T.C.
NIGDE ÖMER HALİSDEMİR UNIVERSITY
GRADUATE SCHOOL OF NATURAL AND APPLIED SCIENCES
MECHANICAL ENGINEERING DEPARTMENT

DESIGN AND OPTIMIZATION OF NOVEL FLOW FIELDS FOR PEM FUEL CELLS

MOHAMMAD ZIAUDDIN CHOWDHURY

August 2017

M.Z. CHOWDHURY, 2017
MASTER OF SCIENCE THESIS
GRADUATE SCHOOL OF NATURAL AND APPLIED SCIENCES OF NIGDE ÖMER HALİSDEMİR UNIVERSITY

T.C.
NIGDE OMER HALISDEMIR UNIVERSITY
GRADUATE SCHOOL OF NATURAL AND APPLIED SCIENCE
MECHANICAL ENGINEERING DEPARTMENT

DESIGN AND OPTIMIZATION OF NOVEL FLOW FIELDS FOR PEM FUEL CELLS

MOHAMMAD ZIAUDDIN CHOWDHURY

Master of Science Thesis

Supervisor
Assoc. Prof. Dr. Bora TIMURKUTLUK

August 2017

The study titled "**DESIGN AND OPTIMIZATION OF NOVEL FLOW FIELDS FOR PEM FUEL CELLS**" and presented by **Mohammad Ziauddin CHOWDHURY** with the help of supervisor **Assoc. Prof. Dr. Bora TIMURKUTLUK,** has been found as Master thesis by the jury at the Department of **Mechanical Engineering** of Nigde Omer Halisdemir University Graduate School of Natural and Applied Sciences.

Head: Assoc. Prof. Dr. Murat GOKCEK, Nigde Omer Halisdemir University

Member: Assist. Prof. Dr. Muhittin BILGILI, Gazi University

Member: Assoc. Prof. Dr. Bora TIMURKUTLUK, Nigde Omer Halisdemir University

CONFIRMATION:

This thesis has been found appropriate at the date of …./…./20.... by the jury mentioned above who have been designated by Board of Directors of Graduate School of Natural and Applied Sciences and has been confirmed with the resolution of Board of Directors dated …./…./20.... and numbered ……………

....../...../20...

Assoc. Prof. Dr. Murat BARUT
DIRECTOR

DECLARATION OF THESIS

I hereby announce that all the information in this document have been acquired and demonstrated in accordance with academic rules and ethical conduct. Besides, I also acknowledge the proper authority of the reference in accordance with the rules and regulations beyond the original contribution of this thesis works.

Mohammad Ziauddin CHOWDHURY

ÖZET

PEM YAKIT PİLİ İÇİN YENİ AKIŞ ALANLARININ TASARIMI VE OPTİMİZASYONU

CHOWDHURY, Mohammad Ziauddin
Niğde Ömer Halisdemir Üniversitesi
Fen Bilimleri Enstitüsü
Makina Mühendisliği Anabilim Dalı

Danışman : Doç. Dr. Bora TİMURKUTLUK

Ağustos 2017, 140 sayfa

Bu çalışmada, deneysel ve sayısal yaklaşım ile akış alanı optimizasyonu incelenmiştir. Yenilikçi yakınsak-ıraksak akış alanı tasarımı, bu çalışmanın özgün yanını ortaya koymaktadır. Deneysel sonuçlara göre belirli yakınsak akış alanlarının hücre gücü, diğer iki geleneksel serpantin akış alanına göre %19-27'lik bir artış göstermiştir. Sayısal model doğrulanmasında deneysel sonuçlara göre sadece % 1'den az sapma göstermiştir. Performans üzerinde önemli etkisi olan kanal geometrik parametrelerinden kanal derinliği, genişliği ve kaburga genişliği sayısal çalışma ile optimize edilmiştir. Sonuçlar, 1,0 mm kanal derinliği, 1,0 mm kanal genişliği ve 0,5 mm kaburga genişliğinin kabul edilebilir basınç düşüşü ile en iyi performansa sahip olduğunu göstermiştir. Geleneksel akış alanı tasarımları kütle transferi, basınç düşüşü ve hücre performansı bakımından serpantin akış alanı tasarımının paralel akış alanı tasarımından daha iyi bir performans gösterdiği görülmüştür. Son olarak, paralel ve serpantin yakınsak-ıraksak akış alanların karşılaştırmasında, sayısal sonuçlar güç yoğunluğu bakımından modifiye edilmiş serpantin akış alanında geleneksel serpantin akış alanına göre %2, modifiye edilmiş paralel akış alanında ise geleneksel paralel akış alanına kıyasla %16 oranında bir iyileşme sağladığını ortaya koymuştur.

Anahtar Sözcükler: Yakınsak ıraksak akış alanı, deneysel, matematiksel model, su yönetimi, basınç kaybı, kütle transferi, kanal geometrisi, serpantin, paralel.

SUMMARY

DESIGN AND OPTIMIZATION OF NOVEL FLOW FIELDS FOR PEM FUEL CELLS

CHOWDHURY, Mohammad Ziauddin

Nigde Ömer Halisdemir University
Graduate School of Natural and Applied Sciences
Department of Mechanical Engineering

Supervisor : Assoc. Professor Dr. Bora TIMURKUTLUK

August 2017, 140 pages

In this study, flow field optimization is carried out through experimental and numerical approach. Novel convergent and divergent flow field concept are proposed for this study, which is a case of originality. The experimental results showed 19-27% improvement in the cell performance for specific convergent flow field compare to the other two conventional serpentine flow fields. The numerical model is developed by validating the experimental case study having only less than 1% error of deviation. Considering the valid numerical model, channel geometry, comparative study of conventional parallel and serpentine as well as convergent and divergent flow fields are studied. The straight channel geometry is optimized for channel depth, width and rib width. The result show that 1.0 mm of channel depth and width as well as 0.5 mm of rib width provide the best performance with acceptable pressure drop. For the conventional flow fields study, analyzing mass transport, pressure drop and cell performance, where the results reveal that the serpentine design outperform parallel flow field pattern. Finally, from the numerical study of convergent and divergent flow fields, the result indicate an improvement for specific modified serpentine and parallel by 2% and 16% cell power density comparing conventional ones respectively with improved mass transport and water management.

Keywords: PEM fuel cell, convergent divergent flow field, experimental, mathematical model, water management, pressure drop, mass transport, channel geometry, serpentine, parallel.

GENİŞLETİLMİŞ ÖZET

1.1 Giriş

Son iki yüzyılda, fosil yakıtlar sanayileşme ve modernleşme için en etkili enerji kaynakları olmuştur. Günümüzde hâlâ fosil yakıtlar bizim en önemli enerji kaynaklarımızdır. Bununla birlikte, hızla artan enerji talebini yakın gelecekte karşılayacak kadar büyük ölçüde fosil yakıt rezervi bulunmamaktadır. Bu nedenle, son yıllarda yoğun bir şekilde yenilenebilir ve sürdürülebilir enerji sistemleri üzerine araştırmalar yapılmaktadır. Yakıt pilleri sürdürülebilir ve çevreye zararsız enerji üreteçleri olduklarından dolayı, artan enerji talebini karşılayabilecek ve fosil yakıtlı enerji sıstemlerinin yerini alabilecek sistemler olarak değerlendirilmektedir. Bu yüzden, insan toplumunun refahı için yakıt pili teknolojilerini geliştirmek çok önemlidir. Yakıt hücresi ilk olarak yaklaşık 200 yıllık bir süre önce icat edilmiş, ancak NASA'nın uzay programları için alternatif bir enerji kaynağı olarak yakıt hücresi teknolojisi kullanmasına kadar potansiyel bir enerji kaynağı olarak öncelik verilmemiştir. İlk olarak Sir William Grove tarafından yakıt hücresi kavramı ortaya konulmuştur. Yakıt hücreleri basitçe bir enerji dönüştürme aygıtı olarak tanımlanabilir.

Yakıt pilleri, elektrolit çalışma sıcaklığına ve kullanılan yakıt türüne göre sınıflandırılmaktadır. Farklı yakıt pili türleri aşağıda verilmiştir.

PEM yakıt pilleri elektrolit olarak düşük sıcaklık polimer membran kullanarak sof hidrojen yakıt ile çalışmaktadır. PEM yakıt pillerinde gerçekleşen kimyasal reaksiyonlar aşağıda verilmiştir:

Anot: $H_2 = 2H^+ + 2e^-$

Katot: $1/2\ O_2 + 2H^+ + 2e^- = H_2O$

Doğrudan metanol yakıt pillerinde yakıt olarak metanol kullanılır ve bu nedenle yüksek enerji depolama kapasitesine sahiptirler. DMYP içerisinde kimyasal reaksiyonlar aşağıdaki gibi gerçekleşir:

Anot: $CH_3OH + H_2O = CO_2 + 6H^+ + 6e^-$

Katot: $3/2\ O_2 + 6H^+ + 6e^- = 3H_20$

Katı oksit yakıt pilleri en yüksek enerji verimliliği sağlayan yakıt pilleridir. Yüksek çalışma sıcaklığına sahip düşük maliyetli metal katalizörler kullanılır. KOYP'de kimyasal reaksiyonlar aşağıdaki gibi gerçekleşir:

Anot: $O^{2-} + H_2 = H_2O + 2e^-$

Katot: $1/2\ O_2 + 2e^- = O^{2-}$

Alkali yakıt pillerinde, katot tarafındaki negatif iyonlar elektrolit üzerinden anota geçerler ve anotta hidrojen ile birleşerek su ve elektron üretirler. AYP özellikle CO_2 emisyonlarına karşı çok hassastırlar. AYP'de gerçekleşen kimyasal reaksiyonlar aşağıda verilmiştir:

Anot: $2\ OH^- + H_2 = H_2O + 2e^-$

Katot: $1/2\ O_2 + H_2O + 2e^- = 2\ OH^-$

Fosforik asit yakıt pillerinde elektrolit olarak fosforik asit kullanılmaktadır ve FAYP'ler safsızlıklara daha toleranslıdır. FAYP'de gerçekleşen kimyasal reaksiyonlar şu şekildedir:

Anot: $H_2 = 2H^+ + 2e^-$

Katot: $1/2\ O_2 + 2H^+ + 2e^- = H_2O$

Eriyik karbonatlı yakıt pilleri, lityum karbonat ya da potasyum karbonat gibi erimiş karbonat tuzunu elektrolit olarak kullanır. Gerçekleşen kimyasal reaksiyonlar aşağıdaki gibidir:

Anot: $H_2 + CO_3^{2-} = H_2O + CO_2 + 2e^-$

Katot: $1/2\ O_2 + CO_2 + 2e^- = CO_3^{2-}$

Otomotiv sektörü büyük miktarda enerji gerektirmekte ve sürekli talep artmaktadır. PEMYP'leri düşük sıcaklıklarda çalışan, çevre dostu, sessiz, titreşimsiz ve hızlı bir şekilde aktif hale geçebilen sistemlerdir. Bu nedenle otomotiv sektöründe kullanımı için oldukça uygun olmaktadır.

PEM yakıt hücresi fiziksel sistemi bileşenlerine göre üç kategoriye ayrılabilir. Bunlar;

1. Temel bileşen
2. Aksesuarlar
3. Çevre elemanları

PEM yakıt pili temel bileşenleri son plaka, çift kutuplu plaka, akım toplayıcı, gaz difüzyon tabakası, katalizör tabaka ve membrandan oluşmaktadır. PEM yakıt pili aksesuarları içerisinde soğutma plakaları, nemlendirici, regülatörler, conta, kütle akışı denetleyicisi, elektronik yük, sıcaklık sensörleri, hidrojen tankı, valfler, hava filtresi ve radyatör gibi elemanlar bulunmaktadır. Soğutma pompası, kompresör ve sirkülasyon pompası v.b. gibi çevre elemanları PEM yakıt hücresinin ve yardımcı aksesuarlarının düzgün ve verimli çalışması için kullanılan ekipmanlardır.

Tezin amacı gerçekleştilecek çalısmaların sırasına göre aiağıda maddeler halınde sunulmuştur.

- PEM yakıt pili deney düzeneği geliştirmek
- Yeni ve verimli akış alanı tasarlamak
- Geliştirilmiş akış alanı tasarımını tasarlanmış geleneksel akış alanı ile karşılaştırmak
- Tasarlanan akış alanları arasındaki hücre performans farkını ölçmek
- Sayısal model geliştirmek
- Sayısal modeli deney sonuçlarıyla doğrulamak
- Doğrulanmış sayısal modelle uyum içinde kanal geometrisi optimizasyonu yapmak
- Var olan geleneksel akış alanı modelini karşılaştırma yapabilmek için analiz etmek
- Geliştirilen akış alanının iç karmaşık olgularını daha iyi anlamak için sayısal analizini yapmak

1.2 Literatür Taraması

PEM yakıt pili ile ilgili ilk çalışmalarda tek boyutlu modeller geliştirilmiş (Springer ve diğ., 1991; Bernardi ve diğerleri, 1992) ve ilerleme kaydedilerek iki boyutlu model geliştirilmüştür. (Gurau ve diğerleri, 1999; Siegel ve diğerleri, 2004). Daha sonra üç boyutlu modele dayanan araştırma çalışmaları (Hontanon ve ark., 2000; Berning ve diğerleri, 2003; Wang ve ark., 2004) yapılmıştır. Farklı çalışma grupları PEM yakıt pili modeli oluşturmak için zaman bağımlı (Um ve diğ., 2000; Khakbaz-Baboli ve diğerleri, 2008; Khajeh-Hosseini-Dalasm ve diğerleri, 2010), zaman bağımsız (Manso ve ark., 2011; Santamaria ve diğerleri., 2013;), tek fazlı akış (Dawes ve ark., 2009; Grigoriev ve diğ., 2013),iki fazlı akış (Shah ve diğerleri, 2007; Mancusi ve diğerleri, 2014), izotermal (Rostami ve diğerleri, 2016; Santamaria ve diğerleri, 2013) ve izotermal olmayan (Lobato ve diğerleri, 2010; Lin ve diğerleri., 2010; Xing ve ark., 2016) gibi durumler uygulayarak sayısal çalışmalar gerçekleştirmişlerdir.

Bazı araştırmacılar ise PEM yakıt hücresi içerisinde gerçekleşen kütle transferi ve elektrokimyasal prosesler gibi karmaşık olayları daha iyi anlayabilmek için hem deneysel hem de sayısal teknikler geliştirmişlerdir. Nötron görüntüleme (Owejan ve diğerleri, 2007 ve Hickner ve diğerleri., 2008), gaz kromatografisi (Mench ve diğerleri, 2003; Yang ve diğ., 2005), X-ray mikrotomografi (Sinha ve ark., 2006; Lee ve diğerleri, 2008), şeffaf hücre (Tuber ve diğerleri, 2003; Zhang ve diğerleri, 2006; Spernjak ve diğerleri, 2007; Kumbur ve diğerleri, 2006; Hussaini ve diğerleri., 2009) gibi çalışmalar bu tekniklerden bazılarıdır. Deneysel ölçüm ile ilgili zorluklar alternatif sayısal modelleme tekniklerinin geliştirilmesi ihtiyacını doğurmuştur.

Literatürde gerekleştirilen çalışmalar inceledığinde genel olarak akış olanı tasarımının hücre performansı üzerinde önemli olan etkisinin olduğu gorulmektedir. Bu yuzden bu deneysel ve sayısal olarak karşılaştırmalı bir incelenmiştir.

1.3 Deneysel Düzenek

Deneysel çalışmada tüm akış alanı tasarımı için 4,73 cm^2'lik aktif kanal alanına sahip bir geometri göz önüne alınmıştır. Geliştirilen farklı akış alanı geometrileri için değişen tek geometrik parametre kanal derinliğidir. İncelenen tekli test hücresinin ayrıntıları Tablo 1.1'de verilmiştir.

Fotoğraf 1.1'de gösterilen toplam altı adet tek serpantinli akış alanına sahip plakalar üretilmiştir. Bu plakalardan iki tanesi 1 mm ve 2 mm kanal derinliğine sahip geleneksel serpantin akış alanlı plakalardır. Diğer dört plaka ise farklı kanal derinliklerine sahip yakınsak-ıraksak akış alanına sahip plakalardır ve Şekil 1.1’de yakınsak-ıraksak akış alanı tasarımı gösterilmiştir.

Çizelge 1.1. Tekli test hücresinin özellikleri

Akış Alan Modeli	Tekli Serpantin
Bipolar plaka (BP) Malzemesi	Grafit
BP boyutu	40 mm*40 mm* 5 mm
Akış kanalında dönüş sayısı	8
Akış kanalı sayısı	9
Kaburga sayısı	8
Toplam Kanal Uzunluğu	206 mm
Aktif Alan	4,73 cm^2
Kanal genişliği	1,5 mm
Kaburga genişliği	1 mm
Akım toplayıcı malzeme	Altın kaplama bakır
Akım toplayıcı kalınlığı	3 mm
Son plaka malzemesi	Paslanmaz çelik
Son plaka boyut	60 mm * 60 mm * 10 mm
Montaj Cıvatası Sayısı	8

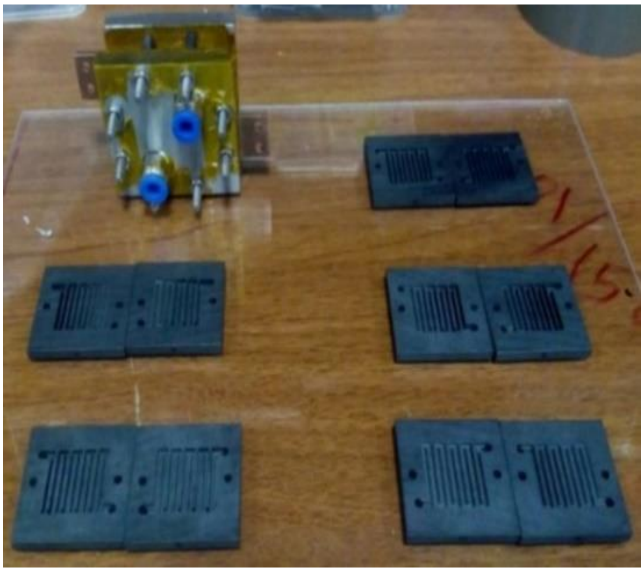

Fotoğraf 1.1. Deneysel çalışmalarda kullanılan farklı akış alanlarına sahip plakalar

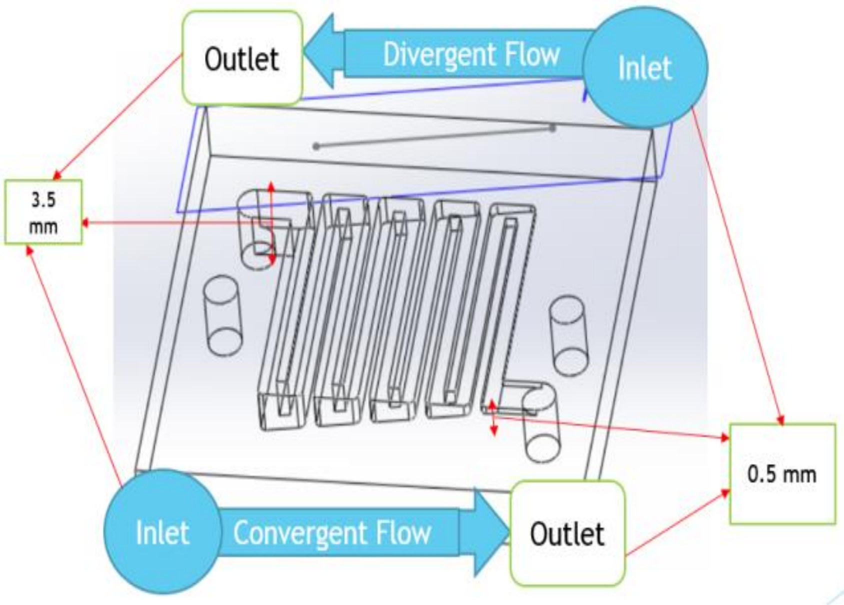

Şekil 1.1. Yakınsak-ıraksak serpantin akış alanı

Deneysel çalışmalarda kullanılan farklı akış alanlarına ait tanımlamalar ve geometrik ölçüler Tablo 1.2'de verilmiştir.

Çizelge 1.2. Farklı akış alanı tanımlamaları

Akış Alanların Adı [C= yakınsak, D= ıraksak, S = sabit derin]	Kanal Derin	
	Giriş mm	Çıkış mm
S1	1	1
S2	2	2
C1	1.5	0.5
C2	2.5	1.5
C3	3	1
C4	3.5	0.5
D1	0.5	1.5
D2	1.5	2.5
D3	1	3
D4	0.5	3.5

Deneysel çalışmalar için gaz difüzyon katmanı ile entegre beş katmanlı membran elektrot grubu (MEG) kullanılmıştır. Kullanılan membran elektrot grubu Fotoğraf 1.2'de, detaylı özellikleri ise Tablo 1.3'te verilmiştir.

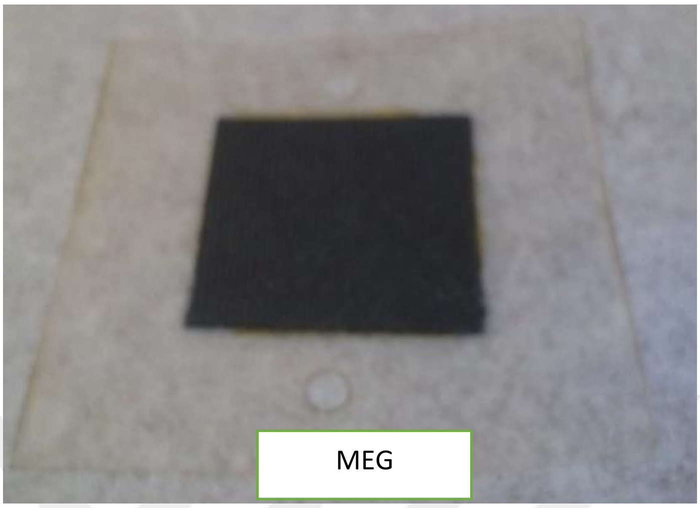

Fotoğraf 1.2. Deneysel çalışmalarda kullanılan MEG

Çizelge 1.3. MEG özellikleri

Membran Tipi	Nafion PFSA NR-212
Membran Kalınlığı	50,8 µm
Gaz difüzyon tabakası (GDT)	Karbon kağıt
GDT Kalınlığı	410 µm
Anot katalizör	0,5mg/cm^2
Anot içeriği	60 wt% Pt
Katot katalizör	0,5mg/cm^2
Katot içeriği	60 wt% Pt
MEG katman sayısı	5
Üretim yöntemi	Sıcak pres

Deneysel çalışmalarda kullanılan Teflon ve Fiberglas sızdırmazlık elemanları Fotoğraf 1.3'te gösterilmiştir.

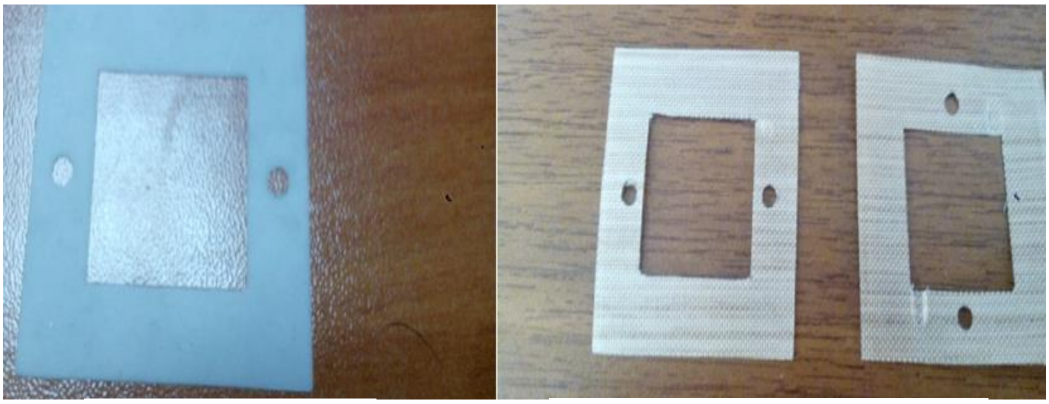

a b

Fotoğraf 1.3. Sızdırmazlık elemanları teflon (a) fiberglas (b)

Bu çalışmada kullanılan deneysel düzeneğin kurulum ile yapılmıştır. Yakıt hücresinin montajı esnasında 3 N-m'lik sıkma torku kullanılmış ve homojen sıkıştırma basıncı sağlamak için hücrenin sekiz cıvatasının sıkıştırma sırası yapilmiştir. Deneysel düzenek şematik olarak Şekil 1.2’te verilmiştir.

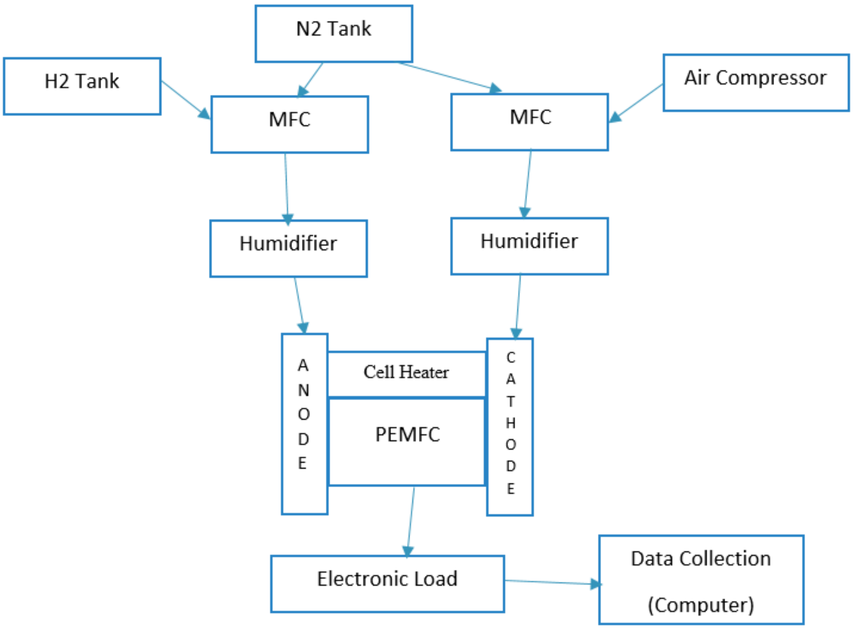

Şekil 1.2. Deneysel düzenek

Deneysel çalışmadan önce montaji tamamlanan hücre üzerinde sabun köpürtme ve su banyosu yöntemi ile gaz kaçak kontrolü yapılmıştır. Deneysel çalışmalarda kullanılan MEG standart prosedür izlenerek aktive edilmiştir. Deney esnasındaki çalışma koşulları Tablo 1.4'te gösterilmiştir.

Çizelge 1.4. Çalışma koşulları

Hücre Sıcaklığı	45 ºC
Giriş H_2 Sıcaklığı	30 ºC
Giriş Hava Sıcaklığı	30 ºC
H_2 Debi Oranı	0,1 SLPM
Air Debi Oranı	0,3 SLPM
Çalışma voltajı	CV 0,5 V
Akış Tipi	Co-flow

1.4 Deneysel Sonuçlar ve Tartışma

Deneysel çalışma neticesindeki sonuçlar geleneksel sabit derinlikli akış alanı geometrisi, yakınsak akış alanı geometrisi ve ıraksak akış alanı geometrisi olmak üzere üç farklı akış alanı geometrisi için karşılaştırılmıştır.

Geleneksel serpantin akış alanına sahip iki dizayndan S1 ve S2'nin performansı Şekil 1.3'de gösterilmiştir. S1 (kanal derinliği 1 mm), S2 (kanal derinliği 2 mm)'den daha iyi performans göstermiştir.

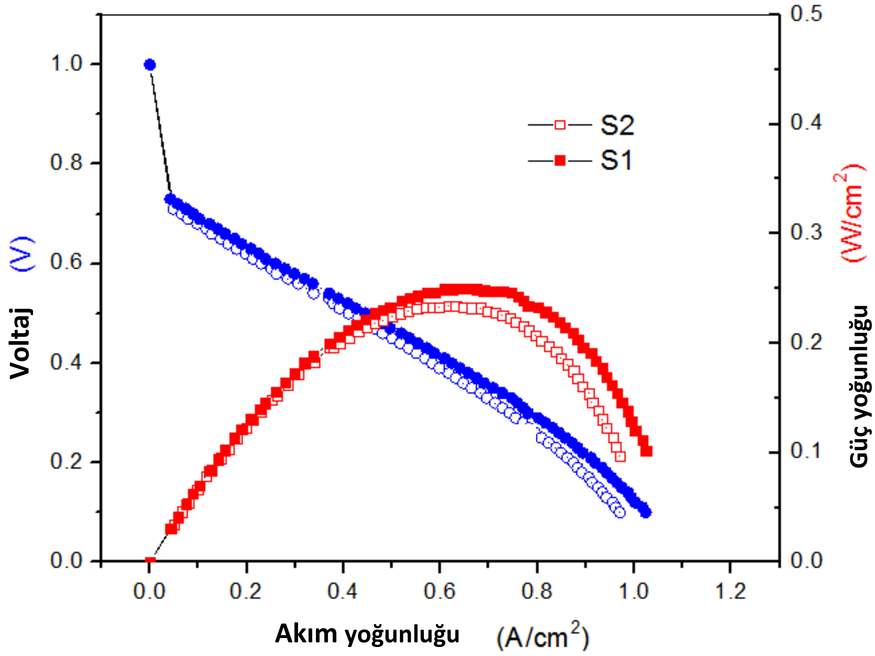

Şekil 1.3. 0,5V, 45ºC'de S1 ve S2 geleneksel kanal tasarımlarının karşılaştırması

Yakınsak ve ıraksak akış alanına sahip geometrilerin performans karşılaştırmaları Şekil 1.4'de verilmiştir. Yakınsak akış alanı geometrisine sahip tasarım bütün durumlarda en iyi performansı göstermiştir.

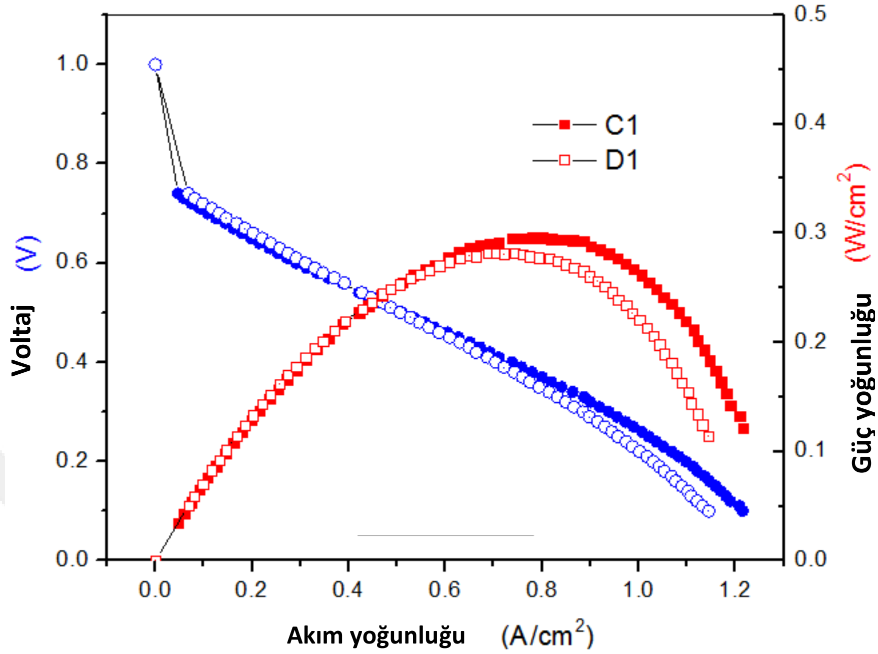

a

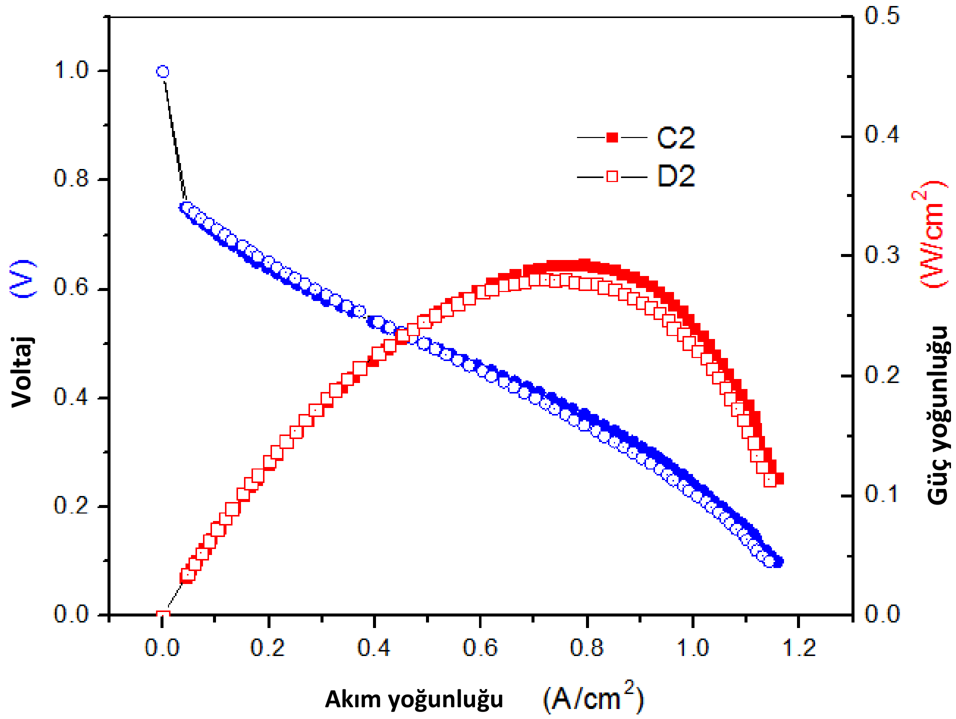

b

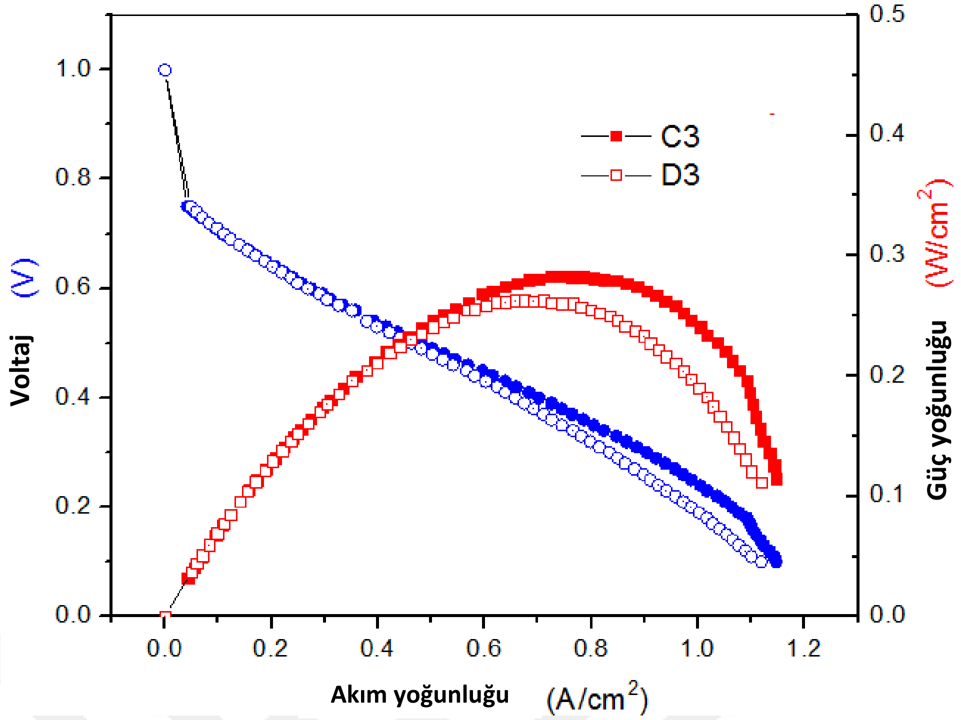

c

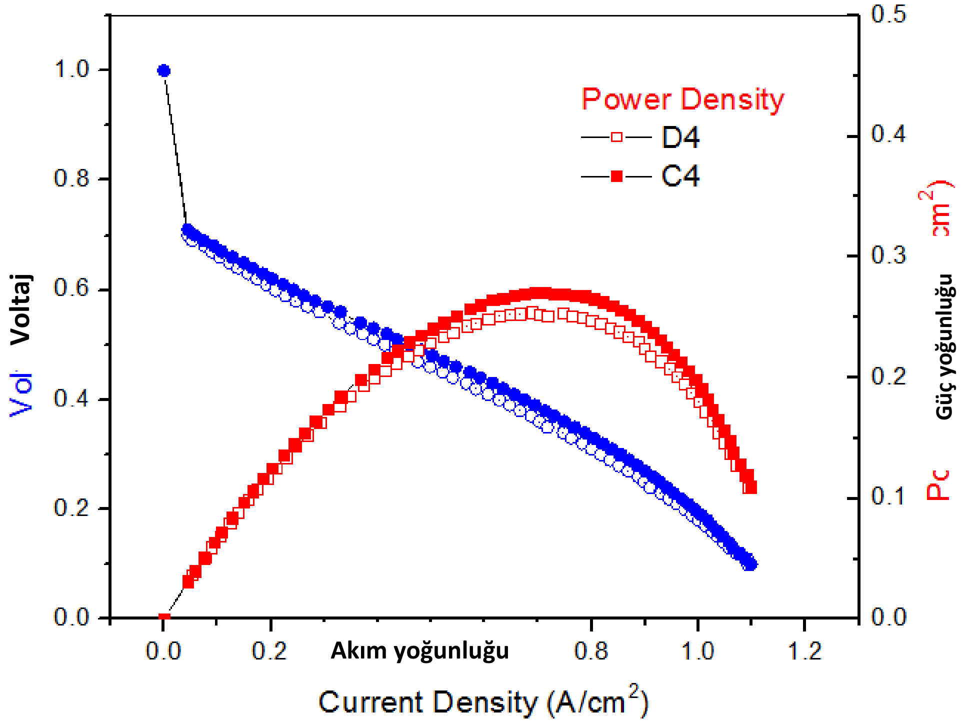

d

Şekil 1.4. Yakınsak-ıraksak akış alanlarının sabit 0,5 V ve 45 ºC hücre sıcaklığında karşılaştırılması D1-C1 (a), D2-C2 (b), D3-C3 (c) ve D4-C4 (d)

Iraksak akış alanları arasındaki karşılaştırma Şekil 1.5'te gösterilmiş olup, D1 konfigürasyonuna sahip tasarım en iyi performansı göstermiştir.

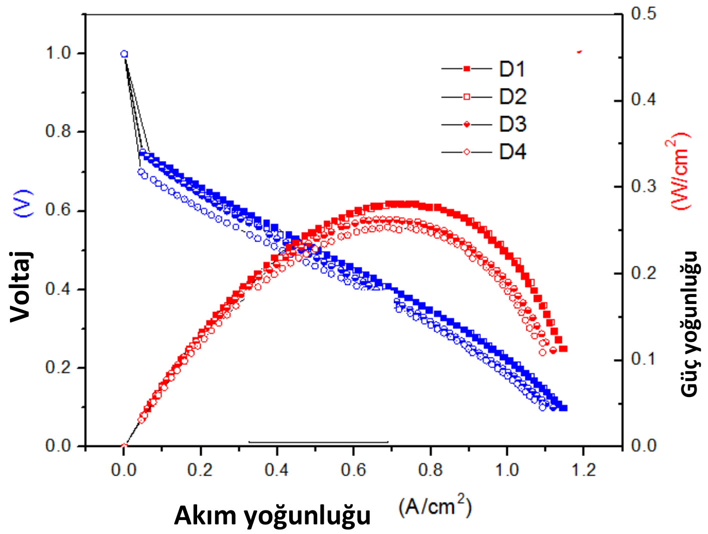

Şekil 1.5. Iraksak akış alanları arasında karşılaştırma

Yakınsak akış alanları arasındaki karşılaştırma Şekil 1.6'te gösterilmiş olup, C1 konfigürasyonuna sahip tasarım en iyi performansı göstermiştir.

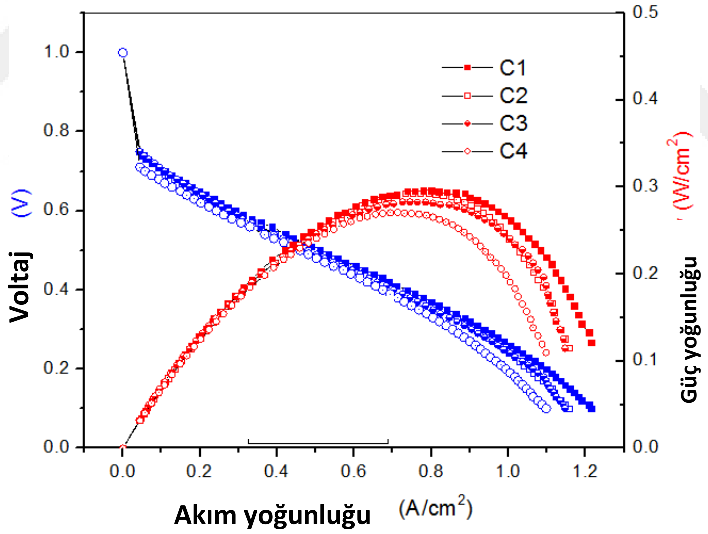

Şekil 1.6. Yakınsak akış alanları arasında karşılaştırma

Deneysel olarak incelenen farklı bütün akış alanlarının hücre performansı Şekil 1.7'de verilmiştir. Bütün konfigürasyonlar için hücre performanslarının sırası ile C1>C2>C3> D1>D2>C4>D3>D4>S1>S2 şeklinde olduğu görülmüştür.

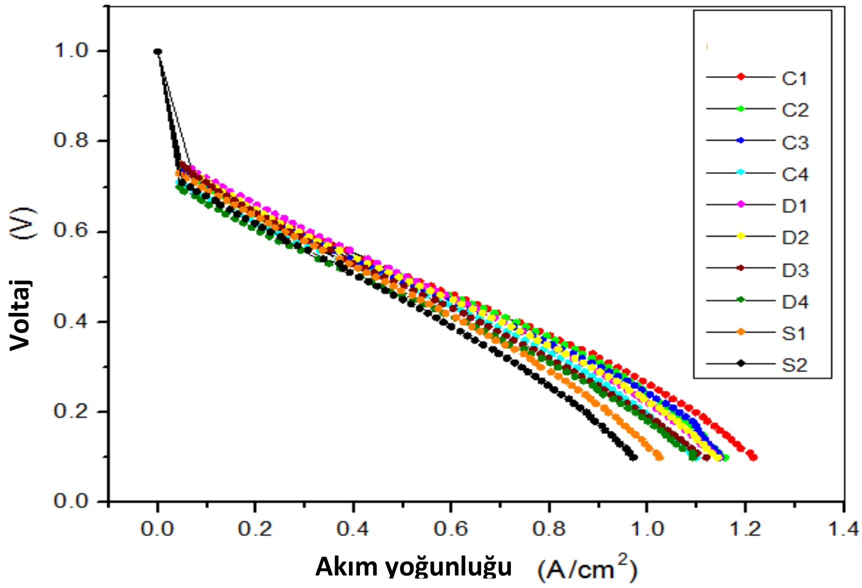

a

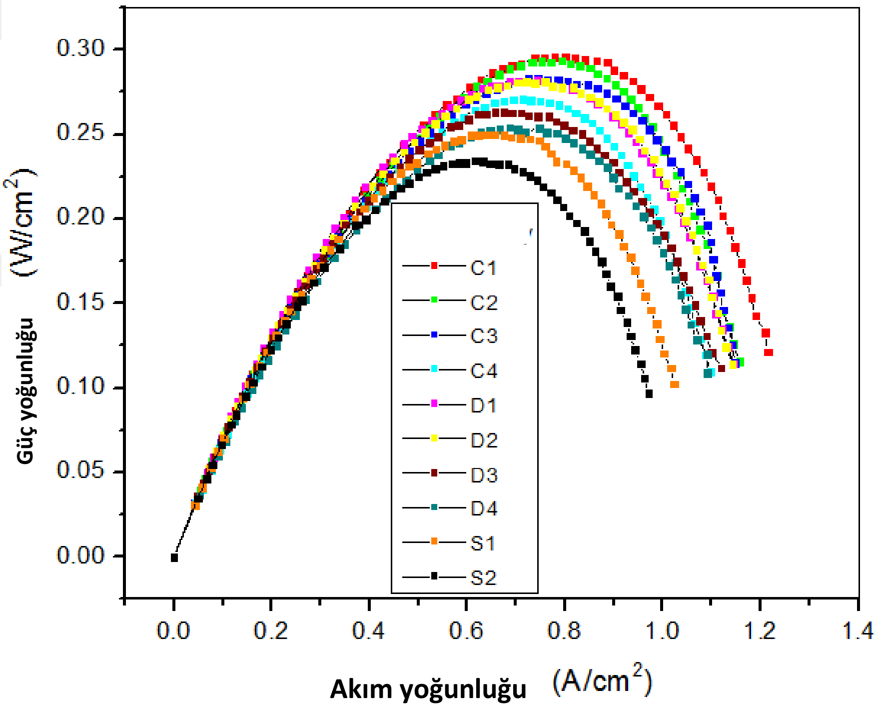

b

Şekil 1.7. Polarizasyon eğrisi (a) ve güç yoğunluğu eğrisi(b)

Şekil 1.8'da geleneksel akış alanı tasarımı ile farklı kanal eğimine sahip yakınsak ve ıraksak tasarımların hücre performansı bakımından karşılaştırılması verilmiştir. Yakınsak kanal tasarımı için C1 konfigürasyonu, ıraksak kanal tasarımı için ise D1 konfigürasyonu en iyi performansı göstermiştir.

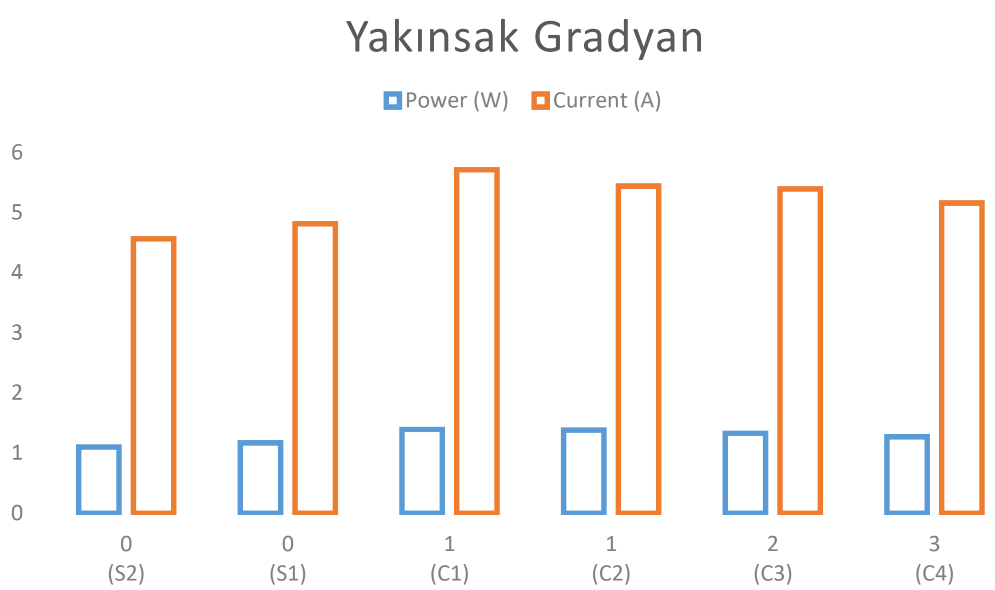

a

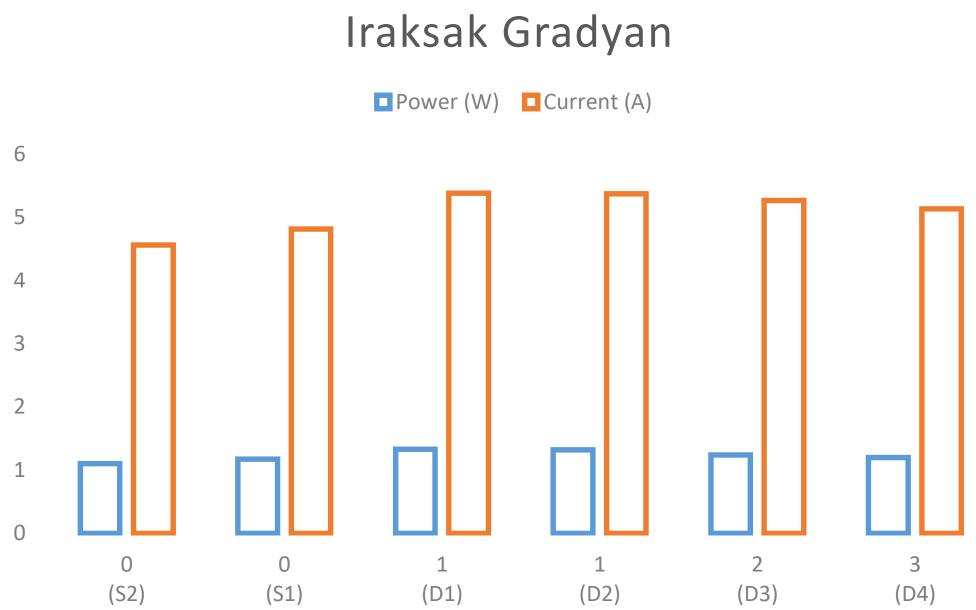

b

Şekil 1.8. Hücre performansı karşılaştırması yakınsak kanal tasarımı (a) ve ıraksak kanal tasarımı (b)

Kanal hacimleri, geleneksel sabit derinliğe sahip kanal tasarımı ve yakınsak-ıraksak kanal tasarımı için kanal geometrisi parametreleri kullanılarak hesaplanmıştır. Toplam kanal hacminin hücre performansı üzerine etkisi Şekil 1.9'de gösterilmiştir. Sonuçlar, kanal hacmi azaldıkça hücre performansının arttığını göstermektedir. Bu yüzden en iyi performans C1 konfigürasyonuna sahip tasarımda elde edilmiştir.

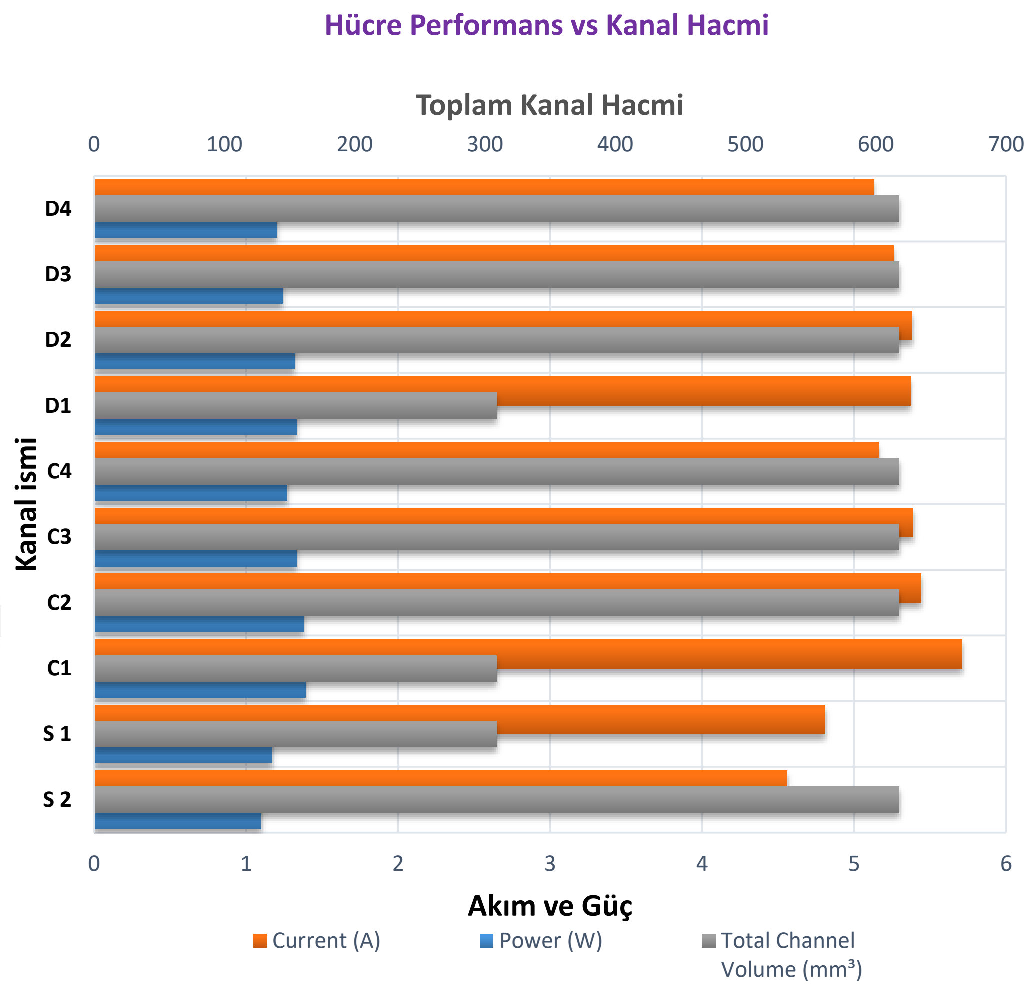

Şekil 1.9. Toplam kanal hacminin (mm^3) hücre performansına etkisi

Deneysel sonuçtan, aşağıdaki tartışma şunu belirtebilir:

- Kanal hacminin azalması ile gaz difüzyonu arttığından dolayı hücre performansı artmaktadır.
- Kanal eğimi azaldıkça yine difüzyon etkilerinden dolayı hücre performansı artmaktadır.
- Suyun hücre içindeki yönetiminin ve akım yoğunluğunun yakınsak akış alanlarında geleneksel ve farklı diğer akış alanlarına kıyasla daha iyi olduğu görülmüştür.
- PEM yakıt hücresinde akış alanı tasarımı için kritik analiz parametresinin hücre hacmi olduğu görülmüştür.

1.5 Sayısal Çalışma

Sayısal çalışmalar için oluşturulan dört farklı geometri yapılmıştır. Kanal geometrisi optimizasyonu için Tablo 1.5'te verilen kanal derinliği, genişliği ve kaburga genişliğine ait geometrik uzunlukların kombinasyonlarını içeren toplam 343 farklı durum incelenmiştir. Bununla birlikte Tablo 1.6'de gösterilen farklı yakınsak ve paralel ve serpantin akış alanları için ise toplam 16 farklı durum incelenmiştir.

Çizelge 1.5. Kanal optimizasyonu için göz önüne alınan geometrik parametreler

Kanal Derinliği (mm)	Kanal Genişliği (mm)	Kaburga Genişliği (mm)
2	2	2
1,75	1,75	1,75
1,5	1,5	1,5
1,25	1,25	1,25
1,0	1,0	1,0
0,75	0,75	0,75
0,5	0,5	0,5

Çizelge 1.6. Yakınsak-ıraksak akış alanı konfigürasyonları

Akış alanı tanımı [C=yakınsak, D=ıraksak, S= serpantin, P=paralel]	Kanal derinliği Giriş/Çıkış (mm)	% Daralma / Genişleme: Girişten çıkışa kanal derinliği
SC1, PC1	1 / 0,75	25%
SC2, PC2	1/0,5	50%
SC3, PC3	1/0,25	75%
SC4, PC4	1/0,1	90%
SD1, PD1	0,75/1	33.33%
SD2, PD2	0,5/1	100%
SD3, PD3	0,25/1	300%
SD4, PD4	0,1/1	900%

Aşağıdaki varsayımlar dikkate alınmıştır:

- Üç boyutlu (3D)
- Tek fazlı akış
- İzotermal
- Laminer akış
- Sabit çalışma koşulları
- Sıkıştırılamaz akış

Sınır ve başlangıç koşulları aşağıdaki gibi alınır:

- İç sınırlar tüm bölgeler için süreklidir.
- Gaz difüzyon katmanları ve katalizör katmanları için simetrik sınır şartları uygulanmıştır.
- Akış kanalı duvarları için kaymama kosulu şartı uygulanmıştır.
- Tüm başlangıç değerleri sıfır olarak atanmıştır.

Aşağıda verilen bilinmeyen değişkenler sayısal olarak çözdürülmüştür.

• ϕ_s— Elektronik potansiyel
• ϕ_l— İyonik potansiyel
• wH_2— Hidrojen kütlesel oranı (anot bölgesinde)
• wH_2Oa— Su kütlesel oranı (anot bölgesinde)
• wO_2— Oksijen kütlesel oranı (katot bölgesinde)
• wH_2Oc— Su kütlesel oranı (katot bölgesinde)
• wN_2— Azot kütlesel oranı (katot bölgesinde)
• u_a and u_c — Anot ve katot bölgelerindeki hız alanı vektörleri
• p_a and p_c — Anot ve katot bölgelerindeki basınçlar

Sayısal çözümler için kullanılan başlıca model parametreleri Çizelge 1.7’de verilmiştir.

Çizelge 1.7. Sayısal model parametreleri

Parametre	Değer
GDL genişliği	400e-6[m]
CL kalınlığı	50e-6[m]
Membran kalınlığı	100e-6[m]
GDL gözenekliliği	0,4
GDL geçirgenliği	1,18e-11[m^2]
GDL Elektrik iletkenliği	222[S/m]
Giriş H_2 Kütlesel oranı (anot)	0,65
Giriş H_2O Kütlesel oranı (katot)	0,03
Giriş oksijen Kütlesel oranı (katot)	0,22
Anot girişi kütle akış hızı	0,00000067[m^3/s]
Katot girişi kütle akış hızı	0,00000201[m^3/s]
Anot viskozitesi	1,19e-5[Pa.s]
Katot viskozitesi	2,46e-5[Pa.s]
Hidrojen molar kütlesi	0,002[kg/mol]
Azot molar kütlesi	0,028[kg/mol]
Su mol kütlesi	0,018[kg/mol]
Oksijen molar kütlesi	0,032[kg/mol]
H_2-H_2O İkili difüzyon katsayısı	9,15e-5*(T/307,1[K])^{1,75}[m^2/s]
N_2-H_2O İkili difüzyon katsayısı	2,56e-5*(T/307,1[K])^{1,75}[m^2/s]
O_2-N_2 İkili difüzyon katsayısı	2,2e-5*(T/307,1[K])^{1,75}[m^2/s]
O_2-H_2O İkili difüzyon katsayısı	2,82e-5*(T/307,1[K])^{1,75}[m^2/s]
Hücre sıcaklığı	Model doğrulama için 318 K, analizler için 353 K olarak alınmıştır.
Referans basıncı	101e3[Pa]
Hücre voltajı	0,9 V
Membran iletkenliği	9,825[S/m]

Farklı geometriler için kullanılan farklı örgü yapılmıştır. Sayısal model için çözüm adımları sırası ile Şekil 1.10'da gösterilmiştir.

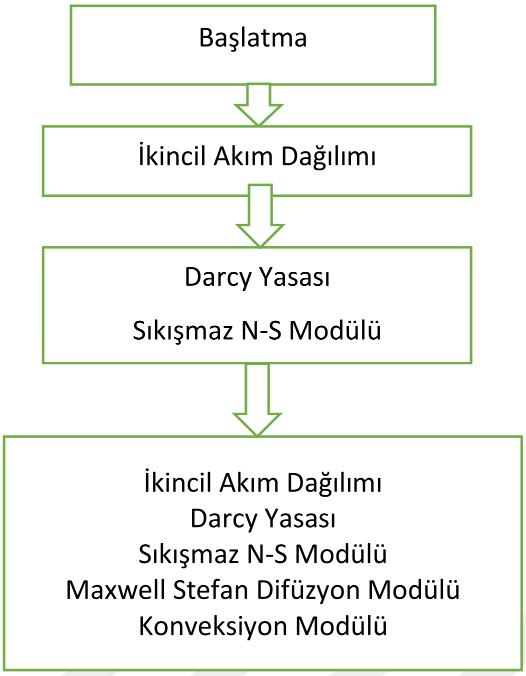

Şekil 1.10. Sayısal model için çözüm adımları

Sayısal model doğrulama sonuçları Şekil 1.11 ve Şekil 1.12 'de gösterilmiştir.

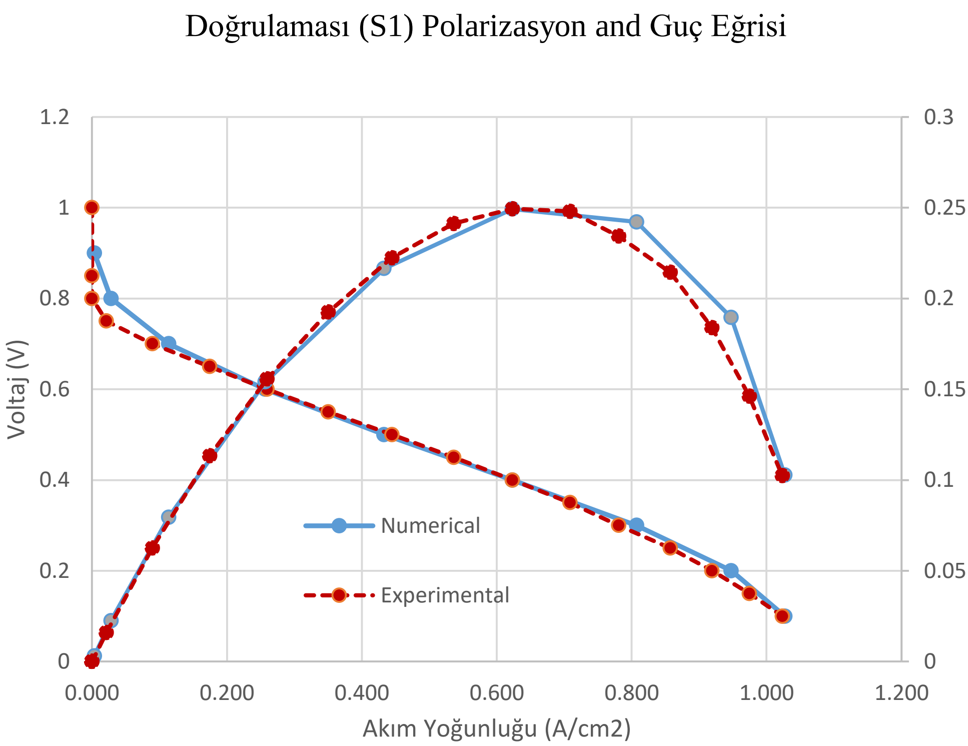

Şekil 1.11. 45°C hücre sıcaklığı ve 30°C gaz sıcaklıkları için S1'in model doğrulamaları Polarizasyon eğrisi ve Güç Yoğunluğu

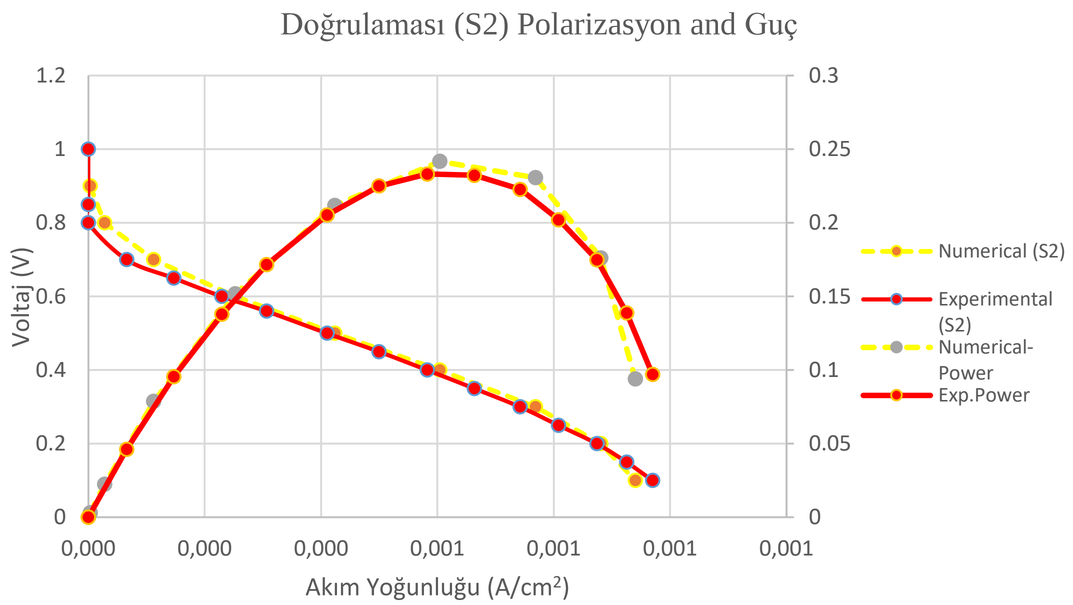

Şekil 1.12. 45ºC hücre sıcaklığı ve 30ºC gaz sıcaklıkları için S2'in model doğrulamaları Polarizasyon eğrisi ve Güç Yoğunluğu

1.6 Sayısal Sonuçlar ve Tartışma

1.6.1 Geometrik optimizasyon

Basınç düşüşü ve akım yoğunluğu dikkate alınarak kanal derinliği, genişliği ve kaburga genişliği için geometrik optimizasyon gerçekleştirilmiştir. Geometrik optimizasyon sonuçları Tablo 1.8'de gösterilmiştir.

Akım yoğunluğu için en önemli parametrenin kaburga genişliği olduğu tespit edilmiştir. Anot basınç düşüşünün etkisinin ihmal edilebilir seviyede olduğu görülmüştür. Kanal derinliği ve genişliği azaldıkça basınç düşüşü artmaktadır. Bu durum katot tarafında daha belirgindir.

Çizelge 1.8. Kanal geometrisi optimizasyon sonucu

Durum	Kanal Geometrisi (D/W/R) mm	Basınç düşmesi (Anode/Cathode) Pa	Akım Yoğunluğu A/cm^2	Kısaltma
Min. Akım Yoğunluğu	2/0.5/2	3.81/22.65	0.61	Katotta düşük akım yoğunluğu ve yüksek basınç düşüşü
Min. Basınç düşmesi	2/2/0.5	0.83/0.89	0.76	Düşük akım yoğunluğu ve en düşük basınç düşüşü
Maks. Akım Yoğunluğu ve Basınç düşmesi	0.5/0.5/0.5	25.96/176.49	0.99	Anot ve katottaki yüksek basınç düşümü ve akım yoğunluğu
Seçilmiş Optimize Edilmiş Model	1/1/0.5	2.26/11.15	0.92	Yüksek akım yoğunluğu ile orta basınç düşüşü

1.6.2 Geleneksel akış alanı analizi

İki farklı geleneksel akış alanı için sayısal çözümler elde edilmiş ve karşılaştırılmıştır. Serpantin akış alanına sahip tasarımın performans bakımından paralel akış alanına sahip tasarımdan daha üstün olduğu görülmüştür.

Serpantin akış alanlı tasarımda reaktanların dağılımı, paralel akış alanı modelinden daha iyidir. Serpantin akış alanına sahip tasarımda basınç düşüşü paralele göre daha yüksektir. Ayrıca suyun hücre içindeki yönetimi serpantin akış alanlı tasarımda daha iyidir.

Serpantin ve paralel akış alanı için hücre performansının karşılaştırılması Şekil 1.13'te gösterilmiştir.

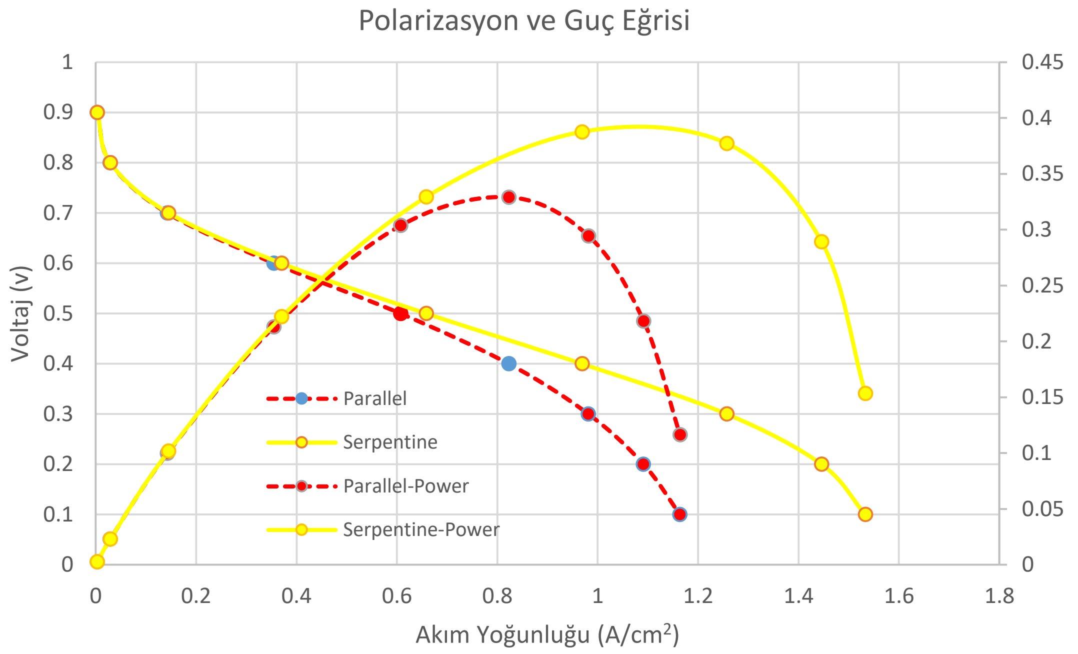

Şekil 1.13. 80 ºC hücre sıcaklığı ve % 100 bağıl nem için Serpantin ve paralel akış alanı hücre performansının karşılaştırılması: Polarizasyon eğrisi ve güç yoğunluğu

1.6.3 Yakınsak-ıraksak akış alanlarının incelenmesi

Yakınsak akış alanına sahip tasarımın hem serpantin hem de paralel akış alanına sahip tasarımlarda diğer akış alanlarına sahip tasarımlara göre daha homojen reaktant dağılımına sahip olduğu görülmüştür.

Yakınsak akış alanına sahip tasarımlar göz önüne alındığında yakınsaklığı artırdıkça hem serpantin hem de paralel akış alanına sahip tasarımlarda basınç düşüşü artmaktadır. Benzer şekilde ıraksak akış alanına sahip tasarımlar göz önüne alındığında ıraksaklığı artırdıkça hem serpantin hem de paralel akış alanına sahip tasarımlarda basınç düşüşü artmaktadır.

Yakınsak akış alanına sahip tasarımlar su yönetimi bakımından ıraksak akış alanına sahip tasarımlardan daha iyi performans göstermektedir. Iraksak akış alanına sahip tasarımlarda ise suyun hücre içerisinde belirli noktalarda birikme yaptığı belirlenmiştir.

Hücre performansı açısından yakınsak, ıraksak ve geleneksel akış alanlı tasarımlar için sayısal sonuçlar karşılaştırılmıştır. Bütün durumlarda yakınsak akış alanına sahip tasarımın performans olarak hem ıraksak hem de geleneksel akış alanına sahip tasarımlardan daha üstün olduğu belirlenmiştir. Yakınsak, ıraksak ve geleneksel akış alanları için hücre performansları akış alanının paralel ve serpantin olması durumu için sırasıyla Şekil 1.14 ve Şekil 1.15'te gösterilmiştir.

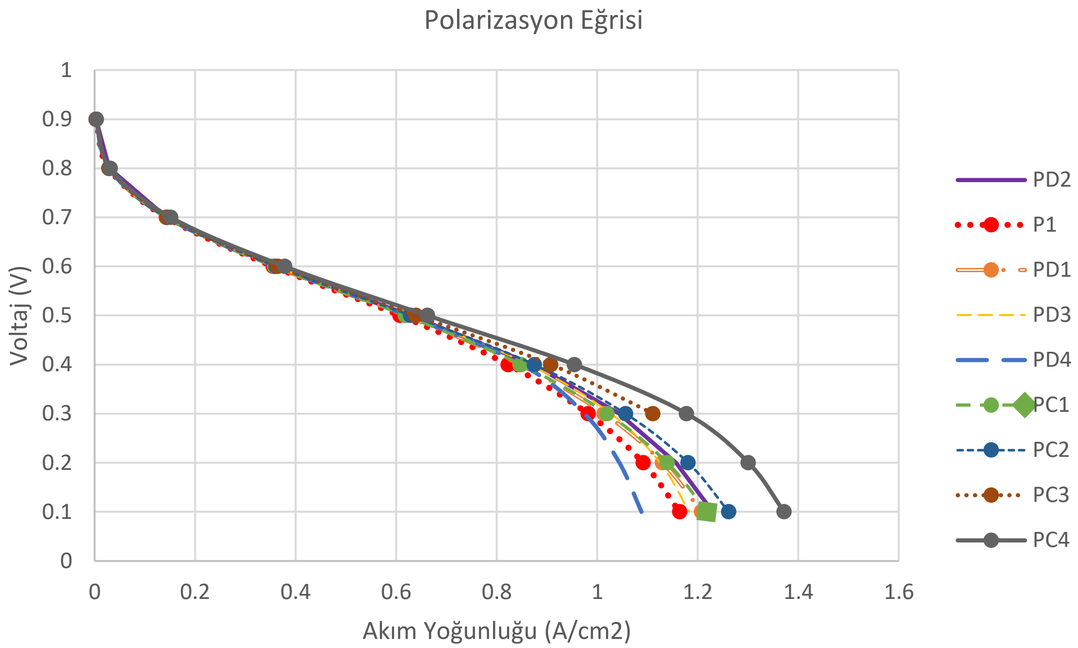

a

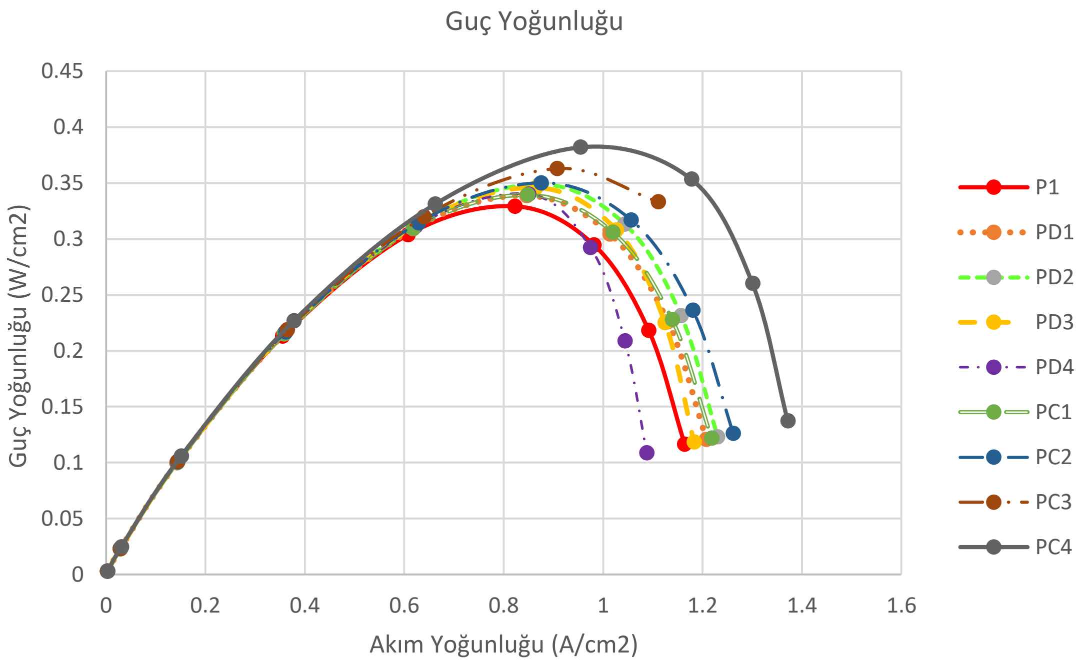

b

Şekil 1.14. Farklı akış alanına sahip tasarımların paralel akış alanı için hücre performanslarının karşılaştırılması polarizasyon eğrisi (a) ve güç yoğunluğu(b)

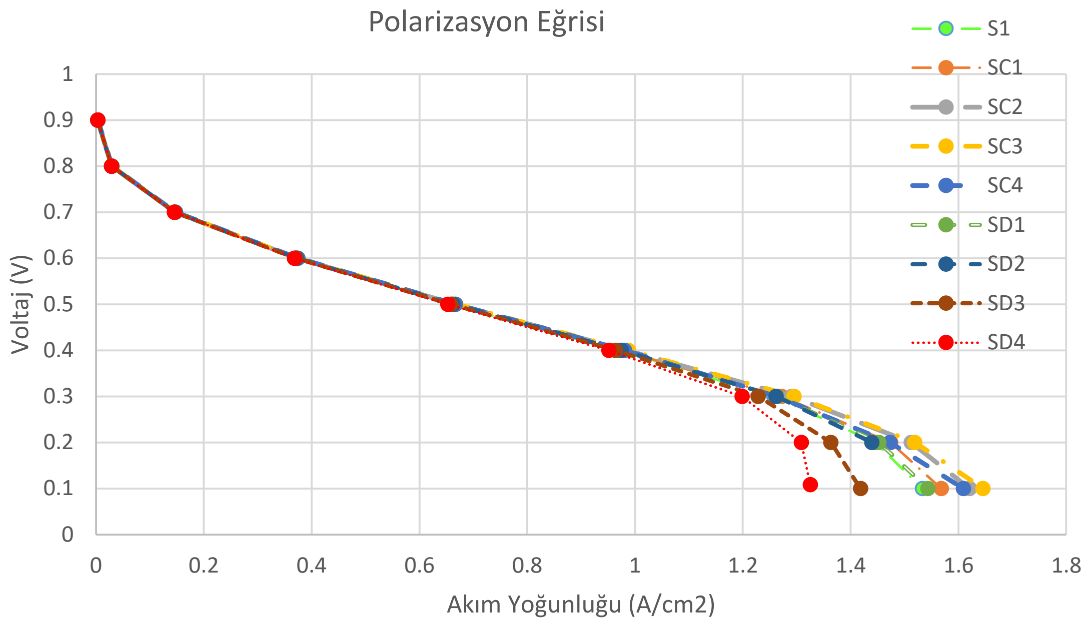

a

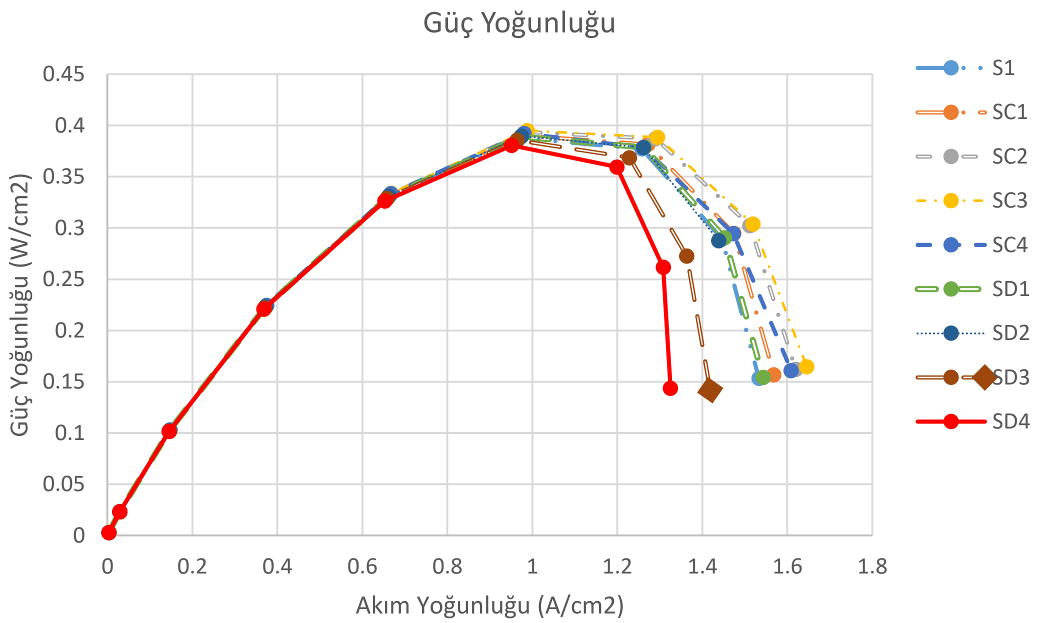

b

Şekil 1.15. Farklı akış alanına sahip tasarımların serpantin akış alanı için hücre performanslarının karşılaştırılması (a) polarizasyon eğrisi (b) güç yoğunluğu

1.7 Sonuç

Bu çalışmada yeni nesil yakınsak ve ıraksak tip kanal geometrisinin PEM yakıt pili çalışma parametrelerine olan etkisi deneysel ve sayısal olarak incelenmiş, geleneksel tasarımlarla karşılaştırımış ve aşağıdaki sonuçlara ulaşılmıştır:

Deneysel çalışmalar aynı şartlar altında test edilen çalışmada önerilen yakınsak kanal tasarımının klasik serpentin tip akış tasarımına göre %19 daha yüksek bir performans sergilediğini ortaya koymuştur.

Deneysel çalışmalarla doğrulanan matematiksel model 343 farklı durum için sayısal olarak çözülmüş ve optimum kanal genişliği, kanal derinliği ve kaburga genişliği sırası ile 1mm, 1mm ve 0,5mm olarak bulunmuştur.

Kanal geometrisi optimizasyonundan sonra matematiksel model çalışmada önerilen yakınsak-ıraksak akış alanı tasarımlarının klasik paralel ve serpentin akış alanlarına uygulanması ile yeniden sayısal olarak çözülmüş ve simülasyon sonuçlarından yeni yaklaşımla modifiye edilmiş serpentin akış tasarımının daha yüksek hücre performansına karşın daha yüksek basınç kaybı sergilediği belirlenmiştir.

Modifiye edilmiş paralel akış tasarımının klasik paralel akış tasarımından %16 ve modifiye edilmiş serpentin akış tasarımının ise geleneksel serpentin akış alanı tasarımından %2 daha yüksek performans sergilediği tespit edilmiştir.

ACKNOWLEDGEMENT

First and foremost, I am obediently paying grattitude to my Creator who gives me knowledge, shows me the way of blessing and mercy. Without His help I could not have been walking in the way now I’m in.

This dissertation could not be accomplished without the support of my supervisor Dr. Bora Timurkutluk as I got continous support, discussion and inspirations from him. Also I am thankful to him for my financial support during the peroid I worked with him in Prof. T. Nejat Veziroglu Clean Energy Research Center.

I am very much thankful to Dr. Yahya Erkan Akansu, with whom I started my journey to PEM fuel cell by working in his TÜBİTAK scientific research project. I also especially thank Dr. Serkan Toros, who introduce me to the numerical skill.

I also deeply recognize the support from Omer Halisdemir University, BAP (Scientific Research Project) YULTEP project scheme for this thesis works.

I also thank Dr. Yusuf Sahin, Dr. Mehmet Khurset Yalcin, Research assistant Omer Genc, Taner Guler, technician Murat Gungordu and other teachers and friends for their immediate and continous help. Beside this, I got love, sympathy and enthusiasum from the neighbours, helpful people and society which I was exposed to during my stay in Turkey.

After all, I am grateful towards my cordial parents, my brothers, sisters, relatives, friends and all well wisher for their love and continous inspirations while I was away from my home country Bangladesh about 6000 km distance. My grattitude will not fulfill until unless I thank my beloved wife for her continous support and sacrifice for me.

TABLE OF CONTENT

LIST OF TABLES

LIST OF FIGURES

LIST OF PHOTOS

LIST OF SYMBOLS AND ABBREVIATIONS

Symbols	**Descriptions**
μ	Dynamic viscosity
A_c	Tafel slope
a_v	Active surface area
C	Carbon
CH_3OH	Methanol
CH4	Methane
CO	Carbon mono-oxide
CO_2	Carbon dioxide
CO_3^{2-}	Carbonate ion
C_x	Species concentration
D_{ij}	Diffusion coefficient
e	Electrolyte phase
e^-	Electron
E_{eq}	Equilibrium voltage
F	Faraday constant
H	Henry’s constant
H^+	Proton
H_2	Hydrogen
H_2O	Water vapor
H_3O+	Hydronium ion
i_a	Anode current density transfer
i_c	Cathode current density transfer
i_o	Exchange current density
i_v	Total current density
k	Permeability
KCO_3	Potassium Carbonate
Li_2CO_3	Lithium Carbonate

M	Molecular mass
N_2	Nitrogen
O_2	Oxygen
OH^-	Hydroxil ion
P	Pressure
Pa	Pressure in the anode compartments
Pc	Pressure in the cathode compartments
Pt	Platinum
R	Universal gas constant
R_i	Species source or sink term
Ru	Ruthenium
S	Current source term
s	Solid phase
T	Temperature
u	Gas velocity
u_a	Velocity field vectors in the anode compartments
u_c	Velocity field vectors in the cathode compartments
V	Voltage
wH_2	Hydrogen mass fraction (in the anode compartment)
wH_2Oa	Water mass fraction (in the anode compartment)
wH_2Oc	Water mass fraction (in the cathode compartment)
wN_2	Nitrogen mass fraction (in the cathode compartment)
wO_2	Oxygen mass fraction (in the cathode compartment)
x	Mole fraction
η	Electrochemical over potential
ρ	Density
φ	Phase potential
φ_l	Ionic potential
φ_s	Electronic potential

Abbreviations	**Description**
AFC	Alkaline Fuel Cell

BOP	Balance of Plant
BP	Bipolar Plate
CL	Catalyst Layer
CNC	Computer Numerical Control
CNG	Compressed Natural Gas
CNT	Carbon Nano Tube
CV	Constant Voltage
DC	Direct Current
DMFC	Direct Methanol Fuel Cell
DOE	Department of Energy, USA
FC	Fuel Cell
FFP	Flow Field Pattern
GDL	Gas Diffusion Layer
IC	Internal Combustion
LIF	Laser Induced Fluorescence
LPG	Liquefied Petroleum Gas
MC	Mass Controller
MCFC	Molten Carbonate Fuel Cell
MEA	Membrane Electrode Assembly
MFC	Mass Flow Controller
NASA	National Aeronautics and Space Administration
N-S	Navier Stokes
OPCF	Open Pore Cellular Foam
PAFC	Phosphoric Acid Fuel Cell
PC	Parallel Convergent
PD	Parallel Divergent
PEM	Proton Exchange Membrane
PEMFC	Proton Exchange Membrane Fuel Cell
PFFP	Parallel Flow Field Pattern
RFC	Regenerative Fuel Cell
RH	Relative Humidity
SC	Serpentine Convergent
SD	Serpentine Divergent

SFFP	Serpentine Flow Field Pattern
SLPM	Standard Liter Per Minute
SOFC	Solid Oxide Fuel Cell
SS	Stainless Steel
YSZ	Yttria Stabilized Zirconia

CHAPTER I

INTRODUCTION

1.1 A Road to Fuel Cell

Since the last two centuries, fossil fuels have been the most dominating energy resource for the industrialization and modernization. Still fossil fuels are the major energy resources of our time. However, fossil fuel reserves are not unlimited in nature for the huge growing demand of energy. Also the environment friendly, sustainable and renewable energy resources become more important for a sustainable growth of human civilization, and in this measure fossil fuel cannot help the cause due to the pollution occurs by the fossil fuel based energy systems. Therefore, from the last few decades, there are intensive search for renewable and sustainable energy system. Fuel cell as a sustainable and environmentally harmless energy device can meet the growing energy demand as well as it can be a replacement of the fossil fuel energy system. So it is an utmost importance to develop better fuel cell technology for the well-being of human society. Although fuel cell invented approximately 200 years ago, it was not well prioritized as a potential energy source until NASA used this technology for the space program as an alternative energy source.

The concept of fuel cell was first developed in the dated back to as old as early nineteen century by Humphry Davy. However, Sir William Grove invented the basic concept of fuel cell in 1839, which was known as gas voltaic battery and in 1889 Charles Langer and Ludwig Mond termed it as fuel cell for the first time. After being suppressed for long time, fuel cell now becomes major research attention due to its concealed potential for the future energy.

Fuel cells can be simply defined as an energy conversion devices where chemical energy of a fuel being directly converted to the electrical energy in an electrochemical way. Thus more chemical energy is directly converted into electrical energy when compared to heat engines that involve a few intermediate conversion steps. Unlike Batteries, fuel cells do not get exhausted and provide continuous power if fuel and oxidant are supplied continuously. Beside the higher energy conversion efficiencies, there is minimal pollution in fuel cells. The basic difference between fuel cells and the existing conventional non-sustainable energy sources can be easily understood from schematic Figure 1.1.

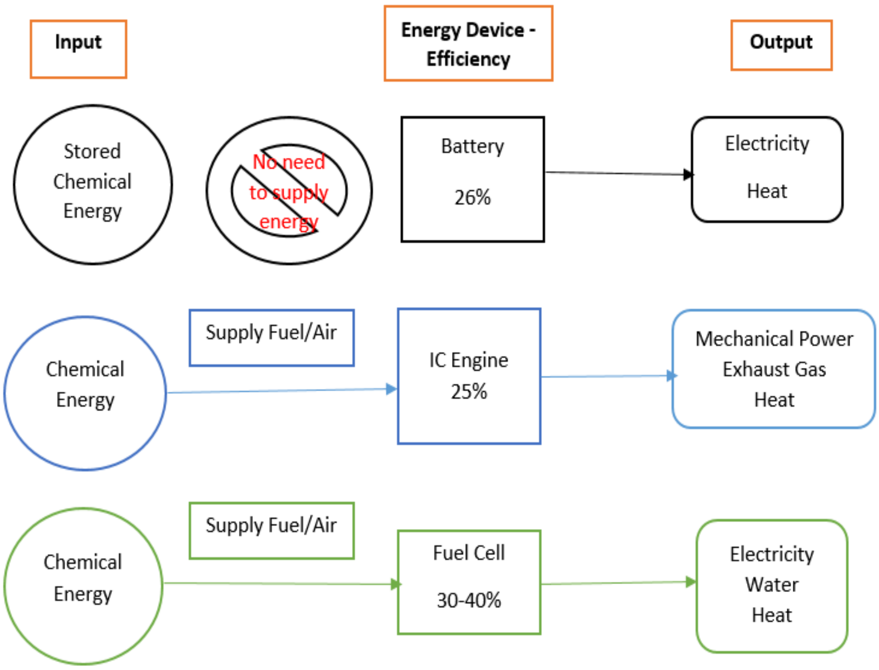

Figure 1.1. Schematic representation of different energy source

The generic type of a fuel cell system consists of anode and cathode electrodes, electrolyte and reactant flow distributor plate. The reactants flow through the distributor plate of the anode and cathode electrode. While flowing through the distributor plate, reactants get diffused to the catalyst layer where the reaction occurs and it is speed up with a suitable catalyst material. Following the formation of ions due to the reduction reactions, ionic exchange occurs through the electrolytes from one side of the electrode to the other side whereas the electron could not pass through the electrolyte rather it is being forced to pass through an external electrical circuit. Thus the electricity is harnessed from the chemical energy directly. Later this electrons participate in the electrochemical reaction for the completion of the chemical and electrical circuit producing byproducts which are released from the cell. The generic fuel cell system is shown in Figure 1.2.

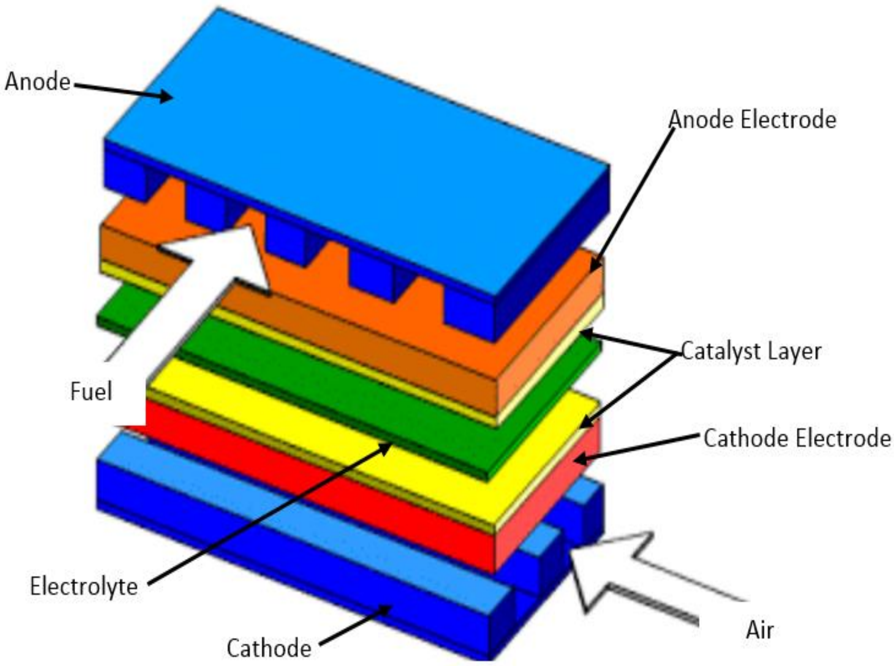

Figure 1.2. Generic Fuel Cell system

Fuel cells have many advantages over the conventional energy systems. Some of the highlighted advantages of the fuel cell systems are as follows:

- High energy conversion efficiency.
- Low maintenance due to having no moving parts.
- Quiet and vibration free operation.
- Zero or low level of pollutant emissions.
- Wide range of opportunity due to the new development of potential electrolyte and material.
- Modular structure.
- Reactants are abundant in nature.
- Depending on the application, different types of fuel cell can be utilized.
- Fuel cells do not need to be recharged and they provide power instantly when supplied with fuel and oxidant.

Like everything exists in the world have demerits, fuel cells are no exception to this. Some of the cons of the fuel cell system are as follows:

- Fuel cell system is very expensive for the large scale industrial implementation
- Durability and reliability problems of some major system components like electrolyte, catalyst layer are of system's disadvantage issues
- Balance of Plants of the fuel cell need energy for a proper system operation
- In some cases, catalyst and electrolyte can be poisoned.

1.2 Taxonomy of Fuel Cell

There are different types of fuel cell which are being developed with the advancement of time. But building an inexpensive, efficient and reliable fuel cell is a far more complicated business. Researchers have designed different types and sizes of fuel cells for the search of higher efficiency and technical variance. Fuel cells are categorized fundamentally by the nature of the electrolyte being employed. It is the determining factor for the electrochemical reactions type in the cell, catalyst suitability, operating temperature, fuel type and usage, cell components physical characteristics and many other factors. Based on these factors, there are different types of fuel cells being developed for different applications. Each type of fuel cell has pros and cons compared to the others. Yet each type of fuel cell which are already developed needs further technical improvements to reduce the cost and expand the application areas.

Broadly, fuel cells can be categorized based on (a) electrolyte nature: Solid electrolyte (PEMFC, DMFC, SOFC) and Liquid electrolyte (AFC, PAFC, MCFC), (b) working temperature: High temperature fuel cell (SOFC, PAFC, MCFC) and Low temperature fuel cell (DMFC, PEMFC, AFC), (c) Fuel and oxidant: Hydrogen (pure) – Oxygen (pure) FC, Hydrogen rich gas - Air FC, Amonia-Air FC, Synthesis gas-Air FC, Hydrocarbon-Air FC. Table 1.1 describes salient features of common fuel cells.

Table 1.1. Common Types of Fuel Cells with their salient features (EG&G Technical Services, Inc., 2004 and Barbir et. al. 2013)

Fuel Cell Type	Electrolyte Nature/ Type	Catalyst	Reactant (Anode /Cathode)	Charge Carrier	Operating Temp. (ºC)	Efficiency/ Application	Inventor/ Year
PEMFC	Solid/ Polymer Membrane	Pt-C/ Pt-CNT	H_2 / O_2	H^+	80-180	40-50% Portable/ Automotive	General Electric/ 1950
DMFC	Solid/ Polymer Membrane	Pt/Ru	CH_3OH / O_2	H^+	50-90	40% Portable	NASA, Jet Propulsion Laboratory/ 1990
SOFC	Solid/ YSZ	Non-precious Metal	H_2, CO, CH_4 / O_2	O^{2-}	550-800	55-60% Industrial	
AFC	Liquid/ KOH	Pt / Non-precious Metal	H_2 / O_2	OH^-	70-120	65-70%	Francis Bacon/ 1959
MCFC	Liquid/ (Li_2CO_3/ KCO_3)	Non-precious Metal	H_2, CO, CH_4 / O_2	CO_3^{2-}	650	60-80%	
PAFC	Liquid/ Phosphoric Acid	Pt	H_2 / O_2	H^+	160-200	40%-80% Thermal-electrical co-generation plant	G. V. Elmore, H. A. Tanner / 1961
RFC	PFSA	Pt	H_2O				

1.2.1 PEMFC

In proton exchange membrane (PEM) fuel cells, protons move through the polymer electrolyte from anode to the cathode to combine with oxygen and electrons, producing water and heat. At present, there are two different types of PEM fuel cell developed which are low temperature (80-100 ºC) PEMFC and another one is high temperature (150-200 ºC) PEMFC. Low temperature operation allows quick startup (less warm-up time) and results in less wear on system components, thus provide better system durability. The electrochemical reactions occurring in PEMFC are:

Anode: $H_2 = 2H^+ + 2e^-$
Cathode: $1/2\ O_2 + 2H^+ + 2e^- = H_2O$

PEMFC is very attractive for the automotive and portable applications. PEMFC will be discussed in more details in the proceeding sections.

1.2.2 DMFC

In direct methanol fuel cell (DMFC), like PEMFC, polymer electrolyte is employed for ionic conductivity. DMFCs, however, are powered by pure methanol, which is usually diluted by water and fed directly to the fuel cell anode. Since liquid methanol can be used as a fuel, no external fuel processing is required and high energy storage densities can be achieved. Unfortunately, the polymer membrane is not impermeable to liquid methanol and the resulting fuel crossover reduces overall system efficiency. The electrochemical reactions occur in DMFC are given below:

Anode: $CH_3OH + H_2O = CO_2 + 6H^+ + 6e^-$
Cathode: $3/2\ O_2 + 6H^+ + 6e^- = 3H_20$

DMFCs are often used to provide power for portable fuel cell applications such as cell phones or laptop computers.

1.2.3 SOFC

In solid oxide fuel cell (SOFC), solid ceramic electrolyte like yttria stabilized zirconia is used for charge transport which occurs from cathode to anode. SOFC operating temperature is relatively higher than any other fuel cell which is about 600-1000ºC. High temperature operation eliminates the need for precious-metal catalyst in SOFC, thereby reducing cost. The efficiency of SOFC is also higher and it is not sensitive to impurity. The electrochemical reactions occurring in SOFC are:

Anode: $O^{2-} + H_2 = H_2O + 2e^-$
Cathode: $1/2\ O_2 + 2e^- = 0^{2-}$

SOFC are suitable for large scale industrial power application.

1.2.4 AFC

Alkaline fuel cell (AFC) uses an alkaline electrolyte such as 40% aqueous potassium hydroxide. In alkaline fuel cells, negative ions travel through the electrolyte to the anode where they combine with hydrogen to generate water and electrons. AFC is very sensitive to impurities especially CO_2. The electrochemical reactions occurring in AFC are as follows:

Anode: $2\ OH^- + H_2 = H_2O + 2e^-$
Cathode: $1/2\ O_2 + H_2O + 2e^- = 2\ 0H^-$

AFCs are high-performance fuel cells due to the rate at which chemical reactions take place in the cell and were used for space applications.

1.2.5 PAFC

Phosphoric acid fuel cells use liquid phosphoric acid as an electrolyte where Teflon-bonded silicon carbide matrix retain acid and platinum catalyst are doped in porous carbon electrodes. PAFCs are more tolerant to impurities. The electrochemical reactions occurring in PAFC are:

Anode: $H_2 = 2H^+ + 2e^-$
Cathode: $1/2\ O_2 + 2H^+ + 2e^- = H_2O$

This type of fuel cell is typically used for stationary power generation.

1.2.6 MCFC

Molten carbonate fuel cell (MCFC) uses molten carbonate salt like lithium carbonate, potassium carbonate as an electrolyte. In molten carbonate fuel cells, negative ions travel through the electrolyte to the anode where they combine with hydrogen to generate water and electrons. The electrochemical reactions occurring in MCFC are:

Anode: $H_2 + CO_3^{2-} = H_2O + CO_2 + 2e^-$
Cathode: $1/2\ O_2 + CO_2 + 2e^- = CO_3^{2-}$

Molten carbonate fuel cells (MCFCs) are currently being developed for natural gas and coal-based power plants for electrical utility, industrial and military applications.

1.3 Motivation Towards PEM Fuel Cell

Automotive sector requires huge amount of energy and the demand is on the rise in every moment. Unfortunately 99% of the automotive sector’s energy system is based on fossil fuel like petroleum, diesel, LPG, CNG etc. With the passage of time, most of the countries are heading towards renewable based energy source to meet the energy demand. This motivation aroused from the global warming impact which is an effect of largely dependence on carbon based energy system releasing carbon di-oxide into the environment burning mainly fossil fuel. Automobile sector is one of the largest area for the release of CO_2 into the environment. So there is an utmost urgency for an alternative green energy source for the automotive sector. Proton exchange membrane fuel cell is a sustainable green energy system which has possibility to replace fossil fuel based energy system for the automotive sectors. PEM fuel cell does not release CO_2, CO and NOx like harmful gases into the environment and the byproduct of the PEM fuel cell is only heat and water. Unlike other fuel cells, PEM fuel cell is working at low temperature which is as low as 80-100 ºC. Also rapid start up system, noiseless and vibration free operation mode made PEM fuel cell more suitable for automotive energy system than any other existing energy systems. Therefore, there is a huge research attraction towards the development of PEM fuel cell technology in the view points of cost, durability and reliability.

1.4 Description: PEM Fuel Cell System

The basic structure of a single PEM fuel cell consists of two end plates, two current collectors, two bipolar plates, two electrodes - anode gas diffusion layer and cathode gas diffusion layer, two catalyst layers - anode catalyst layer and cathode catalyst layer, and one polymer membrane. The MEA, i.e. membrane electrode assembly in PEM fuel cell includes the two catalyst layer and gas diffusion layer of anode and cathode as well as a polymer electrolyte membrane in between the catalyst layers. Besides gasket sealant is used to prevent gas leakage. The assembly bolts are squeezed together to form a single PEM fuel cell unit. The basic construction of a PEM fuel cell is shown in Figure 1.3.

PEM fuel cell physical system components can be divided into three categories based on the system basic functional equipment, essential accessory and efficiency. These are-

1. Fundamental component
2. Accessories
3. Balance of plant

The BOP along with efficient accessories of a PEM fuel cell system is shown schematically in Figure 1.4.

1.4.1 Fundamental component

These type of components include end plate, bipolar plate, current collector, gas diffusion layer, catalyst layer, and a membrane; which are constituents of a unit PEM fuel cell. Without these components PEMFC cannot be considered as an energy device.

1.4.1.1 End plate

Two end plates are used in a single unit or multiple unit based stack of a PEM fuel cell. Normally hard material like steel or cast iron are used for end plates. End plates hold the PEM fuel cell and is responsible for the mechanical integrity of the system. These are the outer most component of the two side of the system. The main purpose of the end plates is to produce a uniform compression within the cell. In this measure, electrodes get contact with the bipolar plates for an effective current collection.

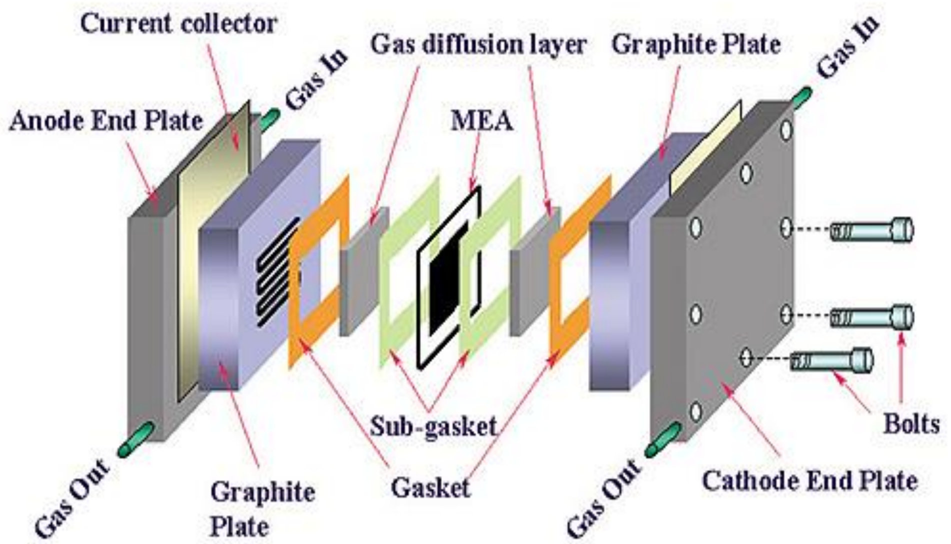

Figure 1.3. Components of single unit PEM Fuel Cell

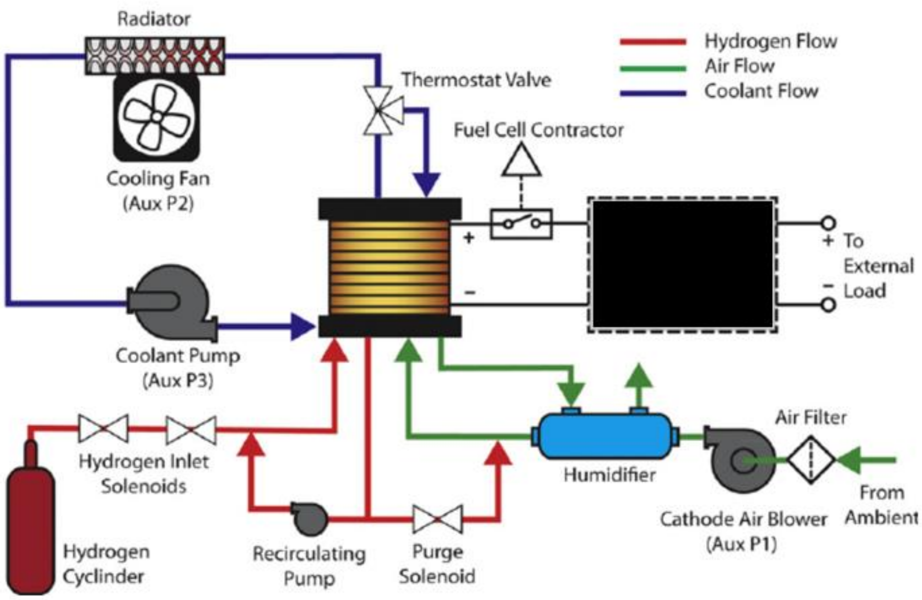

Figure 1.4. PEM fuel cell system with accessories and BOP

1.4.1.2 Current collector

Like the end plate, there are only two current collectors in PEMFC. Both of the current collector seat along with the two sides of the end plates. Current collectors are made of high electron conductive material like copper and usually used with gold plating. Anode side current collector collects electron from the anode electrode through bipolar plate and is connected to an external load. The other current collector of the cathode side is used to receive the electrons from the electronic load to complete the chemical and electronic circuit of the cell.

1.4.1.3 Bipolar plate

It is one of the most important components of PEM fuel cell. Bipolar plate is defined from the nature of its function. In PEM fuel cell stack, one plate is used for both anode and cathode, i.e. bipolar plate has two different polarity of positive cathode and negative anode. But these two are not from the same unit cell rather the bipolar plate's anode is of one cell and cathode of the other unit cell. The major functions of bipolar plates include flow arrangement of reactants along its designed flow field which enhance mass transport of reactants for proper functioning of cell, acting as a medium of electron conductivity and remove waste and water out of the cell.

1.4.1.4 Gas diffusion layer

Gas diffusion layer (GDL) is used in PEM fuel cell which is a porous carbon based cloth or Toray. It is electrically conductive. The function of the gas diffusion layer is to hold diffuse reactants while reactant flow through the bipolar plates. The major priority of the GDL is to protect catalyst layer from physical damage, reduce the chance of flooding in cell catalyst and also to supply reactants to the reaction zones at a uniform concentration.

1.4.1.5 Catalyst layer

Catalyst layer (CL) is one of the major component in PEM fuel cell. At present, Platinum (Pt) based carbon or carbon nanotubes are being used for PEMFC. It is the most expensive component in PEM fuel cell. Since all the reactants take place within these layers, they mainly determine the PEM fuel cell performance.

1.4.1.6 Membrane

The membrane used in PEM fuel cell is a polymer membrane and Nafion is the most widely used. The nature of the polymer membrane is such that it transports proton (H^+) with the presence of water where water acts as a transporter (Hydronium ion: H_3O^+) of proton through polymer membrane. On the other hand, electron cannot pass through the membrane.

1.4.2 Accessories

The accessories are those equipment used for PEMFC system which are required for proper functioning of the PEM fuel cell. These accessories includes- cooling plates, humidifier, regulators, gasket seal, mass flow controller, electronic load, temperature controller, sensors, hydrogen tank, valves, air filter, radiator etc. These equipment are not energy consuming device rather these are for effective controlling as well as help to increase PEMFC system efficiency.

1.4.3 Balance of plant

BOP (Balance of plant) consists of those equipment which are used for the proper functioning of the PEM fuel cell unit and its auxiliary accessories. These equipments consume energy and reduce the total efficiency of the PEM fuel cell system. However, without these equipment PEMFC cannot efficiently work and thereby cell energy efficiency will reduce. These type of component includes- air compressor, cooling pump, recirculating pump, preheater etc.

1.5 Research Justification and Thesis Intent

Staggering number of research efforts have been devoted for the improvement of PEM fuel cell performance during the past 30 years. And with the progress of time, there have been tremendous research improvement. PEM fuel cell consists of many fundamental components like bipolar plate, catalyst layer, polymer membrane, gas diffusion layer wherein each of the component is almost equally important for the research and development of the PEMFC. Since bipolar plate has a significant role in PEMFC, it has wide range of scope to make it more efficient. The energy gained from the PEMFC is in terms of electrical potential. Like any other system, PEMFC has also deviation from the ideal case due to the practical potential loss which are activation, ohmic and concentration loss. Concentration loss occurs due to mal-distribution of reactants mass transport. This type of phenomena can occur largely due to an inefficient bipolar plate flow field design. That's why bipolar flow field design has been a pioneer and dynamic research option in PEM fuel cell.

Experimental approaches were used to be common in the last era for the research of PEMFC flow field design. Since the rapid development of computational software tools, the approach towards the numerical analysis especially for the suitable flow field design has emerged as an effective research tool. Also the experimental tests are being expensive and time consuming. Beside this, the complex internal phenomena like mass transport, pressure distribution and current density distribution, mal-function of flow field in PEM fuel cell cannot be measured with experimental techniques, whereas numerical investigation makes it easier to understand these complex internal phenomena and solve the problems with fast and reliable techniques.

In this study, the main intention for the attainment of the research achievement with the alignment of research interest and justification can be summarized as follows:

- Devise experimental setup of PEM fuel cell
- Design new and effective flow field
- Compare developed flow field design with the conventional flow fields
- Measure the difference of cell performance between the designed flow fields
- Develop a mathematical model
- Validate the model with the experimental results
- Channel geometry optimization in alignment with validated numerical model
- Analyze existing conventional flow field pattern to compare result in between these flow fields to reach to a conclusion of the best available flow fields and also to understand the validity of the developed numerical model in retrospect of research results

- Carry out numerical analysis of the new flow field design for the improvement of conventional flow field
- Numerical analysis of internal complex phenomena of the developed flow field design's model for better understanding

1.6 Thesis Outline

In this thesis, the introductory preceding chapter described the PEM fuel cell research importance in a logical and proceeding way to reach for the thesis research justification and purpose. The upcoming chapter will discuss the research highlight in the light of literature of the past research in accordance with the research purpose and attainment.

The Chapter 3 will discuss the experimental study with detail techniques and tools. The result and discussion of this study are highlighted in Chapter 4. The development of the numerical model and its validation are demonstrated in Chapter 5. Chapter 6 discussed the developed and validated numerical model's case studies for flow field optimization that are being considered for this study within the light of mass transport, pressure drop and water management hence overall cell performance. And Chapter 7 concludes the thesis summary and outcome.

CHAPTER II

LITERATURE SURVEY

In this chapter, the research and development of experimental, theoretical and analytical models regarding flow field designs of proton exchange membrane fuel cells are revisited. There are different approach taken by different studies for the improvement of flow field design. It is analyzed briefly with comparative approach in two different sections of channel geometry and flow field pattern within the scope of mass transport phenomena, electrochemical process and pressure drop in order to investigate final ending result of cell performance.

For the deep understanding of the behavior of the internal mass transport phenomena and electrochemical process researchers have developed both experimental and numerical technique. Experimental technique like neutron imaging (Owejan et. al., 2007; Hickner et. al., 2008), gas chromatography (Mench et. al., 2003; Yang et. al., 2005), x-ray microtomography (Sinha et. al., 2006; Lee et. al., 2008) or even transparent cell (Tuber et. al., 2003; Zhang et. al., 2006; Spernjak et. al., 2007; Kumbur et. al., 2006; Hussaini et. al., 2009) were employed for understanding flow phenomena. The difficulties associated with in-situ measurement have led to the development of alternative numerical modeling techniques. As these experimental techniques are expensive and need critical observation, validated numerical model becomes more popular and reliable.

In the early days, one dimensional models (Springer et. al., 1991; Bernardi et. al., 1992) were studied, then with the progress of time two dimensional models (Gurau et. al., 1999; Siegel et. al., 2004) were developed. From the last decade, there are large scale research studies ongoing based on three dimensional model (Hontanon et al., 2000; Berning et. al., 2003; Wang et. al., 2004) for more accurate, validated and reliable results. Different types of numerical model depending on the assumption of model operating condition like transient (Um et. al., 2000; Khakbaz-Baboli et. al., 2008; Khajeh-Hosseini-Dalasm et. al., 2010) and steady state (Manso et. al., 2011; Santamaria et. al., 2013), single phase flow (Dawes et al., 2009; Grigoriev et. al., 2013) and two phase flow (Shah et. al., 2007; Mancusi et. al., 2014), iso-thermal (Rostami et. al., 2016; Santamaria et. al., 2013) and non-isothermal (Lobato et. al., 2010; Lin et. al., 2010; Xing et. al., 2016) approaches were developed for the PEM fuel cell.

Flow field design for PEM fuel cell is quite challenging issue due to the vast design parameters are associated with the effective flow field design. There are open and wide range of scope to develop for effective cell performance. Mainly the design criteria related with two significant major and primary factor which are uniform flow distribution and pressure drop. First one is associated with the cell performance directly and the second one is related with pumping efficiency being an energy expense for the PEM fuel cell. The impact of these two factors can be more understood from the analysis of Wang et. al. (2015), depicted in Figure 2.1 and Figure 2.2 for uneven flow distribution and high pressure drop case respectively.

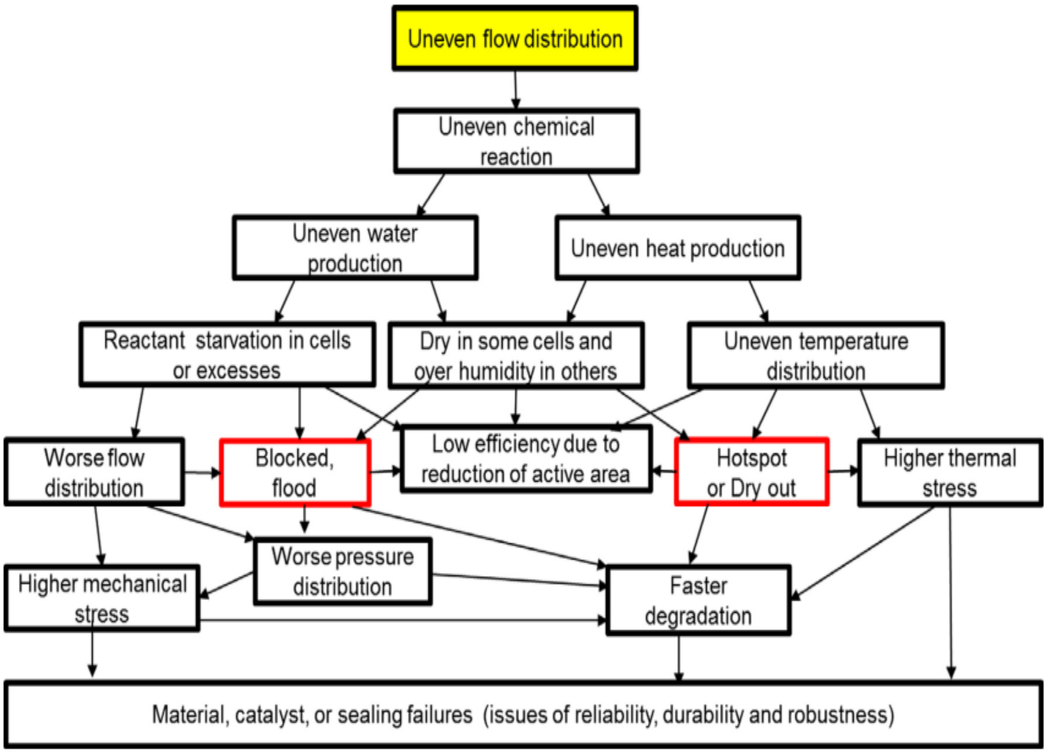

Figure 2.1. Impact of uneven flow distribution in Proton exchange membrane fuel cell durability and reliability [adopted from Wang et. al. (2015)]

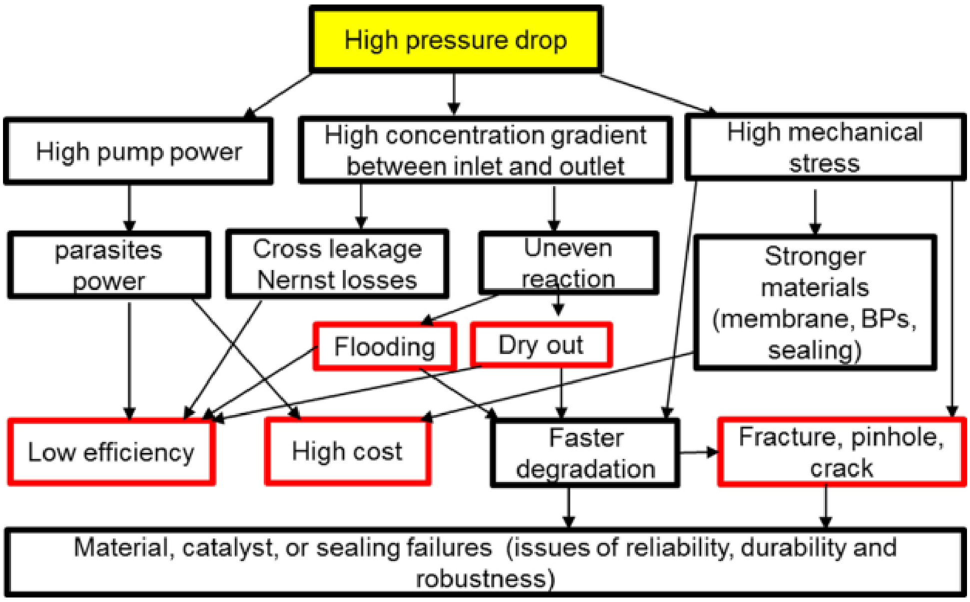

Figure 2.2. Pressure drop effect on PEMFC [adopted from Wang et. al. (2015)]

2.1 Channel Geometry

The cell performance of proton exchange membrane fuel cell largely relies on the proper flow field design. For the effective flow field design, channel geometry is the primary dominant factor. This is because improper channel geometry can results in mal-distribution of reactants transport (Berning et. al., 2003; Rostami et. al., 2016; Yu et. al., 2009; Kreesaeng et. al. 2015; Wang et. al., 2010), faulty water management (Xing et. al., 2016; Salah et. al., 2012; Lorenzini-Gutierrez et al., 2015) and high pressure drop (Akhtar et. al., 2009; Rostami et. al., 2016) across the flow field active area resulting poor cell performance.

Uniform flow distribution, proper water management and reasonable pressure drop in PEM fuel cell are very complex and sensitive issues which are directly related with the cell performance. Enhancement of the flow distribution, liquid water removal and acceptable pressure drop are associated with the channel geometry. Investigations of these behaviors in different flow field designs are important for the advancement of PEMFCs. They facilitate the identification of channel geometries that allow more efficient management of these conditions need to be addressed, and assist to understand the properties which account for this improved performance; thus informing future design processes.

Effective channel geometry includes optimization of channel width (Goebel et. al., 2011; Muthukumar et. al., 2014), rib width (Wang et. al., 2009; Hsieh et. al., 2007), channel depth (Owejan et. al., 2009; Akhtar et. al., 2009; Mckahn et. al., 2015; Chang et. al., 2015) and channel shape (Ashorynejad et. al., 2016; Heidary et. al., 2012; Lu et. al., 2011). Sometimes researchers try to optimize channel geometry with two or even three geometry parameters at a time i.e. cross-sectional area (channel width*Channel depth), aspect ratio i.e. channel width/channel depth (Manso et. al., 2011; Wang et. al., 2007; Cheng et. al., 2007) and channel width/rib width (Higier et. al., 2010; Akbari et. al., 2008; Grigoriev et. al., 2013; Al-Baghdadi et. al., 2007).

Effect of channel depth in PEMFC carried out by Chen et. al. (2004), where it was investigated that a decrease in channel depth results in an increase in the flow velocity as well as a decrease in fuel concentration along the channel. Ferng et. al. (2008) explored that serpentine flow field pattern as superior to parallel flow field pattern by both experimental and numerical analyses. However, they also performed a comparison between uniform channel depth with stepwise different channel depth for which parallel flow field pattern was found better than its uniform channel depth, while there was no significant change for serpentine flow field pattern. Yan et. al. (2008) explored that reducing outlet channel depth results in significant improvement for removing water trapped in porous layer. With the increase in channel height contraction, reactant flow velocities increases so for channel pressure drops. Therefore, the study suggested for an optimal channel height contraction for improved cell performance.

Owejan et. al. (2009) recommended that there must be a minimum channel depth due to the intrusion of GDL while assembling the cell under compression and this can be minimized with reduced channel width. Akhtar et. al. (2009) carried out channel geometry optimization for parallel flow field with the major interest in water droplet kinetics and transport. For three different channel depths of 1.5, 1.0 and 0.6 mm, lower channel depth was found to be advantageous for the better cell performance. Considering 1mm droplet filling in channel length for condensate removal as well as pressure drop analyses, the optimal rectangular channel shape with channel width of 1mm and rib width 0.5mm were found to be superior to other considered channel geometries.

Numerical simulation was employed to modify existing bio-inspired flow field by adding gate in each number of channel by Peitzmeier et. al. (2010). The two types of bio-inspired flow field pattern with leaf and lung type flow field's gate height were calculated by an analytic model, which were analyzed for flow field's velocity distribution considering Gate and without Gate. The results from this study predicted that the addition of gate in the bio-inspired flow field pattern improves the cell performance. Zeroual et. al. (2012) developed two dimensional numerical model considering fluid flow as laminar, unsteady, isothermal and incompressible. Flow fields of the anode and cathode sides were modeled as straight channels. A simulation model was carried out for channel depth effect considering reactants concentration in straight channel, where lower channel depth were preferred from the analyses. Salah et. al. (2012) considered dimensionless pumping efficiency with the channel wettability for water drainage, where the shallower channel found to be superior to deeper channel. Mckahn et. al. (2015) investigated the effect of channel depth on the cell performance. The observation showed that the anode channel depth is less significant than cathode channel depth for the cell performance. The recommended channel depth for anode and cathode were 0.46mm and 0.81 mm respectively. Chang et. al. (2015) experimentally carried out different channel depth of 200, 400 and 600 μm effect for parallel serpentine and 3-serpentine flow fields. It was found that 400μm was superior to other channel depth for the cell performance. Xing et. al. (2016) analyzed channel geometry with multiple outlet and different channel depth for the improved water removal attempt, which asserted better current density resulted from the shallowest channel depth.

Berning et. al. (2003) optimized channel width to land width ratio for channel geometry via 3-D single phase numerical model. Between the three selected channel/land width ratio of 0.8/1.2, 1.0/1.0 and 1.2/0.8, the optimum channel to rib width found to be 1.2/0.8. Shimpalee et. al. (2007) dealt with channel dimension (channel to rib width ratio) parameters for 26- parallel serpentine flow field. Based on the current density and membrane water content as well as temperature distribution, the optimal ratio of channel width to rib width was found as 1.0/0.7 which had superiority over 0.7/1.0 and 0.9/0.9. It was also stressed that the effect of channel/rib width was less sensitive than the effect of channel path length. Hseih et. al. (2007) investigated different channel width to rib width ratio while keeping the same dimension of channel width. Optimal channel to rib width ratio was 0.67 within the range of 0.5-2.0, considering pressure drop for computing power gain/power consumption of the cell. Akbari et. al. (2008) explored that increase in channel width while total channel and rib width kept constant, yields a better cell performance and improve the ‘concentration loss’ region. Al-Baghdadi et. al. (2007) also reached to the same conclusion from the straight cathode channel geometry optimization study as concluding that wider channel width increase current density as well as oxygen molar mass fraction while narrow rib width results in an increase of ohmic loss by increasing contact resistance between bipolar plate and gas diffusion layer. Yu et. al. (2009) addressed interdigitated flow field pattern with different rib width considering mass transport phenomena. It was indicated that the decrease in rib width has a little influence on the improvement of cell performance due to the phenomena of forced convection gas transfer mechanism in the interdigitated flow field.

Higier et. al. (2010) explored in-situ measurements of local current density for the channel to rib width optimization. They suggested wider rib width for higher voltage operation or small channel dimensions would be preferable for better cell performance. Goebel et. al. (2011) carried out rib width with channel span effect on PEM fuel cell performance. At higher voltages and dryer conditions, larger land fraction of flow fields performed better than smaller land fraction for equivalent land width as the contact resistance becomes more important than mass transport resistance although these differences were small. But for the higher current density, land width found to be dominant factor. For better PEM fuel cell performance, reduced land width with a 50% recommended rib fraction for low contact resistance as well as narrow channel width were recommended.

Liu et. al. (2013) numerically investigated channel and rib width as well as rib ratio for the optimal channel design. It was predicted that with the increase of total channel width for fixed rib ratio power density decreased and for fixed total width with the increases of rib ratio power density also decreased. Muthukumar et. al. (2014) numerically analyzed different channel to rib width with fixed ratio. The results suggested narrow channel dimension for better cell performance without the consideration of the channel pressure drop.

Liu et. al. (2005) found out that by reducing the outlet channel cross-sectional area compared to the inlet section in the interdigitated flow field for cathode, can increase oxygen mass transport and water removal rate hence increasing the current density in the outlet section compared to the base model. Cheng et. al. (2007) optimized channel width, depth and gas diffusion layer thickness from a selected dimensions of these parameters, the search model reach to an optimal design of channel width and depth of 0.39 and 1.2 mm respectively resulting an increase of 32% power density from the selected model. Wang et. al. (2008) carried out flow field channel design optimization for parallel and interdigitated flow fields. In this study, the channel aspect ratio and cross-sectional area effect were analyzed for better cell performance. Though there were little difference for aspect ratio variation in interdigitated flow field pattern but a significant change was observed for parallel flow field pattern. The optimal aspect ratio of 1.0 and cross-sectional area of 1.0mm * 1.0mm were determined for the flow fields active area of 23mm*23mm in this study. For single and triple serpentine flow fields, different channel aspect ratio effects were studied by Wang et. al. (2009). The cell performance increases with the decreasing channel aspect ratio for single serpentine although channel aspect ratio have little effect on single serpentine. For triple serpentine, the channel aspect ratio has significant impact on cell performance where the cell performance improved with the decreasing channel aspect ratio. The sub-rib convection improved as the channel aspect ratio decreases for single serpentine flow field. The sub-rib convection was much higher for single serpentine flow than the triple serpentine flow cells and while there was significant effect on triple serpentine.

Maharudrayya et. al. (2004) numerically explored channel aspect ratio, curvature ratio as well as upstream and downstream channel band. The numerical model predicted that increase in numbers of parallel serpentine channels have better performance. Wang et. al. (2010) observed the effect of different channel width in serpentine flow field. The analysis showed that the pressure drop increases with the decreasing channel size. Neglecting pump work, the study suggested for a small channel cross-sectional area for better cell performance. Manso et. al. (2011) explained that for lower channel aspect ratio, local current density becomes non-uniform whereas increase in channel aspect ratio i.e. (channel depth/width), the cell performance increased. Kreesaeng et. al. (2015) dealt with the effect of channel aspect ratio and cross-sectional area of cathode channel geometry for open cathode PEMFC, where it indicated that increasing cross-sectional area results in mal-distribution of oxygen mass transport while increase in aspect ratio improves oxygen mass transport.

Peng et. al. (2008) developed metallic bipolar plate design considering hydro-formability and reaction efficiency for which the recommended optimal channel design of channel depth, channel width, rib width and transition radius were 0.5, 1.0, 1.6 and 0.5 mm, respectively with the highest reaction efficiency (79%) and the acceptable formability (1.0). Chen et. al. (2009) had done experimental study for serpentine micro-channel's bend angle and channel to rib width effect on cell performance. The channel bend angle of 60-120 was found to be superior to those of 90-90 and 30-150 channel bend angle. Also channel to rib width ratio of 0.7/0.5 was proven to be better than 0.8/0.4 and 0.5/0.1 cases. Siefert et. al. (2011) experimentally and numerically investigated parallel flow field pattern's micro-channel effect considering mean voltage loss and amplitude of voltage fluctuation under constant current operation. The objective of this study was to establish channel plurality as a flow field design parameter i.e. to find the optimal number in an active area of a flow field pattern based on the analytical function of air flow rate stoichiometric ratio in relation with channel plurality. Bachman et. al. (2012) experimentally studied channel length effect on parallel flow field with fixed stoichiometry where it explored that longer channel length have better stable cell performance while the case is opposite for interdigitated flow field (Santamaria et. al. 2013).

Besides the channel driven parameters (depth, width and rib), channel shape also play a vital role for the effective channel design. Among the studied channel shape in the literatures are rectangular, semi-circular, trapezoidal, wavy, slanted, tapered or contracted channel etc. Researchers optimized channel shape with different geometric parameters considering water removal characteristics, pumping efficiency, gas diffusion and pressure drop analysis hence impact on overall cell performance.

Jaruwasupant et. al. (2011) analyzed the channel bending curvature effect on PEM fuel cell performance. The type of curvature analyzed in this study were sharp curve, inner radius curve, outer radius curve and smooth curve. The flow characteristics, pressure drop and velocity distribution analysis were carried out for the different types of channel curvature. Comparing between the different channel's curvatures, sharp curve was preferred considering higher chemical reaction in the region due to high pressure drop and non-uniform velocity distribution. They also investigated the effect of different channel depth. It showed that among the different channel depth of 0.8, 1.0 and 1.2 mm, 0.8 mm depth channel had velocity approximate 7.5 m/s and pressure drop of 19,470 Pa. For 1.0 and 1.2 mm depth channel have velocities approximate 6 and 5.5 m/s and pressure drop of 12,380 and 9,410 Pa, respectively. For serpentine flow field various channel bend size were numerically investigated by Rostami et. al. (2016), considering pressure drop and temperature distribution in flow field. It showed that among the different channel bend size of 0.8, 1.0 and 1.2 mm, the later one have comparatively suitable for low pressure drop and better temperature distribution although the molar concentration of oxygen was less in this case than those for other two case.

Owejan et. al. (2007) analyzed the effect of channel cross-sectional by neutron radiography method and found that triangular cross-section channels found to be retained less water than the rectangular cross-section. Sun et. al. (2006) explored the flow cross-over through gas diffusion layer and pressure drop for the channel with trapezoid cross section. The ratio of trapezoidal channel widths were optimized with Reynold's number effect. It concluded as the larger the ratio is, the more the flow cross over it is. Kumar et. al. (2003) dealt with channel design parameters on an account of reactant consumption in flow field for single serpentine. The study predicted that the optimum channel width, depth and rib dimension should 1.5, 1.5 and 0.5 mm respectively for maximum reactant consumption. They also studied different type of channel cross-sectional shapes. The cross-sectional shape of conventional rectangular, triangular and hemispherical shape were comparatively analyzed on the basis of reactants consumption in anode flow field. It was found that channel cross-section of hemisphere found to be superior over triangular and rectangular cross-section. Kuo et. al (2008) also numerically investigated different types of wavy, trapezoidal and ladder shape flow channel which were then compared with conventional rectangular type straight channel. The study presented significant improvement in convective heat transfer and gas flow velocity which enhances improved catalyst reaction performances for wave, trapezoid and ladder shape flow channels compared to the conventional straight channel.

Lu et. al. (2011) examined the flow pattern map, pressure drop and flow distribution for parallel flow field considering two phase flow. The numerical analysis presented that sinusoidal flow channel geometry was shown to be better than trapezoid and rectangular shape where the latter two have almost same performance. Wang et. al. (2012) carried out comparative study between the rectangular, triangular, trapezoidal and semicircular channels with a purpose to explore liquid water removal and oxygen utilization efficiency. The cell performance was predicted triangle channel as the best option, followed by the semicircular, trapezoidal, and the rectangular channel. However, rectangular channel was proven to require the lowest pumping efficiency than the other types of channel cross-section. Salah et. al. (2012) explored water droplet behavior for three different channel shape geometries of rectangular, trapezoidal and triangular considering hydrophobic and hydrophilic conditions. The analyses suggested that with the account of dimensionless pumping efficiency, rectangular channel shape geometry is preferable with 1.0 mm channel width and 0.5 mm channel depth for PEM fuel cell performance. Lorenzini-Gutierrez et al. (2015) numerically investigated channels' water removal characteristics for four alternative designs, corresponding to trapezoidal cross-sections with open angles of 40 (T40), 50 (T50), 60 (T60) and semicircular (SC) cross-section and further compared with conventional rectangular channel cross-section. From the channel surface wettability analysis, it was observed that water was retained in the lower corner of the trapezoid channels while single film formed in continuous curved top wall of the semicircular channel, whereas rectangular channel had two films of water formation. For the mean two phase pressure drop and water content in channel control volume analysis, trapezoid with open angle 60 predicted to be the best suitable channel for PEM fuel cell performance.

Kuo et. al. (2007) presented two-dimensional computational model for conventional straight channel and wavy shape flow channel considering both with buoyancy and without buoyancy effect for different inlet velocity for anode and cathode. Compared to the conventional straight gas flow channel, the wave-like gas flow channel leads to an increase in the output voltage and improves the maximum power density by approximately 39.5%. Velocity found to be higher in the wave-like channel than in the straight channel because the constricted channel area above each crest in the wave-like channel surface generates a nozzle-type effect which accelerates the flow. Kuo et. al. (2008) focused on the forced convection effect in the cathode channel where the numerical model presented a better cell performance with uniform distribution of temperature with increasing gas velocity as well as improved convective heat transfer for wavy shape channel compared with the conventional straight channel. Heidary et. al. (2012) studied wavy shape channel of different amplitude and wave number with the account of Reynolds number. It was observed that there can be an increase of heat convective transfer with the increasing of wavy shape amplitude in the channel. Han et. al. (2014) analyzed three different types of wavy shape flow channel which were then compared with conventional straight channel by validated numerical model. The study asserted that for reducing or delaying reactant concentration loss in the cathode flow channel, wavy shape flow channel performs better than conventional channel. Three different wavy shape channel were studied by means of variation in the wave length. The maximum performance achieved at the wave length of 4 mm. Compared with the conventional one, wavy shape flow channel for cathode improve cell performance by approximately 5%. The velocity and reactant concentration in the channel were better than the conventional one although the differential pressure were much higher in the wavy shape channel. Ashorynejad et. al. (2016) stated that pulsating pressure increases the convective species transport to the reaction sites by means of wavy shape channel in cathode and enhances cell performance just about 5%. In another study, he (2016) concluded that wavy shape channel had very slight improvement in cell performance sacrificing three times more pressure drop than straight channel made it impractical for PEM fuel cell application.

Gurau et. al. (2003) suggested in his patent invention that the fluid flow removal from outlet section can be done by reducing the dimensions of the outlet cross-section. This can be performed by varying channel width or depth of the designed flow field pattern like spiral or interdigitated. Further he explained that this effect can also enhance PEM fuel cell performance. Tapered shape flow channel for cathode side was introduced by Liu et. al. (2006) and found to have an imperative impact on the mass transport with high cell performance and pressure drop. When the pressure loss is taken into account for tapered channel, Yan et. al. (2006) recommended taper height ratio of 0.5 and taper width ratio of 1.8 in his numerical study. Three dimensional isothermal numerical model for single straight channel with varying width, depth were investigated by Kenan et. al. (2011). The converging and diverging channel effect had better current density than the straight channel of uniform depth and width, for low volume and short channel length while predicted for large channel diverging effect was not suitable. Mancusi et. al. (2014) numerically analyzed taper channel for effective water removal in PEM fuel cell. Three different tapering angles were introduced for this study, which are 0, 0.5 and 0.75º. It concluded that the velocity in channel as well as reactant concentration increased with the increase in tapering angle. The same results were observed for the water removal case.

Wawdee et. al. (2015) developed two different approach for modified rib design of down-slanted and up-slanted channel, which were experimentally investigated with the account of water flooding and water removal analyses. The down-slanted channel were preferred than up-slanted due to its better water removal capability.

2.2 Flow Field Pattern

Flow field pattern is equally important like channel geometry. The Proton Exchange Membrane fuel cell has flow-fields which are basically a set of micro channels having geometric dimensions of channel depth, width, land/rib, length, and shape with instinctive flow field pattern. This flow field is responsible for carrying the reactant gases from the inlet manifold to the catalyst layer and then to the electrode where the reaction actually takes place. Therefore, the flow field is an important structural feature of a PEM fuel cell and there have been abundant research carried and it's ongoing. Different flow field patterns have their unique features and its effect on reactant gas delivery, flow distribution, water removal characteristics as well as associated pressure drop have been studied in detail.

Most common flow field patterns found in the literature are serpentine flow field pattern, parallel flow field pattern, interdigitated flow field pattern, pin flow field pattern, spiral flow field pattern, radial flow field pattern and bio-inspired flow field pattern etc. In this section, different flow field pattern's effect on PEM fuel cell performance are analyzed. Both the experimental and numerical studies are taken into consideration for the distinct parametric analyses.

Owejan et. al. (2007) established an optimization model which has 75% of flow channel area of the total area having similarity with bio-inspired flow field pattern. The valid numerical analysis showed the cathode pressure drop for parallel, optimized bio-inspired, and multiple serpentine. For the cell performance, the chronological order was as bio, serpentine and parallel flow field pattern. Different types of micro-channel for hydrogen gas flow were numerically investigated by Choi et. al. (2009). Through the optimization of micro channels, it was reported that flow characteristics like velocity, uniformity and flow rate are highly depended on the channel shape. A 3D numerical model was employed by Jang et. al. (2008) for the analyses of parallel, Z-type and serpentine flow fields performance. The simulation results revealed that serpentine is better than Z-type and parallel, and the later one exhibited worst performance. However, serpentine flow field was found to be superior in terms of oxygen mass transport, velocity and water removal characteristics at the expense of high pressure drop.

Interdigitated, serpentine, parallel and mesh flow fields were investigated by Hsieh et. al. (2008) for transient local current density distribution and liquid water accumulation for certain time period. It was found more uniform and highest current density existed in interdigitated flow field followed by serpentine, parallel and mesh types. However, interdigitated flow field had a high water accumulation relative to other flow fields. For water accumulation analyses in parallel and interdigitated flow fields were numerically performed by Wang et. al. (2008) with different level of RH% for the anode and cathode. The predicted results showed that for the parallel flow field design, the maximum liquid water concentrations occur at the center of the ribs with the minimums at the center of the flow channels; while for the interdigitated flow field design, the maximum liquid water concentrations occur at the outlet flow channels with the minimums at the inlet flow channels.

Hsieh et. al. (2009) conducted pressure drop measurements for different flow fields on the cathode side under various mass flow rates and temperatures on the basis of water accumulation. The analyses presented that pressure drop is the highest for interdigitated flow field followed by serpentine, parallel and mesh types. Lopez et. al. (2009) experimentally investigated water formation, condensation and pressure drop by the flow visualization and image analysis for parallel-serpentine and cascade flow fields. The study concluded that the fluctuation in pressure drop is related to the transient process being inherent to the water formation in the cathode gas flow channel.

Four different types of flow fields were manufactured by MEMS technology by Lu et. al. (2010) for an experimental study of micro PEM fuel. The results indicated that mixed type of serpentine-parallel combination had less pressure drop with better cell performance. Arbabi et. al. (2012) adapted Navier-Stokes equation into two dimensional numerical model for a comparative analysis between conventional flow field patterns. It was found out that total pressure drop in bio-inspired is the lowest, followed by the parallel, 3-serpentine, 1-serpentine. The same order was also obtained for the case of pressure uniformity in the channels of each flow field patterns. Up to 8% performance improvement was reported for bio-inspired flow field pattern than the conventional flow field patterns. Thomas et. al. (2016) designed a flow field with the combination of serpentine-parallel and pin type for open cathode HTPEM fuel cell. This flow field outperformed the parallel-serpentine flow field in both cell performance and pressure drop.

Pressure drop and flow rate were parametrically analyzed for single serpentine, parallel and interdigitated flow fields by Karvelas et. al. (2016). The study also modified these flow fields by smoothing the channel sharp curve which results in relatively low pressure drop and better flow distribution along the channel sections. Especially in case of the serpentine flow field, the smoothing resulted in significant pressure drop. Interdigitated and parallel flow fields were numerically investigated by Santamaria et. al. (2013) for the cold-start performance under 0.2 and 0.4 A/cm^2 using a galvano-static control for the cell environment. Both flow fields became unstable at -6 ºC and cause cell failure at -8 ºC. Under sub-zero condition, the interdigitated flow field was predicted to be the better option than the parallel due to its enhanced water removal capability.

Hwang et. al. (2006) explored the temperature distribution effect on the mass transport and cell performance for parallel and interdigitated flow fields. Cano-Andrade et. al. (2010) numerically investigated the radial flow field for an active area of 10.54 cm^2 with different numbers of channel having 4, 8 and 12 channels. Low pressure drop, more uniform flow and current density distribution hence a better cell performance were reported with the decreasing of the number of channel. Hseih et. al. (2011) concluded that temperature had very low impact on pressure drop for different flow fields of interdigitated, serpentine, parallel and mesh types. Taccani et. al. (2011) numerically investigated 5-serpentine, 4-serpentine and parallel flow fields. The former was found to be superior than 4-serpentine while parallel flow field showed the lowest cell performance. Hashemi et. al. (2012) explored that current density and temperature distribution were much more uniform in serpentine flow field compared to the parallel flow field. Lee et. al. (2013) numerically investigated different flow field patterns of single serpentine, parallel, interdigited and pin type flow fields by keeping an identical active area and operating conditions considering the mass transfer and electrochemical reaction. Single serpentine flow field pattern showed the best performance while interdigitated flow field pattern was almost similar to that of single serpentine and pin flow field being next in line after interdigitated flow field performance. However, parallel flow field pattern showed the worst mass transfer characteristics due to flooding and drying of the membrane caused by uneven flow circulation. The study also presented a quantitative comparison among flow field patterns for the anode and cathode pressure drop, from which it was explored that when the average local current density increases, the anode pressure drop decreases and the cathode pressure drop increases resulting from the internal products of the channel that disturb the flow of the reactants.

A 3D isothermal model of $5cm^2$ active area for two common flow field patterns of serpentine and interdigitated were numerically analyzed on the basis of current distribution by Paulino et. al. (2013). In the serpentine pattern, current generation was concentrated near the gas entrance, while in the interdigitated pattern, current densities were more distributed over the cell area. However the overall cell performance were found to be almost same. In the experimental study by Sreenivasulu et. al. (2013), serpentine and interdigitated flow field patterns were analyzed considering both with and without the anode back pressure. For both cases, 4-serpentine was found to be superior to interdigitated flow field. Flow field patterns of parallel, pin, serpentine, spiral and interdigitated were experimentally carried out by Liu et. al. (2014) for comparative performance analysis. The study demonstrated that serpentine has the best power output of $0.158\ w/cm^2$, which was almost two times higher than the worst case spiral, while rest in order of pin, parallel and interdigitated in ascending order. Also comparison between the different types of serpentine flow field patterns, the symmetric serpentine was the best followed by the 1-serpentine, 2-serpentine and 4-serpentine. A 3-D numerical analysis was carried out for different flow field patterns of conventional serpentine, pin type flow channel with the adoption of porous carbon inserts in uniform and zigzag pattern by Pal et. al. (2015) to minimize cathode side water flooding. Zigzag pin flow field pattern had 2.98% higher cell performance than the uniform pin type and both the pin type flow field patterns had better performance than conventional serpentine but for water management the cases are in opposite order.

Shimpalee et. al. (2006) addressed the effect of channel length on the distribution of current, temperature and electrochemical variables for a commercial size of $200\ cm^2$ serpentine flow field pattern. The analysis showed that the pressure drop and water content increase with the increasing of channel path length. However, 13-parallel serpentine flow field gave a slight advantage over the 26-parallel serpentine flow field due mostly to small differences in the membrane hydration. Jeon et. al. (2008) numerically analyzed flow field pattern comparative study for serpentine flow field patterns of 1-serpentine, 2- serpentine, cyclic- serpentine and symmetric- serpentine. The study considered for high and low humid conditions to explore current density distribution. For high humidity case, double serpentine found to be superior, but there is almost no difference for low humid condition between the serpentine patterns. A three dimensional numerical model was developed by Wang et. al. (2008) for different flow channel design parameters of serpentine, considering local oxygen mass flow rate and liquid water distribution. This study investigated serpentine flow field pattern for the number of channel bends with 7, 11 and 15. The simulation results showed that with the increasing number of channel bend, the limiting current density and cell output power increased. Besides, three different type of 1-serpentine, 2-serpentine and 3-serpentine were compared which showed single serpentine pattern had superiority over 2-serpentine and 3-serpentine. Jaruwasupant et. al. (2011) analyzed number of parallel serpentine channel on the cell performance for 100 cm^2 active channel area. The study considered 1-serpentine, 2-serpentine, 3-serpentine, 4-serpentine, 5-serpentine and 6-serpentine patterns for pressure drop as well as velocity distribution analyses. Based on the numerical analysis, it was found that 6-SFFP has a better cell performance than the other parallel serpentine.

Barreras et. al. (2008) developed three different flow field patterns of diagonal, serpentine and cascade designs and presented a numerical comparative study. Also to observe the flow field characteristics laser induced fluorescence (LIF) trace tracking technique was employed for a mixture of glycerin/water with 49.6% of glycerin and 51.4% of water. From the numerical simulation results based on pressure and velocity distribution, it was observed that diagonal flow field yields a non-uniform flow distribution for both pressure and velocity whereas serpentine flow field provides uniform flow but with a higher pressure drop. The cascade flow field pattern, on the other hand, showed a homogenous flow distribution together with uniform pressure field through the entire flow field. Belchor et. al. (2012) experimentally analyzed serpentine with baffle-serpentine flow field pattern for different cell temperature as well as humid condition of reactants for both anode and cathode. For the no humidification case in cathode, baffle type serpentine exhibited better cell performance than conventional serpentine by retaining water in baffle channel. Meanwhile for the anode case, both with and without gas humidification, conventional serpentine was found to be better than baffle type serpentine. Thitakamol et. al. (2011) investigated interdigitated flow field comparison with the modified mid-baffle interdigitated flow field design considering different cathode stoichiometry for both air and oxygen as reactant. For oxygen as cathode fuel, the performance of the two flow fields are almost similar while for air as cathode fuel, mid-baffle interdigitated flow field outperformed the conventional one due to its more effectiveness for water removal characteristics with the less pressure drop situation. Chen et. al. (2011) analyzed different flow field designs of parallel and serpentine with segmented combination modeling of flow fields. For both co-flow and counter flow comparison, counter flow being more suitable and the newly developed flow field had a better cell performance for low humid condition.

For the improvement of the cell performance, an optimized switching option between parallel-interdigitated flow fields was developed by Santamaria et. al. (2013) facilitating the advantages of the two flow fields by external hardware mechanism. Ku et. al. (2013) developed a modified interdigitated flow field by placing rectangular parallelepiped in varied number through the inlet and outlet sections for separate analyses. The modified interdigitated flow field having optimal number of rectangular parallelepiped in outlet section was better in cell performance than the other configurations including the base model. Parallel, serpentine and combination of serpentine and parallel flow fields were developed by Vazifeshenas et. al. (2015) and numerically investigated for different performance parameter. Soong et. al. (2005) introduced baffle block channel with varied number of baffle block for enhancing reactant diffusion. However, it costs in a higher pressure drop. Liu et. al. (2005) explored the baffle flow field effect for cathode channel on the PEM fuel cell performance. The study investigated the baffle effect on the numbers of baffle block presence as well as the baffle width in the channel. The simulation results showed that the cell performance was better for the case of without the presence of liquid water. It was also found that with the increase in baffle width and the number of baffle blocks, the cell performance increased. All of the baffle block cases were found to be superior to that of the case without baffle. This study also analyzed the air velocity effect on the baffle blocked cathode channel where numerical simulation showed that with the increase in the air velocity the cell performance increased. The high velocity of the reactant gas reduced the mass transfer over potential, delay the occurrence of the mass transport loss, and then increased the limiting current density considerably. Jang et. al. (2006) developed a two dimensional numerical model of baffle blocked channel both for the anode and cathode. The study suggested for an optimal number of baffle block in channel. It was recommended for an optimal number of baffle in flow channel which can increase relative humidity especially in anode side causing better proton transport, but for the case of cathode, increasing relative humidity resulted in less oxygen concentration. Yan et. al. (2006a, 2006b) concluded from the comparative flow fields study that increasing the number of channel can enhance cell performance and baffle presence in the channel can further increase gas diffusion. Yan et. al. (2006c) also claimed that flow area ratio between 40-50% is preferred than 60% considering the interdigitated flow field analytic study. Different types of baffle-serpentine flow field effect on cell performance were compared with conventional 3-serpentine flow field by Wang et. al. (2007). Considering the mass transport and pressure drop the baffle modified serpentine had a better cell performance than the conventional ones. Perng et. al. (2009) showed that better oxygen mass transport occurred by placing a rectangular cylinder in the cathode channel compared with the straight conventional channel. Perng et. al. (2011) also investigated the effect of tapered flow channel as well as the baffle presence in the tapered flow channel. The presence of baffle in the straight channel caused less fuel concentration while tapering channel with baffle resolved the issue by improving the mass transport and convective heat transfer. Li et. al. (2011) explained transient response behavior of overshoot and undershoot voltage loading variation for local current density in five different flow fields which are parallel, Z-type, serpentine, parallel with baffle, Z-type with baffle flow fields. Among them parallel-baffle showed best characteristics followed by baffle-Z, serpentine, parallel and Z-type. Wu et. al. (2012) introduced cuboid rows in channel path for the optimization of serpentine flow field which resulted in an augmented power of 30% and reduction of 275% pressure drop were reported through Taguchi method numerical analysis. Perng et. al. (2014) designed flow channel by placing rectangular obstacle. It was observed that with the presence of rectangular obstacle, the flow channel becomes narrow which create jet type and tapering effect causing more reactant concentration for catalyst layers compared to the conventional straight channel. The presence of rectangular obstacle in the anode and cathode flow channel also numerically investigated by Bilgili et. al. (2015) and predicted an improved performance. Heidary et. al. (2016) demonstrated three different types of parallel flow field of which one was conventional and rest of the two were modified by placing 3 baffle block in different pattern in each channel. The results indicated that the presence of block in parallel channels is advantageous over the conventional one. Heidary et. al. (2016) demonstrated partially and fully blocked straight channel by means of rectangular block obstacle of varied number of block which was compared with conventional straight channel. With the number of obstacle block increase cell performance as fully blocked channel caused increased reactant diffusion. The study also suggested that the block has no effect on the performance for anode channel.

Ramos-Alvarado et. al. (2011) introduced a 3-D numerical study to investigate the constructal flow field with varying branch and outlets. As the number of branch and outlet increase in this studied flow field, the flow and current distribution increased. Inspite of the very low pressure drop in the developed constructal flow field, its performance was way below than the parallel flow field. Ramos-Alvarado et. al. (2012) also developed different optimized symmetric parallel flow fields with the addition of distributor flow channel. With the account of reactants molar mass concentration and pressure drop, optimized Distributor-D type flow field showed a better cell performance than the serpentine with low pressure drop and less pumping power. Guo et. al. (2013) proposed network based optimized pin flow field having better cell performance characteristics with numerical model. Lorenzini-Gutierrez et. al. (2013) demonstrated optimized radially designed tree shape bifurcation type constructal flow field featuring low pressure drop and improved cell performance than conventional parallel flow field. Although the cell performance was less than conventional serpentine, it can be a preferred flow field for stack design considering its low pressure drop.

Leaf and lung type bio-inspired flow pattern developed by Kloess et. al. (2009), were compared with conventional serpentine and interdigitated flow fields under different operating conditions. The numerical results predicted that bio-inspired flow fields can increase the cell performance by 30%. Roshandel et. al. (2012) explored that bio-inspired flow field pattern was far superior to the conventional parallel and serpentine with an increase of power density of 56% and 26% respectively. Also the weight of bio-inspired flow field pattern was less than conventional parallel and serpentine bipolar plates which reduce the material cost. From the numerical simulation result of the mass and velocity distribution, it was observed that eddy formation occurs in serpentine and parallel flow fields whereas homogenous flow distribution existed throughout the bio-inspired flow field pattern. Chen et. al. (2013) carried out numerical simulation for four different types of bio-inspired flow field and compared them with the standard single serpentine flow field pattern. The bio-inspired flow field patterns were differed from each other by number and location of channel branches by creating secondary branch channel. The study also analyzed the effect of humidity, pressure, temperature and stoichiometry on the performance of the proposed flow field patterns. The optimized bio-inspired flow field had 34.6% better performance on the basis of current density comparing to the conventional serpentine channel. Guo et. al. (2014) investigated bio-inspired flow field patterns using Murray's law branching method for interdigitated and non-interdigitated concepts. This flow fields were compared with conventional series-parallel and interdigitated flow field's performance where the bio-inspired interdigitated flow field has 20-25% better cell performance than the conventional ones. Also the interdigitated bio-inspired was found to be superior to non-interdigitated bio-inspired flow field. Arvay et. al. (2015) numerically investigated several flow field designs considering local current density distribution and pressure drop. The flow fields studied were standard parallel, serpentine, interdigitated and other type of flow fields that were modification of the standard flow fields based on biological inspiration naming Murray-parallel, Murray interdigitated-1, Murray interdigitated-2, Pitchfork–7a, Pitchfork–7b, Pitchfork–7c, Pitchfork–9a and Pitchfork–9b. In these simulation studies, interdigitated designs using a Pitchfork pattern and Murray's branching law have more uniform current density distributions but with an increased pressure drops. It was found that different branching patterns with the same number of total branches had little effect on pressure drop but lead to difference in local current density distribution. Increasing the under rib convection area can decrease pressure drop as long as channel lengths is not increased.

Radial flow field pattern of interdigitated type for the cathode channel was numerically investigated by Fries et. al. (2012), which was compared with conventional parallel and serpentine flow field pattern. It was observed that the radial flow field pattern has a relatively low pressure drop than serpentine and better flow distribution than both parallel and serpentine flow field pattern. Also for the dry condition, the limiting current density of radial flow field pattern found to be nearly same to the SFFP. The unconventional radial flow field having four inlet and outlet for cathode side was developed and later numerically analyzed comparing with conventional serpentine flow field pattern by

Ramin et. al. (2014). From this study, it can be concluded that the radial flow field pattern has a better current density than that of conventional flow field patterns since the removal of water is easier as well as reduced channel length cause better mass penetration, and low pressure drop.

Uniform current density gained from foam type flow field was developed by Birgersson et. al. (2006) and compared with the different conventional flow fields for geometric performance analyses. Tsai et. al. (2012) introduced metal foam with multiple inlets having high porosity and pore size improves the reactant distribution and utilization rate. Different types of porous separator flow fields were proposed by Kariya et. al. (2014), as an alternative to the conventional flow fields with low pressure drop and higher cell performance. Carton et. al. (2016) introduced open pore cellular foam (OPCF) as a new form of flow field which was then compared with conventional double channel. This foam type flow field showed an improved mass transport, reduced water flooding and hence increased the cell performance. Kozakai et. al. (2016) developed biporous and monoporous flow field patterns and experimentally compared with conventional serpentine, straight and grid flow fields scrutinizing on pressure drop and current density. It was concluded that bi-porous flow field has the highest current density with an expense of high pressure drop.

Bullecks et. al. (2011) introduced cylindrical flow field which were found to be better comparing to the planar flow field design in the higher potential region. The results indicated that the concentration loss is lower under higher volumetric and gravimetric power density in cylindrical cell than the planar cell. Sierra et. al. (2014) demonstrated tubular type parallel, interdigitated and serpentine flow fields with an aim to observe transport phenomena and cell performance when comparing with the conventional planar type of the same flow fields. The numerical analysis revealed that the pressure drop can be reduced in tubular than planar type bipolar flow fields by introducing uniform mass transport in tubular cell. Water concentration prevailed more in interdigitated followed by parallel and serpentine tubular flow fields. Tubular shape serpentine has more homogenous current distribution due to the angular and twisted flow path lead to uniform mass transport and less pressure drop effect. Lin et. al. (2010) numerically optimized the single serpentine flow field with different channel width and depth on the basis of the maximum local current density. The simulated model was three dimensional, two phase and non-isothermal. The optimal design predicted that the flow channels 1, 3, and 4 are tapered in the flow direction, while channels 2 and 5 being divergent in the flow direction. Compared with the conventional serpentine flow field pattern, the optimized model of serpentine flow field pattern had 22.5% better performance. The same type of study carried out by Wang et. al. (2009).

Chowdhury et. al. (2017) developed convergent and divergent serpentine flow fields which were experimentally investigated and later compared with conventional serpentine flow field pattern. Both convergent and divergent serpentine flow fields were found to be better than the conventional serpentine flow fields of 1 mm and 2 mm uniform depth. The optimized flow field had 19 and 27% better cell performance compared to the conventional serpentine flow fields of 1mm and 2mm uniform depth respectively. Moreover, the water management was found to be better in the newly developed flow fields.

Li et. al. (2005), in their review analysis of bipolar flow field designs, briefly discussed the different parameters of flow field channel design parameter like channel width, rib width, channel depth, channel cross-sectional area as well as cross-section of the channel. Different types of flow field patterns such as serpentine, interdigitated, parallel, integrated and pin types with their modification were also included in the study. The review study by Manso et. al. (2012) about different flow field patterns suggested that the serpentine and interdigitated flow field pattern are suitable if homogenous flow distribution and suitable pressure drop can be achieved. Aiyejina et. al. (2012), in the detail concurrent review research, recommended serpentine flow field with small rib and channel size. Under specific conditions, serpentine flow field having 0.5 mm rib and channel size outperformed other common designs, such as parallel, interdigitated, and Z-type flow fields and could be further improved by utilizing channels of varying depth.

Considering the quality, quantitative and most highlighted literature review studies, serpentine flow field could be most suitable flow field pattern with rectangular shape channel geometry due to their improved mass transport, water management, uniform flow distribution and low pumping efficiency. Based on this conclusion, this study is concentrated further improvement of flow field optimization with both experimental and numerical optimization approach.

CHAPTER III

EXPERIMENTAL STUDY

In this chapter, the experimental setup and different technique employed for experimental study are presented in detail. For this thesis, first the experimental study was carried out by developing new experimental setup. The main purpose of the experimental study was to develop new flow field design and use the experimental results to validate the mathematical model development for detailed numerical analyses to further optimize the flow field. Rather than to develop new flow field pattern, this study was concentrated to improve conventional flow field. Serpentine is one of the widely used flow field pattern for commercial, industrial and academic research. That's why serpentine flow field pattern was selected for the experimental study. So the modification with effective design can further improve the serpentine flow field. For the improvement of the serpentine flow field, the first approach was employed by studying literature research articles for detail understanding of the serpentine pattern. After detailed review, the pros and cons were identified. One of the major problem of the serpentine flow field pattern is having low reactants diffusion in the long channel's outlet section due to the lack of molar concentration which occurs for high pressure drop at that outlet section. Another common and most critical issue for PEM fuel cell is to design effective flow field providing better water removal characteristics and management. Serpentine flow field is one of the better existing flow pattern which is superior to other conventional flow field for its effective water management although there are still demands for more improved water management system. To make a further improvement of serpentine flow field pattern, the novel convergent and divergent serpentine flow field patterns were proposed and postulated to be an improvement factor to resolve the disadvantages possessed by conventional serpentine flow field pattern. The modified design concept proposed in this study is based on increasing or decreasing the flow channel depth with an inclination from inlet to outlet by creating convergent and divergent flow field pattern. Then these conceptual bipolar plate flow fields were designed and manufactured. To understand the effectiveness of the newly developed flow fields, their performances were compared with conventional flow fields by experimental approach.

3.1 Materials and Methods

3.1.1 Design and manufacturing process

For the experimental study, an active channel area of 4.7 cm^2 was considered for all flow field designs. The dimension of the graphite bipolar plates were 40mm*40mm* 5mm. All the single serpentine flow field patterns had 9 total number of internal flow channel with a fixed channel width of 1.5 mm, rib/land width of 1 mm along with the total channel length of 206 mm from inlet to the outlet section. Channel depth was the only geometric parameter of flow field design which was varied for different developed flow fields. The details of the single test cell are provided in Table 3.1. Stainless steel end plates were used for better compression and gold plated copper current collector were used for improved current conductivity.

Table 3.1. Description of test cell

Flow Field Pattern	Single Serpentine
BP Material	Graphite
BP Dimension	40 mm*40 mm* 5 mm
Number of turns in flow channel	8
Number of Flow Channels	9
Number of Ribs	8
Total Channel Length	206 mm
Active Area	4.73 cm^2
Channel Width	1.5 mm
Rib (Land) Width	1 mm
Current Collector Material	Gold plated copper
Current Collector Thickness	3 mm
End Plate Material	Stainless steel
End Plate Dimension	60 mm * 60 mm * 10 mm
Number of Assembly Bolt	8

Total six sets of single serpentine flow fields shown in Photo 3.1, were manufactured for anode and cathode by CNC machine with ArtCam machine generating code program. The designs were created in Solidworks where six of the designed flow fields were mirrored to ensure co-flow experiment of same geometry configuration for both the anode and cathode. Among the six flow field set for the anode and cathode, two of them are conventional serpentine flow fields of 1mm and 2mm channel depth. The other four are convergent flow fields, and these are divergent flow fields as well, which can be understand easily from the depicted in Figure 3.1, where both convergent and divergent flow fields of same set (anode and cathode) have same geometry. The difference between convergent and divergent flow field patterns of same set bipolar plate are only inlet and outlet positions. If the channel depth reduces from inlet to outlet then the flow field is defined as convergent and vice versa, it is divergent. For all of the experiments, anode and cathode have same geometry for different types of flow field analyses. For example if C1 flow field design is used for anode, the same C1 is also used for cathode. All of the flow fields are being defined by its specific name for this study for better explanation and understanding, as shown in Table 3.2.

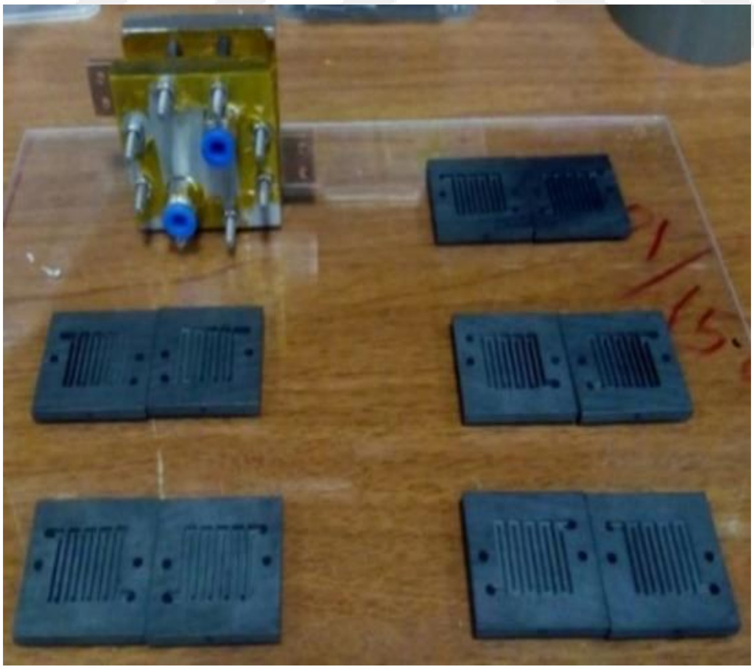

Photos 3.1. Bipolar plates with an assembled fuel cell

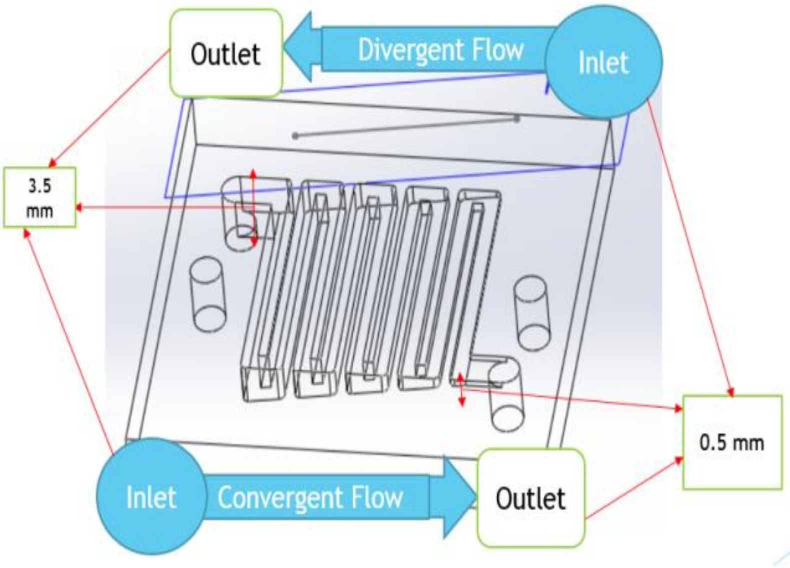

Figure 3.1. Schematic of convergent-divergent serpentine flow field concept

Table 3.2. Definition of flow field patterns

Flow Field Channels Defined Name [C= convergent, D= divergent, S = constant depth]	Channel Depth (mm)	
	Inlet	Outlet
S1	1	1
S2	2	2
C1	1.5	0.5
C2	2.5	1.5
C3	3	1
C4	3.5	0.5
D1	0.5	1.5
D2	1.5	2.5
D3	1	3
D4	0.5	3.5

3.1.2 Membrane electrode assembly

Five layer MEA integrated with gas diffusion layer were used in the experiments. MEAs were produced by hot pressed mechanism with the five layer component of gas diffusion layer and catalyst layer for both the anode and cathode along with the polymer membrane. MEA activation procedure was carried out in the same manner for all of the MEAs. The properties of the experimented MEA is shown in Table 3.3 and used MEA and Gasket sealant shown in Photo 3.2 in details.

Table 3.3. MEA properties

Membrane Type	Nafion PFSA NR-212
Membrane Thickness	50.8 μm
GDL Type	Carbon cloth
GDL Thickness	410 μm
Anode Catalyst	0.5mg/cm^2
Anode Loading	60 wt% Pt
Cathode Catalyst	0.5mg/cm^2
Cathode Loading	60 wt% Pt
Number of Layer of MEA	5
Fabrication Technique	Hot pressed

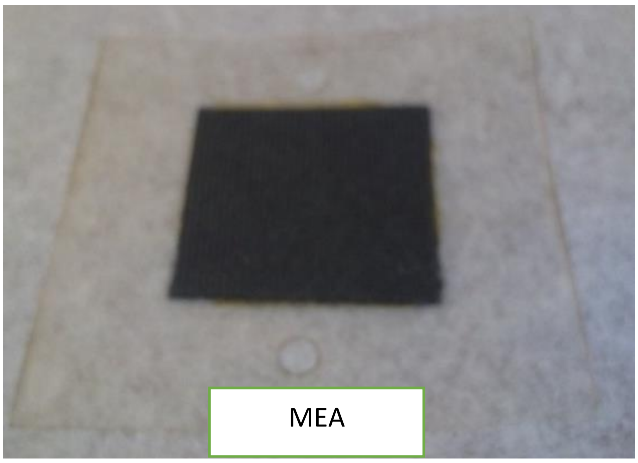

Photo 3.2. MEA used for the experiment

3.1.3 Gasket sealant

Gasket sealant is very important for gas leakage prevention in PEM fuel cell. Two different types of gasket sealant were used for the anode and cathode side. These are Teflon and Fiberglass gaskets shown in Photo 3.3. These gaskets were prepared with required dimensions via laser cutting machine.

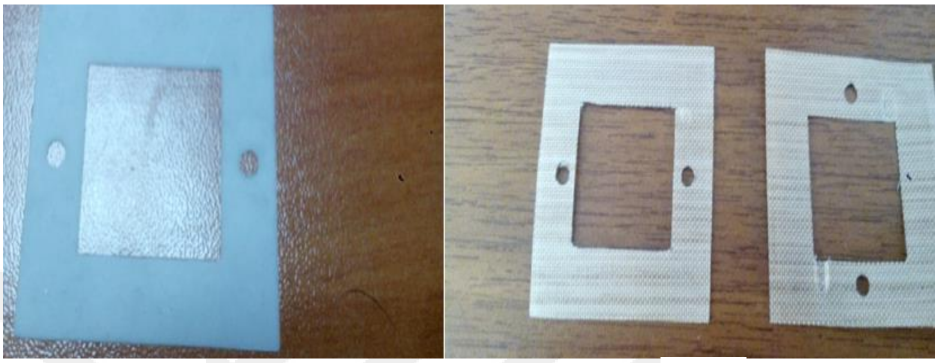

a b

Photo 3.3. Teflon gasket sealant (a) and Fiberglass gasket sealant (b) used for this experiment

3.1.4 Fuel cell assembly procedure

For the electrical insulation between stainless steel end plates and current collector plates, two end plates were electrically insulated by polymer Mylar in the inner side. The Mylar's size were kept same with the end plate dimensions by cutting in laser machine accurately. Two assembly pins were used to assemble the end plates, current collectors, MEA, gasket sealant and bipolar plates. Assembly SS Allen-key bolts were covered by rubber insulator. Total four pieces of polymer pipe inserted between end plate, current collector and bipolar plate instead of the gas sealant O-ring, in the inlet and outlet of the anode and cathode. This new technique ensured no gas leakage between end plate, current collector and bipolar plate. For the fuel cell assembly, 3 N-m tightening torque was applied by a torque wrench for all of the experiment's cell assembly procedure to reduce the effects other than the flow fields. The tightening procedure of the cell's eight bolt in serial is shown in Figure 3.2, for homogenous compression pressure of the cell.

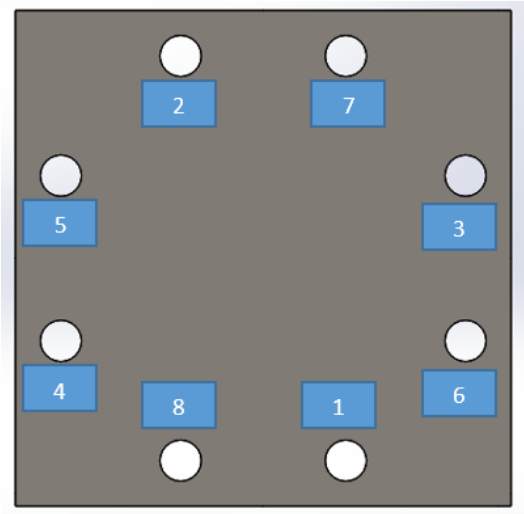

Figure 3.2. Bolt tightening sequence

3.1.5 Experimental setup

The experimental setup was devised in Prof. Dr. T. Nejat Veziroglu Clean Energy Research Center at Nigde Omer Halisdemir University. For this study, standard Arbin Fuel cell test station was used along with other manual setups and equipment required for PEM fuel cell single cell testing. The simple schematic diagram of the experimental setup is shown in Figure 3.3.

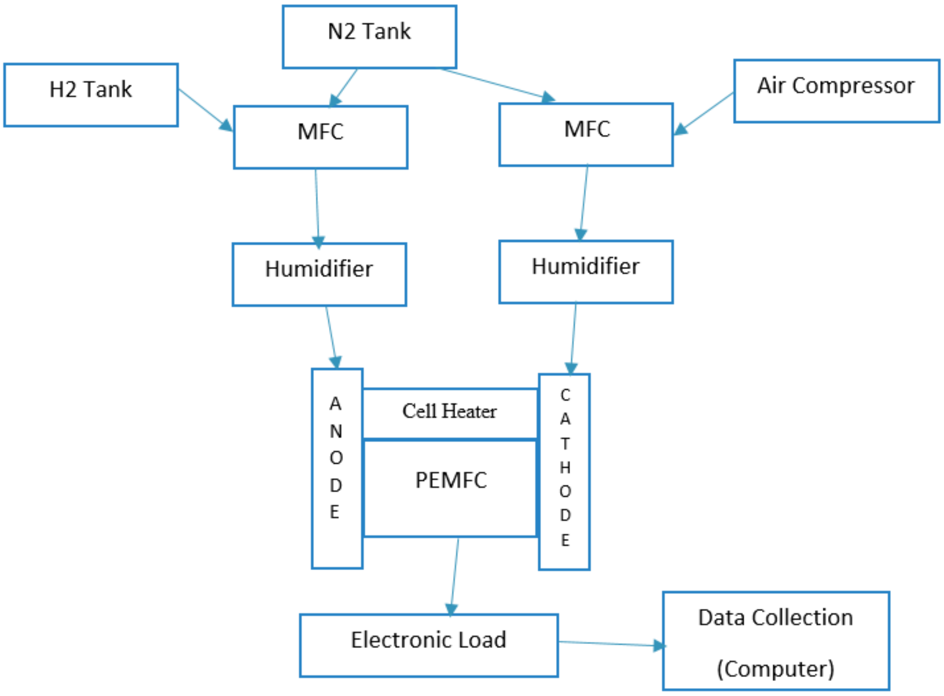

Figure 3.3. Schematic diagram of experimental setup

A thermally insulated box was manufactured by Plexi-glass material shown in Photo 3.4. Fuel cell was placed on a base plate of copper material which was heated by Kapton heater. A temperature controller was used to control the cell temperature inside the box.

a

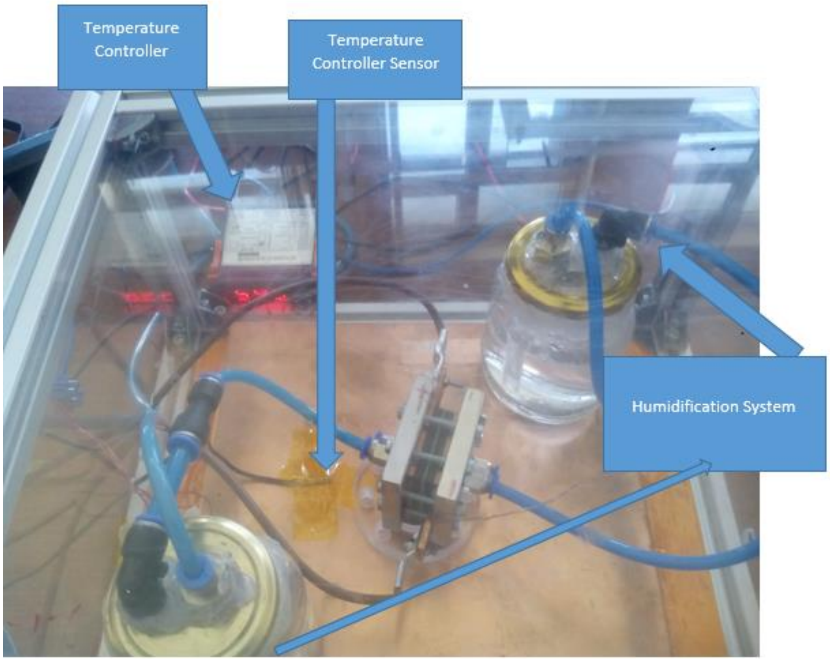

b

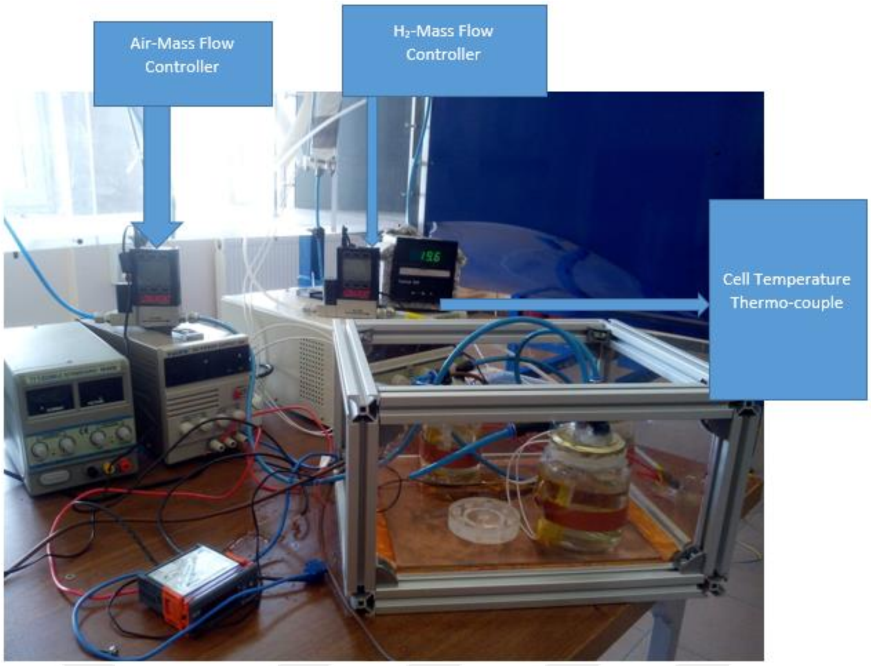

c

d

Photo 3.4. Experimental Setup (a)-(d)

The cell temperature was measured by K-50 type, 6 channel thermocouple of Tactical 306 model. For measuring the cell temperature, each of the bipolar plate was drilled of ϕ1 mm diameter hole in which thermocouple sensors were placed. Hydrogen was supplied from the compressed hydrogen tank and a mass flow controller of ALICAT MC Series was used. Air was supplied from air compressor and a mass flow controller of ALICAT MC Series was used to control air flow rate to the fuel cell cathode side. Two beakers placed in the thermally insulated box were used for hydrogen and air humidification through bubbling process filled with deionized water. A DC Load of BK Precision model of 8514 series was used for testing PEM fuel cell. An IT-E132 isolated communication USB cable was connected to a computer for data collection from the electronic DC load.

3.1.6 Gas leakage prevention technique and test

Gas leakage is a common phenomenon in fuel cell testing. To reduce the gas leakage, high tightening torque applied which sometime cause physical damage of the MEA. Moreover, hydrogen is the lightest gas with molecular size of 2.89 A°, as it can pass through nano-size or even lower space if it finds a path in the flow passage. In the conventional commercial single test model, O-rings are used widely to prevent gas leakage between bipolar plate and current collector. However, this may be a disadvantage for cell tightening torque application. Furthermore, there may be gas leakage through the end plate and current collector. For the prevention of gas leakage between end plates, current collectors and bipolar plates, total 4 numbers of high temperature resistant polymer tube were inserted through the inlet and outlet section by ensuring the proper dimensions matching with inlet and outlet dimension of both anode and cathode side, depicted in Figure 3.4. It is an innovative experimental technique for the single fuel cell test system procedure which has not been described anywhere else. Both soap bubble and water submerging test were carried out to check the gas leakage. The result revealed that the novel technique suggested can fully eliminate the gas leakage even with lower cell tightening torque application. This technique can be a useful measure for future experimental research works and can be further improved by using 3D printing technology.

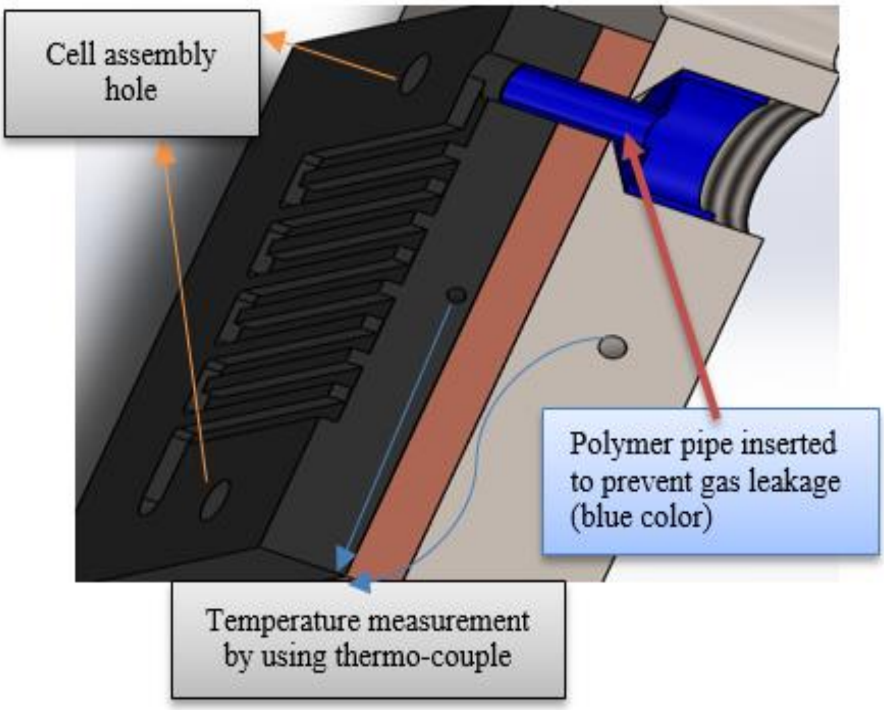

Figure 3.4. Experimental technique to prevent gas leakage between bipolar plate, current collector and end plate for single test cell

3.1.6 MEA activation procedure

MEA activation is very important before starting to take performance data points. It is due to the hot pressed MEA, which first needs to be humidified cautiously with standard procedure, since over humidification can also result in flooding the MEA. First the test cell was initially heated to 70ºC and 100% humidified gases were fed. Then at constant 0.6 V, one hour test was carried out. After that at 0.5V and 0.7V, the test operation were done with 20 minutes sequence for each case three times for a period of two hours. This was followed by a constant current operation of 2 A for 3 hours duration. These process ensured for the proper humidification of MEA for PEM fuel cell testing system.

3.2 Experimental Procedure

After the experimental setup and properly assembly, single cell was tested for gas leakage and then MEA activation was carried out for each MEA. Total 3 MEAs with the same properties were used for this study. For all the flow fields experiment all the same experimental procedure were maintained. The operating conditions of this experimental study kept fixed shown in Table 3.4. The cell temperature kept at 45 ºC, since the best performance was gained at this point for the gases temperature humidification at 30 ºC.

Table 3.4. Operating condition

Cell Temperature	45 ºC
Inlet H_2 Temperature	30 ºC
Inlet Air Temperature	30 ºC
H_2 Flow Rate	0.1 SLPM
Air Flow Rate	0.3 SLPM
Operating Voltage	CV 0.5 V
Flow Type	Co-flow

The performance increased with the increase in flow rates but at excessive higher flow rate flooding occurred which damage MEA. With the context of literature and through several experiments, the suitable mass flow rate for hydrogen and air were fixed at 0.1 slpm and 0.3 slpm. The co-flow arrangements were maintained for all the experiments. After starting the operation, the cells were tested under constant operating conditions for one hour and then the performance data were taken by varying the voltage. The polarization data were collected with 10 mV deviation for a total 90 time steps with 10s delay in each step, resulted to a total 15 minutes experiment for data collection. The same experiment was repeated for three times for each case to obtain more reliable results. There were very little deviations in these experiments which can be neglected.

CHAPTER IV

EXPERIMENTAL RESULTS AND DISCUSSION

In this chapter, the experimental results are analyzed and discussed. The comparative study between the experimented flow field patterns are performed to describe how and why the deviation occurred. The brief conclusions are derived based on the results from the data analyses and experimental observations.

The experimental results from the three different categories of flow field patterns are obtained and compared. These three types of flow field patterns are conventional constant depth flow field pattern, convergent flow field pattern and divergent flow field pattern. The only variable for all the experiments is only the channel depth, which is constant in the uniform channel depth tests or varied from inlet to outlet. Beside these, channel depth gradient is also analyzed for all of the flow fields and compared with zero channel depth gradient for the two constant depth flow fields of 1 mm and 2 mm. Total channel volume in relation with the overall cell performance is also taken into consideration to find an impact factor whether it has any effect on the cell performance. Finally, after all the experiments and observations, the driving parametric influence on the results are discussed.

4.1 Effect of Channel Depth

There were two conventional constant channel depth of 1 mm (S1) and 2 mm (S2) flow fields used for this experiment. Both the anode and cathode flow fields have the same channel depth. The conventional single serpentine of constant channel depth S1 was compared with constant channel depth S2. In both cases same experimental setup and procedures as well as the same operating conditions were used for minimizing other effects. The polarization curve and power density performance comparison are shown in Figure 4.1. It is seen that the performance of the cell with S1 design exhibits a higher performance than that of the cell with S2 design. A similar result was concluded by Kumar et. al. (2003) who found that the cell performance decreases after a channel depth of 1.5 mm. The relatively higher performance of S1 can be attributed to improved gas diffusion due to increased flow velocities since the mass flow rate is kept same for both cases.

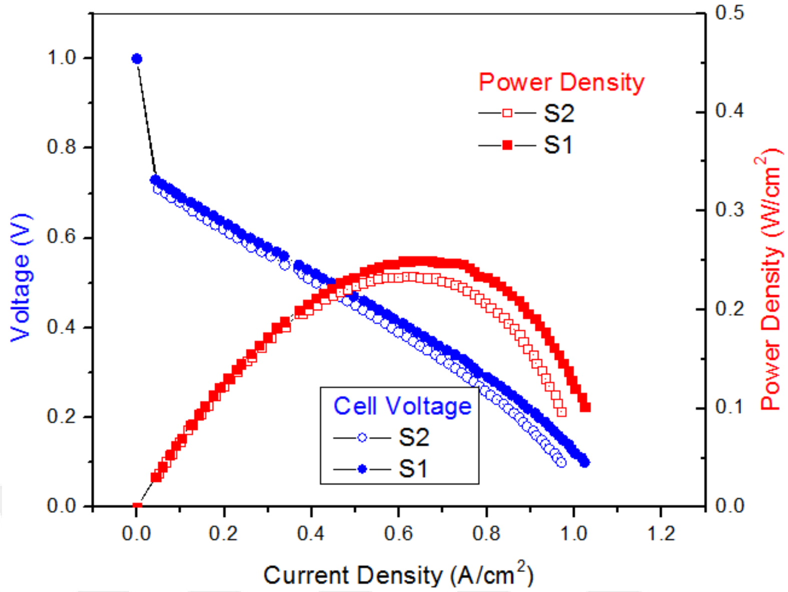

Figure 4.1. Comparison between S1 and S2 conventional constant depth channel single serpentine flow field pattern at 0.5V and 45°C.

4.2 Comparison of Convergent-Divergent Flow Fields

The same convergent flow field can also be the divergent flow field as well if the inlet and outlet of convergent flow field are replaced keeping the same geometric configuration. It can be better understood from Figure 3.1. The divergent and convergent flow field effect for the same bipolar plate are compared in Figure 4.2. The same geometry is used for both anode and cathode. Total four convergent flow fields were compared with the four divergent flow fields. In Figure 4.2(a), the convergent flow field C1 compared with the divergent flow field D1. The inlet and outlet channel depths of convergent flow field C1 are 1.5 mm and 0.5 mm, respectively whereas the divergent flow field D1 has inlet and outlet channel depth of 0.5 mm and 1.5 mm, respectively. The other cases are named in a similar manner and their results are depicted in Figure 4.2 (b)-(d). In all cases considered, the cells with convergent flow field perform better than the cells having divergent flow field. As a result of the continuous decrease in the channel depth of the convergent channel design, the flow velocity has a continuously increasing trend. This behavior improves the gas diffusion into the catalyst layers and certainly increases the cell performance. In addition, since the mass flow rate is kept constant for all the tests, the amount of reactants increases with decreasing the channel dimensions. Therefore, this may improve the reaction rate, leading to an increase in the cell performance. It is also observed that in low operating temperature experiments that the convergent flow fields can serve a better water removal capacity. This may be because of the relative high velocity occurred in the convergent flow fields than divergent flow fields.

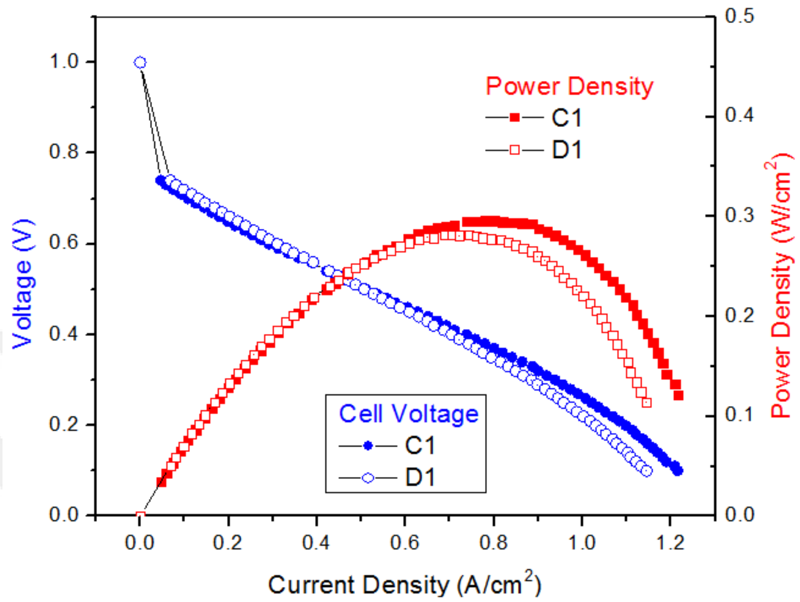

a

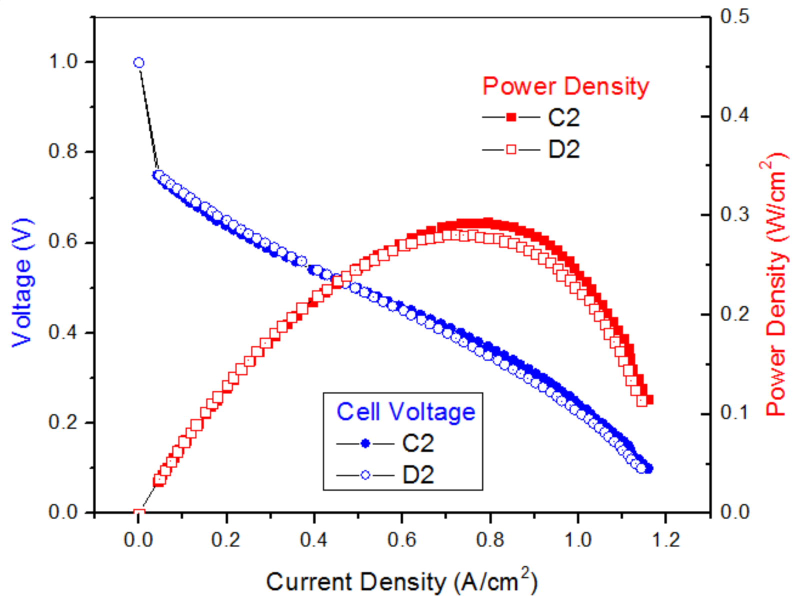

b

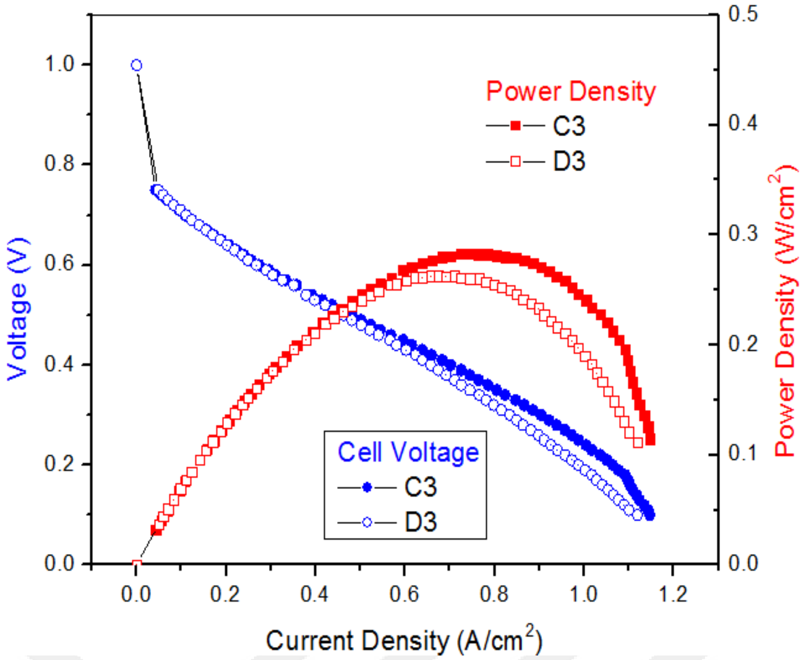

c

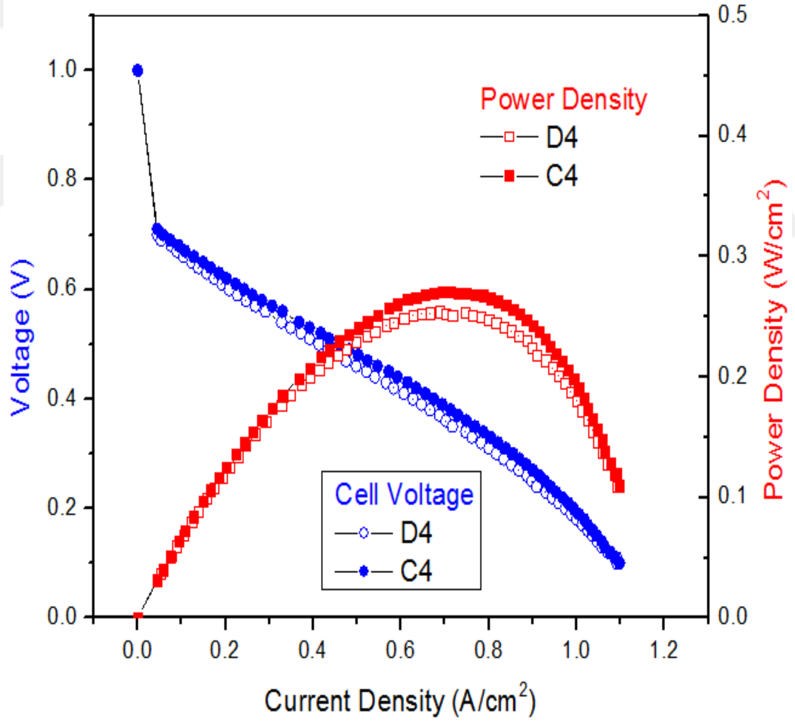

d

Figure 4.2. Comparison of same configured bipolar plate convergent-divergent flow field effect D1 vs. C1 (a), D2 vs. C2 (b), D3 vs. C3 (c) and D4 vs. C4 (d); at 0.5 CV and 45 ºC cell temperature

4.3 Comparison of Divergent Flow Fields

The same configuration of divergent flow fields were used for both the anode and cathode flow field with co-flow arrangement in D1-D4. The channel depths are diverged from inlet to outlet with a uniform angle through the total channel length. The expansion of channel depth from inlet to outlet are 200%, 55.56%, 300% and 600% for the divergent flow fields of D1 (0.5 mm – 1.5 mm), D2 (1.5 mm – 2.5 mm), D3 (1.0 mm – 3.0 mm) and D4 (0.5 mm – 3.5 mm) respectively.

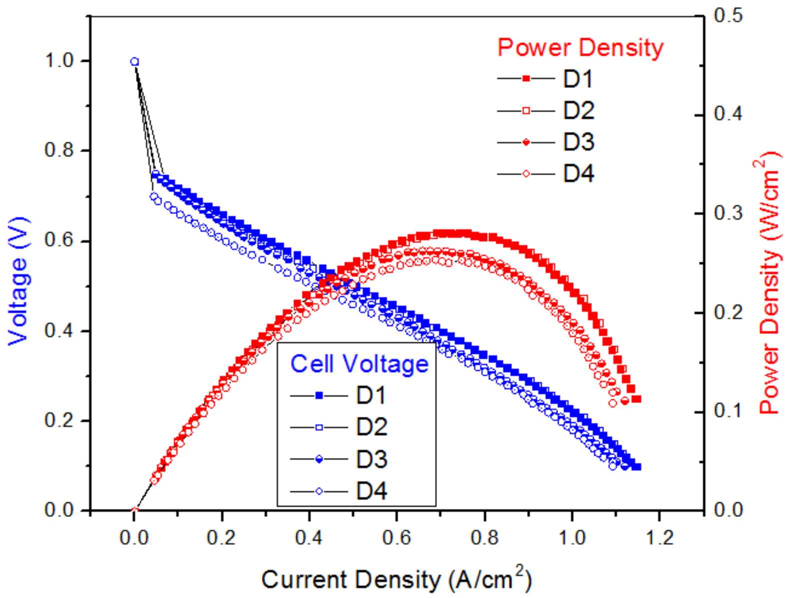

Figure 4.3. Comparison of divergent flow fields

For the same experimental setup procedures and operating conditions, the four different types of divergent flow field's cell performance comparison is shown in Figure 4.3. Divergent flow field of D1 seems to be slightly better than D2, and both D1 and D2 were superior to the other two divergent flow fields of D3 and D4, while divergent flow field D4 was worst in cell performance. These results indicate that the cell performance is inversely proportional to the divergent channel depth.

4.4 Comparison of Convergent Flow Fields

The same bipolar plates described in the divergent flow fields were used for convergent flow field analyses by simply changing the inlet and outlet position, by which transform to convergent flow field.

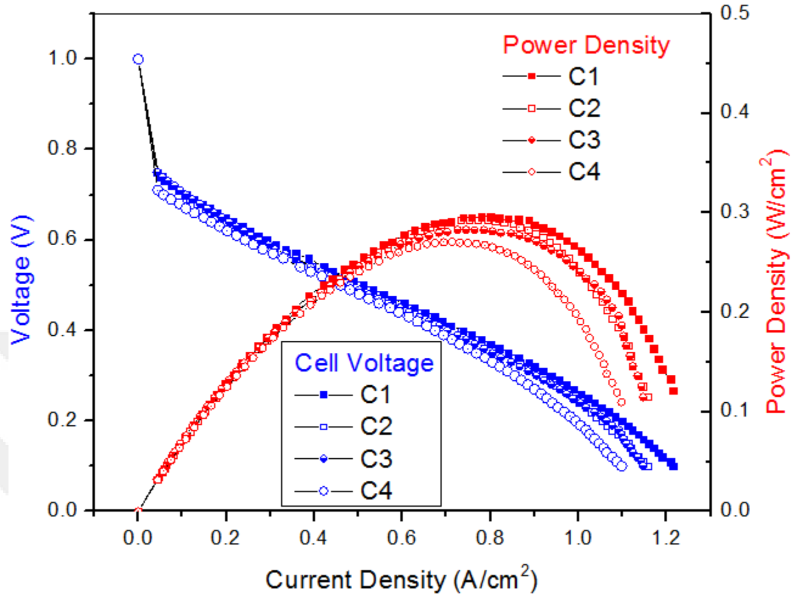

Figure 4.4. Comparison of convergent flow fields

The same geometry and convergent type of flow field were used for both anode and cathode flow fields with co-flow arrangement for each experiment separately. The contraction of channel depth from inlet to outlet are 66.67%, 40%, 66.67% and 85.71% for the convergent flow fields of C1 (1.5 mm – 0.5 mm), C2 (2.5 mm – 1.5 mm), C3 (3.0 mm – 1.0 mm) and C4 (3.5 mm – 0.5 mm) respectively. The channel depth are converged from inlet to outlet with a constant inclination gradient along with the total channel length. For the same experimental setup, procedure and operating conditions, the comparison of the cell performance is shown in Figure 4.4. It is found that the convergent flow field C1 has the best cell performance while convergent flow field C4 exhibits the lowest performance. Although there exists slight difference in the cell performance of C1 and C2, but C1 has higher current density than C2. Therefore it can be concluded that with the decrease in the convergent channel depth, the cell performance tends to increase. This may be due to the improved mass transport with decreasing convergent channel depth.

4.5 Comparison of All Flow Fields

The polarization and power density curves obtained at 45ºC of the cells with all the divergent, convergent and constant depth channels are compared in Figure 4.5 (a) and (b), respectively. It is found that the convergent flow field C1 is the best whereas constant depth channel S2 found to be worst. The descending order of the experimented flow fields overall cell performance is C1 > C2 > C3 > D1 > D2 > C4 > D3 > D4 > S1 > S2. In addition, convergent flow field C4 found to be inferior to the divergent flow fields D1 and D2. This is because the convergent flow field C4 has a higher channel depth gradient which causes reduced reactant gas diffusion.

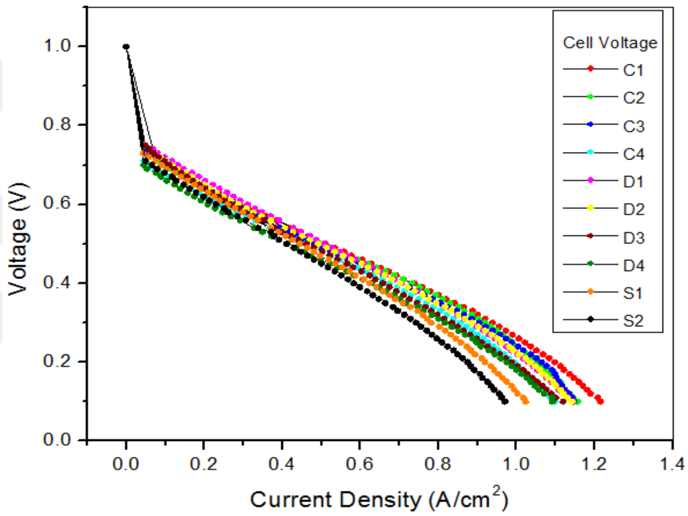

a

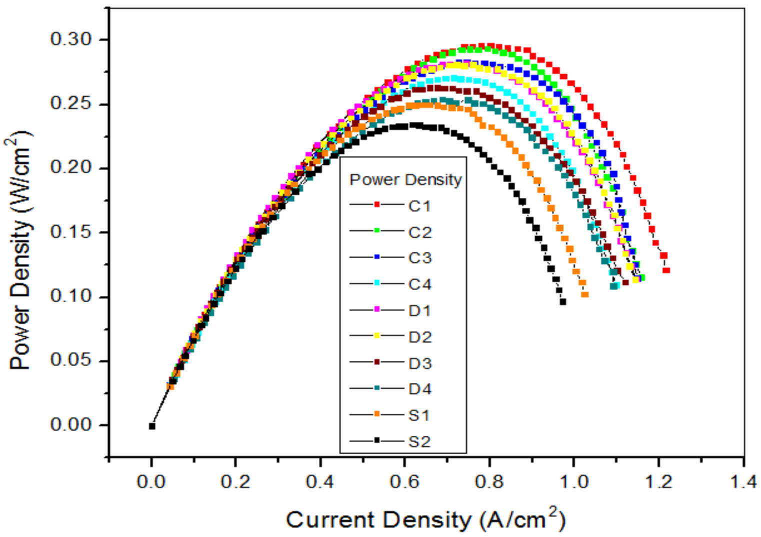

b

Figure 4.5. Polarization (a) and Power density (b) curves of all experimented flow fields tested

4.6 Analysis of Channel Depth Gradient

In Figure 4.6, the effect of channel depth gradient for both convergent flow fields (Figure-4.6a) and divergent flow fields (Figure 4.6b) on the cell power (W) and current (A) are compared. The results of the constant channel depth cases are also included in the figures. For zero gradient of constant depth channel of S1 and S2, former is the superior for the cell peak power and current. For 1 mm channel depth gradient, the convergent flow fields of two different channel's depth of C1 and C2 have small difference in the cell peak power but considerable difference in the current density. The similar results can be also concluded for the divergent flow fields D1 and D2. On the other hand, for 2 mm and 3 mm channel depth gradients, for both convergent and divergent flow fields case, the peak power and corresponding current density tend to decrease with increasing the channel depth gradient.

4.7 Effect of Total Channel Volume

The channel volume are calculated using the channel geometry data in Figure-4.7. The conventional constant channel depth has a rectangular cubic geometry for the calculation of total channel volume whereas a trapezoidal geometry are considered for both convergent and divergent flow fields for total channel volume calculations.

Based on the analytical calculations, the total channel volume for the conventional constant channel depth flow fields of S1 and S2 are 309 mm^3 and 618 mm^3, respectively. The total channel volume of same bipolar plate of both convergent and divergent flow fields have the same total channel volume. The total channel volume of C1 and D1, C2 and D2, C3 and D3, C4 and D4 are 309 mm^3, 618 mm^3, 618 mm^3, and 618 mm^3, respectively. This is somewhat interesting that there are only two different total channel volumes for all flow fields where S1, C1 and D1 have 309 mm^3 while the rest of the flow fields have 618 mm^3 total channel volume.

The effects of the total channel volume on the maximum cell power and the corresponding current at that point for different flow fields considered are compared in Figure 4.8. It is seen that in spite of the same total channel volume, the performances are different. The conventional constant channel depth of S1 (1mm) and S2 (2mm) have 309 mm^3 and 618 mm^3 respectively. However, where S1 having a lower total channel volume has a better cell performance. For the convergent flow field C1 having 309 mm^3 is superior to other convergent flow fields having the same total channel volume of 618 mm^3.

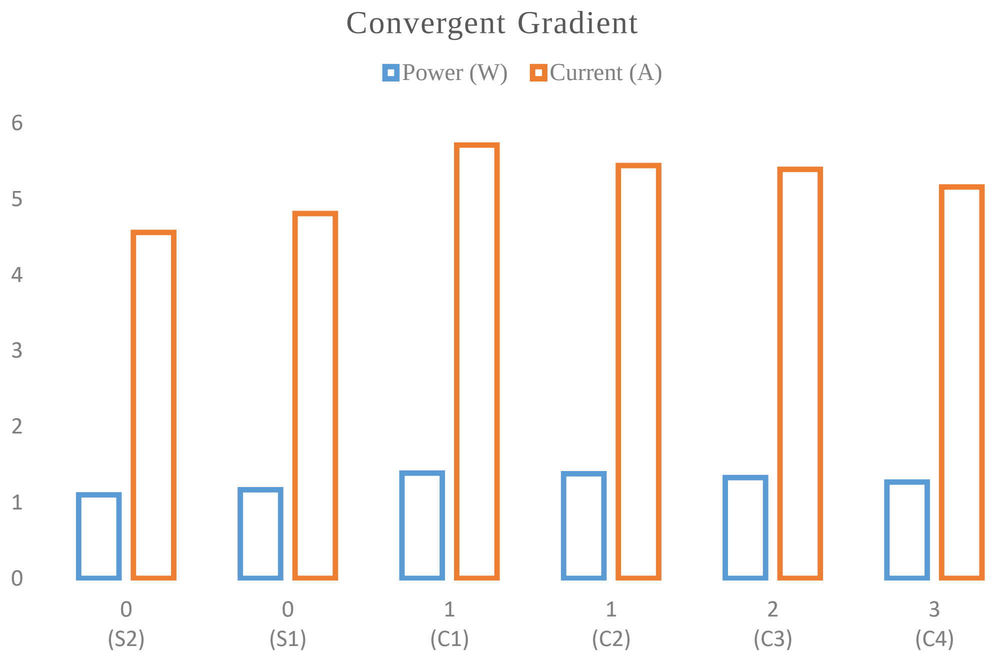

a

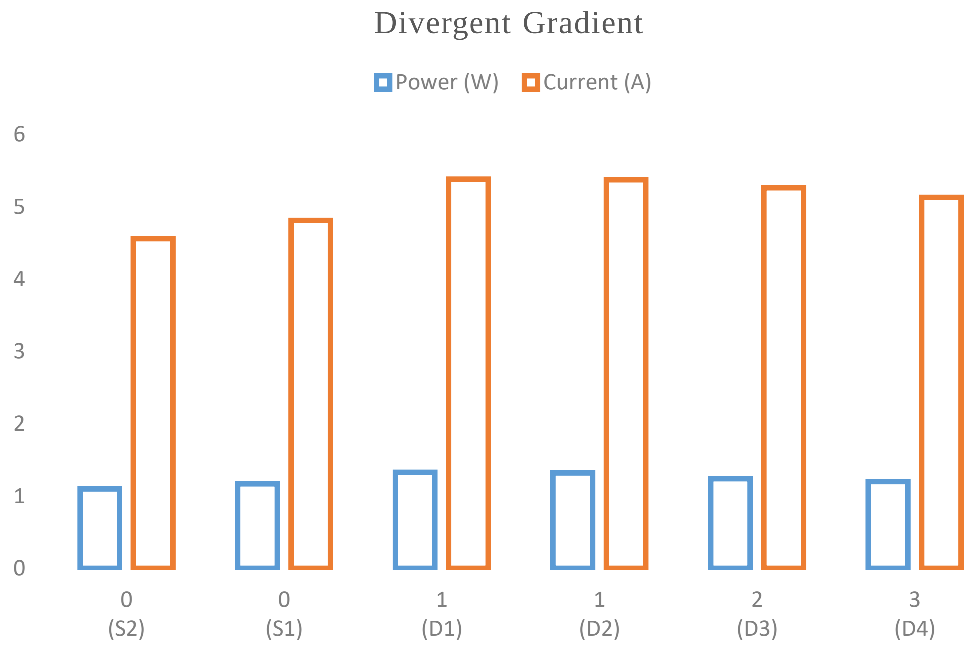

b

Figure 4.6. Cell performance comparison with convergent gradient of channel depth variation (a) and divergent gradient of channel depth variation (b)

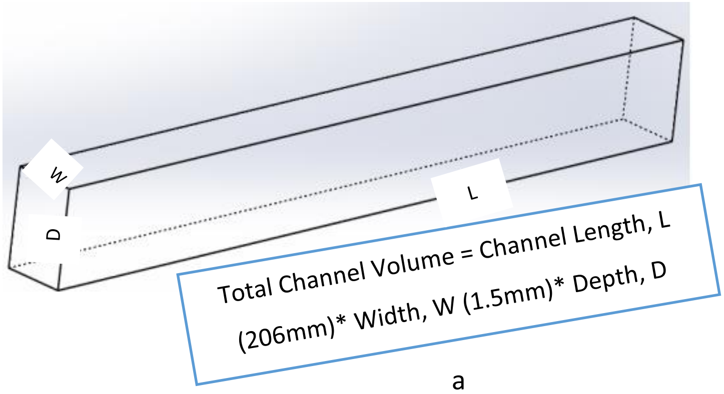

a

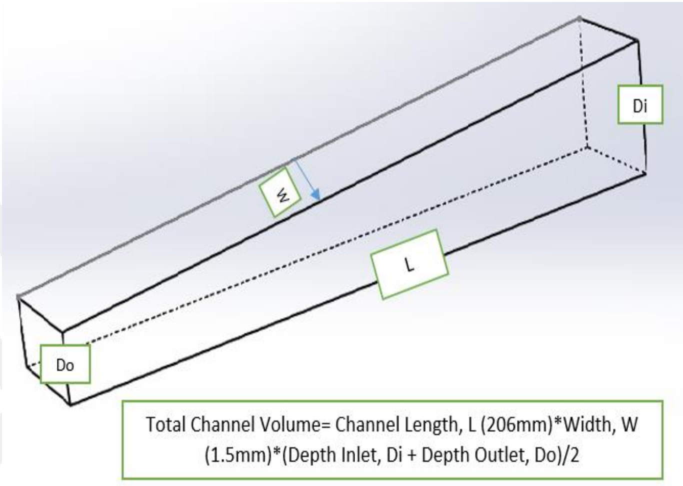

b

Figure 4.7. Conventional constant depth channel flow fields (a) and convergent-divergent flow fields (b)

The divergent flow field D1 has a total channel volume (309 mm^3) shows better cell performance than the other divergent flow fields having the same 618 mm^3 total channel volume. The convergent flow field C1 has the lowest total channel volume, has the best cell performance among all flow fields. According to these results, it can be concluded that the cell performance can be improved by reducing the channel volume. This is mainly due to the improved gas diffusion as a result of the increase in the flow velocities since the mass flow rate is the same for all the tests. Another reason may be the enhanced electrochemical reactions because the amount of reactants increases when the total channel volume decreases for the same mass flow rate.

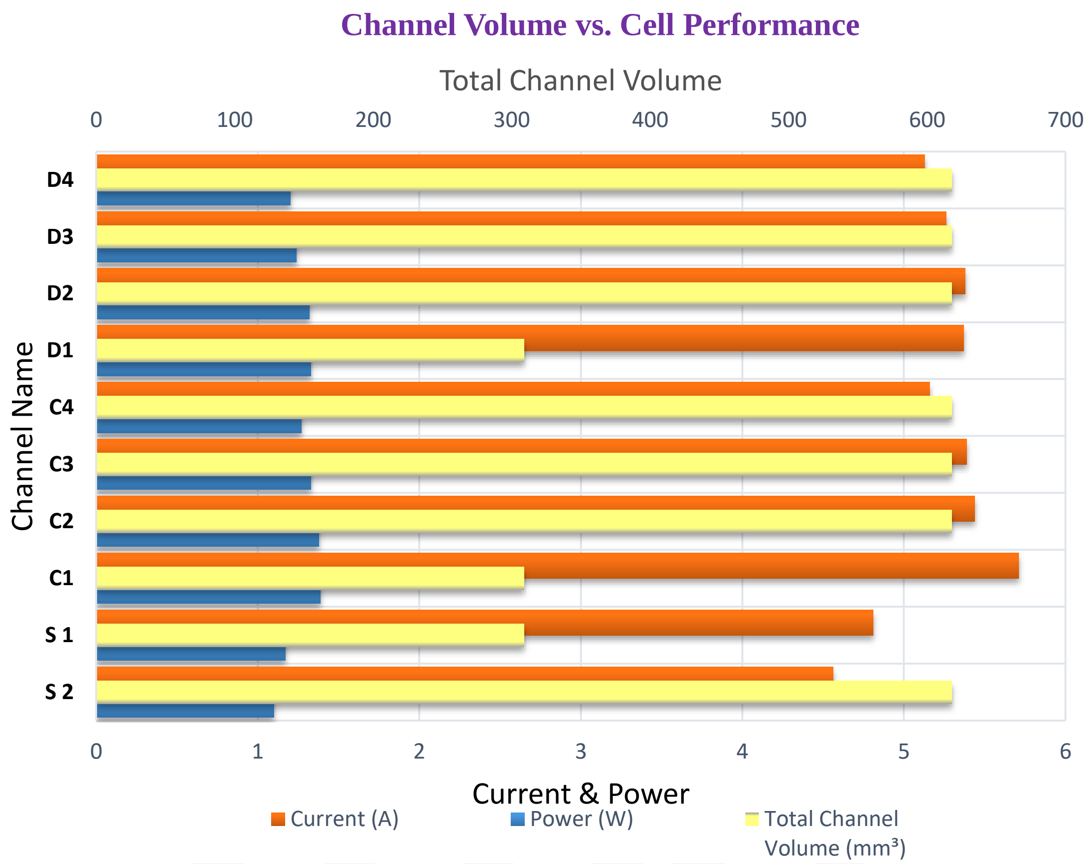

Figure 4.8. Total channel volume (mm^3) effect on the maximum cell performance.

4.8 Discussion

From this experimental study, it was found that both convergent and divergent flow fields perform better than the constant depth channels. At the beginning, convergent flow fields are expected to be better whereas the divergent flow fields should have the worst performance, since the considered hypothesis based on the molecular diffusion rate which is the main drive force. However, the divergent flow fields were found better than constant depth flow fields. This is because of the short channel length and the reactants flow distribution in divergent flow channels were better than conventional constant channel depth flow fields for especially low operating temperature condition. The same results were shown for convergent-divergent effect with numerical analysis for varying channel width and height by Lin et. al. (2010) and Wang et. al. (2010). The convergent flow fields have better performance because as the channel volume decreases with the channel length path, the amount of reactants increase, resulting in a better diffusion rate and enhanced electrochemical reaction rates.

As the experimental study was carried out at low temperature, two phase flow was existed in the GDL, CL as well as in the flow channels (Carton et. al., 2014). For the conventional constant depth channel flow fields, the water accumulation in the channels was observed in the final few internal channels which were the same in the divergent flow fields as well. In the divergent flow fields, although there was water accumulation occurred but due to the divergence in the channel the fuel passed with an ease comparative to the standard constant depth channel. Also for the shorter experimental study time period may be another reason which is not enough to analyze the water accumulation effect in details. Else otherwise, there would be a major drawbacks in the cell performance in divergent flow fields compare to the conventional flow fields. But for the case of convergent flow fields, the water accumulation in the flow channels were almost negligible comparing with the divergent and conventional flow fields. This is due to the increase of fluid velocity due to the channel convergence effect which played a major role to remove liquid water from the channels. For this reasons, the convergent flow fields can be considered to be superior to the divergent and conventional flow fields' cell performance.

The convergent flow fields lead to a favorable PEM fuel cell performance than both divergent and conventional flow fields. The maximum power output was 1.39 W obtained from C1 convergent flow field whereas worst was 1.1 W obtained from S2 flow field. Convergent flow field C1 provided 19% and 27% increased cell power performance comparing with the two conventional flow fields of S1 (1mm) and S2 (2mm), respectively. From this experimental study it can be concluded as follows based on the experimental results and observations:

a) Decreasing in channel depth leads to a better diffusion of reactants especially before the outlet section, resulting in an increase of reactants concentration in decreasing channel volume for the convergent flow fields.
b) The smaller the channel depth gradient between the inlet and outlet channel volume for divergent and convergent flow fields is, the higher the current density is. Because of this reason C1 was found to be superior to the other convergent flow fields and D4 was found to be worst among all divergent and convergent flow fields.
c) Water management and current density were found to be better in convergent flow fields than conventional and divergent flow fields.

d) There should be an optimum channel depth gradient of convergent flow fields for higher cell performance as well as the total channel volume should be a critical analytic parameter for bipolar plate flow field design in PEM fuel cells.

Overall, it can be concluded that the developed novel convergent serpentine flow field pattern improves the water management and current density, hence total cell performance of the PEM fuel cell than the conventional serpentine flow field. For detail understanding the internal complex phenomena of the studied flow fields, numerical approach is recommended.

CHAPTER V

NUMERICAL STUDY

The complex physical and electrochemical phenomena occurring in PEMFC operation cannot be directly observed or examined via experimental analyses. That is why numerical approach is widely conducted. In this study, a mathematical model, governing fluid flow, heat and mass transfer and electrochemical reactions taking place in PEMFC is developed. The model is then numerically solved by a commercial software of Comsol Multiphysics ®. After the validation of the mathematical model with the experimental results, the model is solved for various flow fields for the numerical optimization of the novel convergent-divergent flow fields that are suggested.

5.1 Numerical Model Setup

5.1.1 Computational domain

Four different geometric models are considered for four different case studies. These are shown in Figure 5.1-5.4. The same experimental model that were studied in chapter 3 and 4, i.e. the case of conventional constant channel depth of S1 and S2 serpentine flow fields, were developed for numerical model validation in alignment of experimental model. The difference between S1 and S2 is only channel depth, which is 1.0 mm for S1 and 2.0 mm for S2. The general view of S1 and S2 is shown in Figure 5.1. The single straight channel geometry shown in Figure 5.2 was developed for channel geometry optimization. The third case for numerical study was conventional flow field pattern of parallel and serpentine shown in Figure 5.3 (a) and (b) respectively, for comparative numerical study. Different types geometric model of convergent and divergent flow fields of parallel and serpentine were developed for numerical study which is one of the major purpose of this thesis work. The general schematic of these convergent and divergent for parallel and serpentine are shown in Figure 5.4 (a) and (b) respectively.

All the geometries comprise seven computational sub-divisions as anode and cathode flow channels, gas diffusion layers, catalysts and electrolyte. The flow channels are responsible for the reactant transport and removal of the byproduct of water.

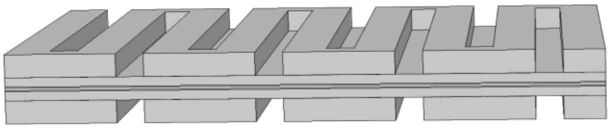

Figure 5.1. The geometry used to validate the mathematical model

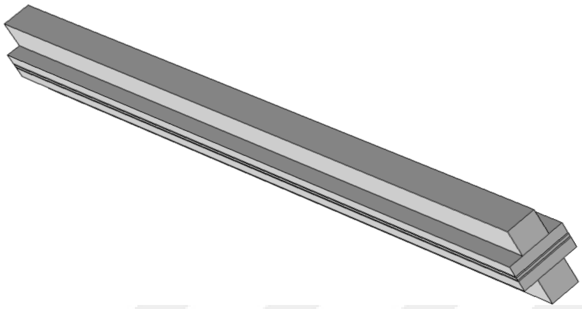

Figure 5.2. Straight channel geometry

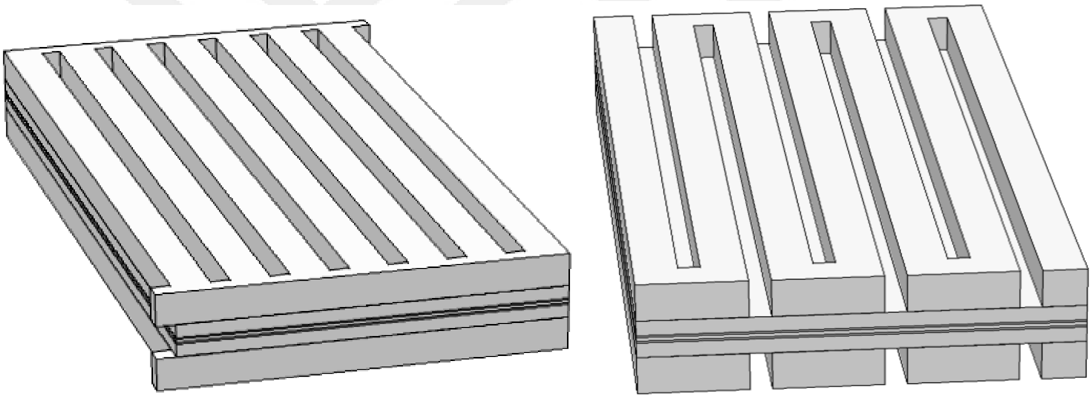

a

b

Figure 5.3. Geometry of the numerical model of conventional el (a) and serpentine (b) flow field pattern

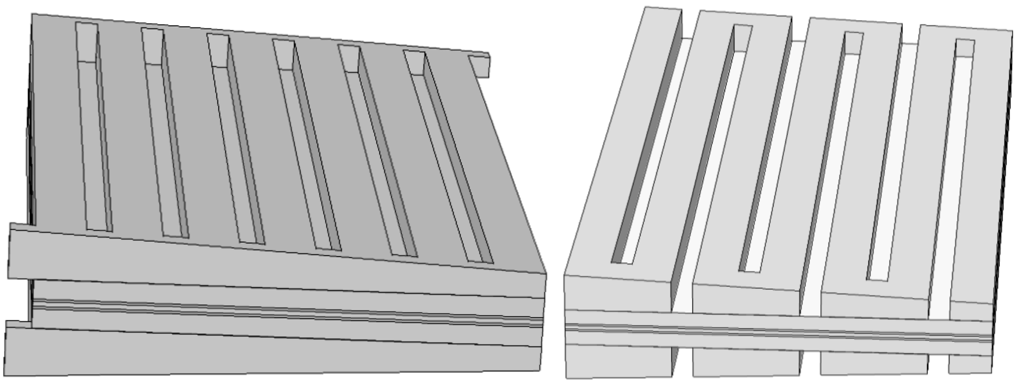

a

b

Figure 5.4. Geometry of the numerical model of convergent-divergent parallel (a) and serpentine (b) flow field pattern

Therefore, the reactants which are to involve in the electrochemical reactions within the corresponding catalysts diffuse from these channels to the related gas diffusion layers first. The anode and cathode catalyst are responsible for the oxidation of hydrogen and reduction of oxygen, respectively. Thus, mass transport is coupled with reactant consumption and product generation beside the convective and diffusive flux. The ionic transport occurs from the anode to the cathode through the electrolyte while the electronic conduction exist in all solid parts except the membrane.

For the channel geometry optimization, a total of 343 case studies are considered for wide ranges of channel depth, width and rib width considering permutation and combination of these parameters shown in Table 5.1. For the comparative study of conventional parallel and serpentine flow fields, the optimized channel geometric parameters are used for these flow field design. On the other hand, the different types of convergent and divergent parallel and serpentine flow fields, the same optimized channel geometric parameters are used except there are variations in the channel depth. Total 16 case are considered for different convergent and divergent flow fields of parallel and serpentine by developing different geometric models shown in Table 5.2.

Table 5.1. Considered channel geometry case studies for optimization

Channel Depth (mm)	Channel Width (mm)	Rib Width (mm)
2	2	2
1.75	1.75	1.75
1.5	1.5	1.5
1.25	1.25	1.25
1.0	1.0	1.0
0.75	0.75	0.75
0.5	0.5	0.5

Table 5.2. Convergent-divergent flow field's case study

Flow Field Channels Defined Name [C=convergent, D=divergent, S= serpentine, P=parallel conventional FFP]	Channel Depth Inlet/Outlet (mm)	% Contraction / Expansion: Inlet to Outlet Channel Depth
SC1, PC1	1 / 0.75	25%
SC2, PC2	1/0.5	50%
SC3, PC3	1/0.25	75%
SC4, PC4	1/0.1	90%
SD1, PD1	0.75/1	33.33%
SD2, PD2	0.5/1	100%
SD3, PD3	0.25/1	300%
SD4, PD4	0.1/1	900%

5.1.2 Assumptions

For this numerical model the following assumptions were made:

- Steady state operating conditions
- All gases and gas mixture behavior are considered as ideal gas and gas mixture conditions
- Isothermal model
- Single phase incompressible flow without any phase change
- There is no crossover of reactants and water vapor through electrolyte membrane
- Electrolyte is electrically non-conductive, only proton can pass through electrolyte
- Current collection only occurs at land area i.e. non-flow channel portion
- The effect of gravity is neglected
- Gas compositions are fixed at the inlets of both the anode and cathode
- Back pressure effect neglected
- No film resistance for GDL and catalyst layer

5.1.3 Governing equations

5.1.3.1 Electrochemical model

A mathematical model is developed based on two major consequences of PEMFC, which are the charge phenomena and fluid flow dynamics. The electricity is generated as a result of the electrochemical reactions taking place in the anode and cathode electrodes. This electrochemical process is related with the charge production, transport and conservation. Thus, the mathematical model in this study considers the related theories by developing associated governing mathematical equations. In PEMFCs, the bipolar plate rib surface, porous electrodes and membrane are the charge transport mediums, while the porous catalysts are responsible for the charge production. The hydrogen oxidation reaction (HOR) occurs at anode catalyst as follows:

$$H_2 \rightarrow 2H^+ + 2e^- \tag{5.1}$$

Therefore local current density for HOR is developed using the linearized concentration depended Butler-Volmer equation can be derived as follows:

$$i_a = i_{o,a}\left(\frac{\alpha_{a,a}+\alpha_{c,a}}{RT}\,F\eta_a\right) \tag{5.2}$$

where $i_{o,a}$ is the anode exchange current density, R is the ideal gas constant, F represents the Faraday constant, T stands for the operation temperature in K and η_a shows the anode overpotential. $\alpha_{a,a}$ and $\alpha_{c,a}$ is the anodic and cathodic charge transfer constant for the anode, respectively. The anode exchange current density $i_{o,a}$ can be calculated as a function of the local H_2 concentration C_{H_2} and the reference H_2 concentration $C_{H_2,ref}$ as follows:

$$i_{o,a} = 10^5\left(\frac{C_{H_2}}{C_{H_2,ref}}\right)^{0.5} \tag{5.3}$$

Similarly, in the cathode catalyst, the oxygen reduction reaction (ORR) occurs:

$\frac{1}{2}O_2 + 2H^+ + 2e^- \rightarrow H_2O$ (5.4)

The local current density in the cathode for ORR can be expressed using cathodic Tafel equation:

$$i_c = -i_{o,c} 10^{\eta_c / A_c} \tag{5.5}$$

$$i_{o,c} = \left(\frac{C_{O_2}}{C_{O_2,ref}}\right) \tag{5.6}$$

In the above equation, $i_{o,c}$ represents the cathode exchange current density and C_{O_2} and $C_{O_2,ref}$ is the local and reference O_2 concentration, respectively. A_c represents Tafel slope while η_c is the cathode overpotential.

The potential difference between the solid matrix and the electrolyte for the electrodes is the electrochemical overpotential (η) which can be defined as a function of electronic (ϕ_s) and ionic (ϕ_l) phase potential as well as equilibrium voltage (E_{eq}) as:

$$\eta = \phi_s - \phi_l - E_{eq} \tag{5.7}$$

The continuity of current density (i) can be expressed as:

$$\nabla . i = 0 \tag{5.8}$$

As in the PEMFC, there are two types of charge, which are electronic (i_s) and ionic (i_l). Then, Eqn. (8) can be rearranged as:

$$\nabla . i_s + \nabla . i_l = 0 \tag{5.9}$$

Applying Ohm's Law to the charge transfer with the account of electronic (S_s) and ionic (S_l) charge source term, Eqn. (9) becomes:

$$\nabla . (-\sigma_s \nabla \phi_s) = S_s \quad ; \quad \nabla . (-\sigma_l \nabla \phi_l) = S_l \tag{5.10}$$

where σ is the electrical conductivity. Due to the electrochemical reactions in the anode and cathode catalyst layers, the current source terms are linked to the corresponding local two-phase current densities of the anode and cathode, respectively, as follows:

$$S_s = -i_a \;\; ; \quad S_l = i_a \tag{5.11}$$

$$S_s = -i_c \;\; ; \quad S_l = i_c \tag{5.12}$$

The total local current density for the active surface area for the anode and cathode electrode kinetics becomes, respectively:

$$i_{v,a} = a_{v,a}\, i_a \quad ; \quad i_{v,c} = a_{v,c}\, i_c \tag{5.13}$$

Therefore, the agglomerated charge module with the account of the charge source terms, the total local current density and charge transport for both the anode and cathode can be expressed in generalized form, respectively, as follows:

$$\nabla . i_s = S_s - i_v \; ; \; \nabla . i_l = S_l + i_v \tag{5.14}$$

5.1.3.2 Fluid flow in channels

The reactant gas flows in the gas channels are governed by the continuity equation for the conservation of mass and Navier-Stokes equations describe the momentum conservation of Newtonian fluids. Based on the model assumptions, the final forms of continuity and Navier-Stokes equations are given below, respectively:

$$\nabla . u = 0 \tag{5.15}$$

$$\rho u . \nabla u = \nabla . \left[-P + \mu \left(\nabla u + \mu (\nabla u)^T \right) \right] \tag{5.16}$$

where u is the flow velocity, μ is the dynamic viscosity of the gas mixture, ρ shows the gas mixture density and P is the pressure.

The multi-component diffusion and convection in the flow channels are described by the Maxwell-Stefan equation to solve the mass fraction (ω) fluxes. The mathematical form of the Maxwell-Stefan equation is used as:

$$\frac{\partial}{\partial t}\rho\omega_i + \nabla.\left[-\rho\omega_i \sum_{j=1}^{N} D_{ij}\left(\frac{M}{M_j}\left(\nabla\omega_j + \omega_j \frac{\nabla M}{M}\right) + (x_j - \omega_j)\frac{\nabla P}{P}\right) + \omega_i \rho u\right] = R_i \quad (5.17)$$

D_{ij} terms in the Eqn.(17) are the Maxwell-Stefan diffusivities and they are listed in Table 2. The combined molecular weight M_j can be calculated as follows:

$$M_j = \sum_i \left(\frac{\omega_i}{M_i}\right)^{-1} \quad (5.18)$$

The diffusion coefficients in the porous anode and cathode layers needs to be correlated with the porosity of the medium (ϵ). The effective diffusion coefficients for the anode and cathode layers can be expressed as follows:

$$D_{jk}^{eff} = D_{jk}\epsilon^{1.5} \quad (5.19)$$

The density of mixture gas is a function of mixture components and is described by the following equation:

$$\rho = \left(\sum_i x_i M_i\right) P/(RT) \quad (5.20)$$

where x_i and M_i is the molar fraction and molecular weight of specie i, respectively.

On the anode side, the hydrogen transport equation is solved first and then the mass fraction of water is obtained. Similarly, for the cathode side, the transport equations are solved for two species, since the third one can be easily obtained from the mass balance equation. These are given in Eqn. (21) and Eqn. (22), respectively.

$$w_{H_2O} = 1 - w_{H_2} \tag{5.21}$$

$$w_{N_2} = 1 - w_{O_2} - w_{H_2O} \tag{5.22}$$

5.1.3.3 Gas diffusion and catalyst layers

For the porous gas diffusion layers and catalyst layers, the velocity distribution is formulated by Darcy's law and for the mass conservation continuity equation is used as given below, respectively:

$$u = -\frac{k}{\mu}\nabla P \tag{5.23}$$

$$\nabla . (\rho u) = R_i \tag{5.24}$$

where k is the permeability for the corresponding domain. Since reaction only occurs in the catalyst layer, the source terms (R_i) for hydrogen, oxygen and water are defined by using Faraday's Law as follows, respectively:

$$R_{H_2} = -\frac{i_a}{2F} M_{H_2} \qquad R_{O_2} = -\frac{|i_c|}{4F} M_{O_2} \qquad R_{H_2O} = -\frac{|i_c|}{4F} M_{H_2O} \tag{5.25}$$

5.1.4 Numerical model parameters

The considered major numerical model parameters for solution solver are shown in Table 5.3.

Table 5.3. Major parameters of the numerical model

Parameter	Value
Open volume fraction for gas diffusion in porous electrode	0.3
Permeability of catalyst layers (m^2)	2.36 x 10^{-12}
Reference pressure (Pa)	101.325 x 10^3
Open circuit cell voltage (V)	0.9
Membrane conductivity (S/m)	9.825
Anodic transfer coefficient	1
Cell temperature (K)	353

Table 5.3. (Continue)Major parameters of the numerical model

Parameter	Value
GDL width (m)	400 x 10^{-6}
Catalyst layer thickness (m)	50 x 10^{-6}
Membrane thickness (m)	100 x 10^{-6}
GDL porosity	0.4
GDL permeability (m^2)	1.18 x 10^{-11}
GDL electric conductivity (S/m)	222
Inlet H_2 mass fraction (anode)	0.65
Inlet H_2O mass fraction (cathode)	0.05
Inlet oxygen mass fraction (cathode)	0.20
Anode inlet mass flow rate (m^3/s)	0.00000067
Cathode inlet mass flow rate (m^3/s)	0.00000201
Anode viscosity (Pa·s)	1.19 x 10^{-5}
Cathode viscosity (Pa·s)	2.46 x 10^{-5}
Hydrogen molar mass (kg/mol)	0.002
Nitrogen molar mass (kg/mol)	0.028
Water molar mass (kg/mol)	0.018
Oxygen molar mass (kg/mol)	0.032
H_2-H_2O binary diffusion coefficient (m^2/s)	11.676 x 10^{-5}
N_2-H_2O binary diffusion coefficient (m^2/s)	3.266 x 10^{-5}
O_2-N_2 binary diffusion coefficient (m^2/s)	3.044 x 10^{-5}
O_2-H_2O binary diffusion coefficient (m^2/s)	3.578 x 10^{-5}
Cathodic transfer coefficient	1
Tafel slope, A_c (mV)	-95
Oxygen reference concentration (mol/m^3)	40.88
Hydrogen reference concentration (mol/m^3)	40.88
Electrolyte phase volume fraction	0.3

5.1.5 Boundary and initial conditions

The boundary and initial conditions for this numerical study are defined and set as follows:

- The internal boundary are continuous for all domains
- Symmetric boundary conditions are assigned for gas diffusion layers and catalyst layers
- No slip condition is applied for flow channel walls
- All initial values are set to zero
- Convective flux boundary applied
- For inlet and outlet, constrain outer edges are set to zero
- Reference pressure is set to 1 atm for working conditions
- Inlet flow rates for anode and cathode are constant
- Open circuit voltage is considered as 0.9V
- Electrolyte and electric potential are set to zero for cathode while electrolyte potential is zero for anode and cathode at initial conditions

5.1.6 Numerical model variables

The following unknown variables are solved in the model:

- ϕ_s—The electronic potential
- ϕ_l—The ionic potential
- wH_2—The hydrogen mass fraction (in the anode compartment)
- wH_2Oa—The water mass fraction (in the anode compartment)
- wO_2—The oxygen mass fraction (in the cathode compartment)
- wH_2Oc—The water mass fraction (in the cathode compartment)
- wN_2—The nitrogen mass fraction (in the cathode compartment)
- u_a and u_c —The velocity field vectors in the anode and cathode compartments
- p_a and p_c —The pressure in the anode and cathode compartments

The solution can be achieved by coupling two reacting flow in porous media, concentrated species modules for both the anode and cathode interfaces to secondary current distribution interface.

5.1.7 Meshing of the geometries of interest

Structural mesh structure is considered for straight channel geometry which is an advantage of the continuity of the geometry. For other cases, tetrahedral meshes are employed due to the non-continuity of the geometry.

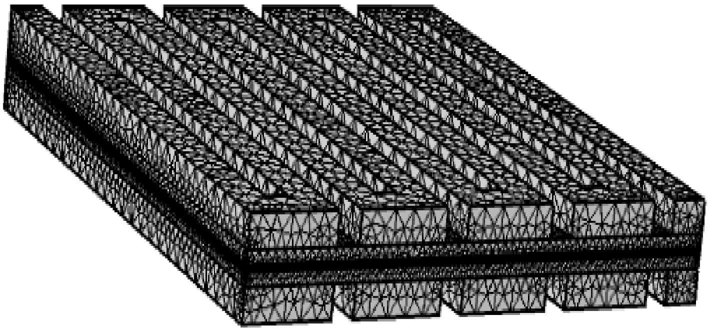

Figure 5.5. Mesh structure of the geometry used for the numerical model validation case

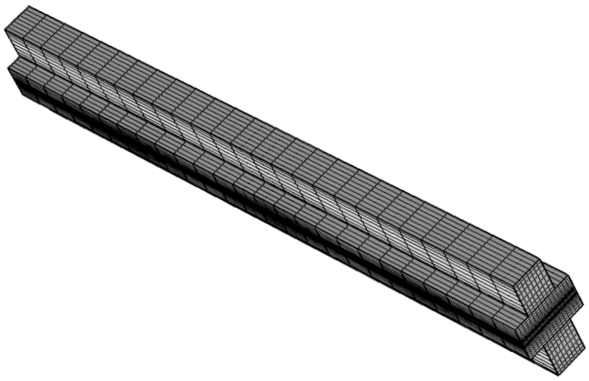

Figure 5.6. Mesh structure of straight channel geometry

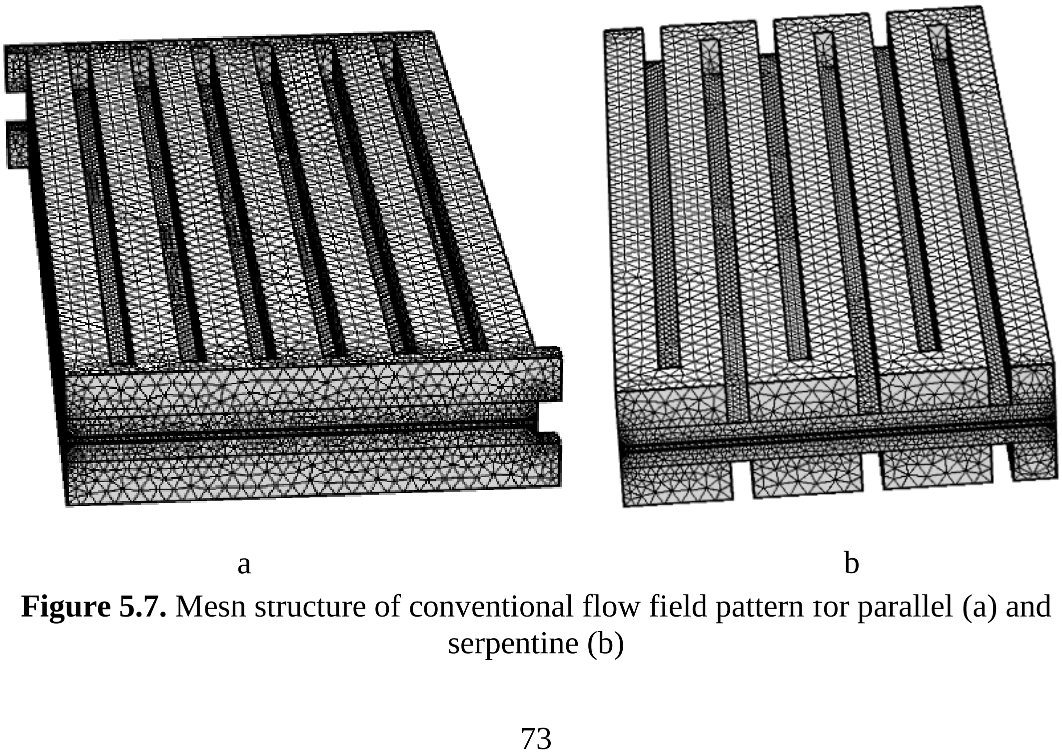

a b

Figure 5.7. Mesn structure of conventional flow field pattern ror parallel (a) and serpentine (b)

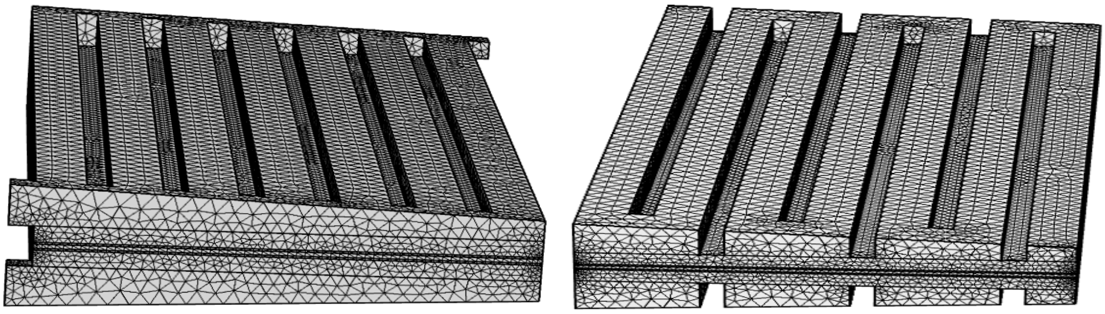

b

a

Figure 5.8. Mesh structure of conventional flow field pattern for parallel (a) and serpentine (b)

The mesh structure of the case used to validate the mathematical model is shown in Figure 5.5. For the straight channel numerical model, structural meshes are used shown in Figure 5.6. The mesh structure of the conventional flow field patterns for parallel and serpentine are shown in Figure 5.7 (a) and (b) respectively. For the cases of different convergent and divergent flow field for parallel and serpentine, the common tetrahedral mesh structures employed are shown in Figure 5.8 (a) and (b), respectively.

5.1.8 Numerical solution technique

The solver based on the finite element technique, is used to solve the governing equations developed. The stationary nonlinear solver is used since the source terms of the current conservation equation make the problem non-linear. Furthermore, the convergence behavior of this non-linear solver is highly sensitive to the initial estimation of the solution.

To accelerate the convergence, the following procedures are adopted: the Conductive Media DC module is firstly solved based on the initial setting; secondly, Darcy's Law and Incompressible Navier-Stokes modules are solved together using the results from the previous calculation as initial conditions. After the previous two modules converge, all the coupled equations including Maxwell-Stefan Diffusion and Convection module are solved simultaneously until the final convergence is obtained as shown in Figure 5.9.

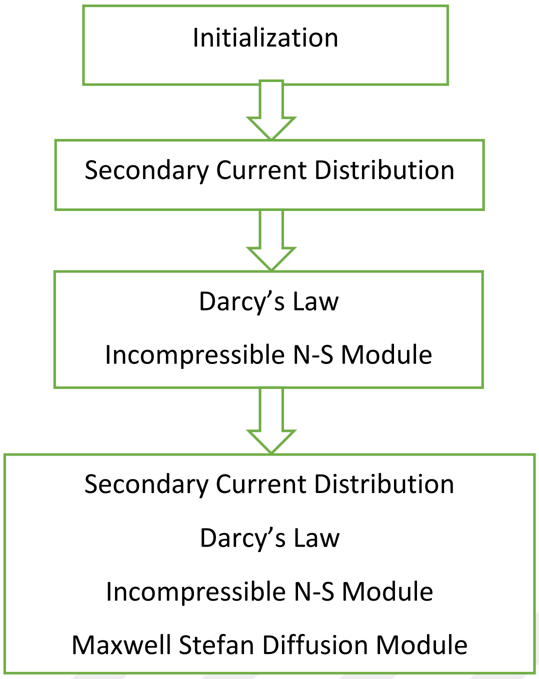

Figure 5.9. Sequence of solver configuration for the numerical model

5.2 Validation of the Numerical Model

The experimental performance result of the conventional constant channel depth of S1 (1.0 mm) design at 45ºC is compared to that obtained from the numerical analysis for the same geometry and operating conditions in order to validate the developed mathematical model. The validation of S1 flow field pattern results are shown in Figure 5.10. When both the polarization and power curves obtained from experimental and numerical studies are considered, it is clearly seen that the numerical results agree well with the experimental results. The error is calculated to be only less than 1%, indicating the successful validation of the mathematical model.

To ensure a further accuracy, the same operating conditions along with the other major parameters are used to validate the other conventional serpentine flow field pattern, S2 having 2.0 mm constant channel depth comparison. The comparison of the experimental and numerical performance results obtained for the cell with S2 flow pattern is shown in Figure 5.11. In this second validation case the error is also less than 1%, indicating match between the numerical and experimental results. Therefore, after this double check validation, the validated model is used for the following numerical analyses to optimize the novel flow fields that are being suggested in this study.

Validation (S1) of Polarization and Power Curve

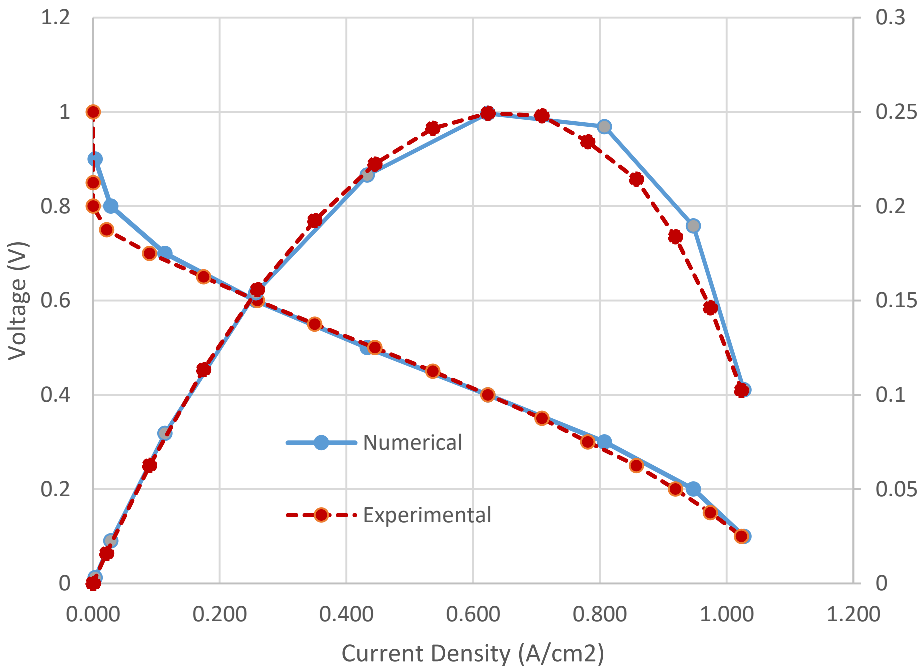

Figure 5.10. Validation of mathematical model considering S1 design

Validation (S2) of Polarization and Power

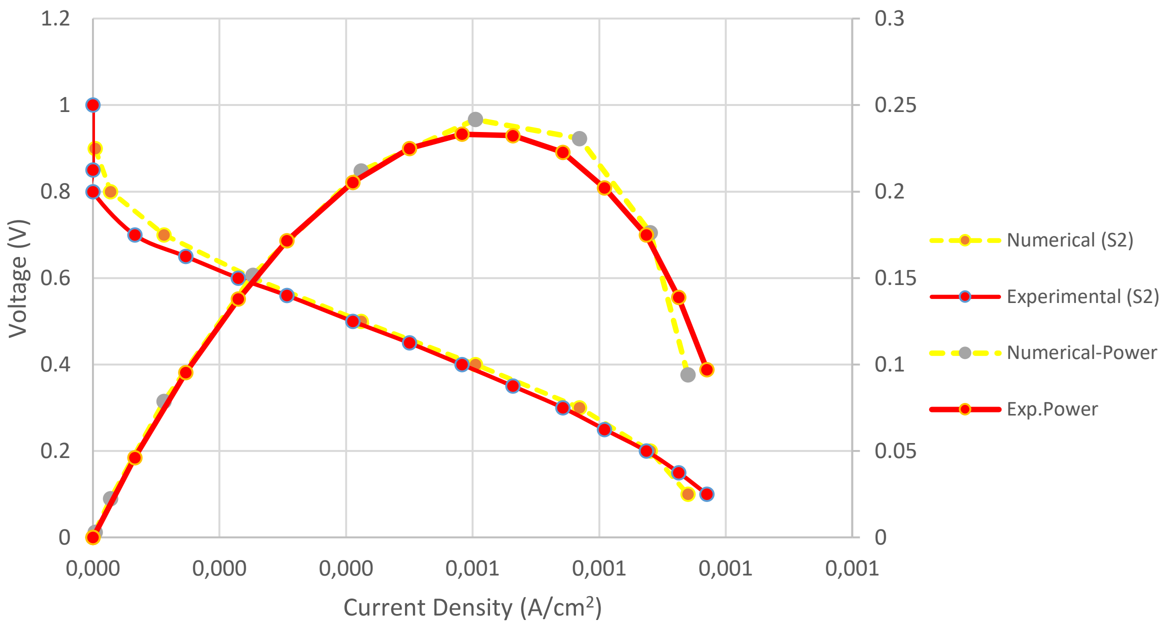

Figure 5.11. Validation of mathematical model considering S2 design

CHAPTER VI

NUMERICAL RESULTS AND DISCUSSION

In this chapter, the numerical results obtained for flow field design optimization are demonstrated. These cover optimization of three different case studies, which are geometric optimization, selection of suitable flow field pattern and modified selected conventional flow field pattern optimization considering the previous two cases. All the numerical studies employ the validated mathematical model and related parameters. Thus, it is ensured that the case studies discussed in this chapter are well0suited for numerical analyses. The analyses are based on the cell current density, flow distribution, mass fraction, pressure drop and water management.

6.1 Geometric Optimization

In PEM fuel cells, there are three major geometric parameters for the flow field design optimization. These can be counted as the channel depth, channel width and rib width. For the proper optimization of the flow field design, these three geometric parameters should have suitable dimensions for improving PEM fuel cell performance. In this study, a straight channel geometry is considered for these parameters, which are analyzed for wide range of dimensions from 2 mm to 0.5 mm, descending with 0.25 mm for each of the parameter. Moreover, these seven dimensions for each parameter are analyzed with all possible combinations giving a total 343 case study for a 25 mm long straight channel geometry of a full scale PEMFC domain. The channel geometry with recommended cell temperature of 80ºC by Department of Energy (DOE, USA) is considered together with the major parameters from the validated numerical model. The model is numerically solved for various channel widths, channel depths and rib widths. The predicted current densities, anode and cathode pressure drops under a constant operating voltage of 0.4 V are compared. According to these results, the optimum dimensions for the channel depth, channel width and rib width are decided.

6.1.1 Effect on cell current density

Since the maximum cell performances are obtained around an operating voltage of 0.4 V, the numerical analyses are carried out at this operating voltage. For different constant channel depths, the predicted current densities are shown in Figure 6.1 (a)-(g) with various channel width change along with rib width variation. It is seen that the general behavior of the current density is almost same for all the different graphical cases of constant channel depths with the change in channel/rib width variation. With the decrease in rib width from 2.0 mm to 0.5 mm, the cell current density increased for constant channel depth and width. For the constant channel depth and rib width, current density increased until channel width decreases from 2.0 mm to 1.0 mm, then current density started to decrease with the decrease of channel width for 0.75 mm to 0.5 mm corresponding to the rib width range of 2.0 mm to 1.0 mm. However, for the cases of constant channel depth, for lower rib width of 0.75 mm and 0.5 mm, with the decrease of channel width, current density again started to gain. For the constant channel width to rib ratio, with the decrease in channel depth current density is ameliorated.

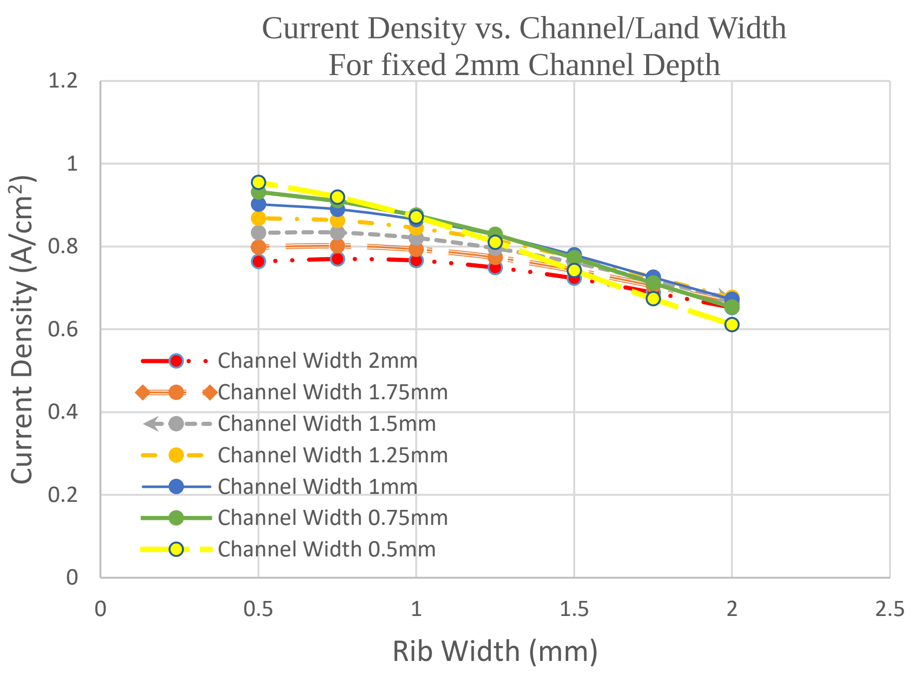

a

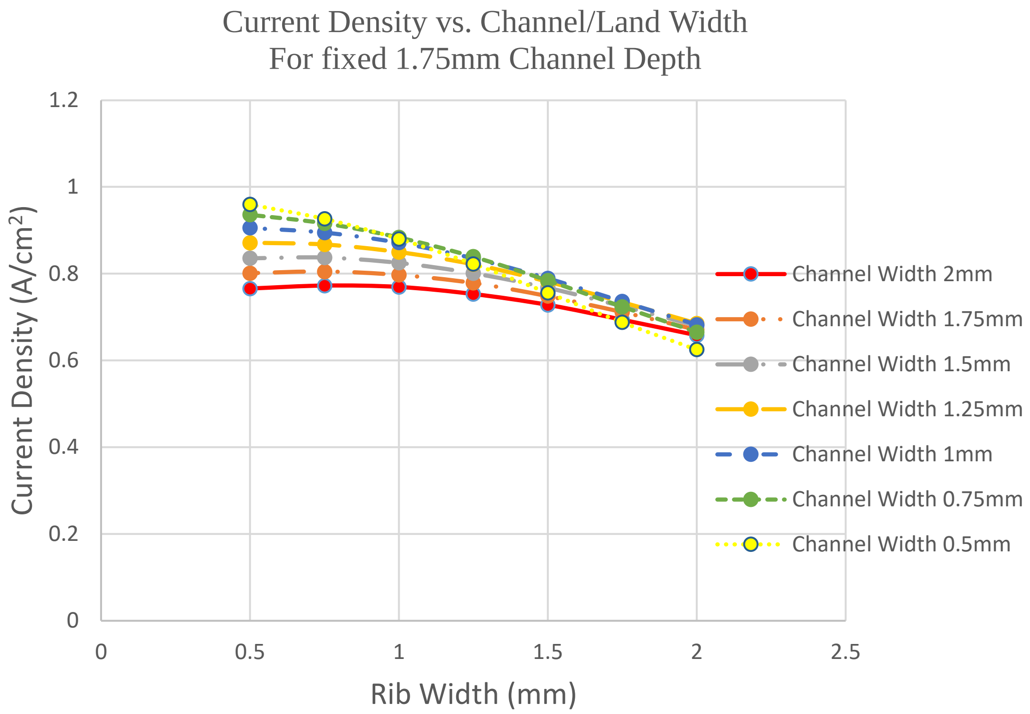
Current Density vs. Channel/Land Width
For fixed 1.75mm Channel Depth
Current Density (A/cm²)
Rib Width (mm)
1.2
1
0.8
0.6
0.4
0.2
0
0
0.5
1
1.5
2
2.5
Channel Width 2mm
Channel Width 1.75mm
Channel Width 1.5mm
Channel Width 1.25mm
Channel Width 1mm
Channel Width 0.75mm
Channel Width 0.5mm

b

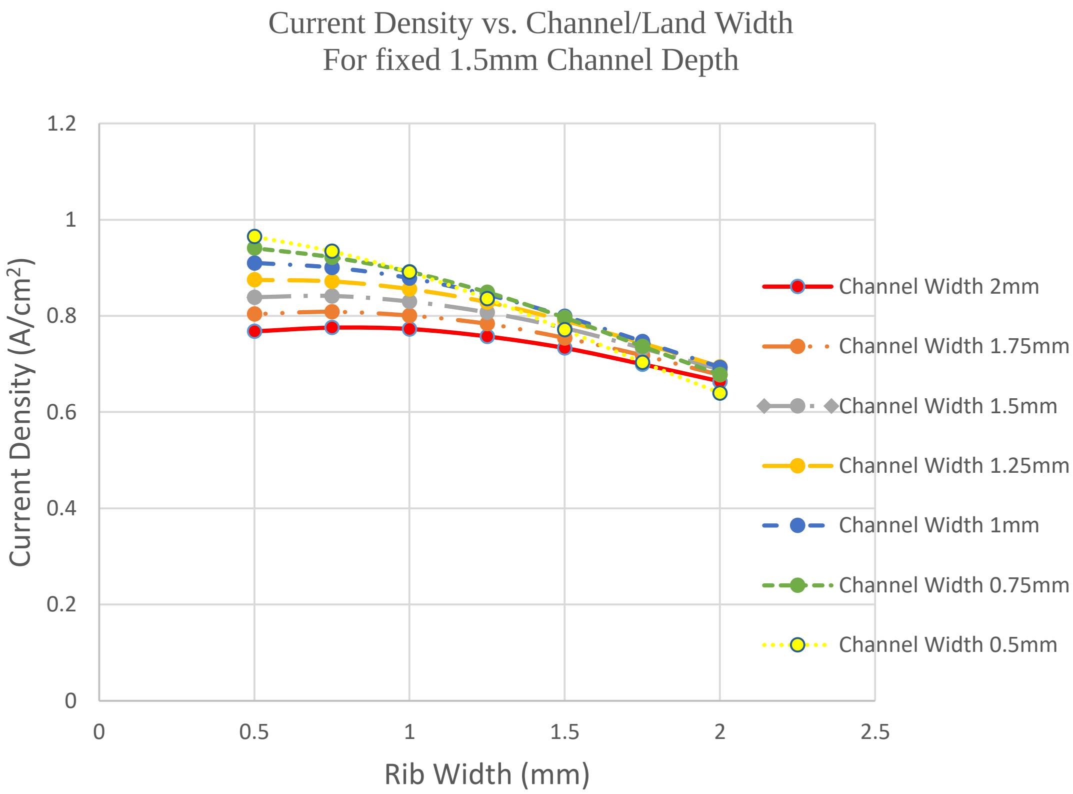
Current Density vs. Channel/Land Width
For fixed 1.5mm Channel Depth
Current Density (A/cm²)
Rib Width (mm)
1.2
1
0.8
0.6
0.4
0.2
0
0
0.5
1
1.5
2
2.5
Channel Width 2mm
Channel Width 1.75mm
Channel Width 1.5mm
Channel Width 1.25mm
Channel Width 1mm
Channel Width 0.75mm
Channel Width 0.5mm

c

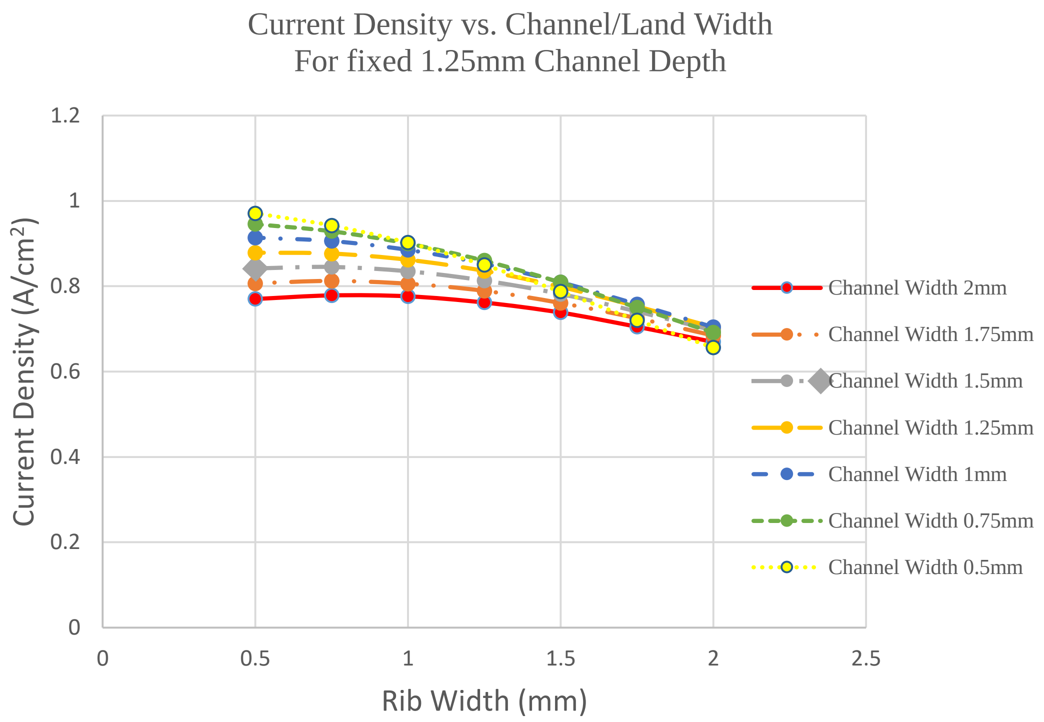
Current Density vs. Channel/Land Width
For fixed 1.25mm Channel Depth
Current Density (A/cm²)
Rib Width (mm)
Channel Width 2mm
Channel Width 1.75mm
Channel Width 1.5mm
Channel Width 1.25mm
Channel Width 1mm
Channel Width 0.75mm
Channel Width 0.5mm

d

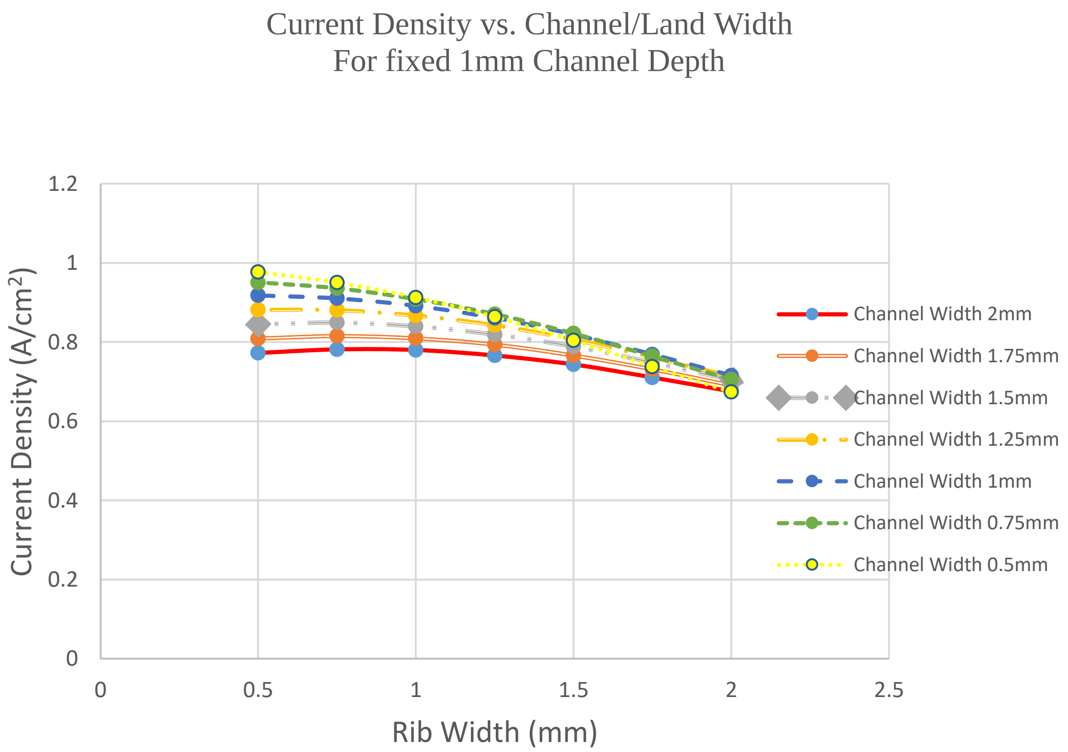
Current Density vs. Channel/Land Width
For fixed 1mm Channel Depth
Current Density (A/cm²)
Rib Width (mm)
Channel Width 2mm
Channel Width 1.75mm
Channel Width 1.5mm
Channel Width 1.25mm
Channel Width 1mm
Channel Width 0.75mm
Channel Width 0.5mm

e

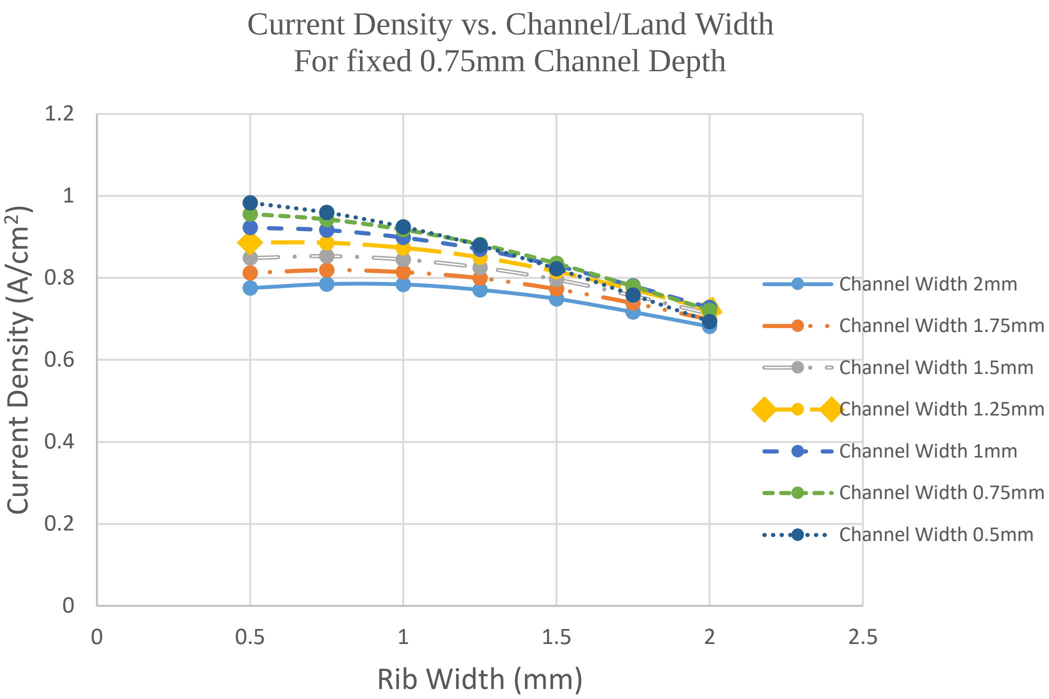

f

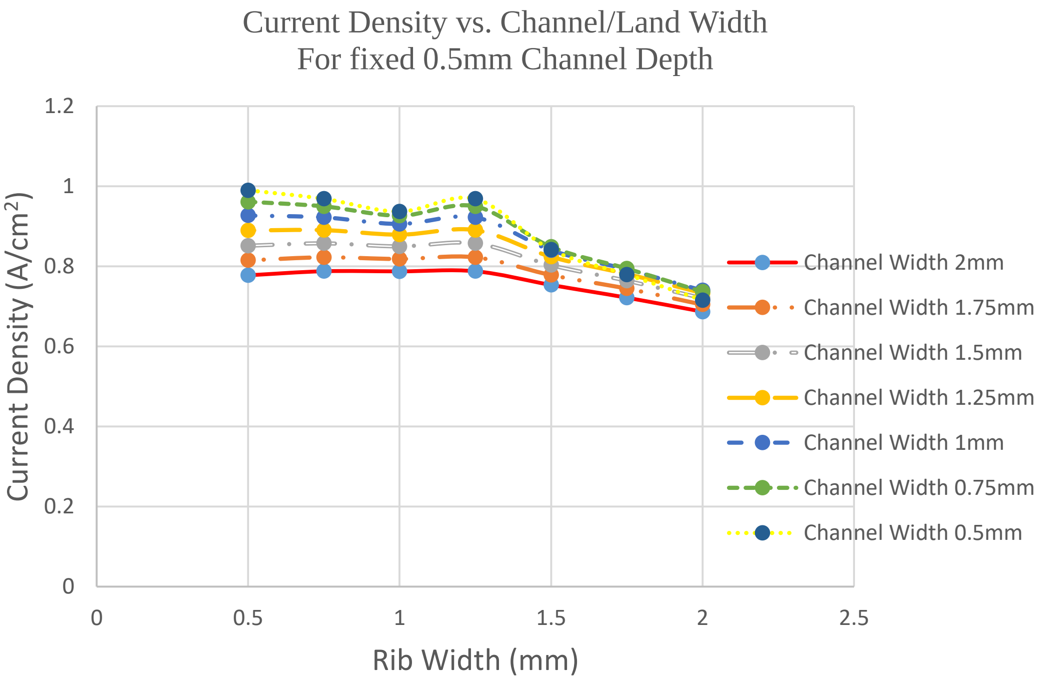

g

Figure 6.1. Variation of the current density with varying channel /rib width change for different constant channel depths of 2.0 - 0.5mm for different case (a) - (g)

6.1.2 Anode pressure drop

The effect of the channel depth, channel width and rib width on the anode pressure drop at an operating voltage of 0.4 V are depicted in Figure 6.2. It is observed that, for a given channel depth and width, the rib width has a negligible effect on the anode pressure drop. On the other hand, the anode pressure drop is found to increase with decreasing the channel dimensions. Moreover, the anode pressure drop becomes noticeable especially for the small channel sizes. This is reasonable since the velocity increases with the decreasing of the channel depth and width.

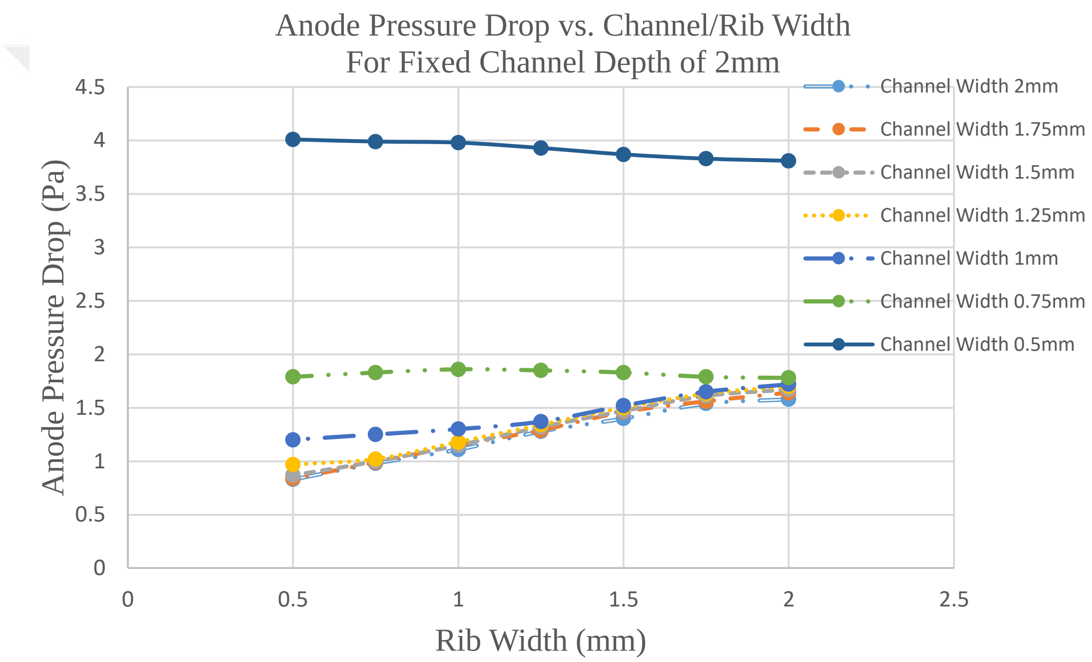

a

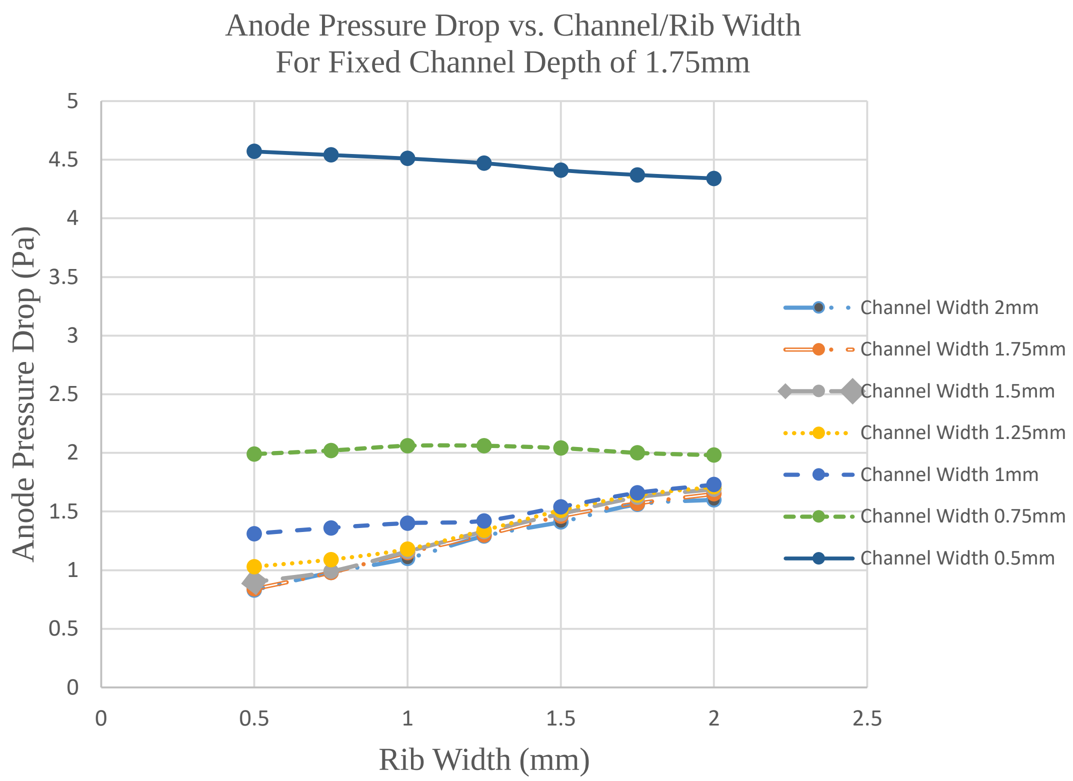
Anode Pressure Drop vs. Channel/Rib Width
For Fixed Channel Depth of 1.75mm
Anode Pressure Drop (Pa)
Rib Width (mm)
Channel Width 2mm
Channel Width 1.75mm
Channel Width 1.5mm
Channel Width 1.25mm
Channel Width 1mm
Channel Width 0.75mm
Channel Width 0.5mm

b

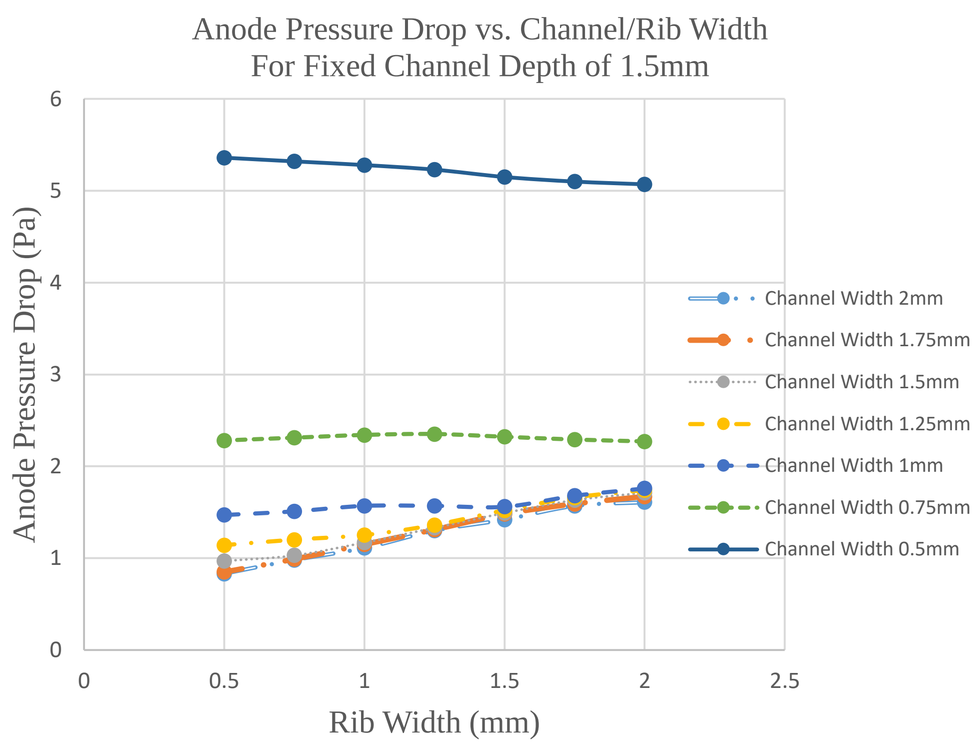
Anode Pressure Drop vs. Channel/Rib Width
For Fixed Channel Depth of 1.5mm
Anode Pressure Drop (Pa)
Rib Width (mm)
Channel Width 2mm
Channel Width 1.75mm
Channel Width 1.5mm
Channel Width 1.25mm
Channel Width 1mm
Channel Width 0.75mm
Channel Width 0.5mm

c

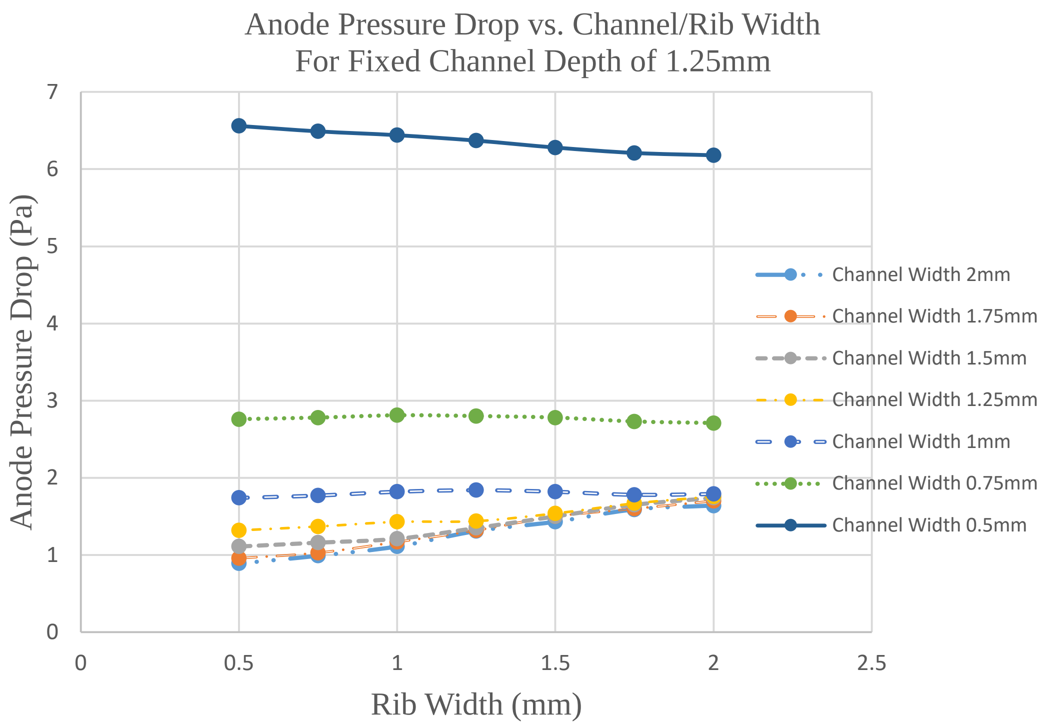

Anode Pressure Drop vs. Channel/Rib Width
For Fixed Channel Depth of 1.25mm
Anode Pressure Drop (Pa)
Rib Width (mm)
Channel Width 2mm
Channel Width 1.75mm
Channel Width 1.5mm
Channel Width 1.25mm
Channel Width 1mm
Channel Width 0.75mm
Channel Width 0.5mm

d

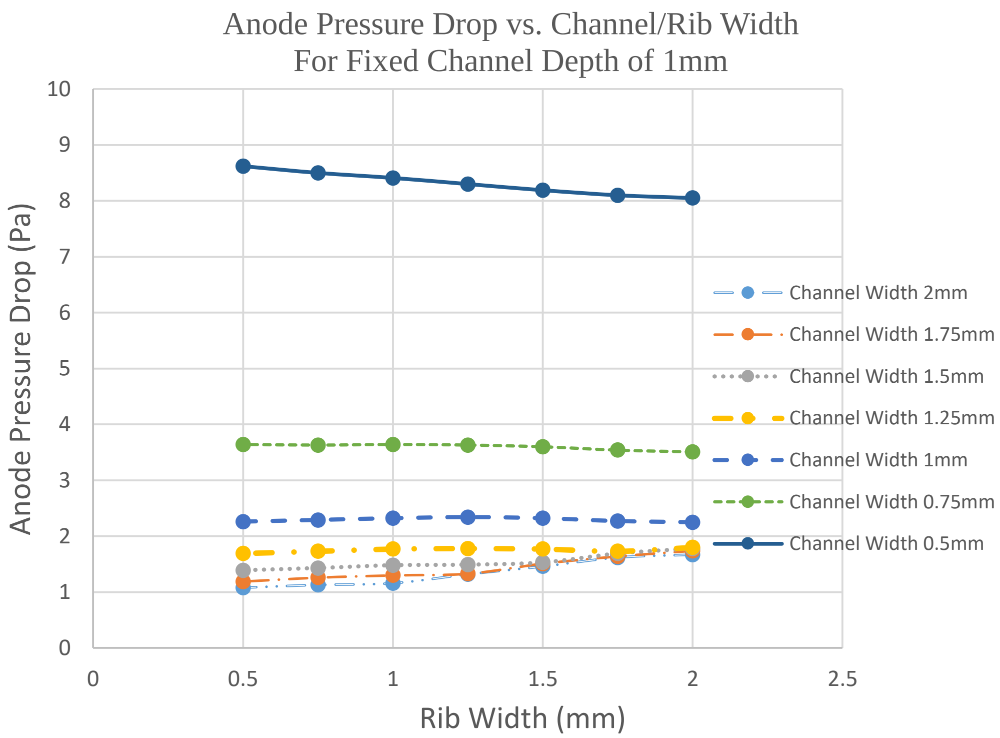

Anode Pressure Drop vs. Channel/Rib Width
For Fixed Channel Depth of 1mm
Anode Pressure Drop (Pa)
Rib Width (mm)
Channel Width 2mm
Channel Width 1.75mm
Channel Width 1.5mm
Channel Width 1.25mm
Channel Width 1mm
Channel Width 0.75mm
Channel Width 0.5mm

e

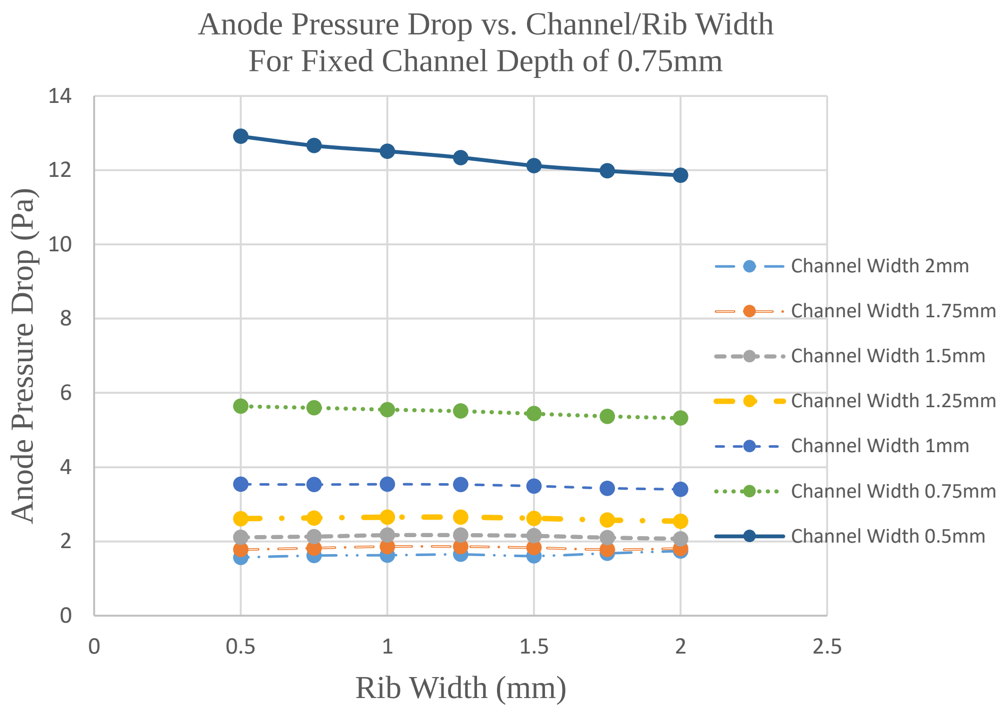

f

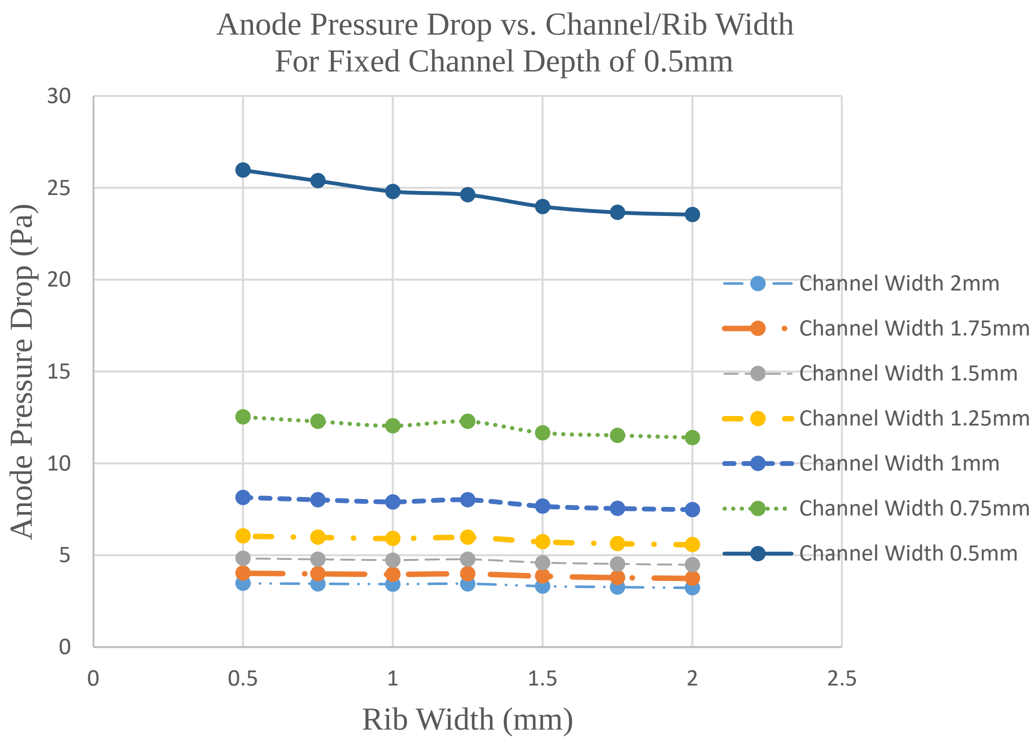

g

Figure 6.2. Variation of the anode pressure drop with varying channel /rib width change for different constant channel depths of 2.0 - 0.5mm for different case (a) - (g)

6.1.3 Cathode pressure drop

For different constant channel depth, variation in cathode pressure drop are shown in Figure 6.3 (a)-(g) with different channel width that changes along with different rib width.

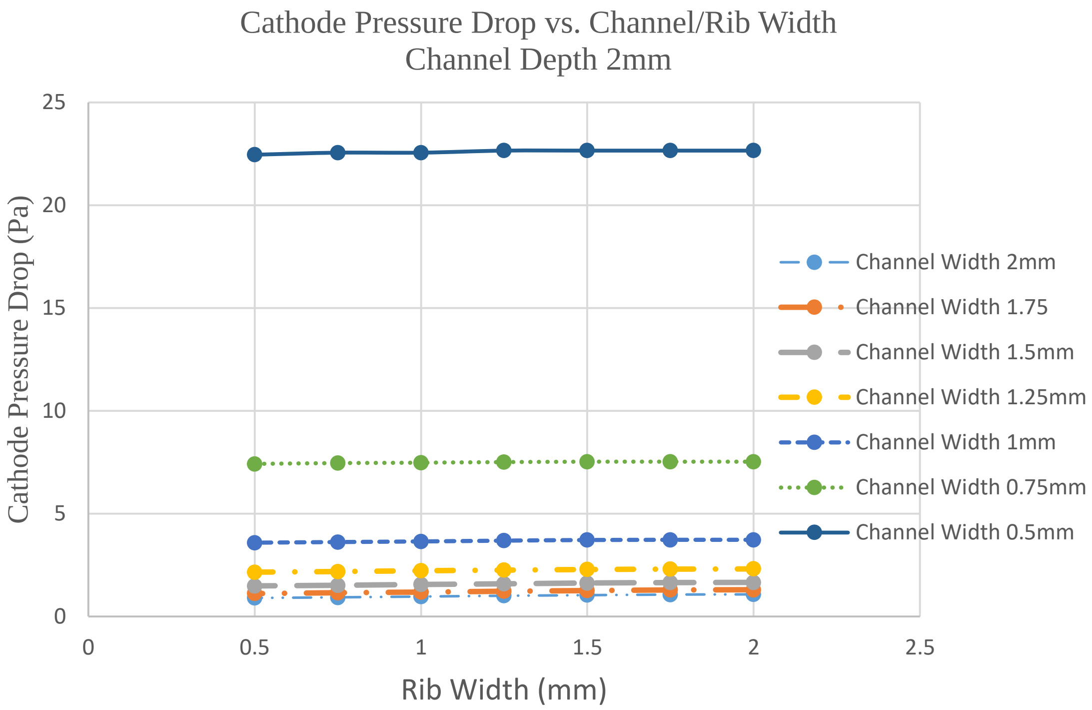

a

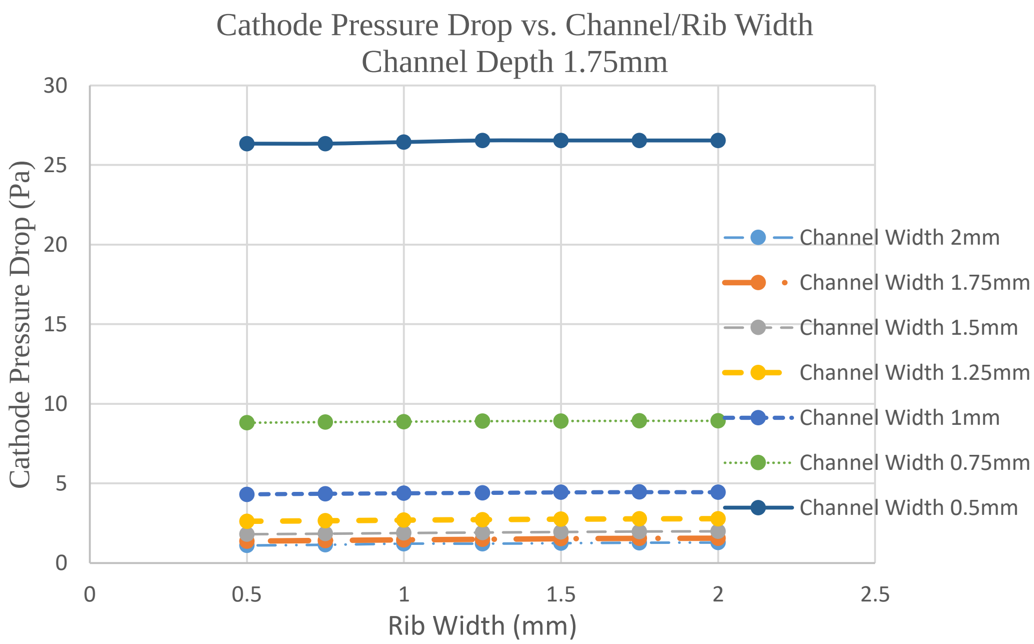

b

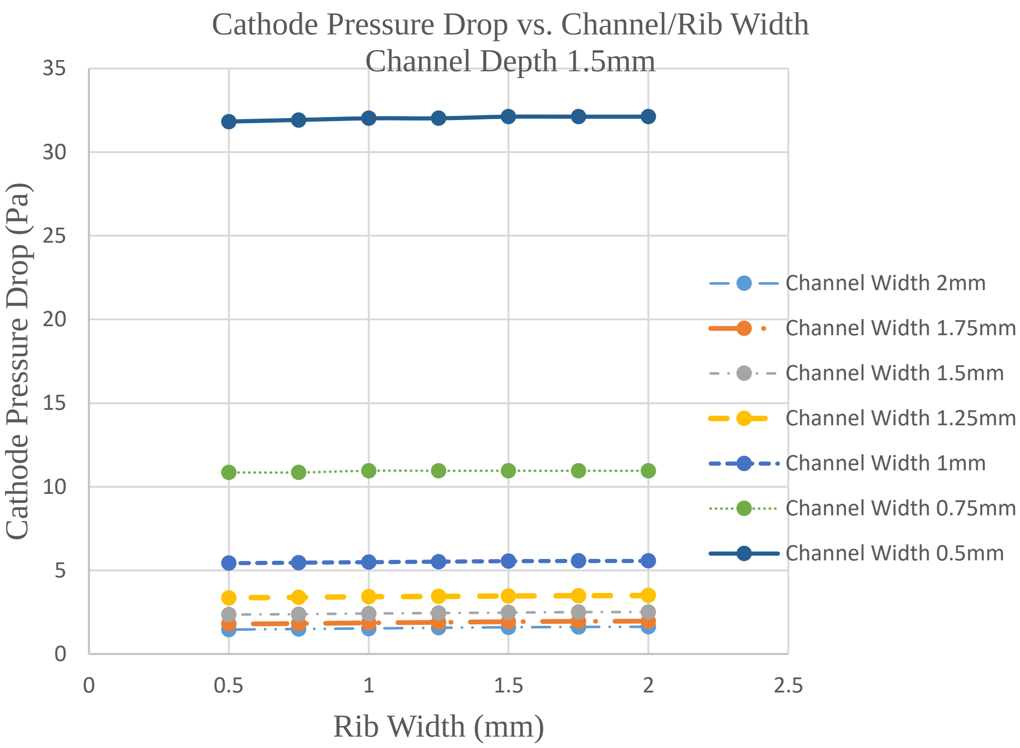
Cathode Pressure Drop vs. Channel/Rib Width
Channel Depth 1.5mm
Cathode Pressure Drop (Pa)
Rib Width (mm)
Channel Width 2mm
Channel Width 1.75mm
Channel Width 1.5mm
Channel Width 1.25mm
Channel Width 1mm
Channel Width 0.75mm
Channel Width 0.5mm

c

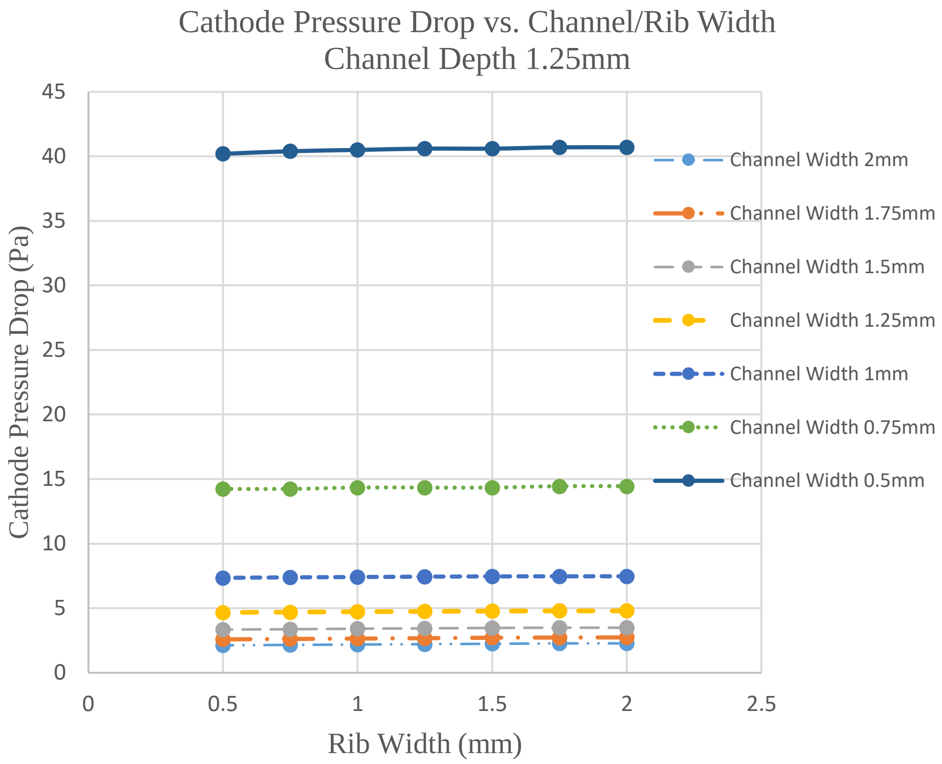
Cathode Pressure Drop vs. Channel/Rib Width
Channel Depth 1.25mm
Cathode Pressure Drop (Pa)
Rib Width (mm)
Channel Width 2mm
Channel Width 1.75mm
Channel Width 1.5mm
Channel Width 1.25mm
Channel Width 1mm
Channel Width 0.75mm
Channel Width 0.5mm

d

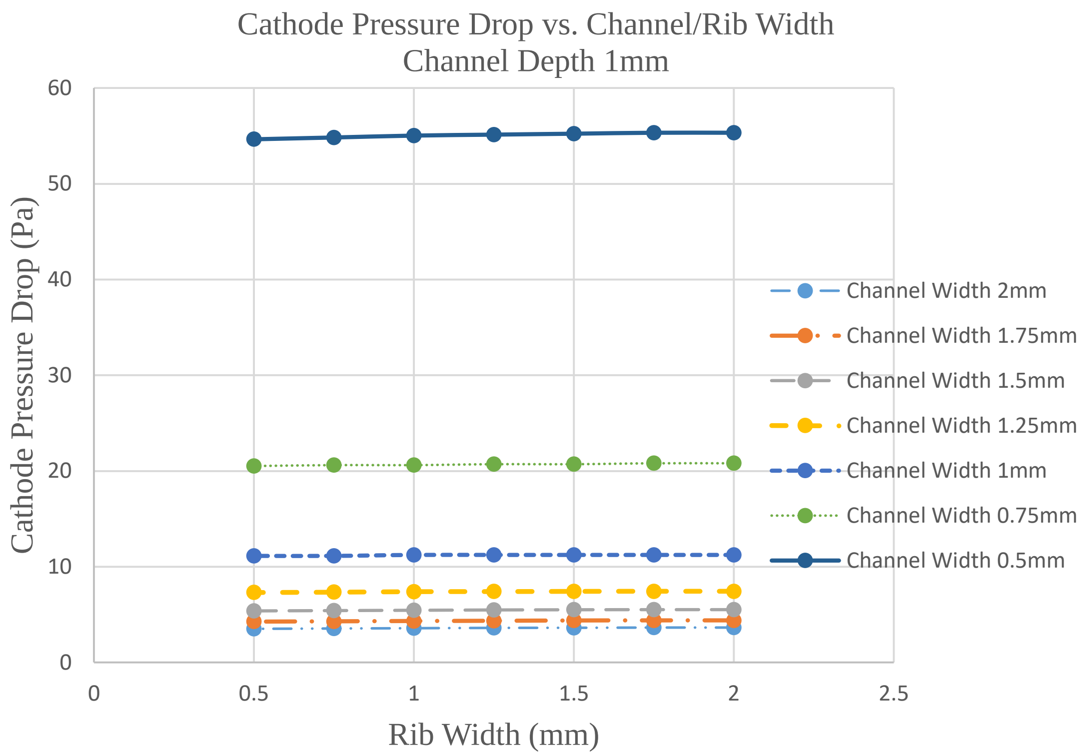

Cathode Pressure Drop vs. Channel/Rib Width
Channel Depth 1mm
Cathode Pressure Drop (Pa)
60
50
40
30
20
10
0
0
0.5
1
1.5
2
2.5
Rib Width (mm)
Channel Width 2mm
Channel Width 1.75mm
Channel Width 1.5mm
Channel Width 1.25mm
Channel Width 1mm
Channel Width 0.75mm
Channel Width 0.5mm

e

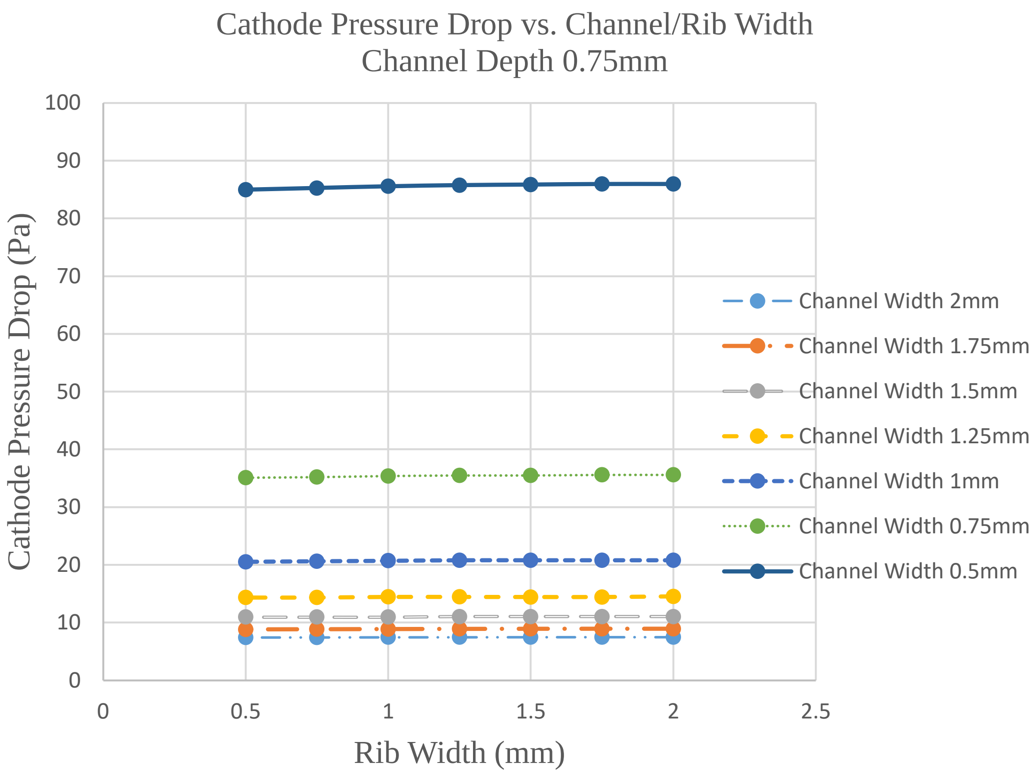

Cathode Pressure Drop vs. Channel/Rib Width
Channel Depth 0.75mm
Cathode Pressure Drop (Pa)
100
90
80
70
60
50
40
30
20
10
0
0
0.5
1
1.5
2
2.5
Rib Width (mm)
Channel Width 2mm
Channel Width 1.75mm
Channel Width 1.5mm
Channel Width 1.25mm
Channel Width 1mm
Channel Width 0.75mm
Channel Width 0.5mm

f

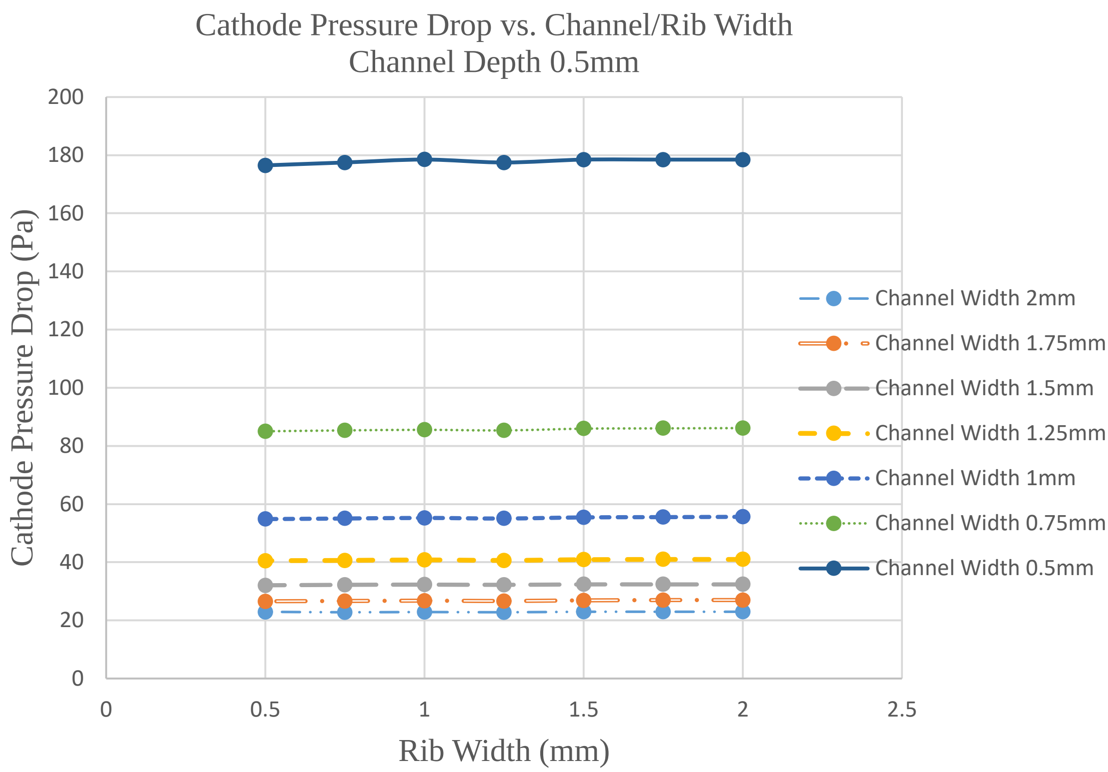

g

Figure 6.3. Variation of the cathode pressure drop with varying channel /rib width change for different constant channel depths of 2.0 - 0.5mm for different case (a) - (g)

Similar to the results for the anode pressure drop, the rib width is found to be ineffective for the cathode pressure drop as expected. Similarly, the cathode pressure drop seems to be strongly depended on the channel depth and width especially when they are lower than 1.0 mm. From the results, it can be observed that, a cathode pressure drop of 178 Pa is predicted for the 25 mm straight channel when all other dimensions are set to 0.5 mm whereas under the same conditions the corresponding anode pressure drop is found to be only 26 Pa. This can be explained for the defined cathode flow rate which is three times higher than that of the anode, yielding higher cathode velocities in the same order for a given channel cross-section. Although the friction coefficients and fluid properties are different, one can expect a higher pressure drop in the cathode channel. This is confirmed by the numerical results obtained from all cases.

6.1.4 Geometry optimization

For the geometry optimization, the cases of current density and pressure drop have been scrutinized. A suitable channel geometry for PEMFC should have neither high pressure drop nor low current density. From the previous case studies, two points are obvious: (1) rib width has no pressure drop effect and (2) the anode pressure drop is negligible compared to the cathode pressure drop. Meanwhile, each of the geometric parameter has noticeable consequences on the current density. Contemplating on all of these issues, maximum and minimum cases of pressure drops as well as current density are analyzed for a suitable channel geometry.

The final geometry is selected such that the cell should provide an acceptable power density along with a moderate pressure drop as well as compact geometry. The selected case studies of the numerical results for the geometry optimization for the maximum and minimum of the cell current density, anode and cathode pressure drop along with the optimization case that are considered for pressure drop analyses. The results of the analyses together with the selected dimensions are summarized in Table 6.1 for the optimization of channel geometry.

The maximum current density of 0.99 A/cm^2 is found for the channel geometry of 0.5 mm for the channel depth, width and rib width case. But in this case, high cathode pressure drop occurred which is about 177 Pa. On the other hand, if the lower pressure drop is considered from the numerical results, which is as low as 1.0 Pa and is highly considerable as the channel pressure drop for the suitable geometry. But the corresponding current density for this case is only 0.76 A/cm^2, which is not considerable. Also the channel depth and width of 2.0 mm is not suitable for compact PEMFC cell. So further looking into the numerical results, it is observed that, for the channel depth of 1.0 mm, channel width of 1.0 mm and rib width of 0.5 mm case, the current density is 0.92 A/cm^2 and the corresponding anode and cathode pressure drop are 2 Pa and 11 Pa respectively, which has the expected cell performance along with considerable pressure drop as well as having a compact channel geometry. Therefore, from the channel geometry optimization analyses, it is decided that, the channel depth of 1.0 mm, channel width of 1.0 mm and rib width of 0.5 mm are the most suitable dimensions considering the cell current density and pressure drop.

Table 6.1. Channel geometry optimization analysis

Case	Channel Geometry ($C_d/C_w/R_w$) mm	Pressure Drop (Anode/Cathode) Pa	Current Density A/cm^2	Summary
Min. Current Density	2/0.5/2	3.81/22.65	0.61	Current density lower side and cathode pressure drop higher side
Min. Pressure Drop	2/2/0.5	0.83/0.89	0.76	Current density in lower side
Max. Current Density and Pressure Drop	0.5/0.5/0.5	25.96/176.49	0.99	Anode and cathode pressure drop are very high
Selected Case	1/1/0.5	2.26/11.15	0.92	Considerable pressure drop with high current density

6.2 Conventional Flow Field Pattern Analysis

Among the quite few flow field patterns developed, parallel and serpentine flow field patterns are the most widely investigated for research and development as well as for wide spread industrial usage. That's why these two field patterns are chosen for this numerical study. Further a comparative analyses between parallel and serpentine flow fields considering pressure drop, mass transport and cell performance are performed. Three dimensional models having 2 cm^2 active area are considered. From the geometry optimization, the channel depth, width and rib dimensions obtained as 1.0 mm, 1.0 mm and 0.5 mm, respectively are used for the numerical comparison of the conventional parallel and serpentine flow fields.

6.2.1 Species distribution

In the anode, hydrogen and water vapor mixture are the transported species whereas oxygen, nitrogen and water vapor mixture are transported in the cathode channel. The major concerning species for the PEMFC cell performance are hydrogen and oxygen for anode and cathode respectively. Therefore, the mass fraction of hydrogen and oxygen are analyzed at an operating voltage of 0.4 V, since the maximum cell performance is achieved at this condition. The hydrogen mass fractions along the anode flow channel obtained for parallel and serpentine flow fields are compared in Figure 6.4.

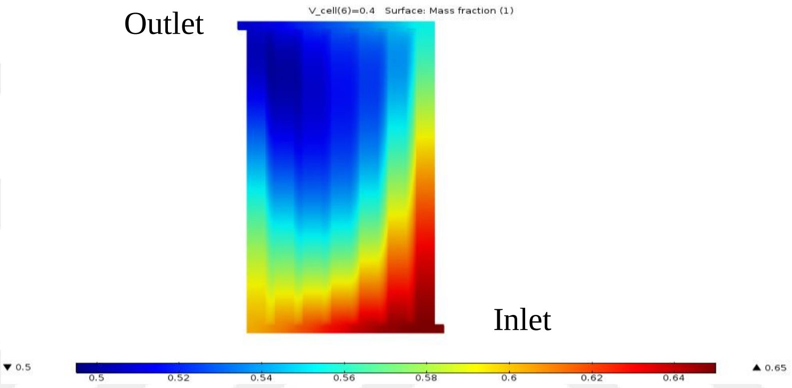

a

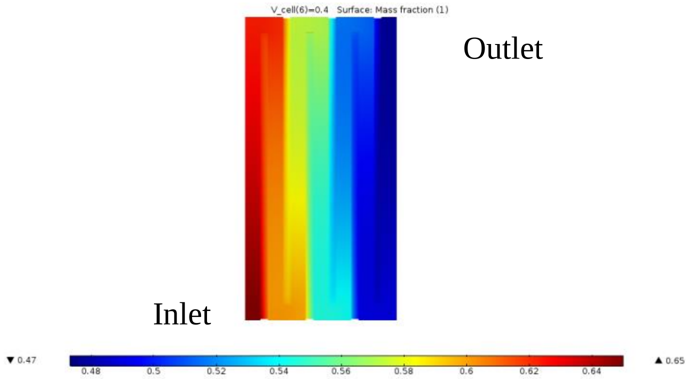

b

Figure 6.4. Hydrogen mass fraction distribution in parallel (a) and serpentine (b) FFP

The hydrogen concentration tends to decrease from inlet to outlet for both flow fields as expected due to the continuous consumption for the anode electrochemical reaction. However, the distribution of hydrogen along the flow field were almost homogenous for both parallel and serpentine. So there were enough flow rate for hydrogen to be uniformly distributed along the flow fields.

For the cathode channel, oxygen mass fraction distribution are illustrated in Figure 6.5, for both parallel and serpentine flow field pattern.

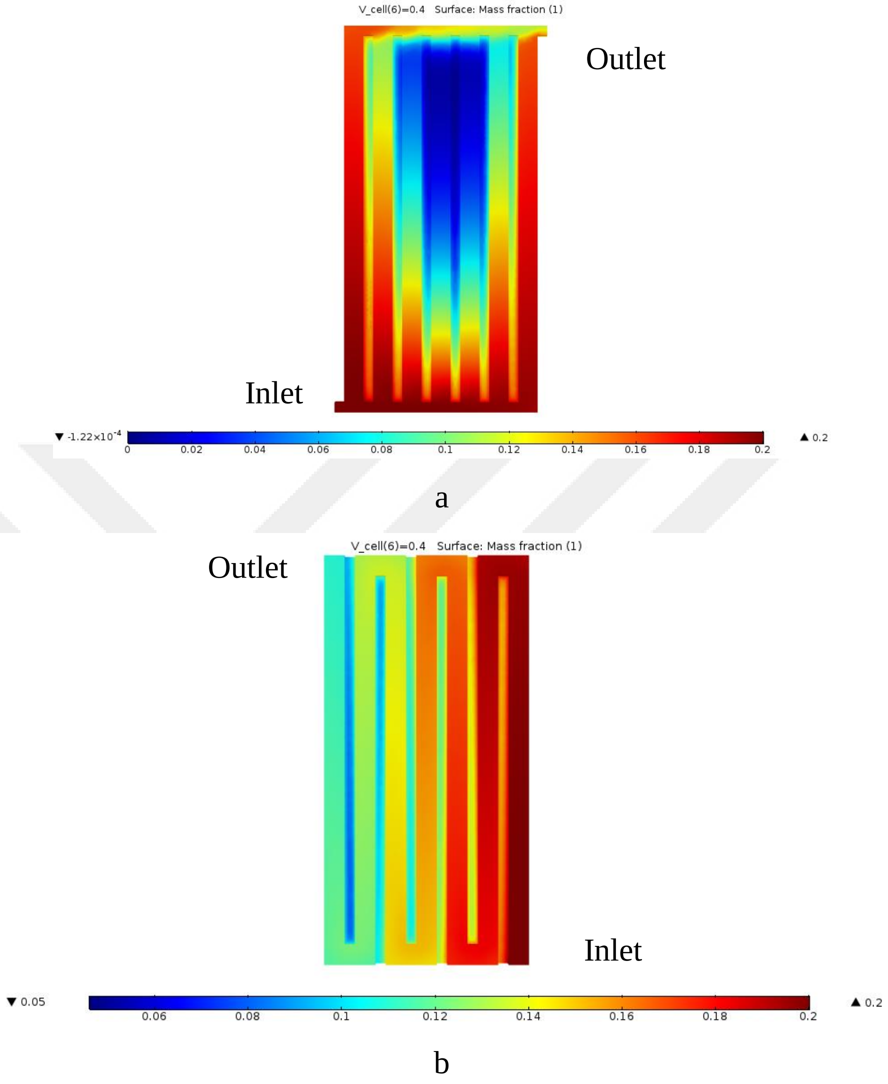

Figure 6.5. Oxygen mass fraction distribution in parallel (a) and serpentine (b) FFP

From the numerical results, it can be observed that, unlike reactants distribution in anode, oxygen is not homogeneously distributed along the cathode channel. This is due the phenomenon of the complex gas mixture and low mass fraction of oxygen in the cathode channel. In parallel flow field pattern, oxygen has mal distribution especially in the middle parallel channels, whereas in the serpentine flow field, distribution of oxygen is more uniform than parallel without any mal-distribution.

6.2.2 Pressure drop

Pressure distribution for the anode and cathode channels in the parallel flow field pattern are depicted in Figure 6.6.

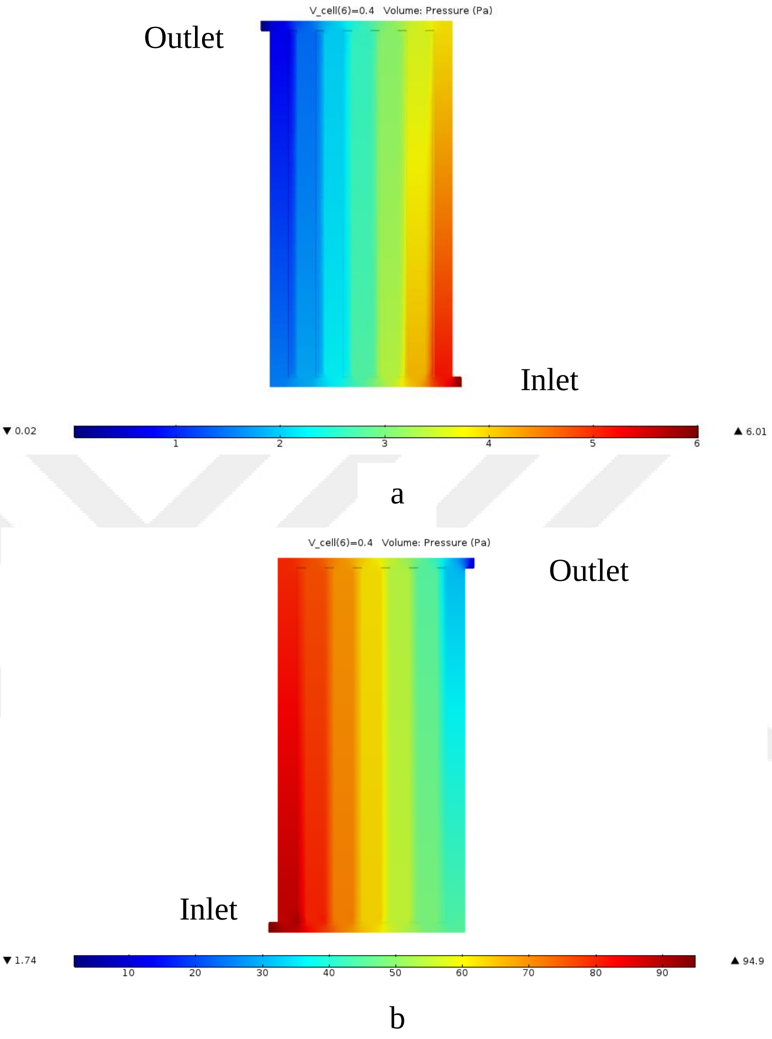

Figure 6.6. Pressure drop in parallel flow field for anode (a) and cathode (b) channels

It can be observed that the anodic pressure drop is very low compared to the cathode side. The anode pressure distribution are more uniform throughout the flow field, whereas for the cathode side, the adjacent inlet channels have uniform pressure distribution, while in proceeding channels high pressure drop occurred.

On the other hand, in the serpentine flow field pattern, the pressure drop was much higher for both anode and cathode than the parallel flow field pattern as given in Figure 6.7. Especially the cathode pressure drop is noticeable.

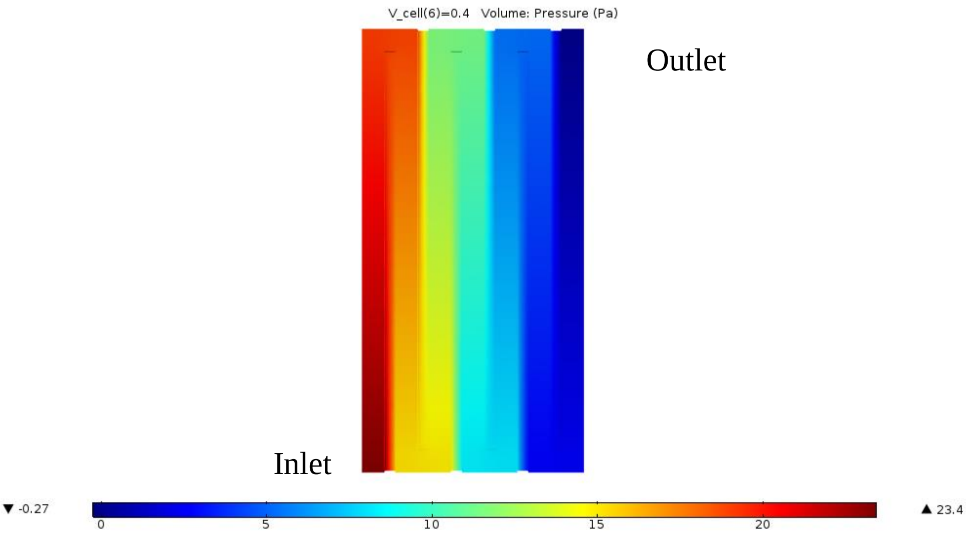

a

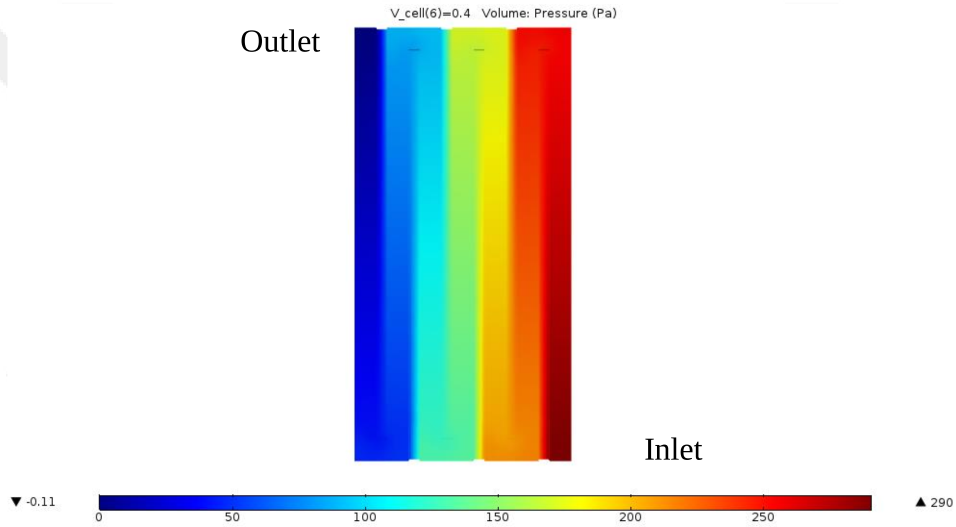

b

Figure 6.7. Pressure drop in serpentine flow field for anode (a) and cathode (b) channels

6.2.3 Water management

The variation of the water mass fraction in the anode and cathode flow channels predicted for parallel and serpentine flow fields are illustrated in Figure 6.8 and Figure 6.9, respectively.

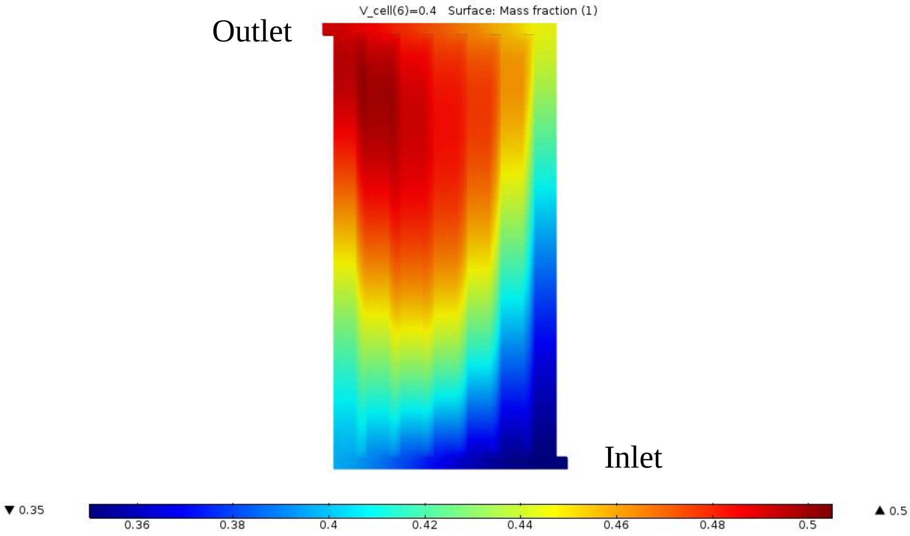

a

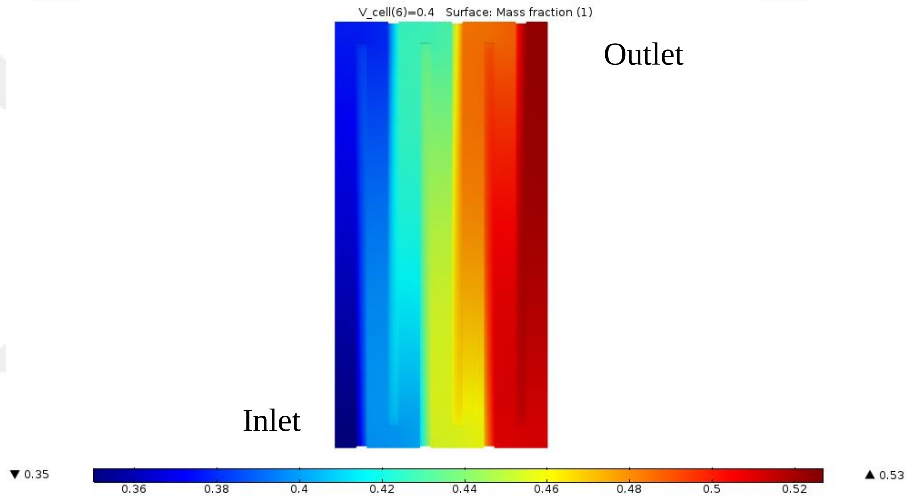

b

Figure 6.8. Water distribution in anode channels of parallel (a) and serpentine (b)

It is seen that in the anode channels for the both flow fields, water mass fraction increases from the inlet to outlet. This behavior is reasonable since hydrogen in the anode channel is consumed due to the electrochemical reaction, leading to an increased water mass fraction.

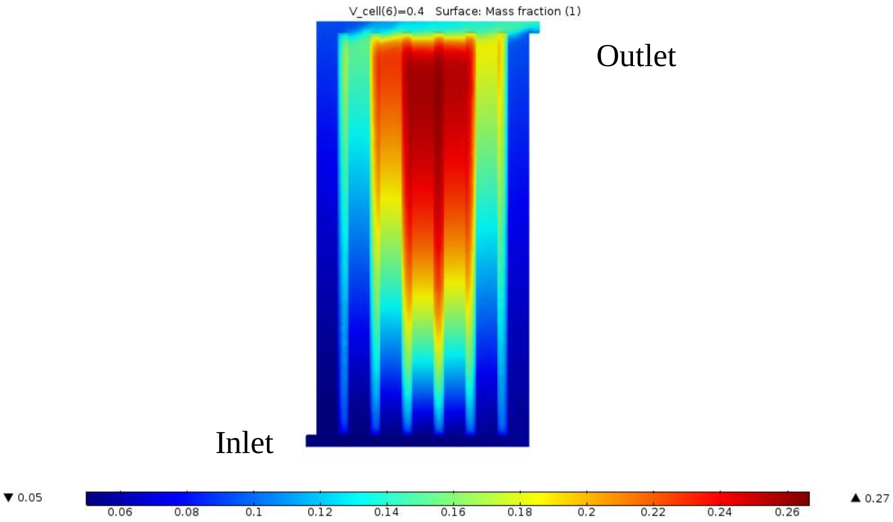

a

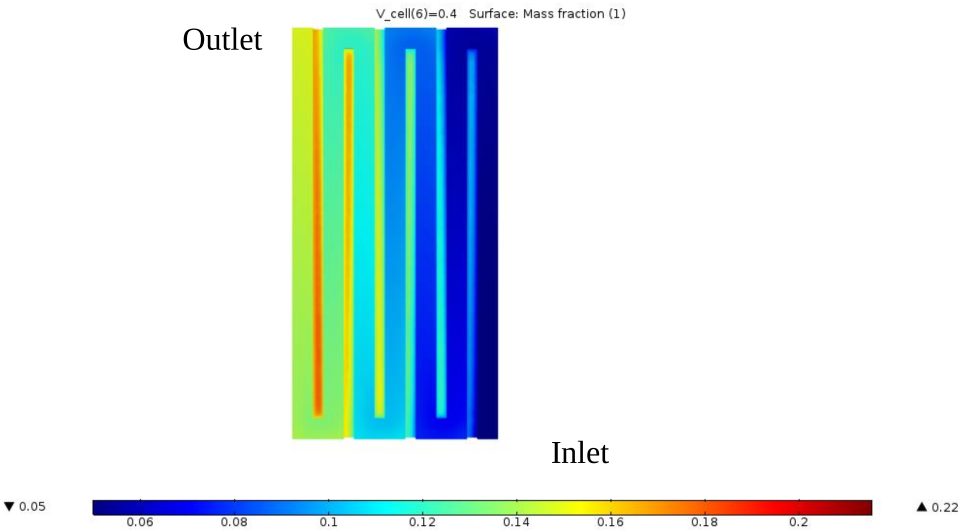

b

Figure 6.9. Water distribution in cathode channels of parallel (a) and serpentine (b)

A similar behavior can be observed also in the cathode flow channels for the both flow fields. On the other hand, the increase in the water mass fraction in this case, is not only due to the oxygen consumption but also due to the water generated from the cathode electrochemical reaction.

6.2.4 Cell performance

The performance comparison of the cells with parallel and serpentine flow fields is depicted in Figure 6.10. From the numerical results, the serpentine flow field has relatively higher cell performance than parallel flow field, which is also indicated in the literature.

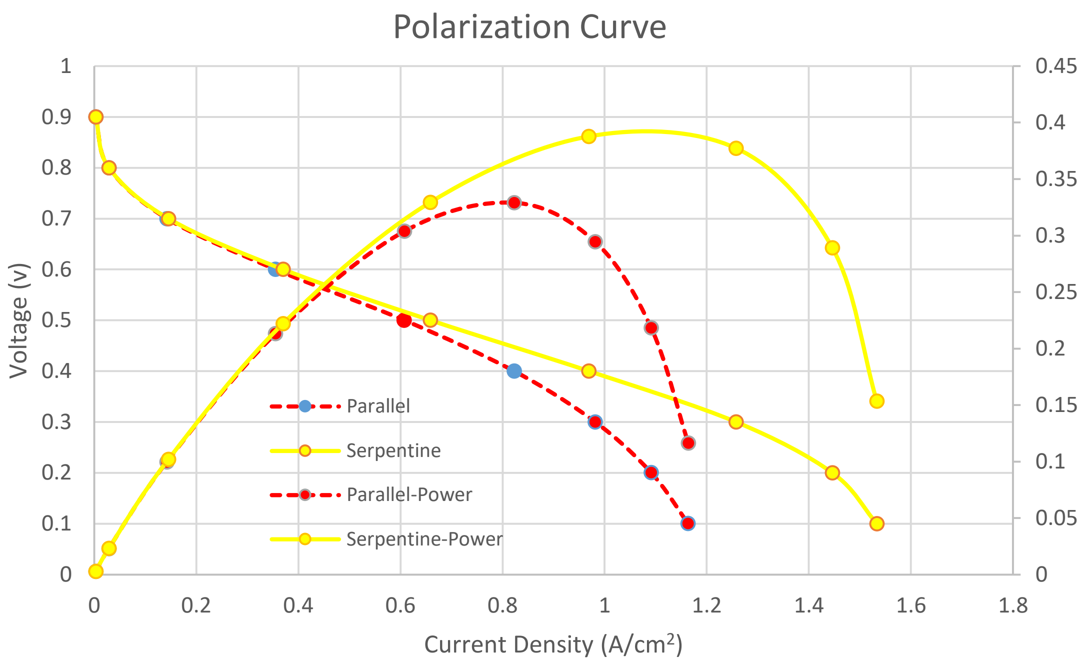

Figure 6.10. Comparison between serpentine and parallel flow field pattern Polarization curve and Power density at 80 ºC cell temperature and 100%RH

6.3 Investigation of Convergent and Divergent Flow Fields

Innovative convergent and divergent flow field patterns are experimentally investigated as explained in chapter 3 and 4. In the experimental study, the channel depth is taken as a bit higher dimensions, which is not practical for PEM fuel cell compact stack design. For this reason, the channel dimensions are considered similar to the conventional designs in line with the literature and the geometry optimization carried out numerically in the previous sections. Like the experimental study as described before, the same convergent flow field is the divergent flow field as well by switching in between the inlet and outlet. For this case study, both parallel and serpentine flow field pattern are modified with the convergent and divergent concept. The parameters of the validated numerical model are introduced to ensure the accuracy of the results. The parallel and serpentine flow field pattern modified by convergent and divergent design techniques. The modified convergent and divergent serpentine and parallel flow field patterns that are numerically studied in this thesis works are described in the previous chapter**.**

6.3.1 Species distribution

The hydrogen mass fraction distributions along the different convergent and divergent parallel flow fields are shown in Figure 6.11. For the convergent parallel flow fields, the hydrogen distribution and flow become more dominant at the adjacent inlet channels. Another noticeable thing is that hydrogen mass fraction density decreases in the outlet section with the increase of convergence due to the increasing consumption of hydrogen.

For divergent parallel flow field case, the hydrogen flow through inlet manifold to the outer most parallel channel become more prominent with the increase of divergence. The low dense reactant region also transfer from the mid channel to the inner corner of the outlet manifold with the increase of divergence.

For serpentine convergent and divergent flow field, the hydrogen mass distribution is shown in Figure 6.12. For the convergent serpentine cases, the hydrogen distribution along the channel path seems to be improved with the increase in the convergence from inlet to outlet channel depth. For the divergent serpentine flow field case, hydrogen concentration increased in the inlet adjacent area by higher sub rib convection as the divergence increase from inlet to the outlet along the channel depth.

The oxygen mass fraction distribution along the different convergent and divergent parallel flow fields is shown in Figure 6.13. For the convergent parallel flow fields, the oxygen distribution and flow become more dominant in the inner most inlet channels which passes through exit manifold with the increase of convergence. The most important point is that, lower dense oxygen mass fraction region is reduced with the increase of the convergence.

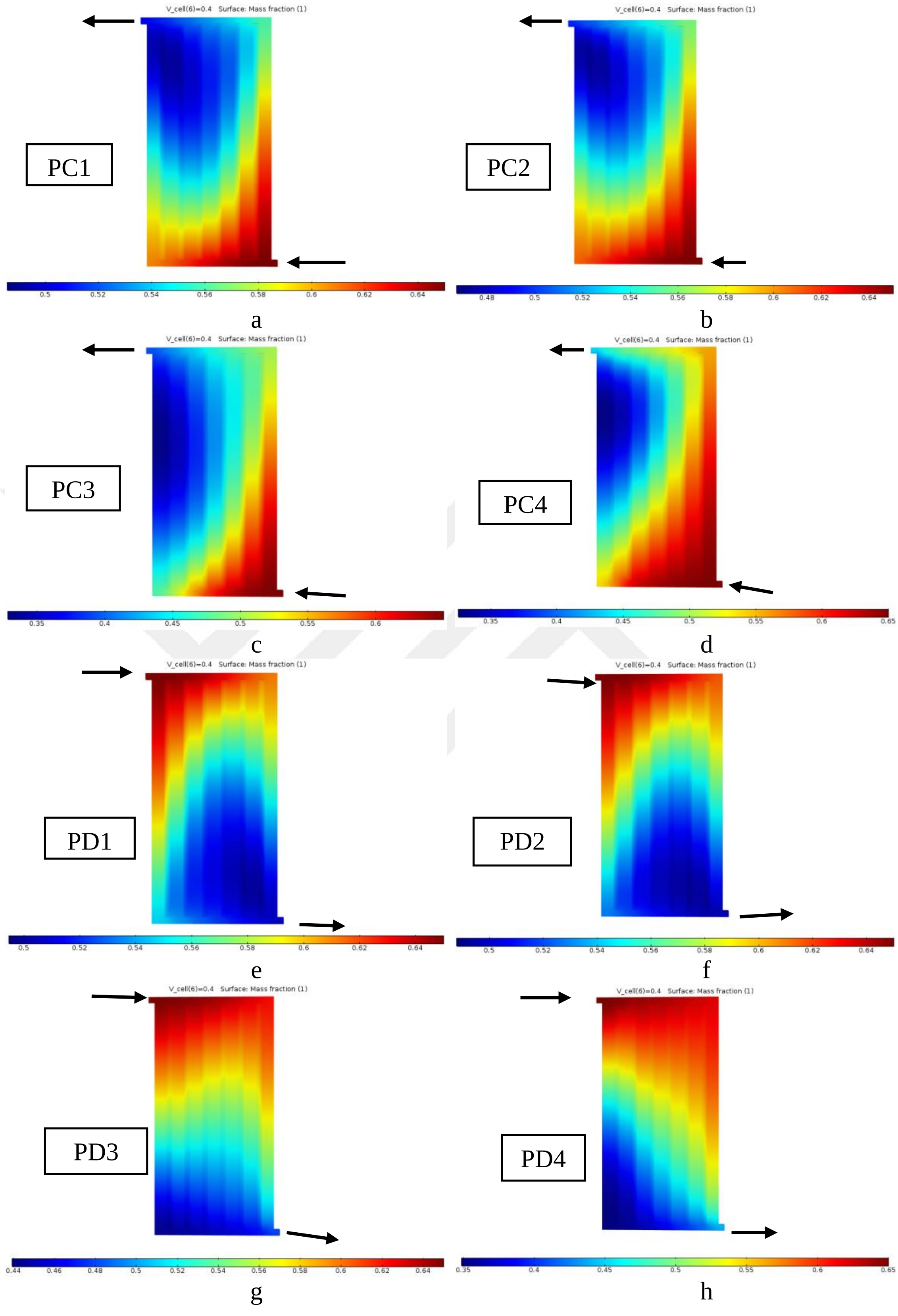

Figure 6.11. Hydrogen mass fraction distribution in different parallel convergent (a)-(d) and divergent flow field patterns (e)-(h)

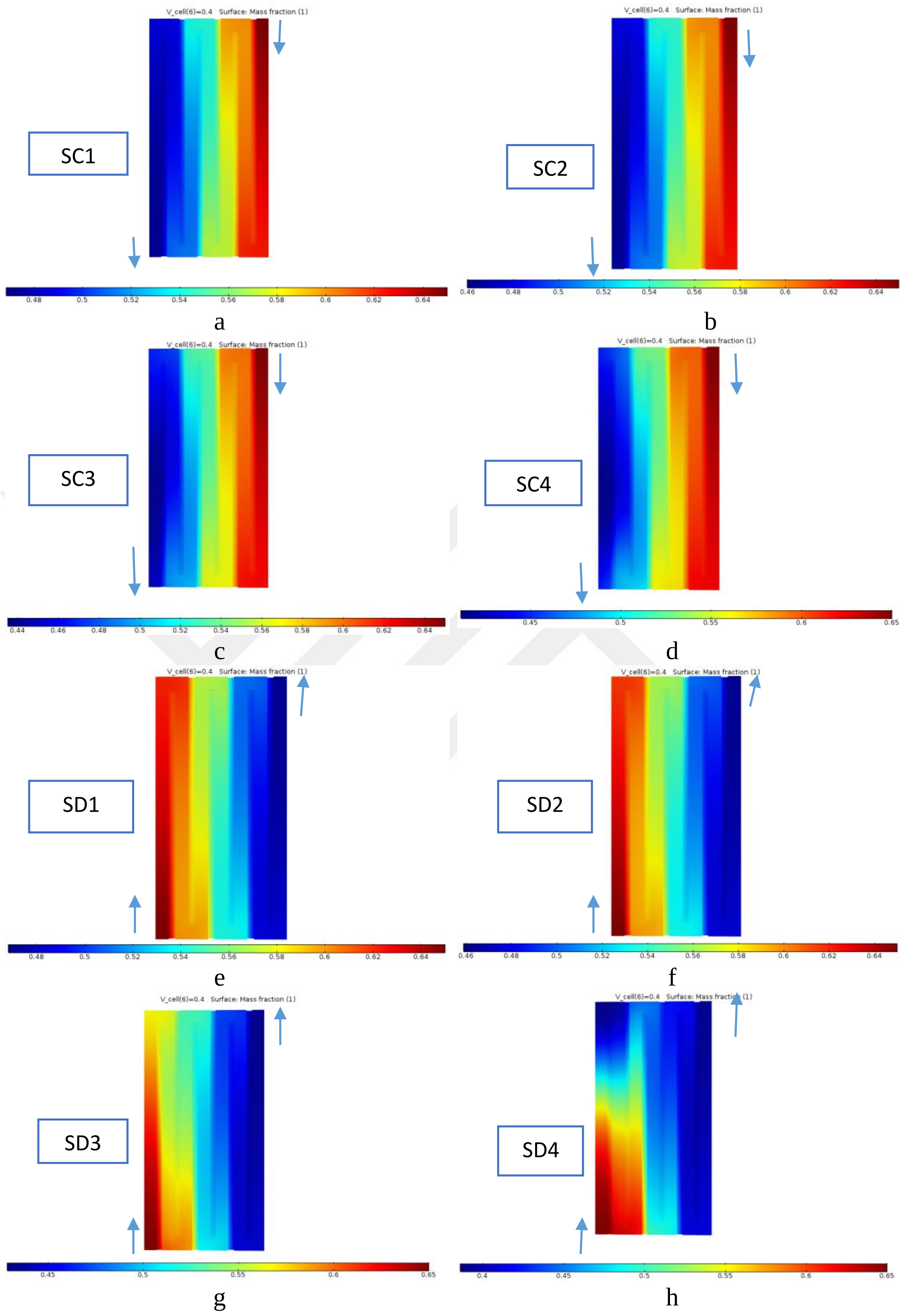

Figure 6.12. Hydrogen mass fraction distribution in different serpentine convergent (a)-(d) and divergent flow field patterns (e)-(h)

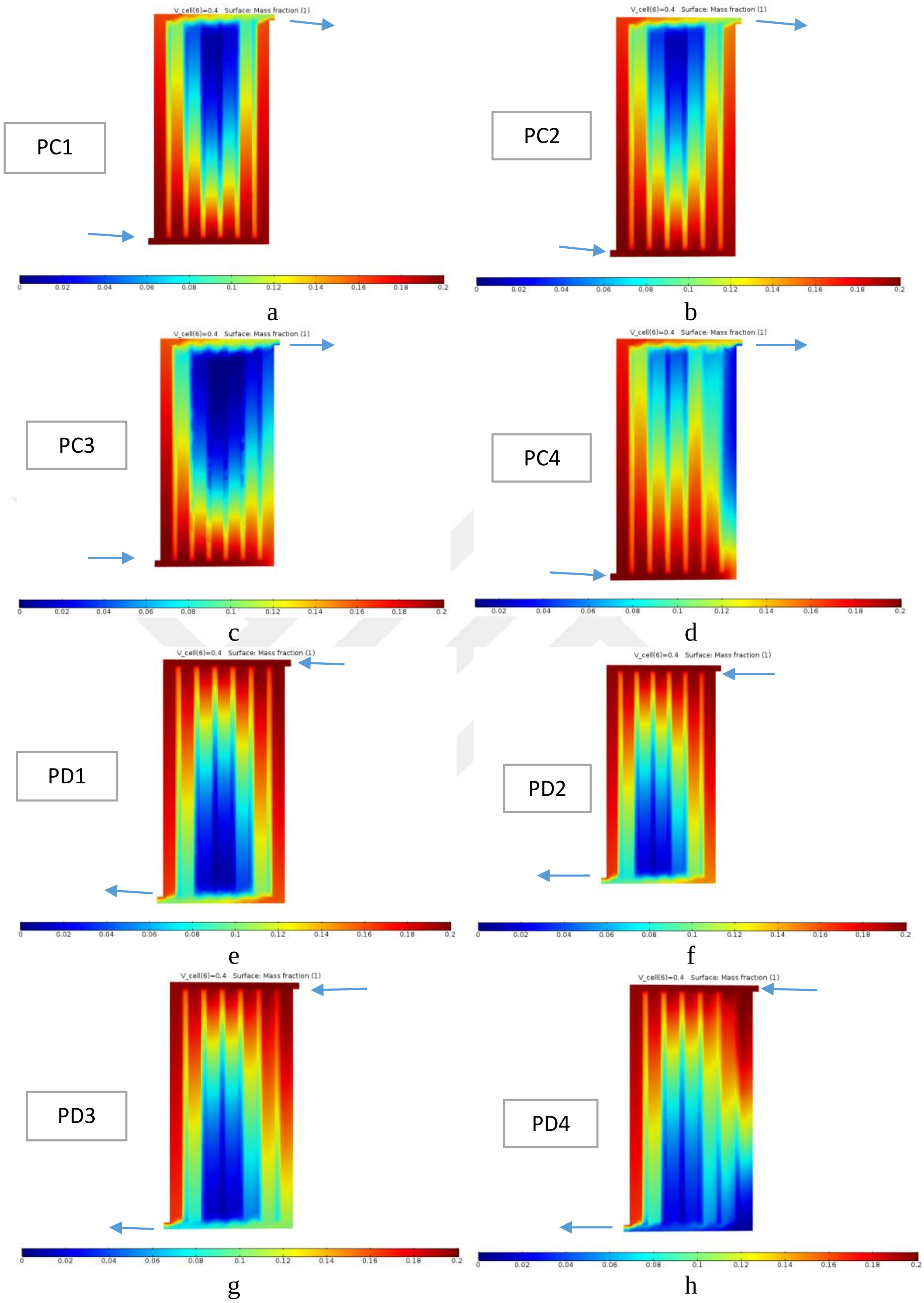

Figure 6.13. Oxygen mass fraction distribution in different parallel convergent (a)-(d) and divergent flow field patterns (e)-(h)

For divergent parallel flow field case, the oxygen flow through inlet manifold to the inner most parallel channel becomes more prominent with the increase of divergence. The low dense reactant region increases from the mid channel to the inner corner of the outlet manifold with the increase of divergence.

The oxygen mass fraction distribution along the different convergent and divergent serpentine flow fields is demonstrated in Figure 6.14. For the convergent serpentine flow fields, the oxygen concentration has a decreasing trend in the outer most channel with the increase of convergence. In the case of divergent serpentine flow field patterns, for extreme divergence case oxygen concentration is more at the inlet zone basically due to the sub rib convection while overall reactant concentration uniformity is reduced with the increase in the divergence.

6.3.2 Pressure drop analysis

The anodic pressure drop for different types of convergent and divergent parallel flow field patterns is depicted in Figure 6.15. The anode side pressure drop is found to be very low for both convergent and divergent parallel flow fields except for the extreme convergence and divergence cases.

In the extreme case of convergence and divergence parallel flow fields, there is a high pressure drop occurred at the outlet compared to that of the inlet while in the former case the high reactant pressure exists throughout the flow field. For the serpentine convergent and divergent flow field, the pressure distribution in the anode channels is demonstrated in Figure 6.16.

The anode pressure drop increases with the increase in convergence and divergence from inlet to outlet along with the channel depth. For both convergent and divergent cases, the pressure drop mainly occurred in the channel outlet and inlet sections, respectively and it becomes more prominent with the increase of the convergence and divergence. The cathode pressure drop of convergent and divergent flow fields for parallel are shown in Figure 6.17. The cathode pressure distribution characteristics are similar to the anode pressure distribution of the parallel flow field. The pressure drop increases with the increase of the convergence and divergence of the different parallel flow field patterns. Also high pressure zones again exist in the extreme convergent and divergent cases.

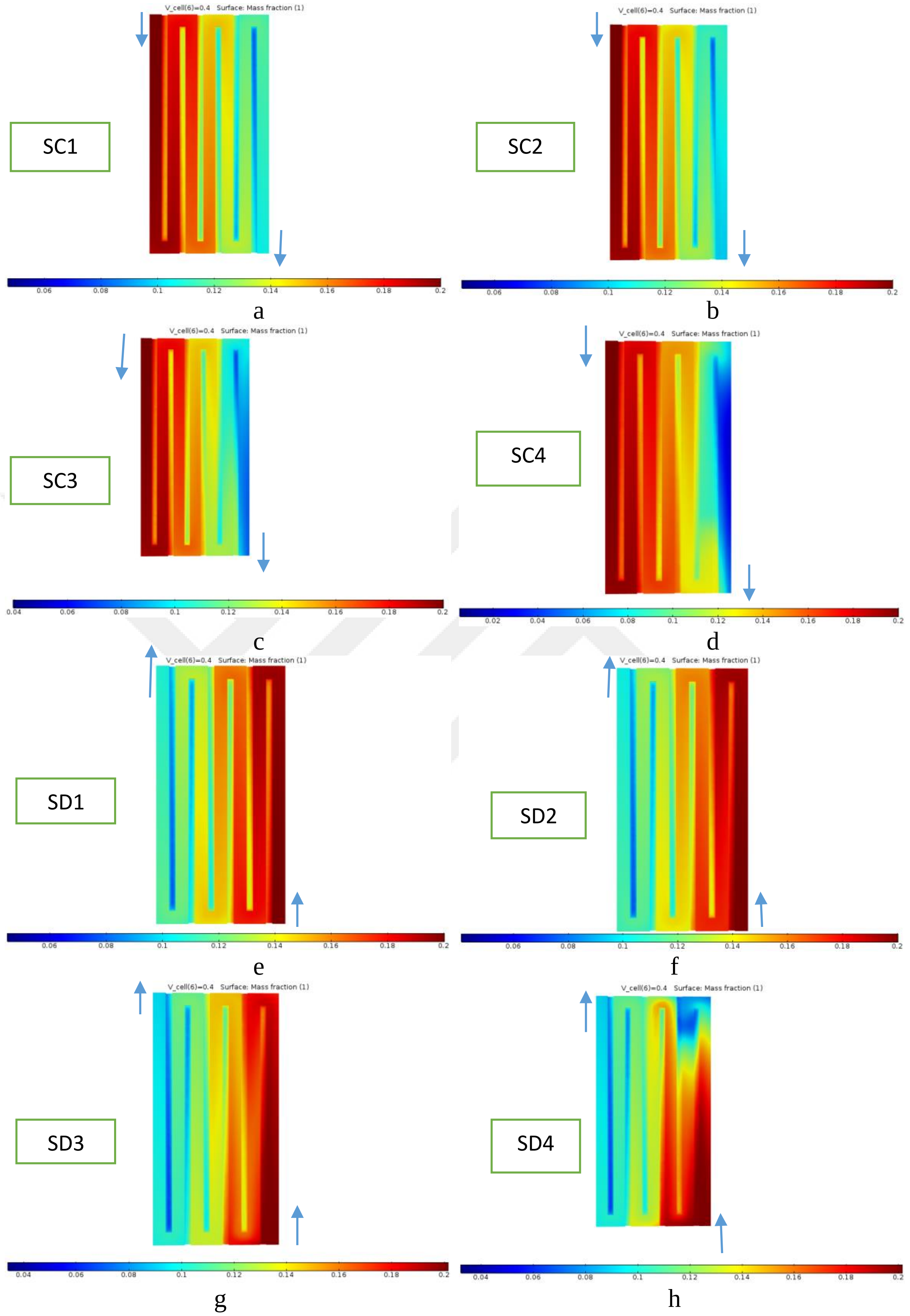

Figure 6.14. Oxygen mass fraction distribution in different serpentine convergent (a)-(d) and divergent flow field patterns (e)-(h)

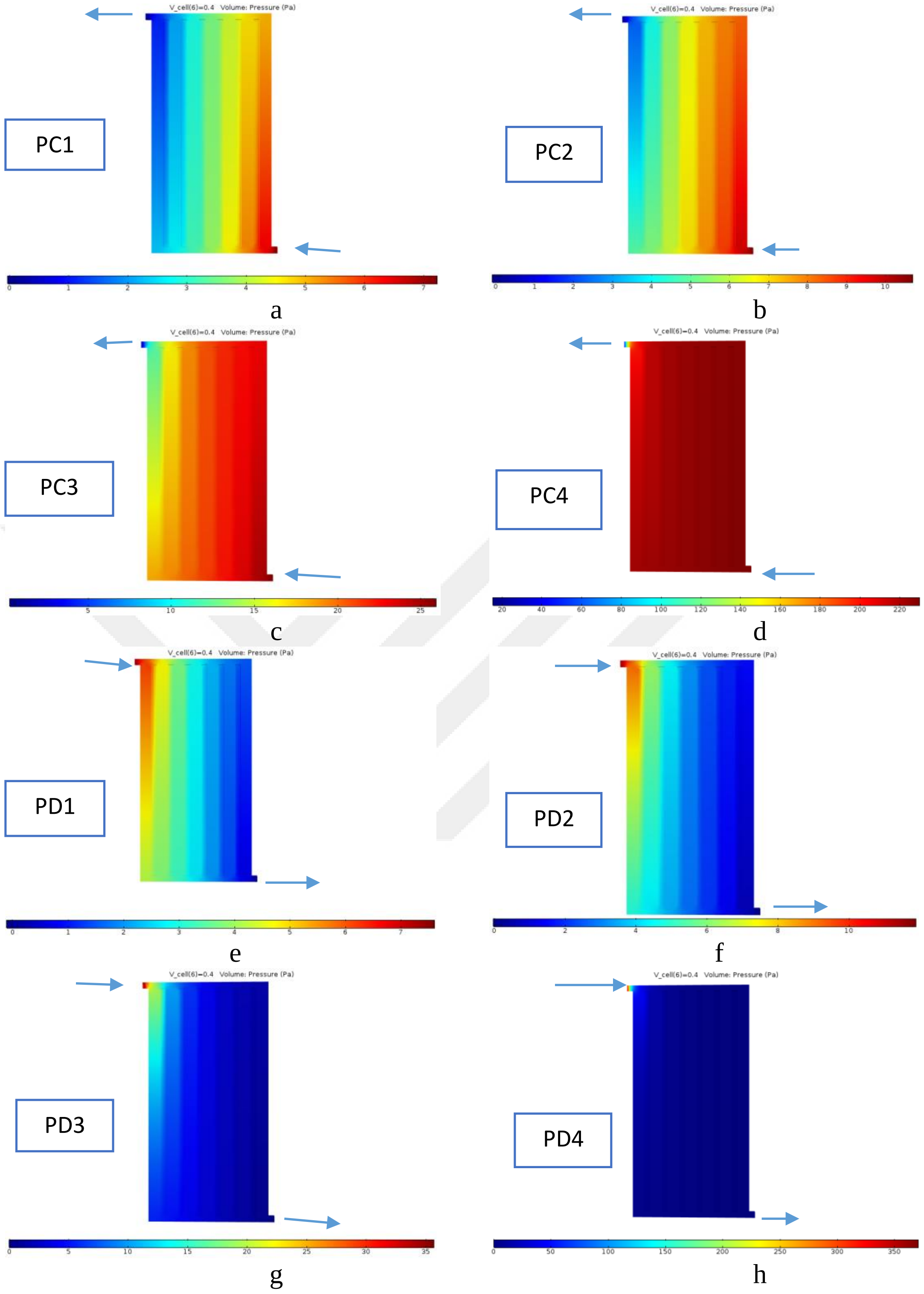

Figure 6.15. Anode Pressure Drop in different parallel convergent (a)-(d) and divergent flow field patterns (e)-(h)

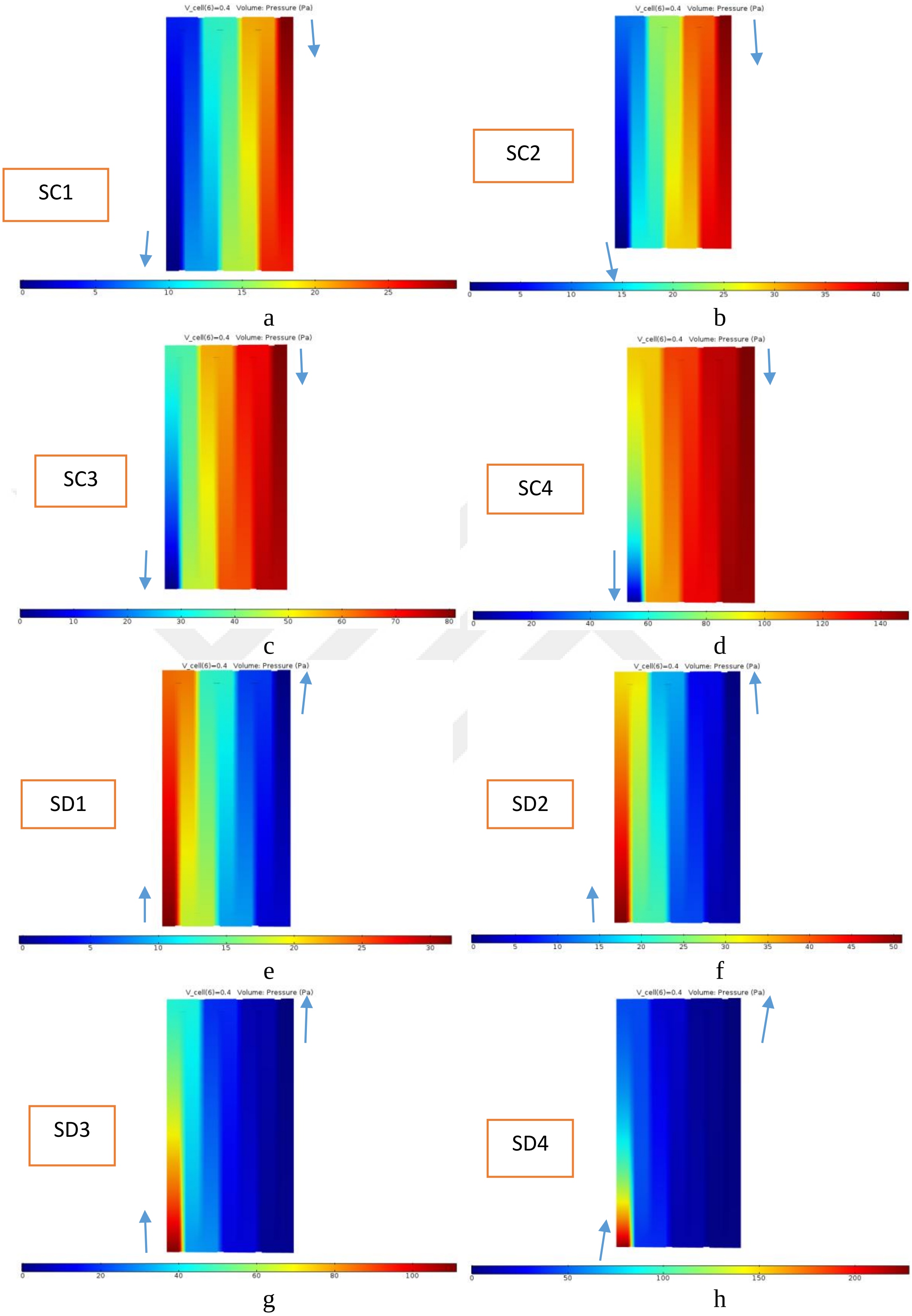

Figure 6.16. Anode pressure drop in different serpentine convergent (a)-(d) and divergent flow field patterns (e)-(h)

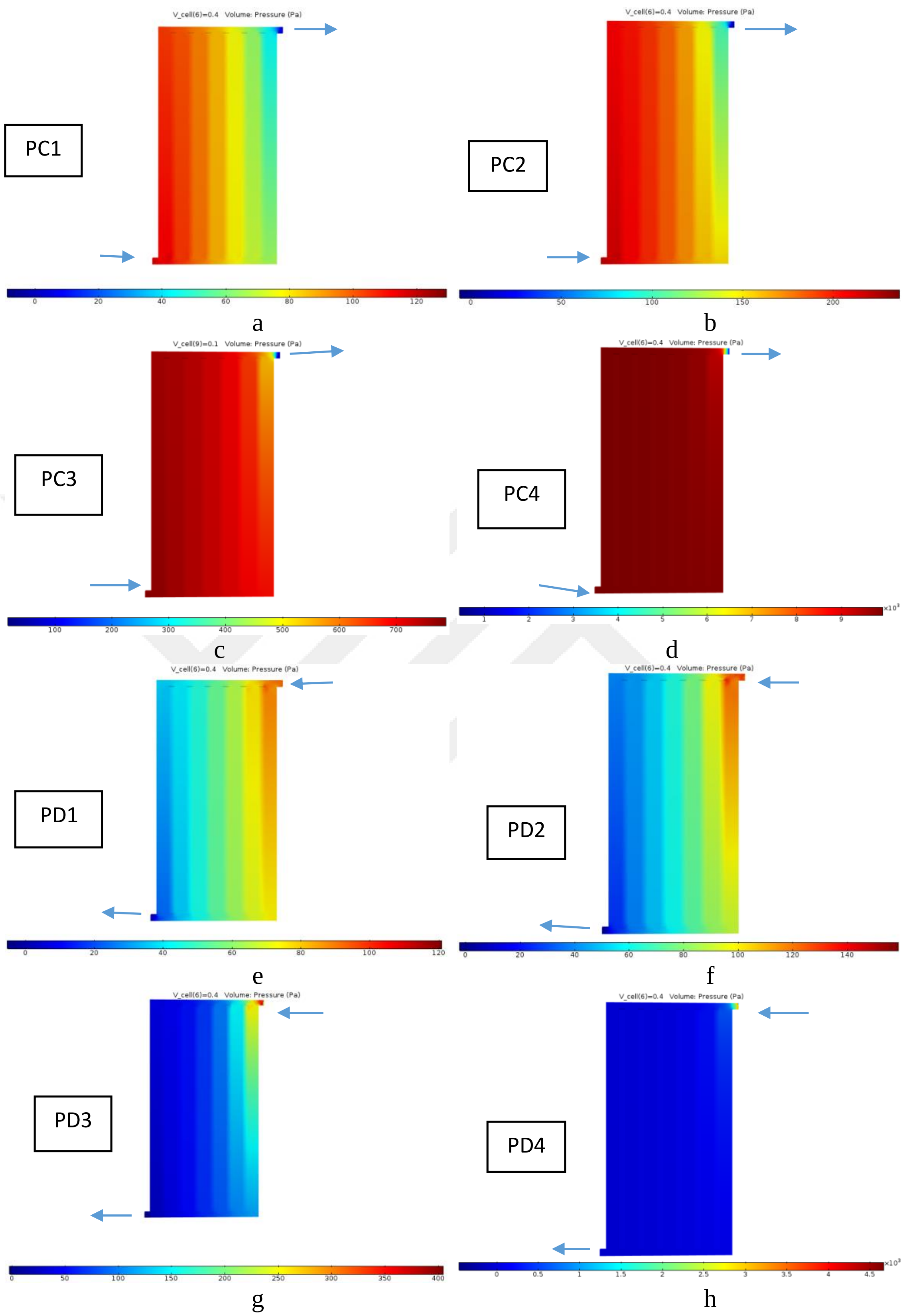

Figure 6.17. Cathode Pressure Drop in different parallel convergent (a)-(d) and divergent flow field patterns (e)-(h)

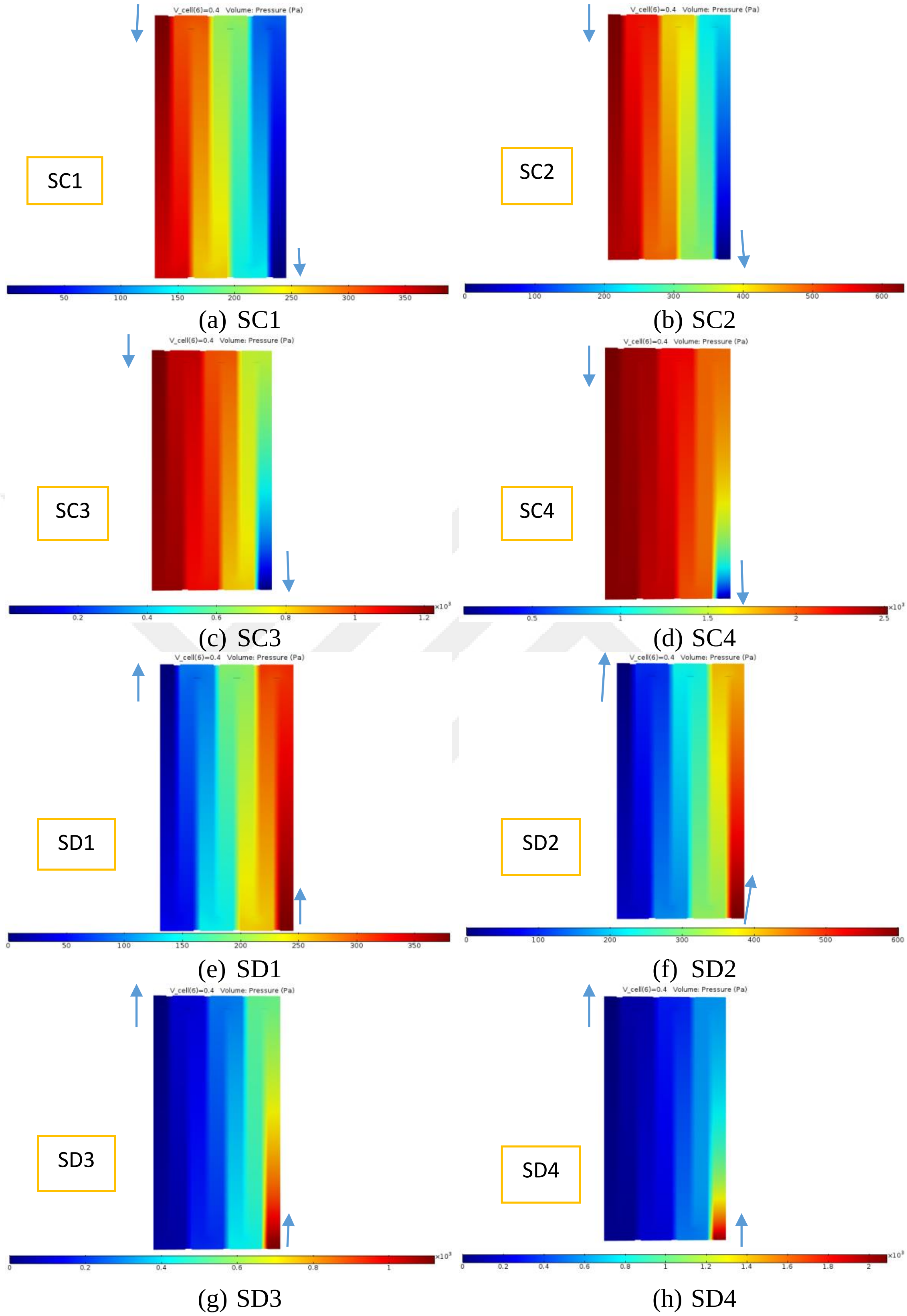

Figure 6.18. Cathode Pressure Drop in different serpentine convergent (a)-(d) and divergent flow field patterns (e)-(h)

For the serpentine convergent and divergent flow field patterns, the pressure distribution is depicted in Figure 6.19. The cathode pressure drop characteristics for different convergent and divergent flow fields are also similar to that of serpentine flow field's anodic pressure drop except relatively higher pressure drop.

6.3.3 Water management analysis

Water vapor distribution in the anode for different convergent and divergent parallel flow fields is demonstrated in Figure 6.19. For the convergent types, the water concentration increases near the outlet. Meanwhile for divergent case water concentration dominated in the mid channel and even worse case of water accumulation occurred in the outlet manifold inner corner for the extreme divergent case of (g) and (h) as shown in Figure 6.20.

The numerical results obtained for the water distribution in anode for different convergent and divergent serpentine flow fields are shown in the Figure 6.20. From the simulation results, it can be seen that the water distribution along the serpentine path for different convergent and divergent flow fields gradually reduces from the inlet towards the outlet except in the extreme divergence case illustrated in Figure 6.21 (h), where the water vapor is non-uniformly distributed due to sub-rib convection.

The water distribution in cathode channels for different parallel convergent and divergent flow fields is demonstrated in Figure 6.21. From the simulation results, it can be observed that water accumulated in the mid-channel in the different parallel convergent and divergent flow fields again except the extreme convergent and divergent cases. For the extreme convergent case, the water removal is found to be exceptionally improved while in the extreme divergence case the water accumulation seems to be much higher than usual cases.

The water distribution in cathode channels for different serpentine convergent and divergent flow fields is illustrated in Figure 6.22. The water removal is quite uniform for the different convergent flow fields especially it increased with the increase in the convergence. Meanwhile the water accumulates before the outlet section channel and it gets worse in the extreme divergence case with a considerable accumulation after the inlet initial channel.

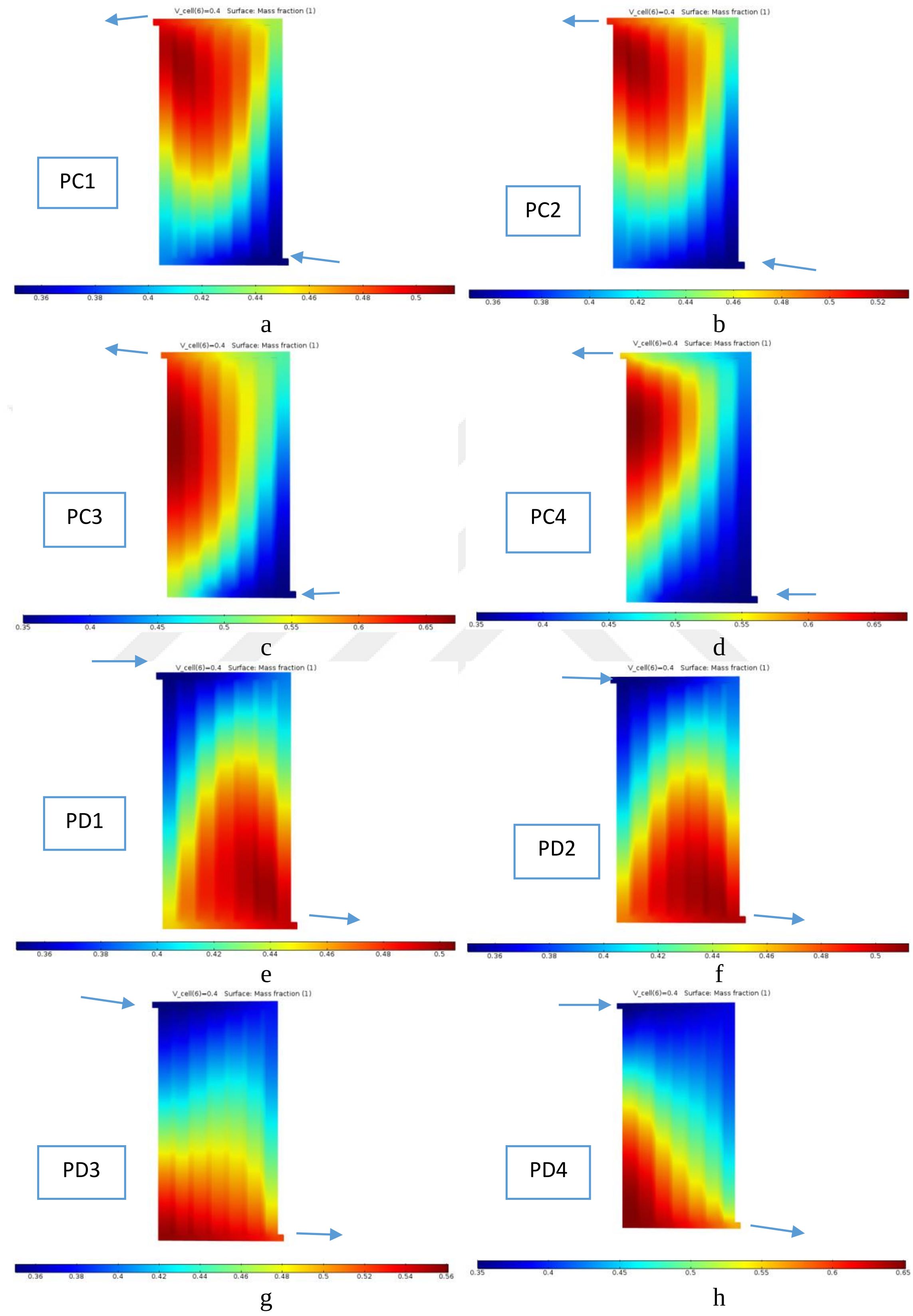

Figure 6.19. Anode water distribution in different parallel- convergent (a)-(d) and divergent flow field patterns (e)-(h)

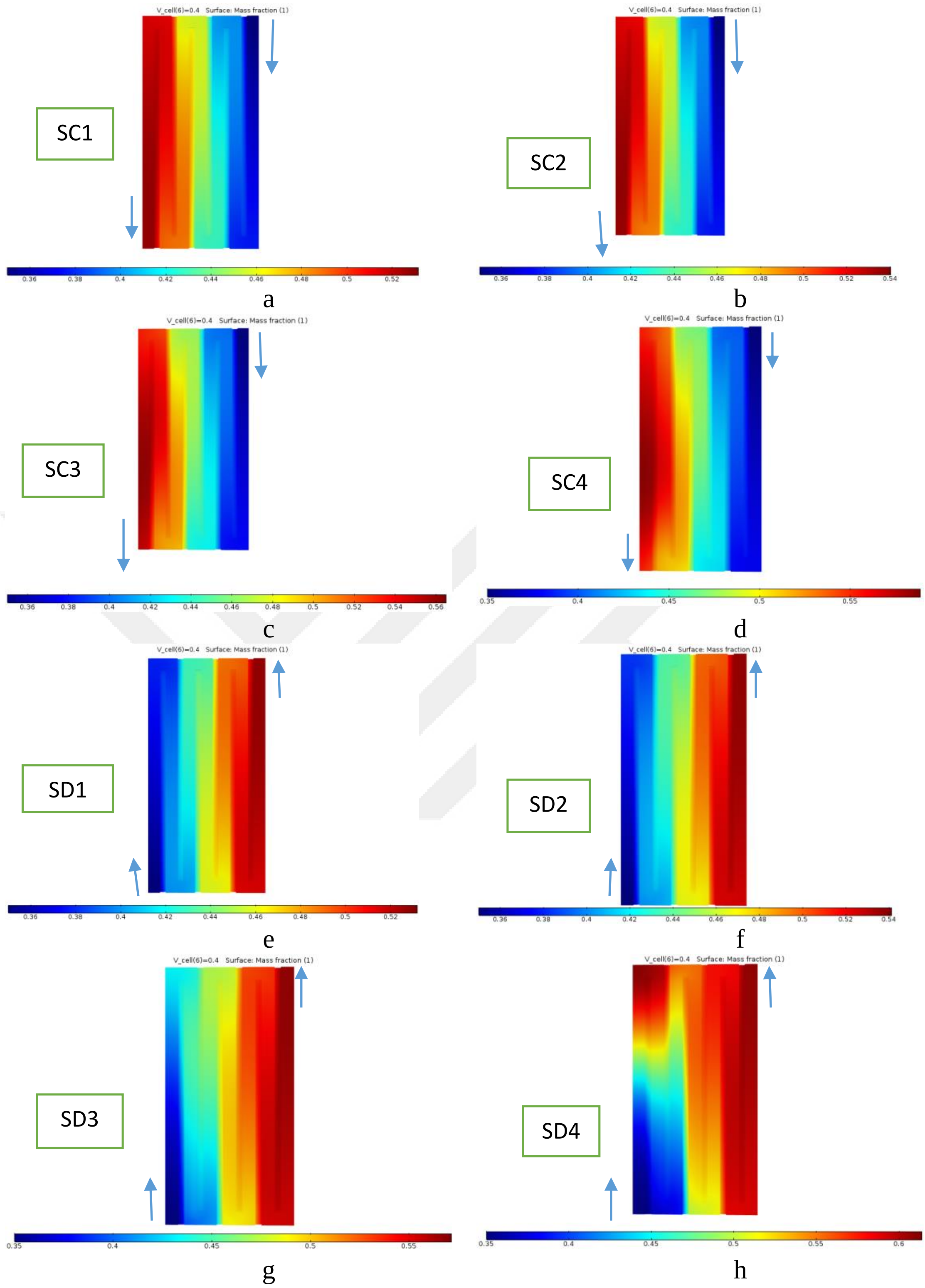

Figure 6.20. Anode water distribution in different serpentine- convergent (a)-(d) and divergent flow field patterns (e)-(h)

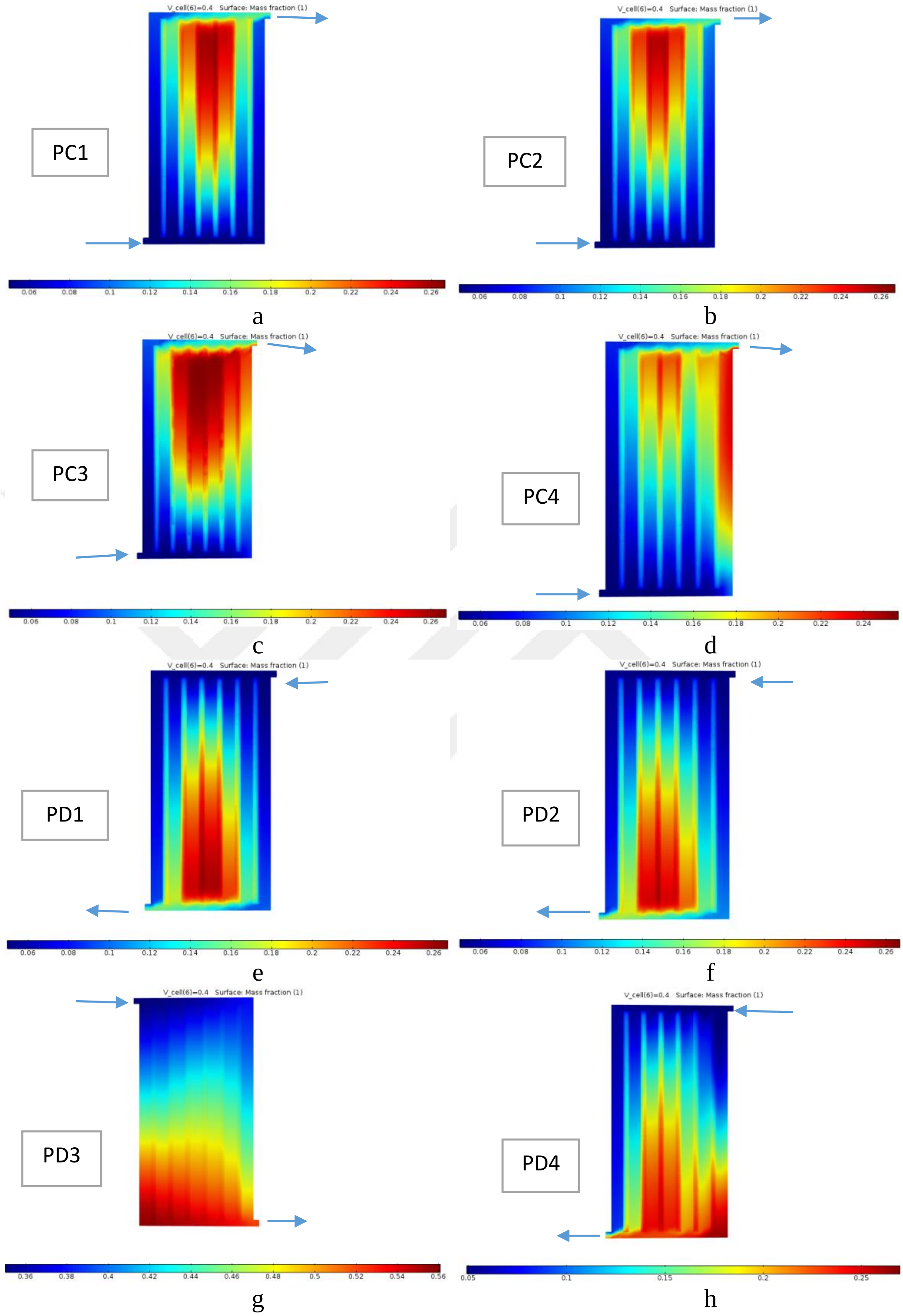

Figure 6.21. Cathode water distribution in different parallel- convergent (a)-(d) and divergent flow field patterns (e)-(h)

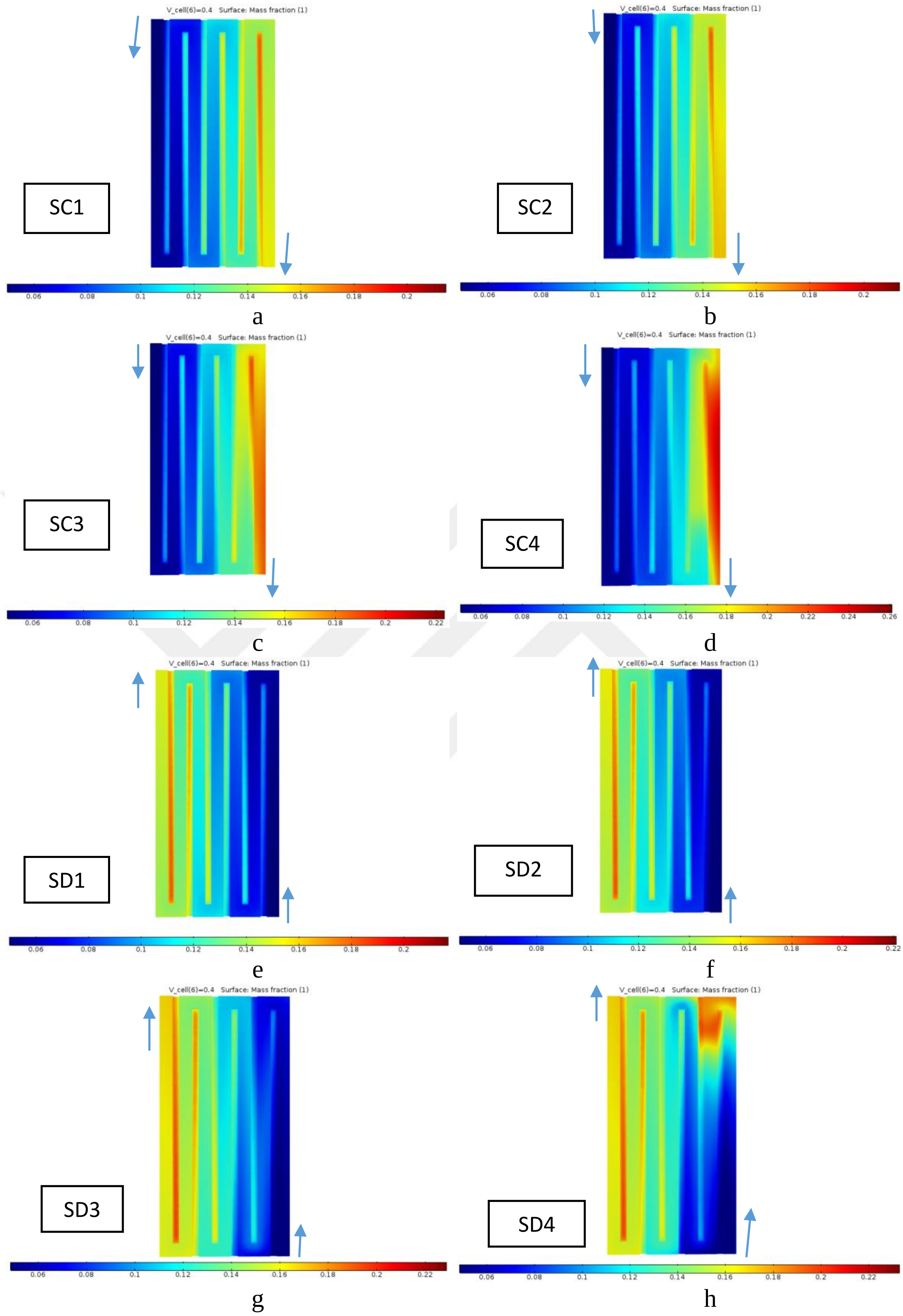

Figure 6.22. Cathode water distribution in different serpentine- convergent (a)-(d) and divergent flow field patterns (e)-(h)

6.3.4 Cell performance analysis

The cell performance of serpentine and parallel type convergent and divergent flow field are compared from the numerical results. The comparison between different convergent and divergent flow fields and the conventional ones for parallel and serpentine are shown in Figure 6.23 and Figure 6.24, respectively.

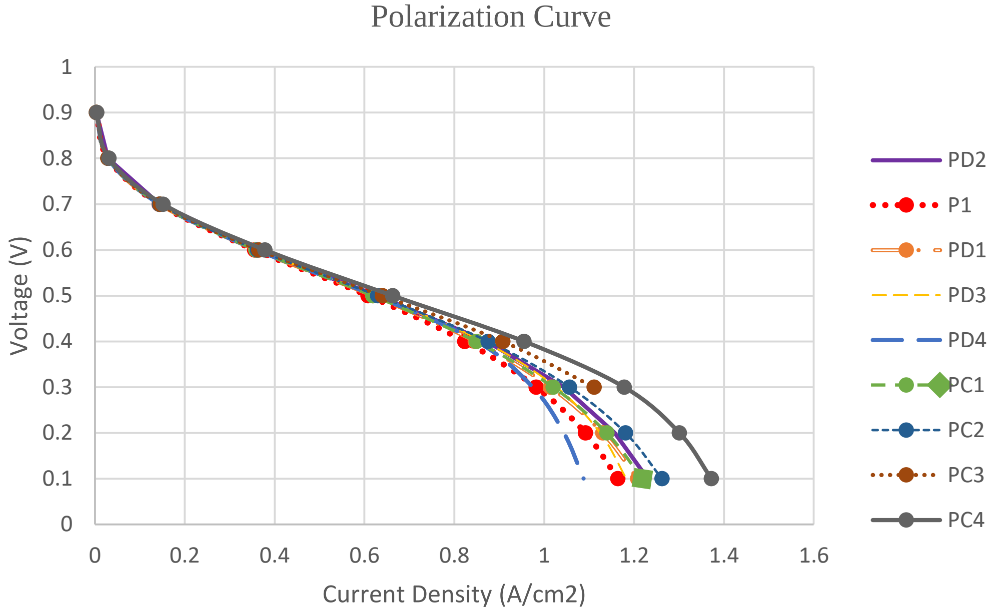

a

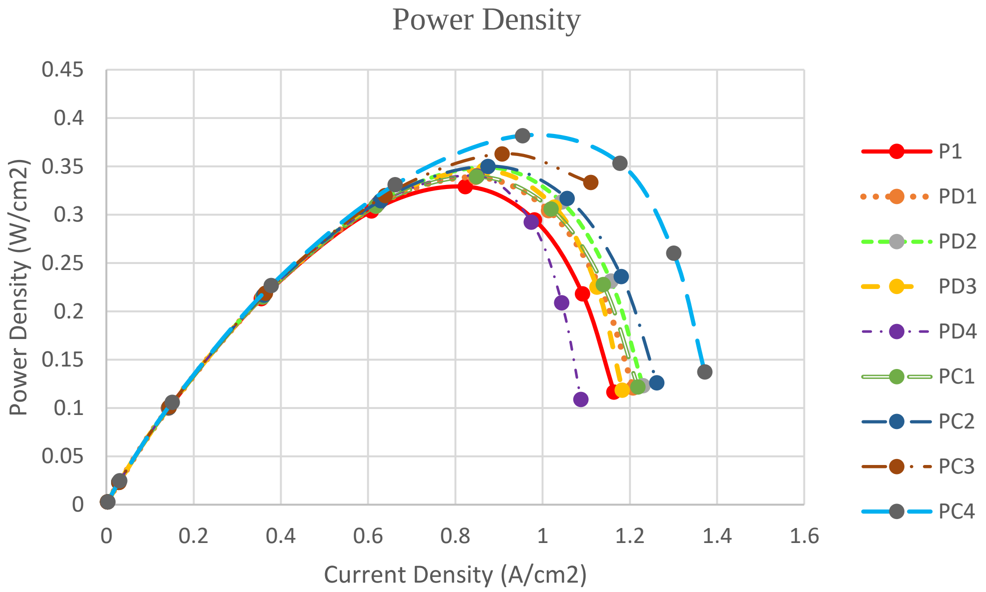

b

Figure 6.23. Cell performance comparison for different convergent and divergent parallel flow field patterns in (a) and (b)

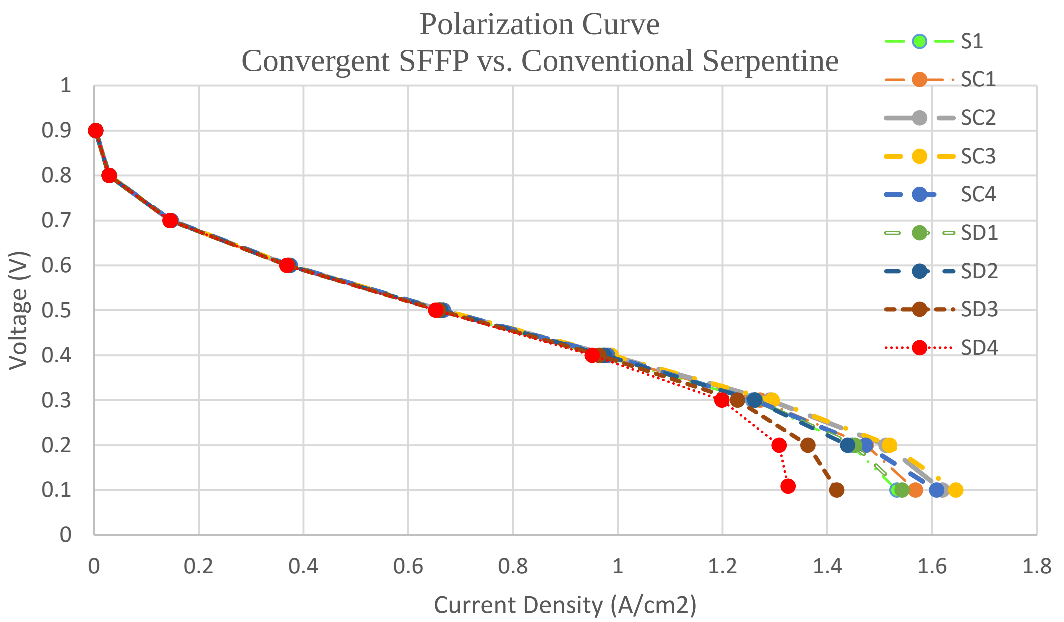

a

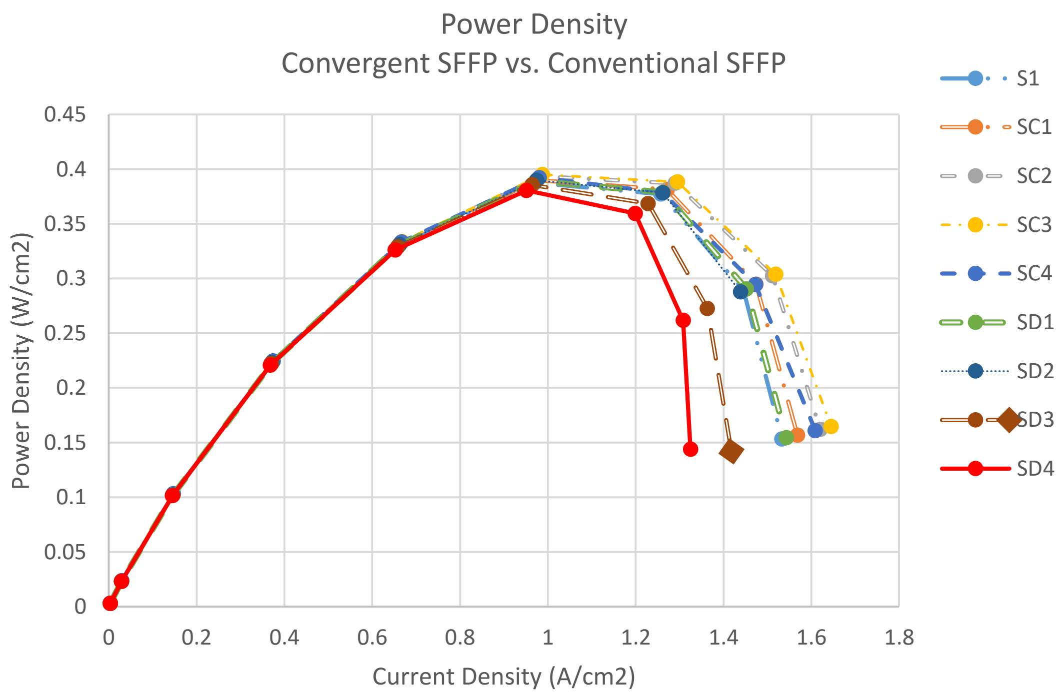

b

Figure 6.24. Cell performance comparison of different convergent and divergent serpentine flow field patterns in (a) and (b)

From this comparative study, it can be seen that all the convergent and divergent flow fields are found to be better than conventional parallel flow field and PC4 is the best among all parallel flow fields. Meanwhile, for the serpentine flow field comparative study, convergent flow fields are better than divergent counterpart and SC3 flow field shows the best cell performance not only for the among serpentine but also all the numerically studied flow field patterns.

6.4 Discussion

The numerical model is developed on the platform of Comsol multi-physics software. The model is developed with standard research procedure with porous flow physics, fluid flow dynamics and electrochemistry. After the major mathematical parameters being in alignment with the literature survey, the numerical model is validated by considering the same operating conditions as the experiments. The numerical model is found to be well in a well agreement with the experimental case study. For the more accuracy and certainty, the same developed numerical model is run for another experimental case study and shows again an error less than 1%.

For the geometry optimization case with a wide range of channel dimension for each of the geometric parameter through 343 different case with parametric sweeps, optimized channel depth and width are decided to be 1.0 mm while rib width is chosen as 0.5 mm considering the cell performance and pressure drop.

The conventional flow field study of parallel and serpentine is carried out where serpentine flow field outperform parallel flow field by an approximately 18% improvement in the power density. The serpentine flow field also shows a better water management and reactant mass transport than that in parallel except it has a relatively higher pressure drop.

Parallel convergent flow field’s performance can be increased by increasing the convergence and for this reason PC4 as the extreme convergent case has a higher power density than the other types of convergent, divergent and conventional parallel flow fields. However, PC4 has excessive higher pressure drop in outlet. Despite it can be a perfect candidate for the removal of the back pressure operation as well as improved mass transport characteristics than conventional ones, especially reduced water accumulation in mid channel which is one of the major drawbacks of the conventional parallel flow field phenomena. On the other hand, divergent flow fields shows a slight improvement in the cell performance which is not worthy of modification. In addition to this, the water accumulation gets worse as the divergence increased for the divergent parallel flow fields. The modified serpentine convergent and divergent flow fields exhibit an improved performance than the conventional ones, although the extreme divergence case of SD3 and SD4 have lower performance than the conventional serpentine. All the convergent flow fields found to be superior to the divergent as well as conventional one. Convergent serpentine SC3 found to be best among all with a relatively higher pressure drop. From the convergence criteria it is observed that there should be an optimum convergence due to excessive water removal in cathode and high pressure drop. That's why the extreme convergent serpentine flow field pattern (SC4) has a lower cell performance than that of optimum SC3. SC3 is found to be optimum not only due to higher cell power density but also had better mass transport characteristics, water removal and considerable pressure drop.

Finally the special outcome of the numerical analysis can be mentioned briefly as follows:

- The convergent concept is superior candidate than divergent
- The anode pressure drop is negligible compared to the cathode pressure drop
- The water management in cathode channel is more critical than that of anode.
- The oxygen uniformity along the flow field is very critical.
- The cathode channel is more critical due to the lower mass fraction of oxygen in air as well as complex gas mixture and water generation.

CHAPTER VII

CONCLUSION

The flow field design optimization of proton exchange membrane fuel cell is carried out by both experimental and numerical approaches in this study. The novel convergent and divergent flow field design concept is developed and optimized by the comparative analyses.
The summary of this study can be footnoted as follows:

The primary approach for the developing new flow field designs is to make a postulate based on the flow physics and phenomena. The concept is proposed for the convergent and divergent flow phenomena which can improve PEM fuel cell by increasing reactant diffusion as well as improved water management. After that detailed related research studies are explored for the development of experimental and numerical work out.

According to the developed concept, flow fields are manufactured, experimental setup is developed and experimental study is carried out.

From the experimental results, it is found out that the suggested flow fields are in favor such that 19% better performance can be obtained from the novel convergent serpentine flow field than the conventional one.

Due to the limitation of time and cost of experimental measurement as well as for the further certainty, accuracy and authenticity of the theoretical as well as experimental approach, numerical tools are employed.

For the numerical study, the first and foremost is to validate the mathematical model with experimental study which is carried out by the double validation of the two experimental case studies and an error of less than 1% considering the same operating conditions and other major parameters is observed. This made the numerical model accurate enough for this thesis research works that are in alignment as a possible replacement of the extended experimental study.

The geometry optimization for the channel depth, width and rib width is investigated with staggering 343 number of different case studies for wide ranges of dimensions of the channel geometry parameters to search for the suitable and optimized flow field designs. The optimum flow field design is found to be 1.0 mm of channel depth and width as well as 0.5 mm of rib width.

With the considered channel geometry parameters, the most popular and conventional parallel and serpentine flow field patterns are modeled using validated numerical model parameters. The outcome of the comparative analyses between these two flow fields are well in agreement with the retrospect literature studies.

The innovative novel proposal of the convergent and divergent flow fields for the modification of the two conventional flow field patterns are then investigated numerically. The numerical results show that, the selected modified convergent parallel flow field design improves the cell power density by 16% compare to the conventional one. Meanwhile, selected convergent serpentine improve not only the cell power density by 2% but also sensitive issues like mass transport and water management are predicted to be better as well.

Finally, it can be concluded that the novel convergent flow field design concept studied and developed in this thesis research works by both experimentally and numerically, will add a fuel to the ongoing research and development of the flow field design for PEM fuel cell. This developed design concept can be a breakthrough flow field design concept in the future for the commercial and industrial Proton exchange membrane fuel cell stack development.

REFERENCES

Aiyejina, A. and Sastry, M.K.S., “PEMFC flow channel geometry optimization: A review”, ***Fuel Cell Sci. Technol*** 9(1), 011011-011034, 2011.

Akbari, M.H. and Rismanchi, B., “Numerical investigation of flow field configuration and contact resistance for PEM fuel cell performance”, ***Renewable Energy*** 33, 1775–1783, 2008.

Akhtar, N., Qureshi, A., Scholta, J., Hartnig, C., Messerschmidt, M. and Lehnert, W., “Investigation of water droplet kinetics and optimization of channel geometry for PEM fuel cell cathodes”, ***International Journal of Hydrogen Energy*** 34, 3104-3111, 2009.

Al-Baghdadi, M.A.R.S. and Al-Janabi, H.A.K.S., “Parametric and optimization study of a PEM fuel cell performance using three-dimensional computational fluid dynamics model”, ***Renewable Energy*** 32, 1077–1101, 2007.

Arbabi, F., Roshandel, R. and Moghaddam, G.K., “Numerical modeling of an innovative bipolar plate design based on the leaf venation patterns for PEM fuel cells”, ***International Journal of Engineering*** 25 (3), 177-186, 2012.

Arvay, A., French, J., Wang, J.C., Peng, X.H. and Kannan, A.M., “Modeling and simulation of biologically inspired flow field designs for proton exchange membrane fuel cells”, ***The Open Electrochemistry Journal*** 6, 1-9, 2015.

Ashorynejad, H.R. and Javaherdeh, K., “Investigation of a waveform cathode channel on the performance of a PEM fuel cell by means of a pore-scale multi-component lattice Boltzmann method”, ***Journal of the Taiwan Institute of Chemical Engineers*** 66, 126–136, 2016.

Ashorynejad, H.R., Javaherdeh, K., Akker, H.E.A.V.D., “The effect of pulsating pressure on the performance of a PEM fuel cell with a wavy cathode surface”, ***International Journal of Hydrogen Energy*** 41, 14239-14251, 2016.

Bachman, J., Charvet, M., Santamaria, A., Tang, H.Y., Park, J.W. and Walker, R., “Experimental investigation of the effect of channel length on performance and water accumulation in a PEMFC parallel flow field”, ***International Journal of Hydrogen Energy*** 37, 17172-17179, 2012.

Barbir, F., PEM Fuel Cells Theory and Practice, 2nd ed., **Elsevier**, London, 2013.

Barreras, F., Lozano, A., Valino, L., Mustata, R. and Marın, C., “Fluid dynamics performance of different bipolar plates Part I. Velocity and pressure fields”, ***Journal of Power Sources*** 175, 841–850, 2008.

Belchor, P.M., Forte, M.M.C. and Carpenter, D.E.O.S., “Parallel serpentine-baffle flow field design for water management in a proton exchange membrane fuel cell”, ***International Journal of Hydrogen Energy*** 37, 11904–11911, 2012.

Bernardi, D. and Verbrugge, M., “A mathematical model of the solid polymer electrolyte fuel cell”, ***J. Electrochem. Soc.*** 139 (9), 2477–2491, 1992.

Berning, T. and Djilali, N., “Three-dimensional computational analysis of transport phenomena in a PEM fuel cell—a parametric study”, ***Journal of Power Sources*** 124, 440–452, 2003.

Bilgili, M., Bosomoiu, M. and Tsotridis, G., “Gas flow field with obstacles for PEM fuel cells at different operating conditions”, ***International Journal of Hydrogen Energy*** 40, 2303–2311, 2015.

Birgersson, E. and Vynnycky, M., “A quantitative study of the effect of flow-distributor geometry in the cathode of a PEM fuel cell”, ***Journal of Power Sources*** 153, 76–88, 2006.

Bullecks, B., Rengaswamy, R., Bhattacharyya, D. and Campbell, G., “Development of a cylindrical PEM fuel cell”, ***International Journal of Hydrogen Energy*** 36, 713-719, 2011.

Cano-Andrade, S., Hernandez-Guerrero, A., Spakovsky, M.R.V., Damian-Ascencio, C.E. and Rubio-Arana, J.C., “Current density and polarization curves for radial flow field patterns applied to PEMFCs (Proton Exchange Membrane Fuel Cells)”, ***Energy*** 35, 920–927, 2010.

Carton, J.G. and Olabi, A.G., “Three-dimensional proton exchange membrane fuel cell model: Comparison of double channel and open pore cellular foam flow plates”, ***Energy***, 1-11, 2016.

Chang, D.H. and Wu, S.Y., “The effects of channel depth on the performance of miniature proton exchange membrane fuel cells with serpentine-type flow fields”, ***International Journal of Hydrogen Energy*** 40, 11659-11667, 2015.

Chen, Y.S. and Peng, H., “Predicting current density distribution of proton exchange membrane fuel cells with different flow field designs”, ***Journal of Power Sources*** 196, 1992–2004, 2011.

Chen, T., Liu, S., Gong, S. and Wu, C., “Development of bipolar plates with different flow channel configurations based on plant vein for fuel cell”, ***Int. J. Energy Res.*** 37, 1680–1688, 2013.

Chen, F., Wen, Y.Z., Chu, H.S., Yan, W.M. and Soong, C.Y., “Convenient two-dimensional model for design of fuel channels for proton exchange membrane fuel cells”, ***Journal of Power Sources*** 128, 125–134, 2004.

Chen, T.Y., Chen, C.H. and Chen, C.H., “The experimental study of the effect of flow pattern geometry on performance of micro proton exchange membrane fuel cell”, ***International Journal of Mechanical*** 3(7), 803-807, 2009.

Cheng, C.H., Lin, H.H. and Lai, G.J., “Design for geometric parameters of PEM fuel cell by integrating computational fluid dynamics code with optimization method”, ***Journal of Power Sources*** 165, 803–813, 2007.

Choi, I., Shin, G., Choi, K.S. and Kim, H.M., “Performance Evaluation of Micro PEM Fuel Cell Through the Numerical Analysis and Fabrication of Micro Channel”, ***World Electrical Vehicle Journal*** 3, 408-412, 2009.

Chowdhury, M.Z. and Akansu, Y.E., “Novel convergent-divergent serpentine flow fields effect on PEM fuel cell performance”, ***International Journal of Hydrogen Energy***, http://dx.doi.org/10.1016/j.ijhydene.2017.04.079, 2017.

Dawes, J.E., Hanspal, N.S., Family, O.A. and Turan, A., “Three dimensional CFD modelling of PEM fuel cells: an investigation into the effects of water flooding,” ***Chem. Eng. Sci.*** 64, 2781–2794, 2009.

EG&G Technical Services Inc., Fuel Cell Handbook, 7th ed., **U.S. Depatrment of Energy**, West Verginia, 2004.

Ferng, Y.M., Su, A. and Lu, S.M., “Experiment and simulation investigations for effects of flow channel patterns on the PEMFC performance”, ***Int. J. Energy Res.*** 32, 12–23, 2008.

Friess, B.R. and Hoorfar, M., “Development of a novel radial cathode flow field for PEMFC”, ***International Journal of Hydrogen Energy*** 37, 7719–7729, 2012.

Goebel, S.G., “Impact of land width and channel span on fuel cell performance”, ***Journal of Power Sources*** 196, 7550–7554, 2011.

Grigoriev, S.A., Kalinnikov, A.A., Kuleshov, N.V. and Millet, P., “Numerical optimization of bipolar plates and gas diffusion electrodes for PBI-based PEM fuel cells”, ***International Journal of Hydrogen Energy*** 38, 8557-8567, 2013.

Guo, N., Leu, M.C. and Koylu, U.O., “Network based optimization model for pin-type flow field of polymer electrolyte membrane fuel cell”, ***International Journal of Hydrogen Energy*** 38, 6750-6761, 2013.

Guo, N., Leu, M.C. and Koylu, U.O., “Bio-inspired flow field designs for polymer electrolyte membrane fuel cells”, ***International Journal of Hydrogen Energy*** 39, 21185-21195, 2014.

Gurau, V., Barbir, F. and Liu, H., “Two-dimensional model for the entire sandwich of a PEM fuel cell,” ***Electrochemical Society Proceedings*** 98(27), 479–503, 1999.

Gurau, V., US Patent No. 6.551.736, 2003.

Han, S.H., Choi, N.H. and Choi, Y.D., “Simulation and experimental analysis on the performance of PEM fuel cell by the wave-like surface design at the cathode channel”, ***International Journal of Hydrogen Energy*** 39, 2628-2638, 2014.

Hashemi, F., Rowshanzamir, S. and Rezakazemi, M., CFD simulation of PEM fuel cell performance: Effect of straight and serpentine flow fields, ***Mathematical and Computer Modelling*** 55, 1540–1557, 2012.

Heidary, H. and Kermani, M.J., “Enhancement of heat exchange in a wavy channel linked to a porous domain; a possible duct geometry for fuel cells”, ***International Communications in Heat and Mass Transfer*** 39, 112–120, 2012.

Heidary, H., Kermani, M.J., Advani, S.G. and Prasad, A.K., “Experimental investigation of in-line and staggered blockages in parallel flow field channels of PEM fuel cells”, ***International Journal of Hydrogen Energy*** 41, 6885-6893, 2016.

Heidary, H., Kermani, M.J. and Dabir, B., “Influences of bipolar plate channel blockages on PEM fuel cell performances”, ***Energy Conversion and Management*** 124, 51–60, 2016.

Hickner, M.A., Siegel, N.P., Chen, K.S., Hussey, D.S., Jacobson, D.L. and Arif, M., "In situ high resolution neutron radiography of cross-sectional liquid water profiles in proton exchange membrane fuel cells", ***J. Electrochem. Soc.*** 155, B427, 2008.

Higier, A. and Liu, H., "Optimization of PEM fuel cell flow field via local current density measurement", ***International Journal of Hydrogen Energy*** 35, 2144-2150, 2010.

Hontanon, E., Escudero, M.J., Bautista, C., Garcia-Ybarra, P.L. and Daza, L., ***J. Power Sources*** 86, 363–368, 2000.

Hsieh, S.S. and Chu, K.M., "Channel and rib geometric scale effects of flow field plates on the performance and transient thermal behavior of a micro-PEM fuel cell", ***Journal of Power Sources*** 173, 222–232, 2007.

Hsieh, S.S. and Huang, Y.J., "Measurements of current and water distribution for a micro-PEM fuel cell with different flow fields", ***Journal of Power Sources*** 183, 193–204, 2008.

Hsieh, S.S., Huang, Y.J. and Her, B.S., "Pressure drop on water accumulation distribution for a micro PEM fuel cell with different flow field plates", ***International Journal of Heat and Mass Transfer*** 52, 5657–5659, 2009.

Hsieh, S.S., Her, B.S. and Huang, Y.J., "Effect of pressure drop in different flow fields on water accumulation and current distribution for a micro PEM fuel cell", ***Energy Conversion and Management*** 52, 975–982, 2011.

Hussaini, I.S. and Wang, C.Y., "Visualization and quantification of cathode channel flooding in PEM fuel cells", ***J. Power Sources*** 187(2), 444–451, 2009.

Hwang, J.J. and Liu, S.J., "Comparison of temperature distributions inside a PEM fuel cell with parallel and interdigitated gas distributors", ***Journal of Power Sources*** 162, 1203–1212, 2006.

Jang, J.H., Yan, W.M., Li, H.Y. and Chou, Y.C., “Humidity of reactant fuel on the cell performance of PEM fuel cell with baffle-blocked flow field designs”, ***Journal of Power Sources*** 159, 468–477, 2006.

Jang, J.H., Yan, W.M., Li, H.Y. and Tsai, W.C., “Three-dimensional numerical study on cell performance and transport phenomena of PEM fuel cells with conventional flow fields”, ***International Journal of Hydrogen Energy*** 33, 156–164, 2008.

Jaruwasupant, N. and Khunatorn, Y., “Effects of difference flow channel designs on proton exchange membrane fuel cell using 3-D model”, ***Energy Procedia*** 9, 326–337, 2011.

Jeon, D.H., Greenway, S., Shimpalee, S. and VanZee, J.W., “The effect of serpentine flow-field designs on PEM fuel cell performance”, ***International Journal of Hydrogen Energy*** 33, 1052–1066, 2008.

Kariya, T., Hirono, T., Funakubo, H. and Shudo, T., “Effects of the porous structures in the porous flow field type separators on fuel cell performances”, ***International Journal of Hydrogen Energy*** 39, 15072-15080, 2014.

Karvelas, E.G., Koubogiannis, D.G., Hatziapostolou, A. and Sarris, I.E., “The effect of anode bed geometry on the hydraulic behaviour of PEM fuel cells”, ***Renewable Energy*** 93, 269-279, 2016.

Kenan, N., Albakri, M. and Khraisheh, M., “Innovative bipolar plates design for increasing fuel cell efficiency”, ***Advances in Sustainable Manufacturing*** 27, 181-186, 2011.

Khajeh-Hosseini-Dalasm, N., Fushinobu, K. and Okazaki, K., “Three-dimensional transient two-phase study of the cathode side of a PEM fuel cell”, ***International Journal of Hydrogen Energy*** 35, 4234–4246, 2010.

Khakbaz-Baboli, M. and Kermani, M.J., “A two-dimensional, transient, compressible isothermal and two-phase model for the air-side electrode of PEM fuel cells”, ***Electrochimica Acta*** 53, 7644–7654, 2008.

Kloess, J. P., Wang, X., Liu, J., Shi, Z. and Guessous, L., “Investigation of bio-inspired flow channel designs for bipolar plates in proton exchange membrane fuel cells”, ***Journal of Power Sources*** 188, 132–140, 2009.

Kozakai, M., Date, K., Tabe, Y. and Chikahisa, T., “Improving gas diffusivity with bi-porous flow-field in polymer electrolyte membrane fuel cells”, ***International Journal of Hydrogen Energy*** 41, 13180-13189, 2016.

Kreesaeng, S., Chalermsinsuwan, B. and Piumsomboon, P., “Effect of channel designs on open-cathode PEM fuel cell performance: a computational study”, ***Energy Procedia*** 79, 733–745, 2015.

Ku, H.W. and Wu, H.W., “Influences of operational factors on proton exchange membrane fuel cell performance with modified interdigitated flow field design”, ***Journal of Power Sources*** 232, 199-208, 2013.

Kumar, A. and Reddy, R.G., “Effect of channel dimensions and shape in the flow-field distributor on the performance of polymer electrolyte membrane fuel cells”, ***Journal of Power Sources*** 113, 11–18, 2003.

Kumbur, E.C., Sharp, K.V. and Mench, M.M., “Liquid droplet behavior and instability in a polymer electrolyte fuel cell flow channel”, ***J. Power Sources*** 161(1), 333–345, 2006.

Kuo, J.K. and Chen, C.K., “The effects of buoyancy on the performance of a PEM fuel cell with a wave-like gas flow channel design by numerical investigation”, ***International Journal of Heat and Mass Transfer*** 50, 4166–4179, 2007.

Kuo, J.K., Yen, T.H. and Chen, C.K., “Three-dimensional numerical analysis of PEM fuel cells with straight and wave-like gas flow fields channels, ***Journal of Power Sources*** 177, 96–103, 2008.

Kuo, J.K., Yen, T.S. and Chen, C.K., "Improvement of performance of gas flow channel in PEM fuel cells", ***Energy Conversion and Management*** 49, 2776–2787, 2008.

Lee, B., Park, K. and Kim, H.M., "Numerical optimization of flow field pattern by mass transfer and electrochemical reaction characteristics in proton exchange membrane fuel cells", ***Int. J. Electrochem. Sci.*** 8, 219–234, 2013.

Lee, S.J., Lim, N.Y., Kim, S., Park, G.G. and Kim, C.S., "X-ray imaging of water distribution in a polymer electrolyte fuel cell", ***J. Power Sources*** 185(2), 867–870, 2008.

Li, H.Y., Weng, W.C., Yan, W.M. and Wang, X.D., "Transient characteristics of proton exchange membrane fuel cells with different flow field designs", ***Journal of Power Sources*** 196, 235–245, 2011.

Li, X. and Sabir, I., "Review of bipolar plates in PEM fuel cells: Flow-field designs", ***International Journal of Hydrogen Energy*** 30, 359–371, 2005.

Lin, L., Zhang, X.X., Feng, H.T. and Wang, X.D., "Optimization of a serpentine flow field with variable channel heights and widths for PEM fuel cells", ***J. Sci. China Tech.*** 53, 453–460, 2010.

Liu, H., Li, P. and Wang, K., "Optimization of PEM fuel cell flow channel dimensions - mathematic modeling analysis and experimental verification", ***International Journal of Hydrogen Energy*** 38, 9835–9846, 2013.

Liu, H., Li, P., Juarez-Robles, D., Wang, K. and Hernandez-Guerrero, A., "Experimental study and comparison of various designs of gas flow fields to PEM fuel cells and cell stack performance", ***J. Front. Energy Res.*** 2(2), 1-8, 2014.

Liu, X.L., Tan, Y.W., Tao, W.Q. and He, Y.L., "A hybrid model of cathode of PEM fuel cell using the interdigitated gas distributor", ***International Journal of Hydrogen Energy*** 31, 379–389, 2005.

Liu, H.C., Yan, W.M., Soong, C.Y. and Chen, F., “Effects of baffle-blocked flow channel on reactant transport and cell performance of a proton exchange membrane fuel cell”, ***Journal of Power Sources*** 142, 125–133, 2005.

Lobato, J., Canizares, P., Rodrigo, M.A., Piuleac, C.G., Curteanu, S. and Linares, J.J., “Direct and inverse neural networks modelling applied to study the influence of the gas diffusion layer properties on PBI-based PEM fuel cells”, ***Int. J. Hydrogen Energy*** 35, 7889-7897, 2010.

López, A.M., Barreras, F., Lozano, A., García, J.A., Valino, L. and Mustata, R., “Comparison of water management between two bipolar plate flow-field geometries in proton exchange membrane fuel cells at low-density current range”, ***Journal of Power Sources*** 192, 94–99, 2009.

Lorenzini-Gutierrez, D., Hernandez-Guerrero, A., Ramos-Alvarado, B., Perez-Raya, I. and Alatorre-Ordaz, A., “Performance analysis of a proton exchange membrane fuel cell using tree-shaped designs for flow distribution”, ***International Journal of Hydrogen Energy*** 38, 14750-14763, 2013.

Lorenzini-Gutierrez, D., Kandlikar, S.G., Hernandez-Guerrero, A. and Elizalde-Blancas, F., “Residence time of water film and slug flow features in fuel cell gas channels and their effect on instantaneous area coverage ratio”, ***Journal of Power Sources*** 279, 567-580, 2015.

Lu, Y. and Reddy, R.G., “Performance of micro-PEM fuel cells with different flow fields”, ***Journal of Power Sources*** 195, 503–508, 2010.

Lu, Z., Rath, C., Zhang, G. and Kandlikar, S.G., “Water management studies in PEM fuel cells, part IV: Effects of channel surface wettability, geometry and orientation on the two-phase flow in parallel gas channels”, ***International Journal of Hydrogen Energy*** 36, 9864-9875, 2011.

Maharudrayya, S., Jayanti, S. and Deshpande, A.P., “Pressure losses in laminar flow through serpentine channels in fuel cell stacks”, ***Journal of Power Sources*** 138, 1–13, 2004.

Mancusi, E., Fontana, E., Souza, A.A.U.D. and Souza, S.M.A.G.U.D., “Numerical study of two-phase flow patterns in the gas channel of PEM fuel cells with tapered flow field design”, ***International Journal of Hydrogen Energy*** 39, 2261-2273, 2014.

Manso, A.P., Marzo, F.F., Mujika, M.G., Barranco, J. and Lorenzo, A., “Numerical analysis of the influence of the channel cross-section aspect ratio on the performance of a PEM fuel cell with serpentine flow field design”, ***International Journal of Hydrogen Energy*** 36, 6795-6808, 2011.

Manso, A.P., Marzo, F.F., Barranco, J., Garikano, X. and Mujika, M.G., “Influence of geometric parameters of the flow fields on the performance of a PEM fuel cell. A review”, ***International Journal of Hydrogen Energy*** 37, 15256–15287, 2012.

McKahn, D.A., “Influence of gas channel depth in self-humidified miniature PEM fuel cells with dead-ended anode”, ***International Journal of Hydrogen Energy*** 40, 7168-7181, 2015.

Mench, M.M., Dong, Q.L. and Wang, C.Y., “In situ water distribution measurements in a polymer electrolyte fuel cell”, ***J. Power Sources***; 124(1), 90–98, 2003.

Muthukumar, M., Karthikeyan, P., Vairavel, M., Loganathan, C., Praveenkumar, S. and Kumar, A.P.S., “Numerical studies on pem fuel cell with different landing to channel width of flow channel, ***Procedia Engineering*** 97, 1534–1542, 2014.

Owejan, J.P., Trabold, T.A., Jacobson, D.L., Arif, M. and Kandlikar S.G., “Effects of flow field and diffusion layer properties on water accumulation in a PEM fuel cell”, ***International Journal of Hydrogen Energy*** 32, 4489–4502, 2007.

Owejan, J.P., Gagliardo, J.J., Sergi, J.M., Kandlikar, S.G. and Trabold, T.A., "Water management studies in PEM fuel cells, Part I: Fuel cell design and in situ water distributions", ***International Journal of Hydrogen Energy*** 34, 3436-3444, 2009.

Pal, V., Karthikeyan, P. and Anand, R., "Performance enhancement of the proton exchange membrane fuel cell using pin type flow channel with porous inserts", ***Journal of Power and Energy Engineering*** 3, 1-10, 2015.

Paulino, A.L.R., Robalinho, E., Cunha, E.F., Passos, R.R. and Santiago E.I., "Current distribution on PEM fuel cells with different flow channel patterns", ***Excerpt from the Proceedings of the 2013 Comsol conference*** in Boston, Boston, USA, p. 1-5, 10 October, 2013.

Peitzmeier, J.A., Kapturowski, S. and Wang, X., "Optimizing bio-inspired flow channel design on bipolar plates of PEM fuel cells", ***Excerpt from the Proceedings of the COMSOL Conference 2010 Boston***, Boston, USA, p. 1-7, 7-9 October, 2010.

Peng, L., Lai, X., Liu, D., Hu, P. and Ni J., "Flow channel shape optimum design for hydroformed metal bipolar plate in PEM fuel cell", ***Journal of Power Sources*** 178, 223–230, 2008.

Perng, S.W., Wu, H.W., Jue, T.C. and Cheng, K.C., "Numerical predictions of a PEM fuel cell performance enhancement by a rectangular cylinder installed transversely in the flow channel", ***Applied Energy*** 86, 1541–1554, 2009.

Perng, S.W. and Wu, H.W., "Non-isothermal transport phenomenon and cell performance of a cathodic PEM fuel cell with a baffle plate in a tapered channel", ***Applied Energy*** 88, 52–67, 2011.

Perng, S.W., Wu, H.W. and Wang R.H., "Effect of modified flow field on non-isothermal transport characteristics and cell performance of a PEMFC", ***Energy Conversion and Management*** 80, 87–96, 2014.

Ramin, F., Torkavannejad, A. and Baheri, S., “The effect of inclined radial flow in proton exchange membrane fuel cells performance”, ***Iranian Journal of Hydrogen & Fuel Cell*** 3, 141-152, 2014.

Ramos-Alvarado, B., Hernandez-Guerrero, A., Elizalde-Blancas, F. and Ellis, M.W., “Constructal flow distributor as a bipolar plate for proton exchange membrane fuel cells”, ***International Journal of Hydrogen Energy*** 36, 12965-12976, 2011.

Ramos-Alvarado, B., Hernandez-Guerrero, A., Juarez-Robles, D. and Li, P., “Numerical investigation of the performance of symmetric flow distributors as flow channels for PEM fuel cells”, ***International Journal of Hydrogen Energy*** 37 (2012) 436-448, 2012.

Roshandel, R., Arbabi, F. and Moghaddam, G.K., “Simulation of an innovative flow-field design based on a bio inspired pattern for PEM fuel cells”, ***Renewable Energy*** 41, 86-95, 2012.

Rostami, L., Nejad, P.M.G. and Vatani, A., “A numerical investigation of serpentine flow channel with different bend sizes in polymer electrolyte membrane fuel cells”, ***Energy*** 97, 400-410, 2016.

Salah, Y.B., Tabe, Y. and Chikahisa, T., “Gas channel optimisation for PEM fuel cell using the lattice Boltzmann method”, ***Energy Procedia*** 28, 125–133, 2012.

Salah, Y.B., Tabe, Y., and Chikahisa, T., “Two phase flow simulation in a channel of a polymer electrolyte membrane fuel cell using the lattice Boltzmann method”, ***Journal of Power Sources*** 199, 85–93, 2012.

Santamaria, A.D., Bachman, J. and Park, J.W., “Design strategy for a polymer electrolyte membrane fuel cell flow-field capable of switching between parallel and interdigitated configurations”, ***International Journal of Hydrogen Energy*** 38, 5807-5812, 2013.

Santamaria, A.D., Cooper, N.J., Becton, M.K. and Park, J.W., “Effect of channel length on interdigitated flow-field PEMFC performance: A computational and experimental study”, ***International Journal of Hydrogen Energy*** 38, 16253-16263, 2013.

Santamaria, A.D., Bachman, J. and Park, J.W., “Cold-start of parallel and interdigitated flow-field polymer electrolyte membrane fuel cell”, ***Electrochimica Acta*** 107, 327–338, 2013.

Shah, A.A., Kim, G.S., Sui, P.C. and Harvey, D., “Transient non-isothermal model of a polymer electrolyte fuel cell”, ***J. Power Sources*** 163, 793–806, 2007.

Shimpalee, S., Greenway, S. and VanZee, J.W., “The impact of channel path length on PEMFC flow-field design, ***Journal of Power Sources*** 160, 398–406, 2006.

Shimpalee, S. and VanZee, J.W., “Numerical studies on rib & channel dimension of flow-field on PEMFC performance”, ***International Journal of Hydrogen Energy*** 32, 842–856, 2007.

Siefert, N.S. and Litster, S., “Voltage loss and fluctuation in proton exchange membrane fuel cells: The role of cathode channel plurality and air stoichiometric ratio”, ***Journal of Power Sources*** 196, 1948–1954, 2011.

Siegel, N.P., Ellis, M.W., Nelson, D.J., and Spakovsky, M.R.V., “A two-dimensional computational model of a PEMFC with liquid water transport,” ***Journal of Power Sources*** 128(2), 173–184, 2004.

Sierra, J.M., Figueroa-Ramırez, S.J., Dıaz, S.E., Vargas, J. and Sebastian, P.J., “Numerical evaluation of a PEM fuel cell with conventional flow fields adapted to tubular plates”, ***International Journal of Hydrogen Energy*** 39, 16694-16705, 2014.

Sinha, P.K., Halleck, P. and Wang, C.Y., “Quantification of liquid water saturation in a PEM fuel cell diffusion medium using X-ray microtomography”, ***Electrochem Solid State Lett.*** 9(7), A344–348, 2006.

Soong, C.Y., Yan, W.M., Tseng, C.Y., Liu, H.C., Chen, F. and Chu, H.S., “Analysis of reactant gas transport in a PEM fuel cell with partially blocked fuel flow channels”, ***Journal of Power Sources*** 143, 36–47, 2005.

Spernjak, D., Prasad, A.K. and Advani, S.G., “Experimental investigation of liquid water formation and transport in a transparent single-serpentine PEM fuel cell”, ***J. Power Sources*** 170, 334–44, 2007.

Springer, T., Zawodzinski, T. and Gottesfeld, S., “Polymer electrolyte fuel cell model,” ***J. Electrochem. Soc.*** 138(8), 2334–2342, 1991.

Sreenivasulu, B., Vasu, G., Rao, V.D., and Naidu, S.V., “Effect of back pressure and flow geometry on PEM Fuel cell performance - an experimental study”, ***International Journal of Applied Science and Engineering*** 11 (1), 1-11. 2013.

Sun, L., Oosthuizen, P.H. and McAuley, K.B., “A numerical study of channel-to-channel flow cross-over through the gas diffusion layer in a PEM-fuel-cell flow system using a serpentine channel with a trapezoidal cross-sectional shape”, ***International Journal of Thermal Sciences*** 45, 1021–1026, 2006.

Taccani, R. and Zuliani, N., “Effect of flow field design on performances of high temperature PEM fuel cells: Experimental analysis”, ***International Journal of Hydrogen Energy*** 36, 10282-10287, 2011.

Thitakamol, V., Therdthianwong, A. and Therdthianwong, S., “Mid-baffle interdigitated flow fields for proton exchange membrane fuel cells”, ***International Journal of Hydrogen Energy*** 36, 3614–3622, 2011.

Thomas, S., Bates, A., Park, S., Sahu, A.K., Lee, S.C., Son, B.R., Kim, J.G. and Lee, D.H., “An experimental and simulation study of novel channel designs for open-cathode high-temperature polymer electrolyte membrane fuel cells”, ***Applied Energy*** 165, 765–776, 2016.

Tsai, B.T., Tseng, C.J., Liu, Z.S., Wang, C.H., Lee, C.I., Yang, C.C. and Lo, S.K., “Effects of flow field design on the performance of a PEM fuel cell with metal foam as the flow distributor”, ***International Journal of Hydrogen Energy*** 37, 13060-13066, 2012.

Tüber, K., Pócza, D. and Hebling, C., “Visualization of water buildup in the cathode of a transparent PEM fuel cell”, ***J. Power Sources*** 124(2), 403–414, 2003.

Um, S., Wang, C.Y. and Chen, K.S., ***J. Electrochem. Soc.*** 147, 4485–4493, 2000.

Vazifeshenas, Y., Sedighi, K. and Shakeri, M., “Numerical investigation of a novel compound flow field for PEMFC performance improvement”, ***International Journal of Hydrogen Energy*** 40, 15032-15039, 2015.

Wang, C.Y., “Fundamental models for fuel cell engineering”, ***Chem. Rev.*** 104, 4727–4766, 2004.

Wang, J., “Theory and practice of flow field designs for fuel cell scaling-up: A critical review”, ***Applied Energy*** 157, 640–663, 2015.

Wang, J.Y., “Barriers of scaling-up fuel cells: cost, durability and reliability”, ***Energy*** 80, 509–21, 2015.

Wang, X.D., Duan, Y.Y. and Yan, W.M., “Novel serpentine-baffle flow field design for proton exchange membrane fuel cells”, ***Journal of Power Sources*** 173, 210–221, 2007.

Wang, X.D., Duan, Y.Y., Yan, W.M. and Peng, X.F., “Local transport phenomena and cell performance of PEM fuel cells with various serpentine flow field designs”, ***Journal of Power Sources*** 175, 397–407, 2008.

Wang, X.D., Duan, Y.Y., Yan, W.M. and Weng, F.B., “Effect of humidity of reactants on the cell performance of PEM fuel cells with parallel and interdigitated flow field designs”, ***Journal of Power Sources*** 176, 247–258, 2008.

Wang, X.D., Duan, Y.Y., Yan, W.M. and Peng, X.F., “Effects of flow channel geometry on cell performance for PEM fuel cells with parallel and interdigitated flow fields”, ***J. Electrochimica Acta*** 53, 5334–5343, 2008.

Wang, X.D., Huang, Y.X., Cheng, C.H., Jang, J.Y., Lee, D.J., Yan, W.M. and Su, A., "Flow field optimization for proton exchange membrane fuel cells with varying channel heights and widths", ***J. Electrochimica Acta*** 54, 5522–5530, 2009.

Wang, X.D., Huang, Y.X., Cheng, C.H., Jang, J.Y., Lee, D.J., Yan, W.M. and Su, A., "An inverse geometry design problem for optimization of single serpentine flow field of PEM fuel cell", ***International Journal of Hydrogen Energy*** 35, 4247-4257, 2010.

Wang, X.D., Yan, W.M., Won, W.C. and Lee, D.J., "Effects of operating parameters on transport phenomena and cell performance of PEM fuel cells with conventional and contracted flow field designs", ***International Journal of Hydrogen Energy*** 37, 15808-15819, 2012.

Wang, X.D., Duan, Y.Y., Yan, W.M., Lee, D.J., Su, A. and Chi, P.H., "Channel aspect ratio effect for serpentine proton exchange membrane fuel cell: Role of sub-rib convection", ***Journal of Power Sources*** 193, 684–690, 2009.

Wang, X.D., Duan, Y.Y. and Yan, W.M., "Numerical study of cell performance and local transport phenomena in PEM fuel cells with various flow channel area ratios", ***Journal of Power Sources*** 172, 265–277, 2007.

Wang, X.D., Yan, W.M., Duan, Y.Y., Weng, F.B., Jung, G.B. and Lee, C.Y., "Numerical study on channel size effect for proton exchange membrane fuel cell with serpentine flow field", ***Energy Conversion and Management*** 51, 959–968, 2010.

Wawdee, P., Limtrakul, S., Vatanatham, T. and Fowler, M.W., "Water transport in a PEM fuel cell with slanted channel flow field plates", ***International Journal of Hydrogen Energy*** 40, 3739-3748, 2015.

Wu, H.W. and Ku, H.W., "Effects of modified flow field on optimal parameters estimation and cell performance of a PEM fuel cell with the Taguchi method", ***International Journal of Hydrogen Energy*** 37, 1613-1627, 2012.

Xing, L., Cai, Q., Liu, X., Liu, C., Scott, K. and Yan, Y., "Anode partial flooding modelling of proton exchange membrane fuel cells: Optimisation of electrode properties and channel geometries", ***Chemical Engineering Science*** 146, 88–103, 2016.

Xing, L., Du, S., Chen, R., Mamlouk, M. and Scott, K., "Anode partial flooding modelling of proton exchange membrane fuel cells: model development and validation", ***Energy*** 96, 80–95, 2016.

Yan, W.M., Mei, S.C., Soong, C.Y., Liu, Z.S. and Song, D., "Experimental study on the performance of PEM fuel cells with interdigitated flow channels", ***Journal of Power Sources*** 160, 116–122, 2006.

Yan, W.M., Chen, C.Y., Mei, S.C., Soong, C.Y. and Chen, F., "Effects of operating conditions on cell performance of PEM fuel cells with conventional or interdigitated flow field", ***Journal of Power Sources*** 162, 1157–1164, 2006.

Yan, W.M., Yang, C.H., Soong, C.Y., Chen, F. and Mei, S.C., "Experimental studies on optimal operating conditions for different flow field designs of PEM fuel cells", ***Journal of Power Sources*** 160, 284–292, 2006.

Yan, W.M., Li, H.Y., Chiu, P.C. and Wang, X.D., "Effects of serpentine flow field with outlet channel contraction on cell performance of proton exchange membrane fuel cells", ***Journal of Power Sources*** 178, 174–180, 2008.

Yang, X.G., Burke, N., Wang, C.Y., Tajiri, K. and Shinohara, K., "Simultaneous measurements of species and current distributions in a PEFC under low-humidity operation", ***J. Electrochem. Soc.*** 152, A759–766, 2005.

Yu, L.J., Ren, G.P., Qin, M.J. and Jiang, X.M., "Transport mechanisms and performance simulations of a PEM fuel cell with interdigitated flow field", ***Renewable Energy*** 34, 530–543, 2009.

Zhang, F.Y., Yang, X.G. and Wang, C.Y., "Liquid water removal from a polymer electrolyte fuel cell", ***J. Electrochem. Soc.*** 153, A225, 2006.

Zeroual, M., Bouzid, S.B., Benmoussa, H. and Bouguettaia, H., “Numerical study of the effect of the inlet pressure and the height of gas channel on the distribution and consumption of reagents in a fuel cell (PEMFC)”, ***Energy Procedia*** 18, 205–214, 2012.

CURRICULAM VITAE

Mohammad Ziauddin CHOWDHURY was born in 24 August, 1988 in Chittagong, Bangladesh. He accomplished his B. Sc. in Mechanical Engineering from Islamic University of Technology, Bangladesh in 2010. After that he was involved in Industrial job in different automotive industry like Tata Motors Ltd., Toyota Motors Corporation and some other heavy industry in Bangladesh. He started his M. Sc. in Mechanical Engineering at Nigde Omer Halisdemir University from September, 2015. Since then he was actively involved in academic research related to mainly fuel cell in Nigde Omer Halisdemir University.

PUBLICATION LIST

❖ Chowdhury, M.Z., Akansu, Y.E., “Novel convergent-divergent serpentine flow fields effect on PEM fuel cell performance”, ***International Journal of Hydrogen Energy***, DOI: 10.1016/j.ijhydene.2017.04.079.

❖ Chowdhury, M.Z., Genc, O., Toros, S., “Numerical investigation of the effect of channel width to land ratio on PEM fuel cell performance”, ***2nd International Hydrogen Technologies Congress***, Cukurova University, Adana, Turkey, 15-18 April, 2017.

❖ Chowdhury, M.Z., Timurkutluk, B., Toros, S., “Numerical investigation of the effect of channel depth on PEM fuel cell performance”, ***2nd International Defense Industry Symposium***, Kirikkale University, Ankara, Turkey, 6-8 April, 2017.

❖ Genc, O., Chowdhury, M.Z., Toros, S., “Numerical analysis of an ejector for micro combined heat and power systems based on 1kw solid-oxide fuel cells, ***2nd International Hydrogen Technologies Congress***, Cukurova University, Adana, Turkey, 2017.

❖ Chowdhury, M.Z., Akansu Y.E., “Effect of convergent-divergent flow fields in single serpentine flow pattern on PEMFCs performance”, ***9th International Conference on Sustainable Energy and Environmental Protection***, p. 75-85, Erciyes University, Kayseri, Turkey, 22-25 September, 2016.